The healing of LASIK flaps

Thesis submitted to Cardiff University for the degree of Doctor of Philosophy in the disciplines of Cell Biology and Biophysics

Christina-Stamatia Kamma (BSc, MSc)

Cell and Molecular Biology and Structural Biophysics Groups,
School of Optometry and Vision Sciences,
Cardiff University
2007

ProQuest LLC
789 East Eisenhower Parkway
P.O. Box 1346
Ann Arbor, MI 48106-1346

"Even youths grow tired and weary, and youth men stumble and fall; but those who hope in the Lord will renew their strength. They will soar on wings like eagles; they will run and not grow weary, they will walk and not be faint."

Isaiah 40:30-31

Acknowledgements

This thesis has been the outcome of hard work and co-operation not only on my behalf, but both my co-supervisors Prof. Keith Meek and Prof. Mike Boulton. A big thank you to both of them for their trust, invaluable help, enthusiasm about the project and their easily approachable manner despite their busy schedules.

I am also extremely grateful to my PhD advisor Dr Julie Albon for her support and advise for all kind of PhD matters ranging from friendly advice and encouragement to practical help with immunohistochemistry and light microscopy. My gratitude also goes to Dr Carlo Knupp for his invaluable help and constant advice on molecular modelling. Also, Dr Sally Hayes for her friendship, her great help with x-ray diffraction data collection and analysis and being there to the rescue at tough times. Dr Craig Boote for his great help with small angle x-ray scattering data collection and analysis. I greatly appreciate the help of Dr Rob Young and Dr Phil Lewis for their help and advice with electron microscopy. Additionally, I am extremely grateful to Richard Earlam and Tony for putting together my ideas, advising and constructing the eye holder that was used for a series of experiments in this thesis. Many thanks also to Prof Tim Wess for allowing me to use the tensiometer in his lab and to Lee Gonzalez for showing me how to use the equipment.

All these years it has been a pleasure to be working at the School of Optometry and Vision Sciences and that's because of the people there for establishing a friendly and pleasant environment. A big thank you to "the most important person in our school" Mrs Susan Hobbs for looking after all the postgrads. Also to Leanne, Stacey and Rosie for always being more than happy to help. Also to Steve, John, Rob and Phil for always being there to help with all the paperwork and technical issues during the years.

I would like to thank all my friends both here in Cardiff and back in Rhodes, especially Debbie, Jen, Missy, Bablin, Linda, Kat, Flick, Stuart, Miguel, Sarah, Kerenza, Rita, Rina, Buki, Jerome, Jacques and Llinos as well as the rest of the postgrads for making my stay here so much enjoyable.

Finally, I'd like to thank my parents, my sisters, my brother and my Federico for believing in my abilities and for constantly supporting me in every possible way; many times in the expense of their own serenity and wellbeing. Tina

Abstract

The aim of this study was to obtain a better understanding in the healing of LASIK-like flaps using an *in vitro* organ culture method in bovine corneas.

At early stages of the PhD, during protocol optimisation, a 5mm trephine was used to injure bovine corneas. At later stages a custom-made eye holder was used to induce LASIK-like incisions in corneas. Immunohistochemistry for α-smooth muscle actin (αSMA) and cytokeratin was used to monitor myofibroblast and epithelial cell expression, respectively, during the wound healing process. Additionally, the effect of certain cytokines (i.e. TNFα, Fas ligand, TGF-β_1 and IL-1α) was tested in terms of corneal transparency, myofibroblast expression and tissue mechanical strength during the healing process. The later series of experiments was an attempt to manipulate and improve wound healing after LASIK. Healing in this *in vitro* system closely followed the effects that are already known from the literature. In addition, preliminary evidence on the cytokine corneas proved that there is a correlation between cytokine type and concentration with the effect in tissue transparency, extend of wound healing response and tissue mechanical strength.

X-ray diffraction also provided important information about collagen ultrastructural changes in the corneas during the healing process. Parameters such as fibrillar diameter, spacing, distribution and orientation were studied. Collagen fibrillar diameter and spacing remained constant for control corneas during the organ culture time-span, indicating that this *in vitro* system does not induce any swelling effects on the tissue. However, injured corneas became significantly swollen ($p<0.05$) during culture. Swelling effects were more severe in trephined corneas than in LASIK-like injured ones. However, collagen fibrillar diameter remained normal in the periphery of injured corneas, but it increased significantly in areas within and around the wound in trephined samples and in the flap incision site for LASIK-like ones. In both types of wounding, collagen orientation changes were observed and were associated with the process of creating the injury. However, in the case of trephine wounded corneas, tissue swelling and changes in collagen orientation reflected the processes of tissue repair. These differences will determine corneal stability and strength follow trauma and, possibly, refractive surgery.

The transparency of the cornea depends on both the collagen and the interstitial proteoglycans. In order to obtain a better insight in ultrastructural changes during the wound healing process molecular modelling techniques were used in order to construct a theoretical model for the core protein of biglycan. This molecule is a dermatan sulphate proteoglycan and its numbers increase up to seven times during wound healing. It is considerably larger than the rest of proteoglycans and molecular modelling also revealed numerous potential collagen interaction sites.

Table of contents

Carrington LM, Albon J, Anderson I, **Kamma C** and Boulton M (2006) Differential regulation of key stages in early corneal wound healing by TGF-beta isoforms and their inhibitors. *Invest Ophthalmol Vis Sci* 47: 1886-1894.

Bibliography

List of figures

loops at the surface of the molecule (indicated by turquoise arrows). Key: Green and aqua→ α-helix and β-sheet, respectively, for the homology model; Red and yellow→ α-helix and β-sheet, respectively, for the crystal structure (A). The homology model of biglycan superimposed with the crystal structure of the same protein. Key: Yellow→ X-ray structure, Red→ homology model (B).

List of tables

List of equations

1. Introduction

1.1 The Cornea

The cornea is a dome shaped transparent layer that is situated at the front of the eye globe. Its anterior part is covered by the tear film and its posterior side is in direct contact with the aqueous humor. Both the cornea and the tear film protect the eye from physical injury and from the invasion of pathogenic micro-organisms. The major function of the cornea is to refract and transmit light to the retina in order for visual function to occur.

The cornea consists mainly of epithelial cells, collagen, proteoglycans, keratocytes, water molecules and endothelial cells (Table 1.1). The organisation of collagen fibrils within the cornea and the lack of any vascular system make the cornea transparent. Corneal transparency is essential for normal visual function. Since there is no blood supply to the cornea, its oxygen is provided by the tear film and the metabolic requirements are provided by the aqueous humour.

Substance	%
Water	78
Collagen	15
Other Proteins	5
Keratocytes	5
Keratan Sulphate	0.7
Chondroitin Sulphate	0.3
Salts	1

Table 1.1: The composition of the cornea.

(Table after Hogan 1971)

The cornea consists of five well-differentiated layers, i.e. the epithelium, Bowman's layer, the stroma, Descemet's membrane and the endothelium (Fig.1.1).

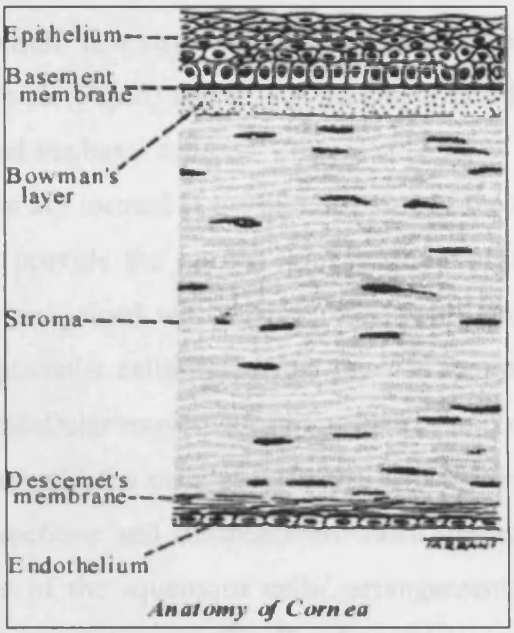

Figure 1.1: Anatomy of the cornea

(Picture after www.northernvision.com 2003)

1.1.1 Tear film

The tear film is the superficial layer of the eye. Its anterior part is in direct contact with the air, whereas its posterior part is adjacent to the epithelial layer of the cornea. Initially it was proposed that the tear film consists of three layers: the lipid, the aqueous and the mucous layer (Wolf 1946). However, this was later challenged by (Dilly 1994) who proposed that the mucous and the aqueous layers are not discrete and they form a single layer. The same review also describes the tear film as a hydrated mucin gel with variable viscosity.

The lipid layer lies at the anterior side of the tear film and it prevents evaporation of the tear film and hence the cornea from the air. This layer is produced by the meibomian glands and the glands of Zeis and Mol. The aqueous portion is the major component of the tear film and it is produced by the main lacrimal glands and the accessory lacrimal glands such as the Krause and Wolfring glands. The mucous portion of the tear film is secreted by conjuctival goblet cells and it is a hydrophilic layer that covers and hydrates the anterior part of the cornea. The tears contain antimicrobial agents (i.e. lysozyme, lactoferrin and IgA) and hence the colonisation of potential pathogens is prevented (Azar 1997, Johnson and Murphy 2004).

1.1.2 Epithelium

The corneal epithelium is a stratified, squamous, non-keratinised epithelium. In human, it is 5-6 cells thick (70μm) and it is subdivided into three different layers: the squamous, the wing and the basal cells.

The squamous cells are located at the anterior part of the epithelium. They are flat, polygonal cells that provide the cornea with a smooth surface (Saude 1993). What is more, these cells are joined with desmosomes and tight junctions. The tight junctions between the squamous cells make this layer a semipermeable membrane that controls the para-intracellular movement of substances and excess fluid from the tear film. Desmosomes between the cells provide the layer with even more adhesion. The existence of tight junctions and desmosomes make the epithelium difficult to penetrate and this feature of the squamous cells' arrangement provides the cornea with protection against physical damage. Finally, the squamous cells have microvilli which attach to the tear film. These tiny projections keep the tear film in place.

The wing cells are flattened, polyhedral and they exist at the middle of the epithelium. In human cornea they are three layers thick and the cells are attached to each other with desmosomes and gap junctions. Wing cells are attached to the squamous cells and basal cells with desmosomes (Remington 1998).

The basal cells are one layer thick, located at the posterior surface of the epithelium and they are attached to each other via desmosomes and gap junctions. The basal cell layer is where mitosis of the epithelial cells takes place. After each mitotic division some of the basal cells differentiate to become middle and superficial cells (Azar 1997). Stem cells at the limbus are responsible for cell replacement and tissue regeneration. Basal cells have a completely different morphology from the cells of the squamous and wing layers since they have cubical or cylindrical forms with varying heights and rounded heads. The basal cells secrete the basement membrane that links the epithelium with the adjacent Bowman's layer below by hemidesmosomes (Young *et al.* 1994). Anchoring fibrils pass from these junctions through the Bowman's layer to plaques of the extracellular matrix of the stroma. Finally, interdigitations and desmosomes link the basal cells with the wing cells above (Saude 1993). Corneal epithelial stem cells are located in the basal epithelial layer of the limbus. These cells are highly proliferative and are responsible for corneal epithelial cell proliferation and differentiation (Stepp and Zieske 2005).

1.1.3 Bowman's layer

Bowman's layer is one of the acellular parts of the cornea and it is 8-14 μm thick. It originates from the mesenchymal cell processes of the superficial stroma during embryogenesis (Azar 1997). It consists mainly of randomly arranged collagen fibrils. Due to its acellular nature it is incapable of regenerating itself after injury. However, its existence seems not to be crucial for proper vision function since some mammalian species do not posses any Bowman's layer at all. Probably its existence in the cornea is correlated with providing the tissue with an extra layer and hence providing it with resistance to mechanical strength.

1.1.4 Stroma

The stroma (or *substantia propria*) is located at the middle of the cornea and it is the thickest layer (500 μm-90% of overall corneal thickness in human). It consists mainly of collagen lamellae, keratocytes and proteoglycans. The stroma is difficult to regenerate after injury and hence it is likely to develop opacities after disturbance.
Types I, III, V, VI, XII and XIV are the main collagens in the corneal stroma (Meek and Fullwood 2001). All collagen fibrils have a uniform diameter and regular spacing. This feature is essential for the maintenance of corneal transparency (section 1.2). Collagen fibrils in any one lamella run in a parallel direction whereas lamellae are at a certain angle to each other and parallel to the corneal surface. With the anterior stroma being an exemption, each lamella runs across the entire cornea, i.e. from limbus to limbus (Remington 1998).

Keratocytes are differentiated mesenchymal fibroblasts and they actively produce and secrete substances for the production, maintenance and repair of proteoglycans, collagen and keratocytes (Azar 1997, Green 2003). They are flattened cells. The morphology and the anatomy of keratocytes differ throughout the stroma and according to Poole *et al* (2003) the keratocytes of the corneal stroma in humans form three distinctive layers (Fig.1.2). The anterior layer is adjacent to the epithelium and Bowman's layer and it has a higher cell density than the bulk of the rest of the stroma. Keratocyte density tends to be the highest in the anterior 10% of the stroma (Patel *et al.* 2001). Additionally, although keratocytes in this layer have a poor lamellar organisation they form an extensive network of branching and interconnecting cell bodies. The central layer has the least keratocyte density and the cells have variable orientation. Finally, keratocytes in the posterior layer have

distinctive morphology and they are denser than the cells at the central layer. Keratocyte cell bodies are larger and are connected by small cell processes (Poole 2003).

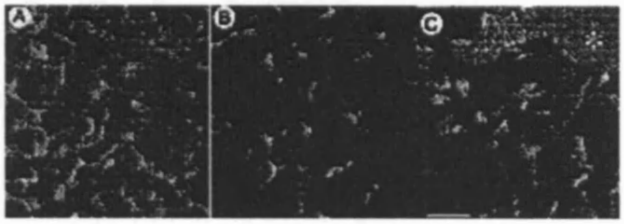

Figure 1.2: Anterior (A), Middle (B) and Posterior (C) stromal keratocytes of a 10-year old individual (Scale bar = 50 μm).

(Picture after Poole 2003)

The ground substance of the stroma is made up of proteoglycans (Fig. 1.3). These are macromolecules composed of a protein core and a carbohydrate glycosaminoglycan (GAG) side chain. GAG's are hydrophilic, negative charged molecules located at specific sites around each collagen fibril (Remington 1998). According to Zieske (2001) the corneal stroma contains two major classes of proteoglycans containing either keratan sulphate side chains or dermatan/chondroitin side chains. Lumican, keratocan and mimecan are the major keratan sulphate PG's, whereas decorin is the major dermatan/chondroitin PG (Fig. 1.3). Another heparan sulphate PG is heparin which exists in the basement membrane (Zieske 2001).

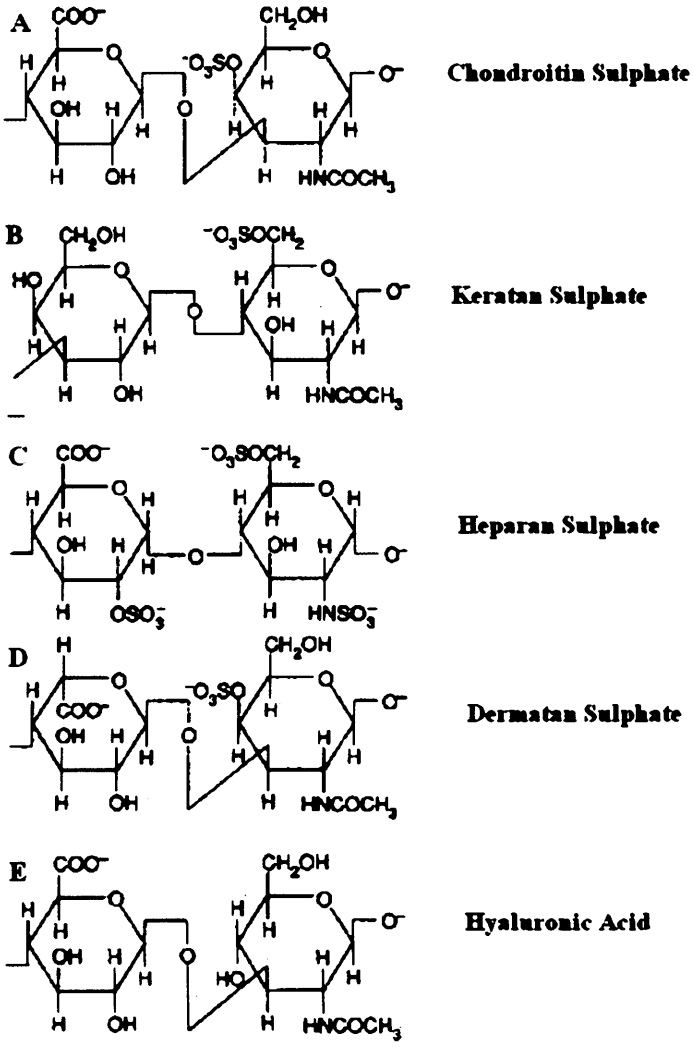

Figure 1.3: Proteoglycans present at the cornea

(Picture adapted from Zmuda-Trzebiatowska 1997)

1.1.5 Descemet's Membrane

Descemet's membrane is an acellular membrane that lies between the stroma and the endothelium. It is 8-10μm thick and consists of three layers. It is composed of type IV collagen, glycine and hydroxyproline (Azar 1997). Descemet's membrane is secreted by the endothelium, it is capable of regenerating itself after a disturbance, it has good antigenic properties and its thickness increases with age (Saude 1993).

1.1.6 Endothelium

The endothelium comprises a single layer of cells. These cells are flattened, hexagonal in shape with oval nuclei. Tight junctions join the cells, whereas intercellular communication is maintained by gap junctions. The main function of the endothelium is the maintenance of corneal hydration and it also allows the passage of ions, glucose, amino acids and water from the aqueous humour to the cornea. Glucose and amino acids diffuse into the cornea through a leaky barrier that is formed by the endothelial adhesions. Water and ions are actively transported by the endothelial pump. The Na^+/K^+-ATP pump system is the most important for water/ion exchange. Endothelial cells rarely divide and they decrease in number with age (Remington 1998). Cell loss is compensated by an increase in endothelial cell size (Azar 1997). In cases where the cell density falls below a critical minimum, corneal hydration increases causing loss of transparency and visual impairment.

1.2 Corneal transparency

Corneal transparency is an essential requirement for visual function to occur. It is mainly due to the collagen and proteoglycan organisation of the stroma. In order for corneal transparency to be established, stromal collagen fibrils need to have uniform spacing. Collagen spacing is mainly controlled by proteoglycans that fill the space between the fibrils. Therefore, the physical and chemical properties of proteoglycans play an important role in establishing and maintaining corneal transparency. In order for an object to be transparent it must fulfil two basic requirements (Meek 2002). Firstly, it must not absorb light. Although glycoproteins in the stromal ECM absorb light in the electromagnetic spectrum below 310nm vision is not affected. In fact the ultraviolet radiation is harmful for the tissues. In contrast, none of the components of the cornea absorbs light in the visible region of the spectrum. Secondly, a transparent object must not scatter light. According to (Freegard 1997) it is essential that as little light as possible should be scattered in the forward direction relative to that transmitted in order for a clear image to be formed. Several models have already been proposed in order to explain light scattering and corneal transparency. The simplest model introduced the theory of the uniform refractive index of all corneal components. It is assumed that spacing between particles is very much less than the wavelength of light and hence light cannot distinguish between the fibrils and the material between them. Therefore light passes

through the tissue without any scattering. In this case, the medium is considered to have a uniform refractive index different from unity. This has the effect of slowing down the light, but there is no scattering of light away in the forward direction. However, this is not the case since it has been shown that there is a small amount of scattering per particle (Maurice 1957). Other models introduced theories such as the perfect crystal or perturbed lattice arrangement of fibrils. The most realistic model was introduced by Hart and Farrell (1969) and proposes that only a short-range order in the packing of the collagen fibrils is required for the appropriate destructive interference of scattered photons to occur. There is disorder in the packing of collagen, but all fibrils are within a small range of distances from each other (Meek 2003).

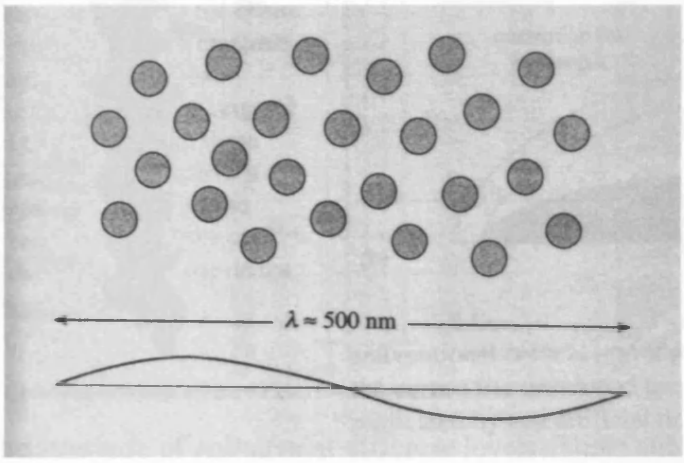

Figure 1.4: Collagen fibrils are within a small range of distances from each other (Picture after Maurice 1957).

1.2.1 Collagen structure and organisation within the cornea

The overall mechanical strength of a connective tissue depends on the interfibrillar interactions of collagen molecules and the interactions of collagen with proteoglycans and water (Cameron 2002). Collagen has a special amino acid composition. Its major feature is that one in every three amino acids is a glycine and it adopts a Gly-X-Y pattern, where usually X is a proline and Y a hydroxyproline. Consequently, collagen does not appear to have a typical α-helical or β-sheet conformation. The collagen helix has a left hand twist instead of the right handed one that is adopted by typical α-helical structures. This is due to the existence of hydroxyproline within the protein structure. This amino acid has a tendency of

inducing a left handed twist and because it appears in high frequency within the collagen structure it causes the whole helix to obtain a left handed twist. A collagen fibril consists of three parallel helices joined together with hydrogen bonds in a left handed twist (Fig. 1.5). According to Rainey and Goh (2002) collagen is either a homotripeptide or heterotripeptide with a repeating primary sequence of $(Gly\text{-}X\text{-}Z)_n$, displaying characteristic peptide backbone dihedral angles. Furthermore, glycine has the smallest side chain of all amino acids and this causes the three chains to pack together very tightly (Woodhead-Galloway 1980).

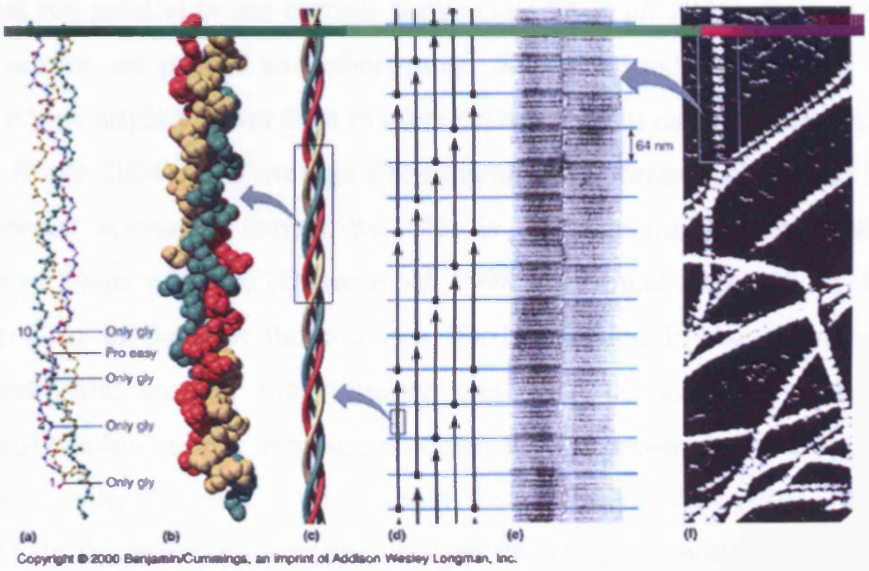

Figure 1.5: The structure of collagen at different levels. Three subunits of the α-helical protein (a) coil together to form a collagen fibre (b and c). In a collagen fibril (d) many fibres are stuck together and separated by 67nm from one another lengthwise. This feature produces the black and white patches in electron micrographs representing collagen fibres (e). Collagen fibrils form lamellae in tissues (f).
(Picture after http://wwwfac.mcdaniel.edu/Chemistry/CH3321JPGs/Proteins/Collagen.jpg 2003)

Collagen organisation within the stroma is essential for corneal transparency. Out of the 19 known collagen types, at least 10 of them are expressed in the adult mammalian cornea (i.e. Types I, III, IV, V, VI, VII, VIII, XII, XIII and XVII). Most collagen types are fibrillar, however types IV, VI and VII are nor fibril forming collagen types (Zieske 2001). Predominantly, types I (85%), III (10%) and V (5%) collagen are present in the human corneal stroma (Marshall 1991). All collagen types are classified into three superfamilies. Class 1 or banded fibrillar collagens and have the typical D-period fibril appearance. Types I, III and V which are predominantly

present at the cornea are Class 1 collagens. Class 2 are fibril associated collagens with interrupted triple helices (FACIT). Such collagen types do not form fibrils by them selves but interact with fibrillar collagens. Types XII and XIV are Class 2 collagens. Class 3 collagens have fibrillar structures, but they are not the same as Class 1 collagens. Type VI is a Class3 collagen (Meek and Fullwood 2001).

Collagen fibrils within the bovine cornea have a diameter of 36 nm approximately and are parallel to one another forming the lamellae. Each lamella is 1-2 μm thick. Central regions in the human corneal stroma consist of about 200 stacked lamellae that run parallel to the corneal surface (Boote *et al.* 2006). Collagen fibrils within the cornea are packed in a short-range order. The axial periodicity corneal collagen is 65nm, slightly lower than in other collagenous tissues (e.g. tendon, 67nm) (Meek and Boote 2004). The average fibril diameter of corneal collagen in humans remains constant across the cornea; its value is in the region of 31nm and it can increase up to 34nm with age (Daxer *et al.* 1998, Meek and Boote 2004). Corneal proteoglycans lie in between the collagen fibrils assisting in the maintenance of normal interfibrillar spacing and therefore preserving transparency at the tissue. Under normal conditions in a transparent cornea the intermolecular spacing between the consituent molecules of a fibril is about 1.8nm (Malik *et al.* 1992, Meek and Boote 2004). In the peripheral cornea, collagen fibrils have a wider spacing than in central parts (Boote 2006). This is mainly due to the existence of chondroitin sulphate, a large PG, at the periphery. The corneal stroma has a tendency to swell easily since hydrophilic PGs attract water molecules (Freegard 1997). If the collagen arrangement within the corneal stroma is disrupted, light scattering might occur and therefore the cornea will not be transparent any more.

1.2.2 Proteoglycan structure, localisation and its role in corneal transparency

It is widely accepted that the properties of the extracellular matrix are highly correlated with its structural characteristics (Berthiaume *et al.* 1996, Fitton *et al.* 1998, Ranucci *et al.* 2000, Wu *et al.* 2003). The Extracellular Matrix (ECM) plays a key role in the maintenance and function of connective tissue and consists predominantly of collagen, proteoglycans, glycosaminoglycans and other minor proteins (Hocking 1998).

Proteoglycans are macromolecules composed of a protein core and a carbohydrate glycosaminoglycan (GAG) side chain. GAG's are highly hydrophilic,

negatively charged molecules located at specific sites around each collagen fibril (Scott 1988) (Fig. 1.3). The core protein of a proteoglycan seems to be the most active part of the molecule and structurally it is a leucine zipper kind of protein that obtains a horse-shoe spatial arrangement. It interacts with the collagen fibrils and the extracellular matrix at specific sites. Consequently, they play an important role in corneal hydration. According to (Cintron 1989) the precise arrangement of PGs presumably reflects specific intermolecular interactions with collagens. Therefore, loss of PGs might cause alterations to the collagen organisation and hence to corneal transparency. For example, lumican, which is a keratan sulphate-containing proteoglycan, seems to play a key role in corneal transparency, since it is a key molecule in the neonatal development of the stromal matrix (Beecher *et al.* 2006) and it was also observed that mice homozygous for a null mutation in this molecule had opaque corneas (Chakravarti *et al.* 1998, Quantock *et al.* 2001).

1.2.3 Hydration of the cornea

It should be taken into consideration that abnormal hydration of the cornea might cause serious disturbances in visual function. Corneal hydration is defined as the weight of water in the cornea divided by the dry weight of the tissue. Under normal conditions corneal hydration is around 3.2 and the tissue remains transparent (Hodson *et al.* 1991).

$$\frac{Wet\_weight - Dry\_weight}{Dry\_weight}$$

Figure 1.6: Equation for cornea hydration. *Wet_weight* is the initial corneal weight. *Dry_weight* is the weight of the tissue after the whole water content is being removed.

The mechanism by which the cornea maintains its level of hydration is called *deturgescence.* This is very important for corneal transparency and in healthy corneas there should be a constant proportion between solids and water (i.e. 22% solids to 78% water) (Saude 1993). In cases where the endothelium is disturbed corneal hydration from the aqueous humour also becomes abnormal. Oedema or corneal swelling might appear, causing rearrangement of collagen fibrils in the stroma. The cornea becomes opaque and this might have severe implications in normal visual

function. The force which the tissue swells is called swelling pressure and it is inversibly related to the hydration of the tissue (Hedbys and Dohlman 1963).

1.3 Corneal shape defects

Refractive errors in the eye are usually corrected by the use of the appropriate visual aids (e.g. spectacles or contact lenses). However, there are cases where the use of visual aids is inadequate and the refractive surgery approach is then preferred. The use of refractive surgery is considered in cases where the refractive error is minimized and hence the patient is able to use no spectacles or much smaller ones for their convenience. Additionally, refractive surgery might also be applied to patients who wish to eliminate completely their refractive error for their careers or jobs requirements or even for vanity.

The refractive power of the eye is predominantly determined by three variables: the refractive power of the cornea, the power of the lens and the length of the eye globe. Myopia or "near sightedness" is the most common refractive error (25% for Caucasians and 13% for African Americans) (Azar 1997). This condition occurs when the cornea is too steeply curved or the eye globe is too long. In this case, the light that enters the eye is focused in front of the retina (Fig. 1.6A). Patients suffering from myopia are unable to see clearly objects that are at a long distance.

Hyperopia or "far sightedness" affects almost 40% of the adult population, but is much less visually significant than myopia. Patients suffering from hyperopia are incapable of seeing clearly objects that are at a near distance. The great majority of young hyperopes regard themselves to be optically "normal", but they may develop presbyopia and manifest hyperopia in their mid to late 30s (Azar 1997). In hyperopia light rays focus behind the retina (Fig. 1.6B) and the diffusion circles, which are formed result in a blurred and indistinctive image (Bores 2001). Hyperopia is a consequence of a too small eye globe or a too flattened cornea.

Almost 95% of the human population have some clinically detectable astigmatism. However, only a 3% - 15% has astigmatism greater than 2 diopters (Azar 1997). In this case, the radius of the curvature is not constant and the refractive powers varies across the cornea. People suffering from astigmatism have a blurred vision for objects situated in both near and long distance (Fig. 1.6C).

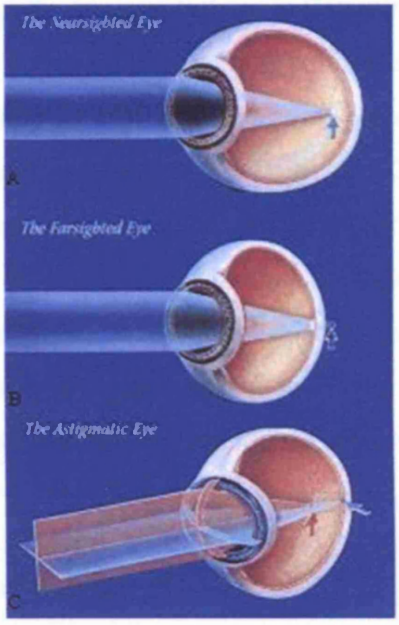

Figure 1.7: In myopia light rays focus in front of the retina (A). In hyperopia light rays focus behind the retina (B). In astigmatism light rays do not focus at any one point, rather an area, resulting in a blurred distorted image (C).

(Picture after www.northernvision.com 2003)

1.4 Refractive surgery

Refractive surgery has been widely used for the correction of corneal shape defects. Refractive surgery originally involved incisions from a blade (i.e. radial keratotomy) but with technological developments excimer lasers are now widely used in order to reshape the cornea and correct various degrees of myopia and astigmatism. The excimer laser is an argon-fluoride gas combination, which is capable of creating a high-power ultraviolet light beam. Laser pulses are usually 193nm and they break organic molecular bonds. They also remove the tissue in the area of application, causing very little thermal damage to the rest of the adjacent tissues (Singerman and Coscas 1992). A number of different laser refractive procedures have been developed; most common of which are radial keratotomy (RK), photorefractive keratectomy (PRK), laser *in situ* keratomileusis (LASIK) and laser epithelial keratomileusis (LASEK).

1.4.1 Radial keratotomy (RK)

In radial keratotomy, microscopic radial incisions are created in the cornea with the aid of an ultra-thin diamond scalpel. RK incisions weaken the outer cornea,

so that it bulges forward slightly as a result there is flattening of the central cornea and a decrease of its refractive power. Experimental studies confirm that the deeper the incisions the more the cornea is centrally flattened postoperatively (Grimmett and Holland 1996). RK is recommended for 1.50 up to 5.00 diopters of myopia. Its advantages include minimal postoperative recovery time, not considerable pain, relatively low cost and it does not involve damage to the central cornea. Disadvantages include permanent weakening of the cornea, endothelial damage, possible infection, high rate of reoperation (up to 30%), regression, hyperopic shift and, for some patients, occasional fluctuation of vision and sensitivity to glare (Chaudhry 1999).

1.4.2 Photorefractive keratectomy (PRK)

In PRK the excimer laser (193nm) sculpts the cornea into a flatter shape to correct vision in myopia. Each pulse of laser energy disrupts the molecular bonds of the cornea and removes 0.2-0.3μm of tissue. Most of the heat is dissipated into the air, and there is minimal thermal or radiation damage to the underlying tissue which remains structurally normal. The laser is programmed to remove more tissue centrally than peripherally for the correction of myopia. As a result, the central cornea is flattened and normal focus ability is obtained. Elliptical ablations are created for the correction of astigmatism. The laser beam quality and the frequency of the pulses administered are controlled by an algorithm (Fagerholm 2000).

PRK proved to be a more precise and a better technique than RK. PRK does not involve deep cuts into the cornea and therefore does not weaken the cornea (Chaudhry 1999).

PRK causes damage in the central cornea, includes considerable postoperative pain and longer recovery, due to the establishment of epithelial debridement after surgery (Shah 2001). Immediately after PRK the anterior part of the stroma is covered by a pseudomembrane (20-100nm thick). It is degraded by plasmin and MMPs within a few hours postoperatively (Corbett and Marshall 1996). In addition, disturbance of the corneal epithelium and Bowman's membrane may lead to an increase of the incidence of corneal haze and scarring. Another drawback is the risk of a decentred ablation, which can result in irregular astigmatism (Singerman and Coscas 1999).

1.4.3 Laser *in situ* keratomileusis (LASIK)

In LASIK an automated microkeratome creates a thin layer of corneal tissue (flap) that covers the area to be sculpted by the laser. This flap allows for rapid recovery of vision and reduces discomfort after surgery. The flap is left hinged at one side, is lifted and placed aside. Then a computer-controlled excimer laser sculpts the underlying cornea, correcting the refractive error. The flap is repositioned without sutures and is secure after a few minutes so that a patch is not required. Visual recovery is typically rapid, and there is little or no postoperative pain (Azar and Farah 1998). Additionally, LASIK is considered to be superior in efficacy and safety when compared to other popular refractive surgery procedures (Shortt *et al.* 2006).

The most important drawback of LASIK is that wound healing response is very poor and occurs only at the edge of the flap. A small increase in the expression of specific cytokines such as HGF and HGF-α is noted shortly after surgery at the flap edge. Proliferative cells of the epithelium release IL-1β, TGF-α and PDGF-BB, trigger keratocyte apoptosis in the stroma near the flap margins (Philipp 2003). ECM proteins such as fibrinogen and tenascin do not seem to appear after LASIK and hence the wound healing process depends only on the epithelial-stromal interaction. The strict localisation of fibrosis marginally at the flap edge, contrary to the minimal fibrosis below the entire flap, suggests that the LASIK interface never heals (Ivarsen 2003). Also there is a decrease in keratocyte numbers and this loss of cell numbers is reported to continue up to 3yrs after surgery (Erie *et al.* 2006). Additionally, epithelial ingrowth results in haze and focal stromal loss at the flap margin (Perez-Santonja 1998). After LASIK the cornea might be weakened, resulting in loss of its biomechanical stability. This causes postoperative keratoectasia and may have severe implications in visual function (Pallikaris *et al.* 2001). The incidence of ectasia after LASIK is not known precisely, but according to American Society of Cataract and Refractive Surgery (ASCRS 2003) has been estimated to be between 0.2-0.66% (Pallikaris *et al.* 2001). Ectasia can be defined as progressive non-inflammatory corneal thinning after surgery resulting in irregular topographic steepening and resultant irregular astigmatism (Chan and Boxer-Walcher 2006). However, it has been recently proposed that insights into the biomechanics and genetics of the cornea may help to further reduce the occurrence of corneal ectasia after LASIK (Rabinowitz 2006). In addition, recent studies suggest different approaches to

enhance the healing response of LASIK flaps and therefore increase the mechanical stability of the tissue. Kymionis *et al.* (2006) proposes that "Intacs" implantation can be an effective approach in preventing post-LASIK ectasia and Abdelkader *et al.* (2006) suggests that the addition of sutures in the corneal flap after LASIK appears to stimulate a stronger wound-healing response at the edge of the flap and therefore to improve the long-term stability of LASIK surgery in borderline thin corneas.

Late traumatic flap dislocations are rare but they have been reported in several cases (Melki 2000, Iskander 2001, Heickell 2004, Landau 2006). The limited peripheral wound healing response after LASIK is not usually enough to secure the flap and make it patent under mechanical or pressure stress (Crawford 2003). This is the reason why people who have had LASIK are disqualified from becoming pilots in combat aircraft jets in certain countries (Levy 2003). LASIK surgery may also induce epithelial defects to the cornea. Epithelial defects or erosion is seen in 1-3% of patients undergoing LASIK. This condition is mainly caused by the tangential shearing effect of friction caused by the movement of the microkeratome over the cornea. It should be taken into consideration that the epithelium in the superior cornea is hypoxic and hence more vulnerable. In rare cases the whole epithelium may slide as a sheet, denuding the whole flap. Patients who develop epithelial defects after LASIK are more susceptible to develop eye infections (Wilson 1998).

1.4.4 Laser epithelial keratomileusis (LASEK)

In this particular approach a thinner flap is created as the corneal epithelium is peeled off. In contrast with LASIK, a microkeratome is not used and the flap is created by chemical agents (i.e. alcohol). There are two basic types of LASEK flap: one with a superior hinge and the other nasal and temporal hinges. The epithelial basement membrane is delaminated using ethanol (18%) placed in an alcohol well for 30 seconds and then washed off with balanced salt solutions (Shah and Kumar 2003). The hinged flap is lifted back and an excimer laser corrects the defect. LASEK is used for the correction of myopia, astigmatism and hyperopia. It is a relative new technique and it is considered as an alternative to PRK because it causes less haze and postoperative pain and as an alternative to LASIK because there are no interface problems and there is less tissue to recover after surgery. However, according to

Litwak *et al.* (2002) LASEK did not result in faster visual rehabilitation than PRK in patients with low to moderate myopia. Indeed, LASIK proved to have a faster recovery time than LASEK.

1.5 Wound healing

Wound healing in general occurs in several different phases: acute inflammation, proliferative stage, angiogenesis and remodelling phase (epithelialisation) (Bale 2000). Blood loss (haemorrhage) after injury is eliminated through vasoconstriction and the coagulation cascades. The coagulation pathway results in the formation of a fibrin clot that seals the damaged blood vessels (Clark 1993). Platelets degranulate and release cytokines (i.e. PDGF, PGF, TGF-β, EGF and IGF) that stimulate various leucocytes. Blood supply increases at the wound site (inflammation). Polymorphonuclear cells and monocytes attack pathogens at the wound site. During the proliferative stage, fibroblast number increases and myofibroblasts appear. Growth factors such as TGF-β, PDGF and EGF regulate the stimulation or the inhibition of the fibroblasts. The action of myofibroblasts is regulated by an autocrine pathway (Bale 2000). Subsequently, epithelial cells migrate over the surface of the wound and restore the epithelial barrier. New vessel formation and subsequent vascular restoration also occur during this phase. Finally, during the remodelling phase cell numbers return to normal levels. Granulation tissue replaces the fibrin clot within the wound. Mature granulation tissue produces a scar, but at the end it is covered by a viable epidermal surface (Iocono 1998).

1.5.1 Corneal Wound Healing

Wound healing in all body parts follows a similar pattern with local variations. In the cornea because of the lack of a vascular system, the inflammatory stage of wound repair and granulation are usually minimal or non-existent. In general, upon injury corneal epithelial cells and activated stromal fibroblasts secrete growth factors and cytokines that have paracrine and autocrine functions (Lim *et al.* 2003). Corneal repair might last up to several weeks after injury and the wound healing response in the cornea can differ for the various refractive surgery approaches discussed in Section 1.4.

1.5.2 Epithelial Wound Healing

Corneal epithelia wound healing occurs in three stages: a) the latent phase, b) cell migration and adhesion and c) cell proliferation. The first phase occurs within 4 to 6 hours after wounding. PMNs are derived from the tear fluid and they remove the necrotic tissue. After epithelial debridement basal cells start flattening and separating (Lu *et al.* 2001). Hemidesmosomal attachments between the basal membrane and the basal cells disappear to approximately 70μm outward from the wound margin. The epithelium immediately adjacent to the wound exhibits lamellipodial and filopodial extensions. During cell migration and adhesion the extension of filopodia and lamellopodia is completed. Cell bodies become larger and they move forward. Finally, once the wound defect is completely covered hemidesmosomes are reformed (Steele 1999). During homeostasis and following injury to the corneal epithelium, the limbal stem cells divide to produce transient amplifying cells (TACs) that proliferate, migrate and differentiate into post mitotic cells (PMCs) and subsequently terminally differentiated cells (TDCs). The later ones replace lost cells in the wound area (Daniels and Khaw 2000).

Cytokines are also considered to have important roles in epithelial wound healing. The levels of IL-1 and IL-6 rise immediately after wounding and they initiate the cascade of epithelial wound healing events. IL-1 induces keratocyte growth Factor (KGF) and HGF expression in corneal fibroblasts, causing epithelial cell proliferation. KGF is a paracrine effector of corneal epithelial cells accelerating corneal epithelial cell growth (Wilson 1999). Cytokines such as the epidermal growth factor (EGF), KGF and HGF induce mitogenic activity and subsequent cell proliferation in corneal epithelial cells (Bansal and Veenashree 2001). In contrast, TGF-β1 and TGF-β2 inhibit and have no effect on epithelial cell proliferation, respectively (Carrington *et al.* 2006). The relationships between EGF, KGF, HGF and TGF-β are thought to be responsible for corneal epithelial wound healing (Baldwin and Marshall 2002). HGF was found to have a delaying and KGF an accelerating effect on epithelial cell proliferation. It was also proposed that HGF causes the formation of an abnormal epithelium but also causes extensive differentiation of keratocytes into myofibroblasts (Carrington and Boulton 2005).

1.5.3 Stromal wound healing

Shortly after wounding keratocytes undergo programmed death (i.e. apoptosis), phenotypic change and finally proliferation and migration (Helena 1998). These processes are stimulated by the presence of certain cytokines. Immediately after wounding keratocyte apoptosis occurs in areas below the epithelial wound. Apoptosis in the corneal stroma is triggered by IL-1α, the Fas-Fas ligand and bone morphogenic protein 2 and 4 (Wilson and Kim 1998, Lim *et al.* 2003). However, a week after surgery keratocyte number is elevated rapidly. These remaining keratocytes start to undergo fibroblastic transformation into myofibroblasts with resulting expansion of the fibroblast population by mitosis after approximately 48 to 72 hours, which reaches its peak between three to six days, whilst new connective tissue is synthesised (Mohan 2003). The new keratocytes are created by mitotic division of cells peripheral to the epithelial defect and they migrate into the wound. The activated fibroblasts under the influence of the TGF-β/CTGF system synthesise new extracellular matrix components (i.e. collagens, glycoproteins, proteoglycans) which form the scar tissue (Lim *et al.* 2003).

During wound healing chondroitin/dermatan sulphate levels increase significantly. Consequently, the newly synthesised collagen fibrils are larger in diameter than normal ones. This variation in collagen fibril diameter may cause disruption of corneal transparency and scarring. Initially, the extracellular matrix, which normally contains high levels of type IV collagen, laminin and proteoglycans (i.e. keratan sulphate, dermatan sulphate and heparan sulphate) is also disorganised (Ishizaki *et al.* 1994, Saika 1998). Stromal remodelling is thought to be controlled, in part at least, by various MMPs, e.g. collagenase, stromelysin and gelatinase. Removal of damaged collagen fibres is performed by polymorphonuclear leukocytes. After almost two years, the lamellar collagen pattern is almost back to normal dimensions but with shorter and narrower lamellae. The strength of corneal scars never reaches that of uninjured corneal tissue (Steele 1999).

1.5.4 Synopsis of corneal wound healing

Shortly upon epithelial/stromal injury epithelial cells are believed to release IL-1β towards the stroma. Stromal cells then release KGF that causes the stem cells in the limbal region to proliferate and differentiate into terminally differentiated

epithelial cells. Myofibroblasts at the wound site in the stroma release HGF that acts as a chemoattractant for the newly formed epithelial cells. This causes the epithelial cell migration towards the wound site in order for the defect to be covered. Shortly after the epithelial cell migration is completed, apoptosis of stromal cells occurs in the stroma. Finally the remaining quiescent keratocytes transform into myofibroblasts and the stromal wound repair process is initiated (Fig. 1.7).

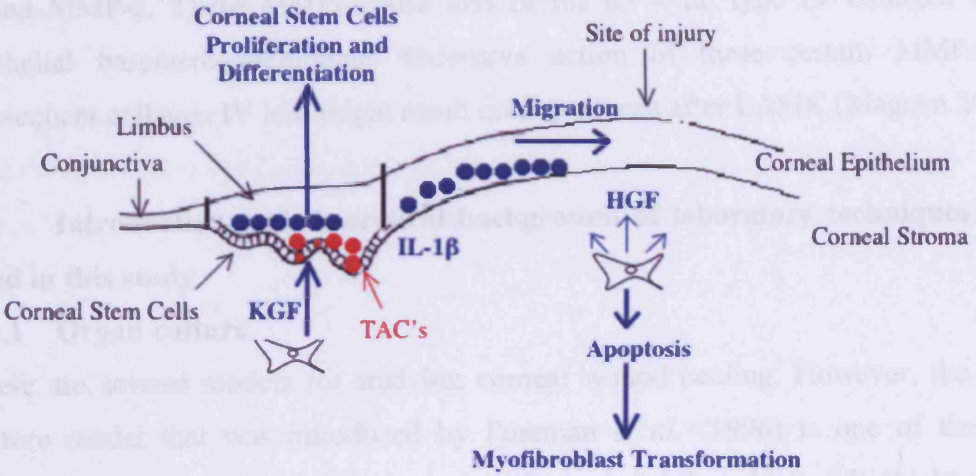

Figure 1.8: Overview of the corneal wound healing process.

1.5.5 Proteoglycan and matrix metalloproteinase alterations during the wound healing process

Several weeks after laser surgery regions of the ECM at the wounded area contain large amounts of unusually large sized proteoglycan molecules (i.e. chondroitin/ dermatan sulphate). Additionally, keratan sulphate appears to be transiently undersulphated, whereas chondroitin/ dermatan sulphate oversulphated. In case of LASIK these alterations in the proteoglycan molecules occur in response to the insult that occurred in the stroma (Quantock *et al.* 2003).

Dermatan sulphate proteoglycans are small leucine rich proteins (SLRPs) with an "arc" shaped spatial conformation and tend to form dimers. The amino-acid sequence of these proteins is characterised by long arrays of leucine-rich repeat motifs of about 24 amino acids in length (Jolles 1994). A feature that is of great interest about SLRPs is that they contain an amphipathic consensus sequence, with leucine as the predominant hydrophobic residue placed in conserved positions (Hocking 1998).

Right after LASIK there is a dramatic reduction of α3 – α6 type IV collagen chains in the epithelial basement membrane at the transected flap. This finding suggests that the LASIK flap acquires an early developmental character during remodelling, since this type of collagen is almost absent during human embryonic development. There are also great amounts of α1 – α3 type IV collagen present. These alterations in type IV collagen may be caused by the selective activity of selected MMPs. Fibrosed areas of the anterior stroma appear to have increased levels of MMP-1 and MMP-2. These MMPs cause loss of the α3 – α6 type IV collagen in the epithelial basement membrane. Extensive action of these certain MMPs and subsequent collagen IV loss might result on flap ectasia after LASIK (Maguen 2002).

1.6 Introduction and theoretical background of laboratory techniques to be used in this study

1.6.1 Organ culture

There are several models for studying corneal wound healing. However, the organ culture model that was introduced by Foreman *et al.* (1996) is one of the most representative. This is a simple air interface model in which full thickness re-epithelialisation of wounds occurs and it is possible to assess the role of growth factors in corneal wound healing (Fig. 1.8).

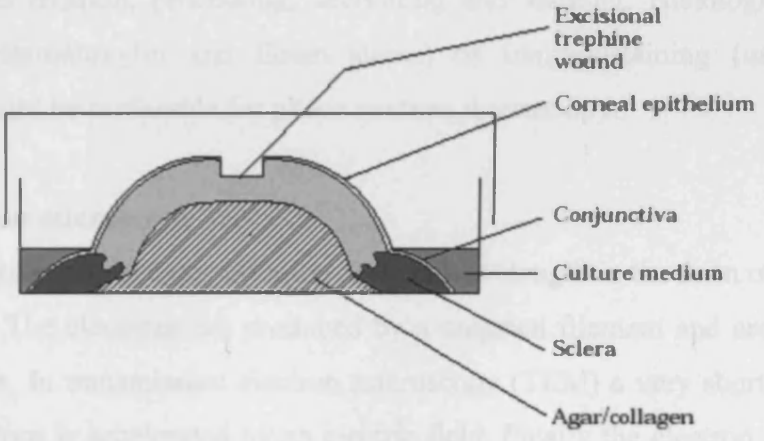

Figure 1.9: Diagram of the organ culture model.
(Picture after Foreman 1996)

This method has various advantages over other methods that have been used for studying wound healing. Firstly, it is less expensive than *in vivo* studies and also it

reduces using animal experiments. Secondly, it is more accurate and reliable than cell culture techniques since the whole organ is cultured and therefore various cell processes (i.e. wound healing) are mimicked more accurately. Finally, in submerged organ cultures, corneas appeared to have epithelial and stromal oedema and keratocyte deterioration (Foreman *et al.* 1996).

Many studies have used successfully corneal organ culture techniques to study the wound healing process (Foreman *et al.* 1996, Carrington and Boulton 2005, Carrington *et al.* 2006, Zhao *et al.* 2006). However, it must be taken into consideration that an in vitro system lacks certain factors essential for the wound healing process. Such parameters are the absence of any tear cytokines, nerve responses and intraocular pressure fluctuations in response to injury. However, the lack of these parameters has not been an issue in previous *in vitro* corneal wound healing studies.

1.6.2 Light microscopy

In light microscopy visible light and lenses are used to magnify the specimens. Light microscopes can magnify up to 1500 times and have a resolution limit of about 0.2μm. There are six different types of light microscopy: dark field illumination, fluorescence microscopy, phase contrast, nomarski or differential interference contrast, polarised light microscopy and confocal (Reed 1998). Preparation of the tissue involves fixation, processing, sectioning and staining. Histological Staining (e.g. using Haematoxylin and Eosin stains) or immunostaining (using various antibodies) might be preferable for phase contrast microscopy.

1.6.3 Electron microscopy

In electron microscopy radiation at short wavelength in the form of an electron beam is used. The electrons are produced by a tungsten filament and are focused by electromagnets. In transmission electron microscopy (TEM) a very short wavelength beam of electrons is accelerated by an electric field. Finally the electron beam passes through the specimen. Then the image is formed on a fluorescent screen. A transmission electron microscope magnifies up to 200 000 times and has a resolution limit of 1nm for biological specimens. It principally uses a fine electron beam, which is subsequently reflected from a metal-coated specimen surface. The secondary electrons that are generated from the specimen-surface impact are collected by a

scintillation crystal that converts each electron impact into a flash of light. Each flash of light generated inside the crystal is then amplified by a photomultiplier and used to build up an image on a fluorescent screen. In histology, chemical agents called histological stains are applied to specimens in order to increase contrast and hence the resolution. Heavy metals are used for specimens for electron microscopy. In TEM contrast is enhanced by incorporating heavy metal salts into the specimens. In this case electron absorption is increased. Immunogold staining is preferred because gold is an electron dense element and more particularly, the use of antibodies allows specific molecules to be stained (Wilson and Walker 1997).

In TEM the tissue undergoes a fixation and embedding procedure. The tissue is initially submerged in a fixative solution (e.g. paraformaldehyde or glutaraldehyde). These solutions cross-link different protein groups within the tissue and preserve the structures. The second step of this procedure involves the staining of the tissue with certain heavy metals, in order for further electron contrast to be achieved. Cuprolinic Blue is extensively used for proteoglycan localisation experiments. This chemical complexes with negatively charged GAGs and it is later enhanced by the addition of tungstate groups (Scott and Stockwell 1967). Then the dehydration and infiltration step follows. In this case, the embedding medium replaces the water content of the tissue. Embedding media are water insoluble solutions. Epoxy resin is an embedding medium and provides support to the tissue when it finally stabilises (polymerises). Once the tissue has been embedded then ultrathin sections (less than 600Å or 70-100 nm) are obtained by using an ultramicrotome. Finally, the section undergoes further staining with a heavy metal salt solution (e.g. OsO_4). This step is carried out in order to enhance contrast under the EM (Meek 1981).

1.6.4 X-ray diffraction

X-rays are electromagnetic radiation with typical photon energies in the range of 100 eV-100 keV. For diffraction experiments short wavelength x-rays (i.e. 1-120 keV) are produced by either x-ray tubes or synchroton radiation.

In the current project synchroton x-ray radiation was used in order to map corneal collagens. Synchroton radiation is emitted by electrons or positrons travelling at close to the speed of light in a circular storage ring. The electron beam hits the tissue and the scattering pattern is related to the structural properties of the tissue. However, precise information about the structural properties of macromolecules

cannot be obtained directly from x-rays, as there are no lenses to bend and focus the scattered x-rays. X-ray images have to further be reconstructed using computer analysis in order to obtain structural information of the scanned tissue (Hendrickson 1986).

X-rays scatter through differing angles when they interact with biological tissues (Fig.: 1.10). Different levels of interference occur as a result and they are dependent on the degree of order in the structure. Perfect or near perfect order will produce true diffraction maxima. Less ordered structures would produce more diffuse interference maxima (i.e. x-ray reflections), which are being produced by the existence of many fibres. The series of reflections arising from a given periodic structure is numbered consequently from the centre of the pattern outward (Meek and Quantock 2001).

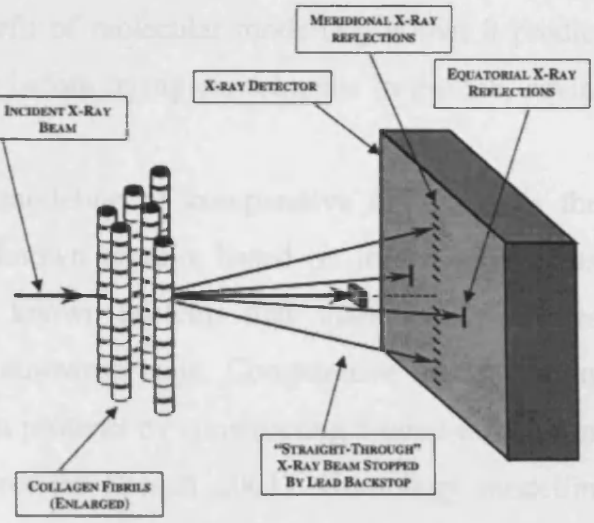

Figure 1.10: Visual representation of the x-ray diffraction technique. A bundle of vertically arranged collagen fibrils produce meridional x-ray reflections, which are parallel to the fibril axes and equatorial reflections and are perpendicular to the fibril axes (Meek and Quantock 2001)

X-ray scattering has been established as a very powerful experimental research tool for examining corneal ultrastucture (Meek and Quantock 2001, Boote *et al.* 2005). The X-ray diffraction technique for generally measuring the interfibrillar spacing and diameter is proven to be more accurate than known TEM techniques. TEM is a time consuming, complex procedure and the whole processing and sample preparation compromises the physical state of the tissue. Consequently, electron

micrographs underestimate the centre-to-centre distance of collagen fibrils (Fullwood and Meek 1993, Meek and Boote 2004). On the other hand x-ray diffraction techniques are less invasive to the tissue and with the improvement of technology is an effective technique that helps in the physical preservation of the tissue during data collection.

1.6.5 Molecular modelling

Molecular modelling is the computer aided prediction of the structure of behaviour of molecules. It is a fast growing and powerful technique that is used in the fields of computational chemistry (i.e. chemoinformatics), biology (i.e. bioinformatics) and materials science for the study of a range of small molecular structures to larger macromolecules and material assemblies. The use of computers and knowledge of programming is essential for molecular modeling methods. The benefit of molecular modelling is that it predicts the behaviour of molecular systems before trying experiments in the lab, saving time, money and effort in research.

Homology modeling or comparative modelling is the prediction of the structure of an unknown protein, based on information of its sequence and the structure of other known proteins that share similar sequence and functional aspects with the unknown protein. Comparative modelling exploits the structural similarities between proteins by constructing a three-dimensional structures of one or more related proteins (Leach 2001). Homology modelling is based on the simple principle that proteins with similar sequence tend to have similar three-dimensional structures (Chothia and Lesk 1986).

1.7 Aims and objectives

This project was based on the simple hypothesis that wound healing in the cornea is incomplete after LASIK surgery. The main aim was then set to identify why corneal wound healing is incomplete after LASIK. The objectives that were set in order to achieve this aim, were to develop an *in vitro* model for studying wound healing after LASIK, identify and test factors that affect wound healing, assess wound healing using histological analysis, mechanical strength testing and transparency

assessment. Finally, ultrastructural analysis was carried out by means of x-ray diffraction, transmission electron microscopy and molecular modelling.

2. Method development for microscopy laboratory techniques

2.1 Organ Culture

Bovine eye globes were obtained from the Ciderford abattoir and transported to the laboratory on ice. Healthy eyes with clear/transparent corneas were processed for organ culture as previously described by Foreman *et al.* (1996) within the same day of slaughter. Initially excess tissue was removed from the exterior of the eyes. The cleared eye globes were submerged in 25% (v/v with PBS) Betadine solution for 3-5min to decontaminate the exterior of the eye globes and then washed with sterile PBS solution. The eyes were then dissected using a surgical blade and their corneas were isolated. Two different groups of corneas were cultured. Half of them were wounded (either trephined or in a LASIK-like manner) and half of them were unwounded and acted as controls. For trephine wounded corneas, a 5mm trephine was used. The wound extended half-way through the stroma and upon wounding the 5mm disc was excised. Trephine wounding was used in this project as a methodological development as well as a correlation to LASIK-like flaps. For LASIK-like incisions a custom made devise that was developed locally was used to create a stromal flap ranging 180-250nm in thickness. After the induction of the wounds the eyes were dissected, the corneas removed and the rest of the eye globe discarded. The posterior endothelial cavity of each cornea was filled with an agar-gelatin support gel (appendix III). As soon as the gel had set at RT the corneas were inverted and placed in a 60mm tissue culture dish (Fig. 2.1). Serum-free Trowells T8 medium containing antibiotics and fungizone (see appendix III) was placed into the dishes up to the limbal area to preserve the corneas during the culture period. The medium was replaced every four days during the culture period. 200μl of medium was dripped at certain times on the corneal surface twice every 24hrs throughout the duration of the experiment, in order to prevent the corneal surface from drying out.

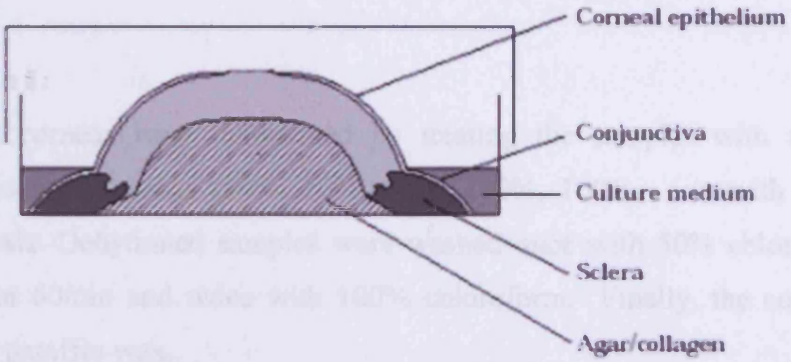

Figure 2.1: Diagram of the organ culture model.
(Picture after Foreman *et al.* 1996)

2.2 Light Microscopy

2.2.1 Preparation of Frozen Sections

Corneas (n=16) were removed from the culture at different time-points (0, 1, 3, 7, 14, 21 and 28 days) and they were bisected. Each half was placed in a foil mould, which was filled with Tissue-Tek OCT compound. The foil container was placed in pre-cooled iso-pentane solution and then placed in liquid nitrogen until the whole block had frozen. Frozen blocks were kept at -20°C.

Frozen blocks were trimmed and 7µm-thick sections were obtained using a cryostat (Fig.2.2). The sections were then transferred to SuperFrost Plus microscope slides and allowed to air-dry for 1-4hrs at RT. The slides were submerged in ice-cold methanol for 5min and then left on the bench to air-dry for 10min. Finally the slides were wrapped in aluminium foil and kept at -20°C until further processing.

Figure 2.2: The Cryostat (Leica, UK)

2.2.2 Preparation of wax sections and method development

Corneas (n=16) were removed from the culture at different time-points (0, 1, 3, 7, 14, 21 and 28 days) and they were fixed in 10% Neutral Buffered Formalin (NBF).

Approach No 1:

Fixed corneas were dehydrated by treating the samples with a series of increasing alcohol dilutions (50%, 70%, 90%, 100%, 100% - v/v with ddH_2O) at 60min intervals. Dehydrated samples were washed once with 50% chloroform (v/v with IMS) for 60min and twice with 100% chloroform. Finally, the corneas were embedded in paraffin wax.

Final protocol:

Steps were repeated as described above but changing two parameters:

1. The tissue was fixed in 10% NBF and processed within 48hrs.
2. Incubation times were eliminated to 30min instead of 60min.

Wax blocks were trimmed and 7μm-thick sections were obtained by using a microtome (Fig. 2.3). The sections were then placed in a water bath (almost 45 °C) and they were allowed to flatten. Finally, the sections were collected from the water bath by floating on to Histobond slides. The slides were allowed to dry overnight in a 56°C oven.

Figure 2.3: The Microtome (leica, UK)

2.2.3 Haematoxylin and Eosin Staining

Wax sections were passed through a series of xylene and alcohol solutions in order to dewax and rehydrate the sections. Initially, the slides were submerged twice in xylene solutions (5min each). Then the sections were passed through a decreasing series of alcohol dilutions (100%, 90%, 70%, 50% - 1min each). The slides were then washed briefly in tap water to remove excess alcohol. The sections were stained with filtered Harris' Haematoxylin for 3min and washed under tap water. Subsequently, the sections were counterstained with Eosin for 1min. The slides were then washed with water very briefly and then passed through an increasing series of alcohol. Finally, the slides were immersed in xylene for 1min and then the sections were mounted with coverslips using Xylene-Mounting medium.

Frozen sections were removed from -20°C and they were let to cool down wrapped at aluminium foil at RT for 30min. Then they were counterstained with Haematoxylin and Eosin. Finally, the sections were mounted by using Hydromount.

2.2.4 Cytokeratin 3 and PAN cytokeratin immunostaining and method development

Several approaches were followed in order to optimise the protocol for immunohistochemistry. In all cases negative control samples were used. Negative controls were not treated with primary antibody.

Approach No 1:

7μm frozen sections were fixed in acetone for 10min and left on bench to air dry for another 5min. Sections were incubated with 0.6% hydrogen peroxide in Methanol for 5min. The slides were subsequently treated with 0.1mg/ml Trypsin containing solution for 30min at 37 °C. Then, the slides were treated with 0.1% (v/v) Triton x100 for 30min at 37°C. The slides were incubated with 20% goat serum for 20min at RT. The serum was tapped off the slides and cytokeratin (ICN Biomedicals) primary Ab (1/100) was applied to slides for 60min at RT. The slides were incubated with goat mouse-IgG biotinylated secondary Ab (1/50) for 1hr at RT and then the staining was developed with diaminobenzidine (DAB). Between each step three PBS washes were taking place. The sections were dehydrated and mounted using Xylene-Mounting medium (DPX) and the slides were kept at RT.

Approach No 2:

Same as above, but frozen sections were left on bench to air dry for 1-4hrs before fixing in acetone and two different dilutions of cytokeratin primary Ab was used (i.e. 1/100 and 1/200). Additionally, PBS washes were performed on the slides and wash time was extended to 10minutes each wash, in order to eliminate hassle to the tissue and avoid epithelium detachment from the underlying stroma.

Approach No 3:

Same as above but slides were left on bench to airdry overnight before the acetone fixation and PAN cytokeratin (1/25, 1/50, 1/100) as well as cytokeratin 3 (1/100) were used as a primary Abs.

Approach No 4:

7μm frozen sections left on bench to air-dry overnight and fixed with acetone as described before. Endogenous peroxidase activity was blocked by treating the slides with 0.6% hydrogen peroxide for 5min. Sections were washed briefly with ddH_2O and washed with PBS (DAKO, pH 7) on the slide for 10min. 20% goat serum was applied to the sections for 20min. The serum was subsequently tapped off the slides and PAN Cytokeratin primary Ab (1/25, 1/50, 1/100) was applied overnight at 4°C. The slides were then incubated with AlexaFluor® goat mouse-IgG at 1/1000 dilution for 2hrs in the dark at RT. The sections were mounted using Hydromount. The slides were then wrapped in aluminium foil, left at 4°C O/N or at -20°C for a longer period. Between each step three PBS washes were taking place.

Approach No 5:

Same as above, but slides were incubated with 10 mg/ml Proteinase K buffer for 20min at 37°C.

Approach No 6-Final optimised protocol:

7μm wax sections were wax cleared and rehydrated. Sections were incubated with 3% hydrogen peroxide in ddH_2O for 5min in order to block endogenous peroxidase activity within the tissue. The slides were subsequently treated with 0.1mg/ml Trypsin containing solution for 30min at 37°C. Then, the slides were treated with 0.1% (v/v) Triton x100 for 30min at 37°C in order to achieve further antigen retrieval. The slides were incubated with 20% goat serum for 20min at RT. The serum was tapped off the slides and cytokeratin (ICN Biomedicals) primary Ab (1/100) was applied to slides for 60min at RT. The slides were incubated with goat mouse-IgG

biotinylated secondary Ab (1/50) for 1hr at RT and then the staining was developed with diaminobenzidine (DAB). Between each step three PBS washes were taking place. The sections were dehydrated and mounted using Xylene-Mounting medium (DPX) and the slides were kept at RT.

2.2.5 α-smooth muscle actin immunostaining and method development

Approach No 1:

Monoclonal α-smooth muscle actin antibody was purchased from Sigma (A 2547). Initially 7μm frozen sections were used. Sections were left on bench overnight in order to achieve better adhesion of the tissue onto the SuperFrost slides. All slides were then fixed in cold acetone for 10min and subsequently were left on bench to air dry for another 10min. Half of the slides that would be stained with peroxidase were treated with 0.6% Hydrogen Peroxide in methanol for 5min in order to avoid background staining caused by any peroxidase activity within the tissue. Meanwhile, the rest of the slides that would be treated with AlexaFluor secondary were kept in PBS. Although 1/400 dilution (i.e. 5μg/ml) of the primary Ab was suggested as optimum by sigma 1/200 was used as well. All slides were incubated with the primary Ab at 4°C overnight. Negative control slides were treated with 25% goat serum. For the peroxidase staining the slides were incubated with goat mouse-IgG biotinylated at 1/50 dilution for 1hr at RT and then the staining was developed with diaminobenzidine (DAB). The sections were mounted using Xylene-Mounting medium (DPX) and the slides were kept at RT. For the fluorescent staining the slides were incubated with AlexaFluor® 488 goat mouse-IgG at 1/1000 dilution for 2hrs in the dark at RT. The sections were mounted using Hydromount. The slides were then wrapped in aluminium foil, left at 4°C O/N or at -20°C for a longer period. Between each step three PBS washes were taking place.

Approach No 2:

7μm wax sections were wax cleared and dehydrated as previously described. Slides were divided in two groups and subsequently in four subgroups (Table 2.1). Half of the slides were treated with 0.1mg/ml Trypsin containing solution for 35min at 37°C and the remaining half of the slides were treated with 20μg/ml Proteinase K containing solution for 35min at 37°C.

Subgroup	Approach
A	Block with 20% Goat serum in PBS for 20 min
B	0.2% BSA in PBS used for Ab dilutions
C	0.05% Tween 20 in PBS for Ab dilutions & washes
D	Plain PBS

Table 2.1: Solutions that used for the four different subgroups of slides.

The slides were then treated with primary Ab (1/200) at 4°C overnight. Negative control slides were treated with 25% goat serum in plain PBS. The following day were incubated with AlexaFluor® 488 goat mouse-IgG at 1/1000 dilution for 2hrs in the dark at RT. The sections were mounted using Hydromount. The slides were then wrapped in aluminium foil, left at 4°C O/N or at -20°C for a longer period. Between each step three PBS washes were taking place.

Approach No 3:

7μm wax sections were wax cleared and dehydrated as previously described. The slides were treated with 20μg/ml Proteinase K containing solution for 20min at 37°C and washed with PBS. All sections were incubated with 20% goat serum for 20min at RT. Goat serum was tapped off the slides and primary Ab dilutions were applied. Half of the slides were treated with primary Ab (1/200 or 1/400) diluted in 0.05% Tween 20, 0.2% BSA, PBS. The other half of the slides were treated with primary Ab (1/200 or 1/400) diluted in 0.05% Tween 20, PBS. Primary Ab incubation was left overnight at 4°C. Negative control slides were treated with 25% goat serum in plain PBS. The following day sections were incubated with AlexaFluor® 488 goat mouse-IgG (1/1000) diluted in either 0.05% Tween 20, 0.2% BSA, PBS or 0.05% Tween 20, PBS for 2hrs in the dark at RT. The sections were mounted using Hydromount. The slides were then wrapped in aluminium foil, left at 4°C O/N or at -20°C for a longer period. Between each step three 0.05% Tween 20, 0.2% BSA, PBS or 0.05% Tween 20, PBS washes were taking place.

Approach No 4-Final optimised protocol:

7 μm wax sections were wax cleared and dehydrated. Sections were incubated with 20%goat serum for 20min at RT. Goat serum was tapped off the slides and primary Ab dilutions were applied. The slides were treated with primary Ab (1/400 or

1/800) diluted in 0.05% Tween 20, 0.2% BSA, PBS at 4°C overnight. The following day sections were incubated with AlexaFluor® 488 goat mouse-IgG (1/1000) diluted in 0.05% Tween 20, 0.2% BSA for 2hrs in the dark at RT. The sections were mounted using Hydromount. The slides were then wrapped in aluminium foil, left at 4°C O/N or at -20°C for a longer period. Between each step three 0.05% Tween 20, 0.2% BSA, PBS washes were taking place.

2.3 Transmission Electron Microscopy (TEM)

2.3.1 Cuprolinic Blue fixation in a critical electrolyte condition

Approach No 1:

Sixteen corneas from the organ culture were fixed with 4% PFA and they stored at 4°C. The tissue was cut into 25mm^2 cubes and the samples washed with PBS and treated with 0.05% Cuprolinic Blue buffer overnight at RT. The tissue was then washed with three changes of 2.5 % glutaraldehyde solution for 15min. Subsequently, the samples were incubated with three changes of both 0.5% sodium tunsgate buffer for 15min and with 0.5% sodium tunsgate in 50% ethanol for 15min. The tissue then was dehydrated by passing it through of a series of increasing alcohol concentrations (50%, 70%, 90%, 100%, 100%, 100% v/v with ddH_2O– 15min each). The samples were incubated with 1:1, 2:1, 3:1 Resin:Ethanol solutions for 1hr with each resin dilution. Then, the samples were incubated with 100% resin for 8hrs for three times. Finally, the tissue was placed in small container and incubated with 100% resin in a 70 °C oven for 8hr.

Approach No 2- Final optimised protocol:

Sixteen corneas from the organ culture were fixed with 4% PFA and they stored at 4°C. The tissue was cut into 25mm^2 cubes and the samples washed with PBS and treated with 0.05% Cuprolinic Blue buffer for almost 24hrs at RT. The tissue blocks then were washed with three 15min washes of 2.5 % glutaraldehyde. Subsequently, the samples were incubated with three changes of both 0.5% sodium tunsgate buffer for 15min and with 0.5% sodium tunsgate in 50% ethanol for 15 min. The tissue then was dehydrated by passing it through a series of a series of increasing alcohol concentrations (50%, 70%, 90%, 100%, 100%, 100% v/v with ddH_2O– 15min each). The tissue was then incubated with propylene oxide for 15min twice. The samples were subsequently incubated with 1:1 medium Epon Resin: Propylene Oxide solution for 1hr. Tissue blocks were then incubated with pure medium Epon Resin for

1hr, twice. At this point, the lids of the vials were removed in order to allow any remaining propylene oxide to evaporate from within the tissue. The tissue was incubated with fresh 100% medium Epon Resin overnight at RT. The next day the tissue was incubated in 100% medium Epon Resin for 6hrs. The resin was renewed twice during the 6hr period. At the end of the six-hour resin incubation the tissue was placed in small container and incubated with 100% medium epon resin in a 60°C oven for 48 hrs.

2.3.2 Sectioning

Sections of 80nm thickness were obtained by using a Reichert-jung Ultracut E Ultramicrotome. The sections were placed on a 3mm copper grid and allowed to air dry.

2.3.3 Staining of ultrathin sections

2.3.3.1 Uranyl Acetate (UA) / Lead Citrate Staining

The grids were placed face down on a drop of 2% Uranyl Acetate (UA) for 15min. Then, each grid was passed over 5 drops ddH_2O in order for the sections to be washed. They were blotted on filter paper in order to remove excess water. The grid was then placed on 2% lead citrate for 10min. Finally, the sections were washed five times with distilled H_2O.

2.3.3.2 Uranyl Acetate (UA) / PTA Staining

UA and PTA containing vials were centrifuged at 14,000 for 5min at RT. Meanwhile, two sheets of filter paper were placed on the bench and soaked with ddH_2O. Parafilm pieces were placed on the filter papers. Copper grids were placed on top of 1% PTA solution drops and left to stand at RT for 10min. Sections were washed with five 3min washes of filtered ddH_2O. Sufficient amount of ddH_2O was applied in a Petri dish until the surface of the dish was covered. A piece of paraffin was placed into the Petri dish and the grids were placed on drops of UA. The Petri dish was transferred in a 45°C oven and the tissue was incubated with the UA for 1hr. Finally, the sections were washed five times with distilled H_2O as described before.

2.3.4 Observing the samples under a TEM

The samples were observed under a JEOL 1010 transmission electron microscope (TEM) at 80kV. The images of the corneal stroma were taken at various magnifications. Electron micrographs were obtained using a Kodak Megaplus 3.0 digital camera, which was attached to the electron microscope.

3. Morphological and cellular assessment of LASIK-like injured corneas

3.1 Introduction

Trephine injured corneas were used as a preliminary to the study of the wound healing response in LASIK-like injured corneas. The extent and the severity of the wound healing response in the cornea depend on the cause of injury. A surgical trephine causes a circular wound that can either extend half way or all the way through the cornea. Once the trephined corneal disc is removed a severe injury is induced in the cornea and an intense wound healing response is caused. However, LASIK-like injuries are not so severe and therefore wound healing response events tend to be milder.

In order to understand the cellular behaviour in trephined and LASIK-like injured corneas the expression of various intracellular proteins within the tissue was monitored. Such proteins include the cytokeratins (CKs) and α-smooth muscle actin (αSMA). Both types of proteins are part of the cytoskeleton, serving different functions to the cells that express them.

Cytokeratins are intermediate filaments. The principal function of the intermediate filaments is to reinforce cells by distributing tensile powers. Cytokeratin (CK) nos. 3, 5 and 12 are the most abundant ones in the adult cornea and they are expressed uniformly all over the tissue. CK 12 forms a heterodimer with CK3 in the cornea, whereas CK5 forms homodimers. CKs 4, 14, 15 and 19 are also present in minor amounts. Additionally, CK 4 is expressed only in the upper corneal epithelial cells from about the third layer upwards and CK 19 expression is restricted to the peripheral regions of the corneal epithelium (Kasper *et al.* 1988).

Actin filaments are 8nm wide and they are thinner and more flexible that other cytoskeleton components and therefore this type of filaments is a characteristic of highly motile cells (Alberts 1994). In the cornea myofibroblasts occur after the transformation of corneal keratocytes (Mohan 2003) after wounding and they express α-smooth muscle actin (αSMA). The main role of myofibroblasts in the wound healing process is to modify the composition of the extracellular matrix, by producing new components and subsequent scaring and wound contraction (Wilson 1998).

In the current study the cellular expression in both the corneal epithelium and stroma was monitored. Epithelial cell response is immediate after injury (Wilson 1999) whereas the stromal wound healing process is slower and occurs when the epithelial one is upon completion (Mohan 2003). In the current study a major part of

the immunohistochemical analysis focused on the LASIK-like injured corneas only because similar experiments have already been performed extensively in the past in trephine wounded bovine corneas (Carrington and Boulton 2005, Carrington *et al.* 2006). Stromal wound healing response is impaired in LASIK (Pallikaris *et al.* 2001, Ivarsen and Moller-Pedersen 2003, Phillip *et al.* 2003) and therefore a significant part of this study was focused on the expression and cell population variation of stromal cells. The aim of this study was to gain a better understanding of both the epithelial and stromal wound healing response in the cornea after LASIK-like incisions.

3.2 Experimental design

3.2.1 Organ Culture

Bovine corneas were organ cultured as detailed in section 2.3.1.

Trephine wounded corneas

Figure 3.1: Control (A) and Wounded (B) bovine corneal samples in organ culture for 24hrs (20x)

Two different groups of corneas (n=32) were cultured. Sixteen were centrally wounded with a 5mm biopsy punch and sixteen were unwounded and acted as controls (Fig. 3.1 and 3.2). The depth of the trephine wound was extending half way through the corneal stroma. The trephined disc was excised using a surgical blade and the corneas were cultured for 0, 1, 3, and 7 days. At the end of each culture period control and wounded corneas were cut in half and processed into wax. During the organ culture the eyes were observed under a microscope in order to monitor the progress and the quality of the culture. The progress of the wound healing was monitored under the microscope, as was the occasional presence of contaminating micro-organisms.

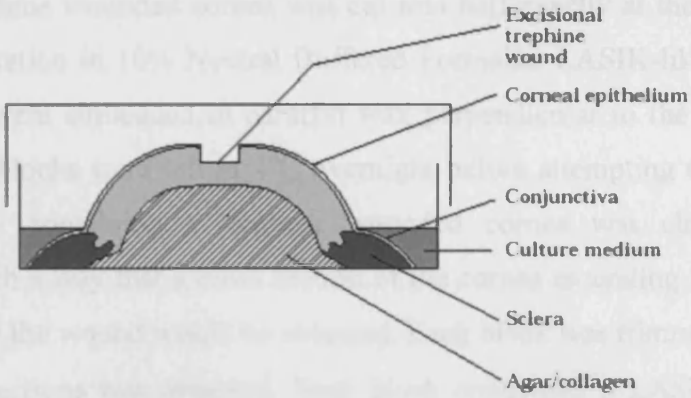

Figure 3.2: Diagram representing a trephine wounded cornea in organ culture (Picture taken from Foreman *et al.* 1996)

LASIK-like injured corneas

Two different groups of corneas (n=48) were cultured. Twenty four were wounded in a LASIK-like fashion using the custom made eye holder (section 2.2.2). Twenty four corneas were unwounded and acted as controls (Fig. 3.3). The corneas were cultured for 0, 1 and 3 days, 1, 2, 3, 4 weeks. At the end of each culture period three control and three wounded corneas were fixed in 10% neutral buffered formalin and wax embedded. Control corneas were cut into halves before fixation, whereas LASIK-like corneas were trimmed close to the flap area before fixation.

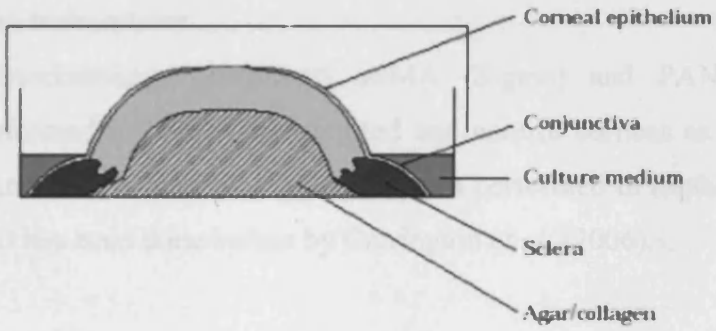

Figure 3.3: The organ culture set up representing a control/uninjured cornea (Picture adapted from Foreman *et al.* 1996)

3.2.2 Wax embedding and tissue sectioning

Each trephine wounded cornea was cut into half exactly at the middle of the wound before fixation in 10% Neutral Buffered Formalin. LASIK-like and trephine injured corneas were embedded in paraffin wax perpendicular to the surface of the wax pot. Tissue blocks were left in 4°C overnight before attempting to cut sections. Each wax block containing a trephine wounded cornea was clamped on the microtome in such a way that a cross section of the cornea extending from limbus to limbus, including the wound would be obtained. Each block was trimmed and a series of 10μm thick sections was obtained. Each block containing a LASIK-like injured cornea was then clamped on the microtome in such a way that a cross section would be obtained, cutting from the flap hinge towards the flap edge. The wax block was then trimmed until the tread in the middle of the flap was obvious. Finally, a series of 10μm thick corneal cross sections were cut from the middle of the flap. Series of 10μm thick corneal cross sections from central regions of control/uninjured corneas were also obtained. The sections were floated as described in section 2.3.2.3 and collected using SuperFrost slides for better tissue adhesion. Slides were then incubated overnight in a 56°C oven.

3.2.3 Haematoxylin and Eosin staining

Haematoxylin and Eosin staining was performed in trephined, LASIK-like injured and control corneas as described in section 2.3.2.5.

3.2.4 Immunohistochemistry

Immunohistochemistry using anti αSMA (Sigma) and PAN-Cytokeratin (DAKO) was performed in LASIK-like injured and control corneas as described in section 2.3.2.7. Anti αSMA immunostaining was not performed in trephine wounded corneas, because it has been done before by Carrington *et al.* (2006).

3.2.5 Cell counts

3.2.5.1 Total cell counts and statistics

LASIK-like (n=24) and control (n=24) corneal cross sections were dewaxed and dehydrated as described in sect.2.3.2.4. Samples had been in culture for 0, 1 and 3

days, 1, 2, 3, 4 weeks. The sections were then mounted with hydromount mountant containing 1μg/ml of bisbenzimide solution. Slides were then placed on the viewing stage of a fluorescent microscope (Olympus, UK). Colour photographs were taken at 10x magnification using the SPOT software package and a digital camera (Leica), which was attached to the microscope. A scale bar was also included in the image. A scale bar was then transferred to the CorelDraw11® software package and transparent rectangular boxes of 100x200μm were constructed. Six images were taken from each corneal sample; above and below the incision site, above and below the incision at the equidistance and above and below the incision at the flap edge (Fig. 3.4). Cell counts of total cells were made by opening the light micrographs in the ImagePro Plus software package and pasting the 100x200μm box on the picture. For each time-point three control sections and three LASIK-like injured samples were photographed, in order for the subsequent statistical analysis to be viable.

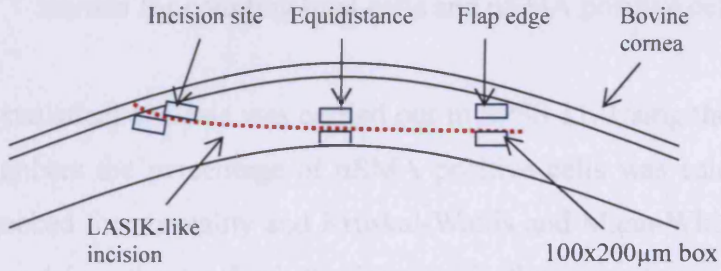

Figure 3.4: Corneal diagram with rectangular boxes (100x200μm) in six positions denoting the location of the area assessed for quantitative total cell counts

The statistical analysis was carried out in SPSS 11. The data was checked for normality and one-way ANOVA and paired t-test were performed in order to check the differences in numbers between the different time-points and various locations.

3.2.5.2 Myofibroblast cell counts and statistics

LASIK-like (n=12) and control (n=12) corneal cross sections were dewaxed and dehydrated as previously described (sect. 2.3.2.4). Corneal samples that had been in culture for 0, 1, 2, 3, 4 weeks were stained with anti αSMA as previously described (section 2.3.2.7). Slides were then placed on the viewing stage of a fluorescent microscope (Leica, UK). Colour photographs of a stromal area proximal to the epithelial plug and below the incision were taken at 20x magnification using the FW400 (Leica) software package (Fig. 3.5). Images were captured using a digital camera (Leica), which was attached to the microscope. Blue (i.e. total cells) and green

(i.e. positive cells) composite pictures were saved separately. Cell counts of total and positive stained cells were done by transferring the light micrographs to the ImagePro Plus software package. For each sample the whole of the picture was selected and cell counts were performed using the software options. For each time-point three control sections and three LASIK-like injured samples were photographed, in order for the subsequent statistical analysis to be viable.

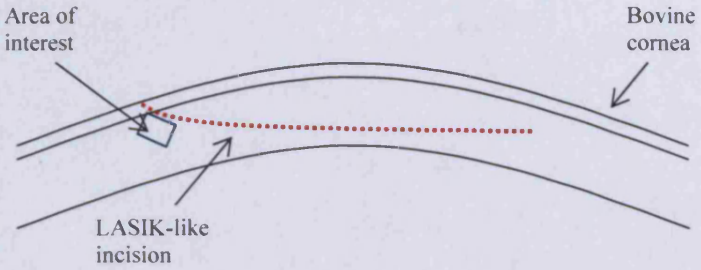

Figure 3.5: Diagram representing a LASIK-like injured cornea indicating the area of interest for counting total cells and αSMA positive cells.

The statistical analysis was carried out in SPSS 11. Using the positive and the total cell numbers the percentage of αSMA positive cells was calculated. The data was then checked for normality and Kruskal-Wallis and Mann-Whitney median tests were performed in order to check the increase in the percentage of positive αSMA cells during the culture period.

3.3 Results

3.3.1 Haematoxylin and Eosin staining

Control/uninjured corneas

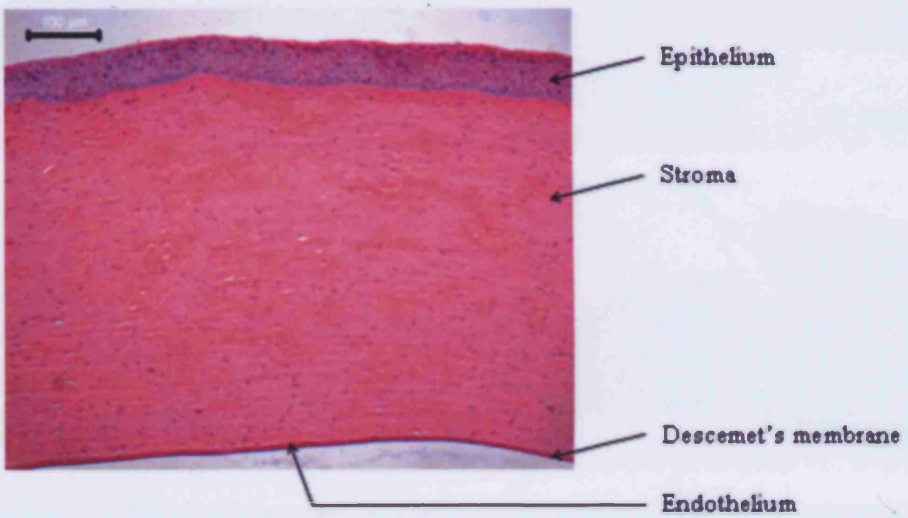

Figure 3.6: Structure of a cross section in a central region of a normal/uninjured bovine cornea. Bovine corneas lack Bowman's layer. Scale bar 100μm.

A normal bovine cornea at time-point 0 hrs is depicted at Fig. 3.6. There are only four distinctive layers present since the bovine species do not possess any Bowman's layer.

Trephine wounded corneas

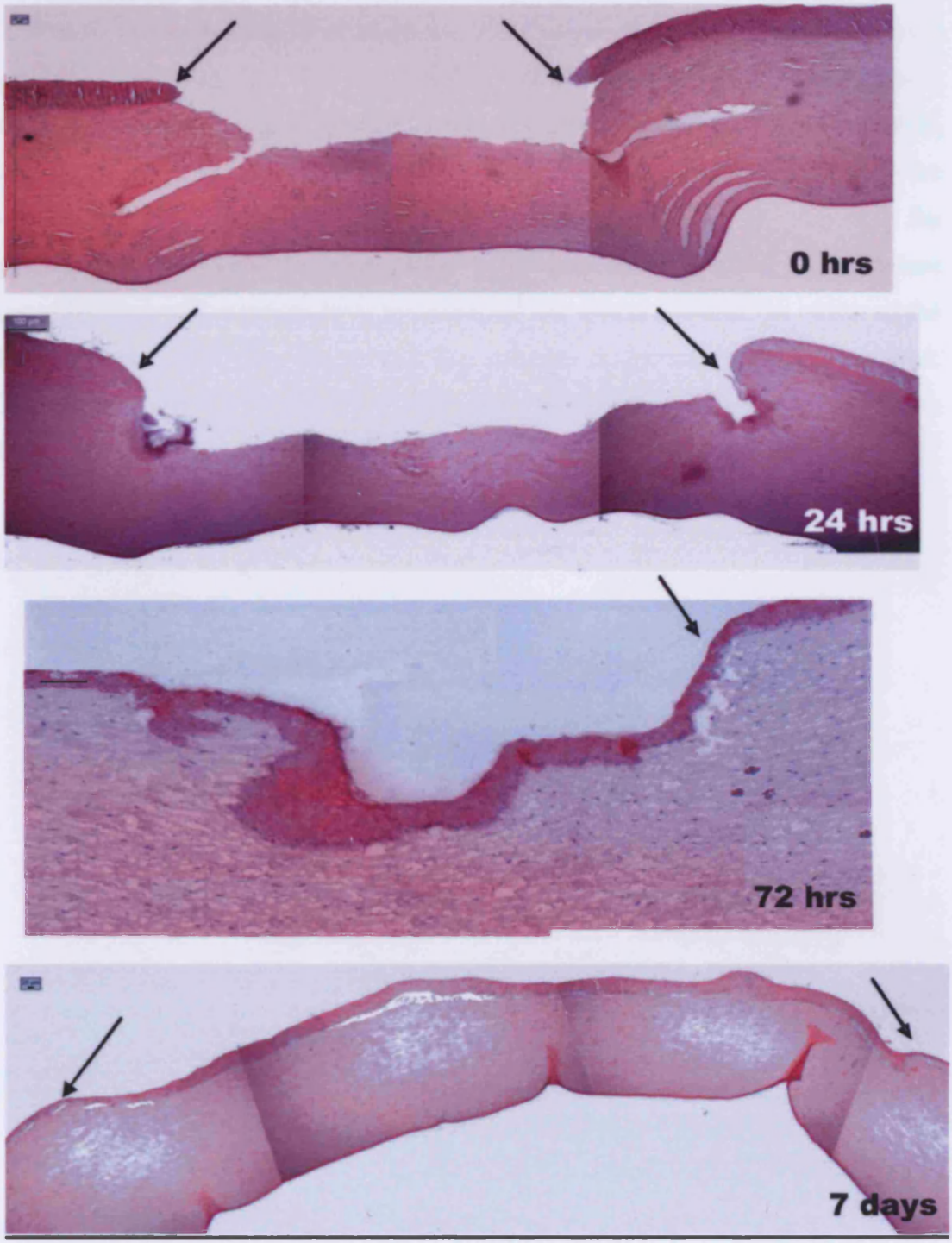

Figure 3.7: Wound healing progress in trephined bovine corneas at different time points. Light micrograph for 72hrs is a focused image in the right side of the wound that shows the formation of a thin layer of epithelium covering the site of injury. This layer becomes thicker at the 7th day after injury (Black arrows indicate the incision site).Scale bars: 0hrs and 7 days=25μm, 24hrs=100 μm, 72hrs=50 μm.

Haematoxylin and Eosin counterstaining was applied to wax sections in order to observe the morphological changes that occur in bovine corneas during the wound healing process (Fig. 3.7). At 0 hrs it can be seen that there are some stromal gaps at the wound edge. These gaps are filled within the first 24 hrs of the culture. However, it is expected to observe a stromal wound healing response at these sites although the overlaying epithelium is not injured. At the same time point (i.e. 24 hrs) the epithelium at the edge of the wound starts to build up. At the third day of the culture the epithelium still migrates from the edges of the wound towards the centre of the wounded area. Finally, by the seventh day complete re-epithelialisation is observed. The epithelium at the wounded area is thicker than the rest of the cornea and it fills the stromal gap that was created initially.

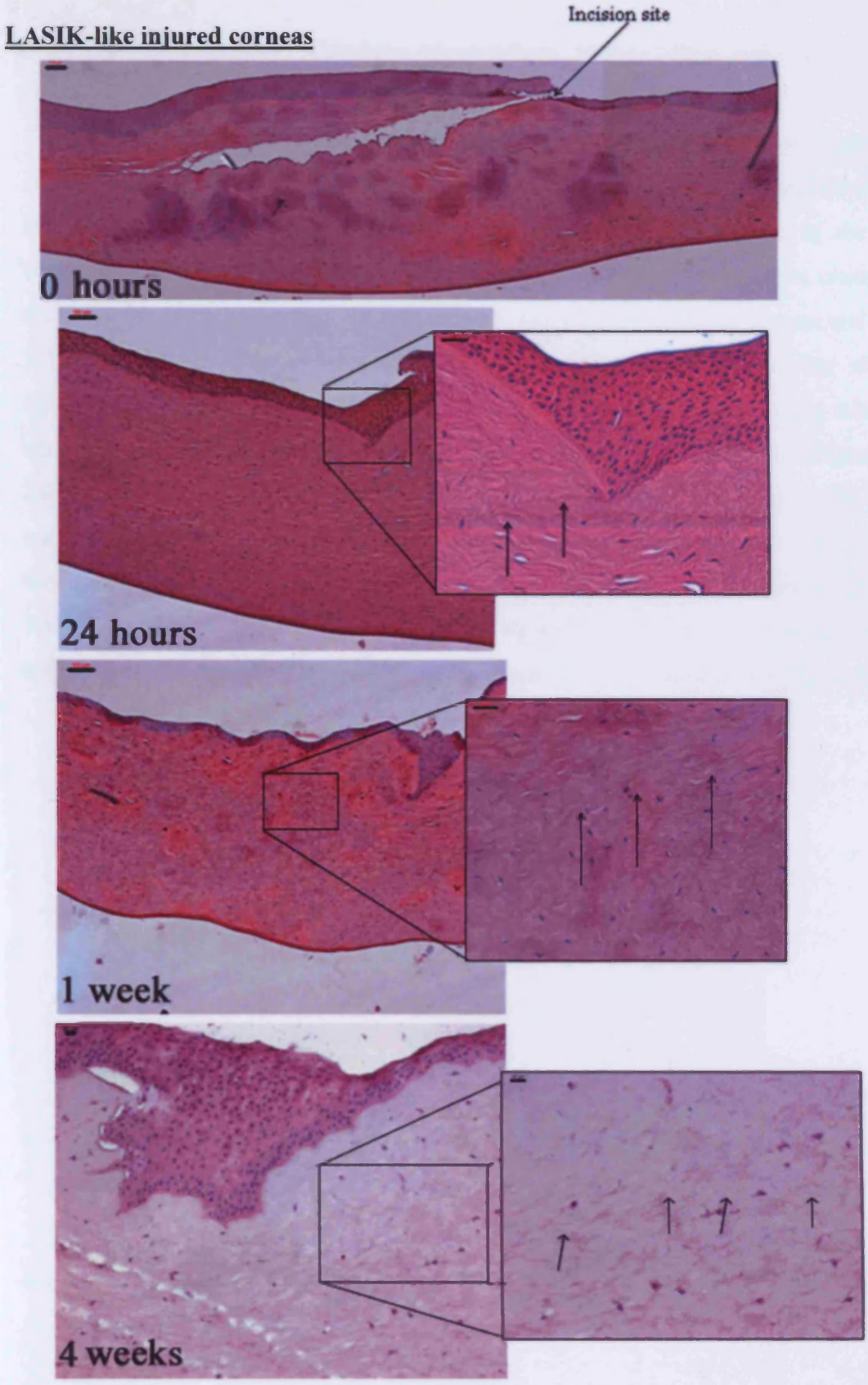

Figure 3.8: LASIK-like injured bovine corneas in culture for up to one month. LASIK-like flap immediately after wounding at 0hrs. Epithelial plug formation within 24hrs post-wounding. Incision still intact within the stroma at 1 and 4 weeks after

injury, respectively. Scale bars: 0 hrs=100μm, 24 hrs=100μm and 30μm, 1 week=100μm and 30μm, 4 weeks=25μm.

Using a surgical blade a LASIK-like flap was induced in bovine corneas cutting initially the epithelial interface, proceeding into the stroma parallel to the cross-sectional plane of the cornea (Figure 3.8 0hrs). The induction of the flap disrupted severely the epithelium at the incision site and stromal gaps were created as the scar was extending within the mid stroma. The depth of the flap was around 180-250μm. Immediately after wounding epithelial cells migrated towards the site of injury. An epithelial plug was created at the incision site. The epithelium in this area was obviously thicker than the epithelium across the rest of the cornea (Figure 3.8 24hrs). By 24hrs complete re-epithelialisation had occurred and epithelial cells covered the stromal gap that was created initially at the incision site. By 1 to 4 weeks the epithelium still migrated towards the stromal gaps (Figure 3.8 1 and 4 weeks). The incision was still obvious within the stroma even at areas proximal to the epithelial plug, suggesting minimal or non existent stromal wound healing response.

3.3.2 Epithelial cells

Control/uninjured corneas

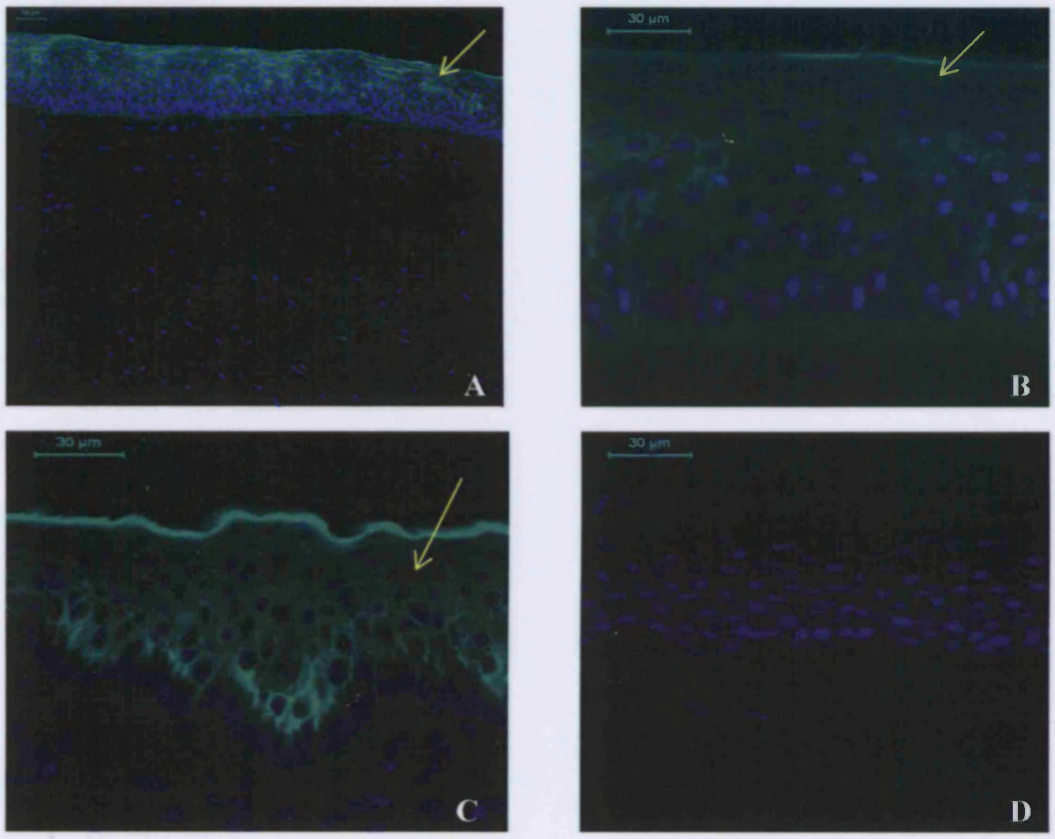

Figure 3.9: Epithelial cell expression in central region of control/uninjured corneas (A and B). Limbal region of control/uninjured cornea (C). Negative control/ central corneal region (D). Yellow arrow indicates site of positive staining for cytokeratin in epithelial cell cytoplasm (Green→ Cytokeratin, Blue→ Biz-benzimide).

In order to assess epithelial cell expression during the wound healing process a two step indirect immunostaining method was performed using a PAN Cytokeratin primary antibody (DAKO). The PAN Cytokeratin antibody is a cocktail of two primary monoclonal antibodies (i.e. AE1 and AE3 clones) and stains cytokeratin isoforms 1-8, 10, 13-16 and 19. Cytokeratins are a diverse family of intermediate filaments that are expressed in epithelial cell cytoplasms. Cytokeratin is only being expressed in terminally differentiated epithelial cells and therefore it is considered as a marker for differentiation. In Fig. 3.9 positive staining within the cytoplasm of corneal epithelial cells is obvious. In central regions of normal corneas it is also apparent that cell population at the upper layers of the epithelium is less dense than that in the suprabasal epithelium. Additionally, there is no positive staining for

cytokeratin at the basal epithelium in the limbal area (Fig. 3.9C). This was expected, as it is believed that the stem cell population of the cornea is based in this area.

LASIK-like injured corneas

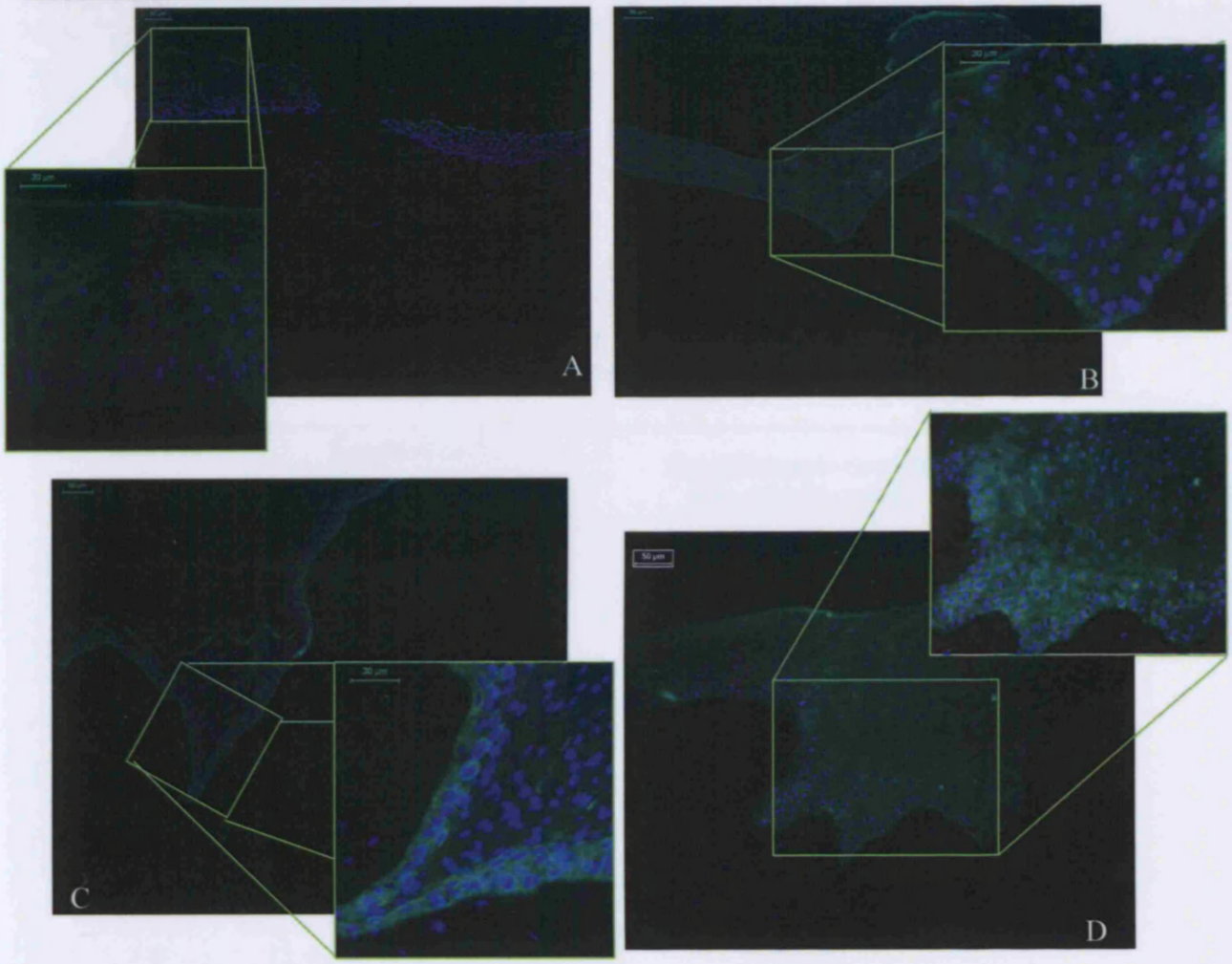

Figure 3.10: Epithelial cell expression LASIK-like injured corneas up to four weeks after injury. Epithelial cells at the site of incision at 0hrs time-point (A). The epithelial pug that was formed within 24hours after injury consisted of terminally differentiated epithelial cells. The epithelium also started to migrate towards the stroma covering gaps (B). The profile of the epithelial cellular behaviour remained the same after 1week (C) and 4 weeks (D) after wounding.

The epithelial plug that was created at the incision site consisted of terminally differentiated epithelial cells at all time-points, as there was positive staining for cytokeratin. The epithelium at the incision site consisted of differentiated epithelial cells soon after injury (Figure 3.10B). Epithelial cells migrated towards the stroma in order to fill gaps that were created after injury. They kept migrating until the end of the culture period as the epithelial plug at the 4weeks time point is considerably bigger compared to the epithelial plug of earlier time-points.

3.3.3 Stromal cells numbers in LASIK-like injured corneas

Days in culture	Incision site		Corneal periphery control (No of cells ± SD)
	No of cells above ± SD	No of cells below ± SD	
0	10 ±3.1	14 ±5.7	15 ±2.2
1	22 ±8.5	23 ±10.9	16 ±6.2
3	14 ±6.0	14 ±2.5	19 ±2.9
7	12 ±3.3	15 ±3.7	14 ±3.3
14	16 ±4.5	15 ±3.1	15 ±1.7
21	12 ±1.2	11 ±2.5	16 ±6.2
28	13 ±1.6	25 ±2.5	19 ±2.9

Days in culture	Equidistance		Equidistance control (No of cells ± SD)
	No of cells above ± SD	No of cells below ± SD	
0	12 ±4.1	10 ±2.6	19 ±2.8
1	23 ±2.5	21 ±6.2	15 ±2.1
3	11 ±2.1	14 ±1.2	15 ±1.2
7	10 ±1.7	12 ±0.9	10 ±3.1
14	11 ±3.7	11 ±2.2	19 ±2.8
21	11 ±0.8	11 ±0.5	15 ±2.1
28	7 ±0.8	8 ±0.5	15 ±1.2

Days in culture	Flap edge		Mid Cornea control (No of cells ± SD)
	No of cells above ± SD	No of cells below ± SD	
0	12 ±3.3	16 ±2.3	19 ±2.9
1	20 ±5.4	16 ±7.1	17 ±1.4
3	15 ±5.4	17 ±2.9	18 ±1.7
7	12 ±3.4	14 ±3.3	10 ±1.4
14	13 ±2.4	12 ±4.2	19 ±2.9
21	9 ±0.8	10 ±0.5	17 ±1.4
28	7 ±0.8	8 ±1.2	18 ±1.7

Table 3.1: Total cell counts for stromal cells from different areas along the LASIK-like flap. For each time-point 3 corneas were used (For cell numbers/mm^2 and also raw data please refer to Appendix 4).

Significant differences in cell numbers above and bellow the incision counts at the incision site at 1wk (0.035) and 4wks (p=0.05) were observed. In specific, cell numbers were higher below the scar at the incision site.

Comparison of cell counts in wounded corneas against controls revealed the following observations.

1. 0hrs significant decrease in equidistance below (p=0.027)

2. 1wk significant decrease in equidistance above (p=0.025)
3. 2wks significant decrease in equidistance below (p=0.034)
4. 3wks significant decrease in "edge" region (p=0.005)
5. 4wks significant decrease in "equidistance" and "edge" regions

(p=0.003 and p=0.001, respectively)

3.3.4 Myofibroblast expression and cell numbers in LASIK-like injured corneas

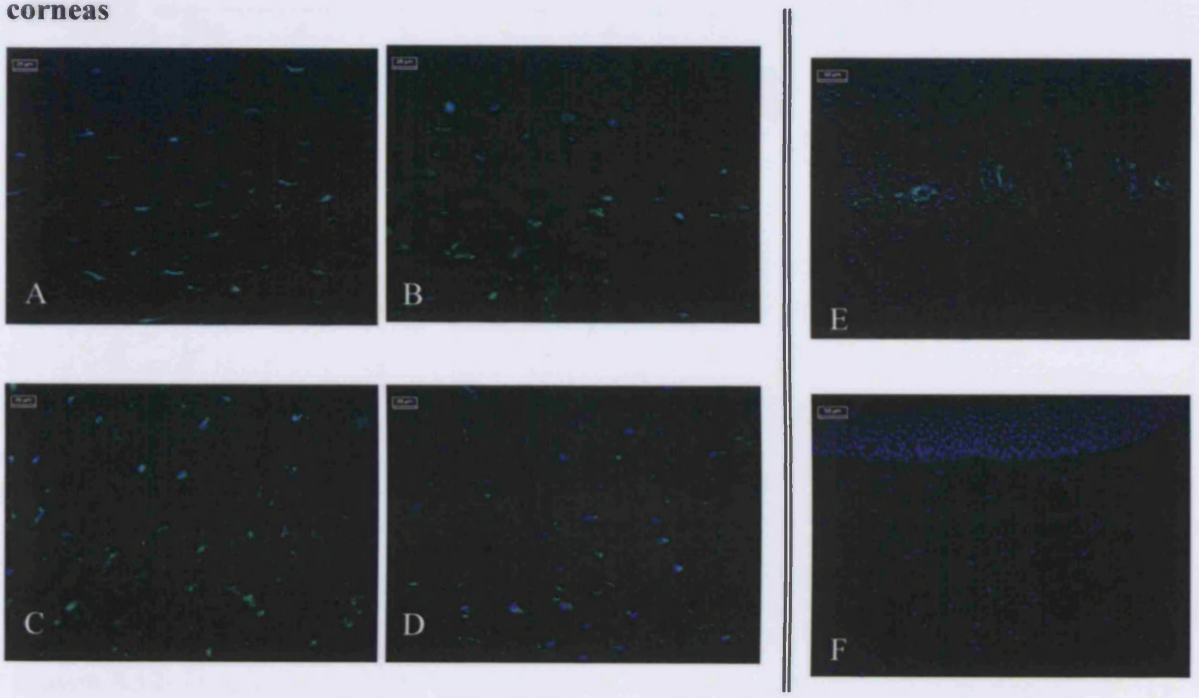

Figure 3.11: Myofibroblast cell expression in LASIK-like corneas. Positive stained cells were first observed at the 1 week time-point (A) and they were present for the rest of the organ culture time span (B-D depict 2-4 weeks, respectively). αSMA staining was also positive in the limbal vessels of all corneas (E). Negative control (F) (Green→ αSMA, Blue→ Biz-benzimide).

αSMA positive staining in LASIK-like injured corneas confirmed the presence of myofibroblasts in scar tissue. Staining was negative at 0, 1 and 3 days after injury. αSMA positive staining became evident at the 1 week time-point and it remained obvious at later time-points of the organ culture. During all the time-points that positive αSMA was observed, myofibroblast expression was only present in a stromal area proximal to the epithelial plug. There was no staining at all in stromal areas close to the middle or the edge of the flap.

Positive staining was also observed in the limbal vessels of all corneas, both injured and uninjured ones (Fig. 3.11E). This was expected as actin filaments are known to surround blood vessels and therefore staining in the limbus for αSMA was considered as a positive control for this series of experiments.

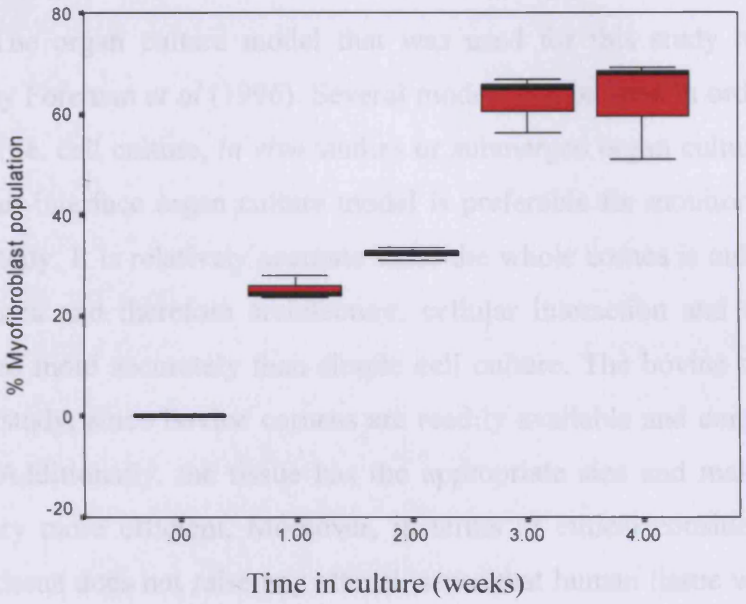

Figure 3.12: Graph representing the increase in % myofibroblast population over a four weeks period after injury in LASIK-like injured corneas. Error bars represent the standard error of mean (B).

According to the statistical analysis, the myofibroblast population was increasing from the first week after injury. Specifically, the Kruskal-Wallis test revealed that there were significant increases in the percentage of positive stained cells between 0 and 1week, 1 and 2 weeks and 2 and 3 weeks ($p=0.011$). There was not a significant change between the 3rd and 4th week percentages suggesting that the myofibroblast population gradually increases during the first three weeks after injury and then it tends to stabilise. The data was further analysed by performing Mann-Whitney median tests that provided with a p value of 0.001. This outcome confirms that the observed response in myofibroblast population increases as the independent variable (i.e. time) increases.

3.4 Discussion and conclusions

The organ culture model that was used for this study has been described before by Foreman *et al* (1996). Several models can be used in order to assess wound healing (i.e. cell culture, *in vivo* studies or submerged organ cultures). However, this simple air-interface organ culture model is preferable for monitoring wound healing in this study. It is relatively accurate since the whole cornea is cultured including the limbal area and therefore architecture, cellular interaction and wound healing are mimicked more accurately than simple cell culture. The bovine species was chosen for this study, since bovine corneas are readily available and commercially cheap to obtain. Additionally, the tissue has the appropriate size and makes handling in the laboratory more efficient. Moreover, in terms of ethical considerations, the use of bovine tissue does not raise any ethical issues that human tissue would do. However, the bovine species is not as ideal as it can be difficult to find appropriate antibodies for immunohistochemistry and the bovine genome is not fully elucidated.

In this study the wound healing process was monitored for several weeks and in agreement with Foreman *et al* (1996) complete re-epithelialisation in trephine wounded cultured bovine corneas occurred within the first 72 hrs post wounding. While re-epithelialisation could be visualized, it was sometimes more difficult to interpret following sectioning. In some micrographs, even at 7 days, the epithelium had detached from the wound surface and in some cases it had fallen off. This artefact represents weak adhesion between the new epithelium and the underlying stromal surface and a requirement of further optimization of the wax embedding and sectioning technique. Furthermore, it should be taken into consideration that the bovine cornea does not possess a Bowman's layer and therefore the connection between the epithelium and stroma might be weaker, compared to other species which posses a Bowman's layer. The wax embedding procedure had to be optimized for the bovine cornea, since extensive treatment of the corneas with the neutral buffered formalin buffer, chloroform and paraffin wax had made them rigid and it was impossible to produce full length sections of the cornea without the sections tending to break or fold up.

Total cell numbers tend to be significantly decreased at later stages of the organ culture time span. In the current study, total stromal cell numbers remain decreased until the end of the organ culture period. This leads to the conclusion that

cell numbers decrease possibly because of the occurrence of apoptosis as a natural response to injury. However, the fact that cell numbers do not increase indicates that there is no cellular proliferation, supporting the existence of a poor wound healing response in LASIK-like incisions.

Total cell counts in stromal cells revealed that there was a significant increase in the cell density at the incision site, below the incision, at 1 and 4 weeks. Later experiments confirmed the existence of myofibroblasts in this area. Additionally, at 0hrs there was a significant decrease in cell numbers at the equidistance region below the incision. This observation might be due to the fact that the blade mechanically removed cells during the induction of the injury in the stroma. Between the 1 and 4 weeks time-points there is a variation in cell numbers along the flap, as there is a significant decrease in cell density when injured corneas are compared to control ones. According to Wilson and Kim (1998) keratocytes in a wounded area undergo cell shrinkage and subsequent apoptosis. Additionally, according to previous studies the stromal response to refractive surgery is characterised by a reduction in size and density of keratocyte cell bodies, and by migration of the remaining keratocytes to repopulate the areas in which cell density has decreased (Rajan *et al.* 2005). What causes keratocyte loss around the wound area right after wounding is still unclear. This might be a homeostatic internal response from living organisms. Besides, it has been proposed by Wilson *et al* (1997) that this might be a defence mechanism in order to prevent the passage of viral material into the eye when a wound occurs. According to Zieske *et al.* (2001) cell proliferation and the appearance of myofibroblasts in a wounded cornea occurs 24-48hrs post wounding. The same report also supports that myofibroblast transformation might take up to one month to become apparent, whereas they do not regress even one year after wounding. The fact that the remaining keratocytes tend to repopulate low cell density areas instead of transforming into myofibroblasts, explains the fact that the stromal wound healing response is impaired in the stroma after LASIK.

In PRK, the wound healing response in the stroma takes place at the stroma-epithelium interface as a result of interaction of a number of cytokines that are released by the injured epithelium (Marshall *et al.* 1988, Wilson *et al.* 1999, Rajan *et al.* 2005). In the case of LASIK, the epithelium is only injured at the incision site and therefore the stromal wound healing response takes place in areas proximal to the incision site, leaving central areas of the flap intact. Keratocyte apoptosis only takes

place in a zone approximately 50μm anterior and 50μm posterior to the incision in stromal areas close to the epithelial plug (Helena *et al.* 1998, Wilson *et al.* 2001, Mohan *et al.* 2003, Dawson *et al.* 2005).

Attempts to optimize immunostaining for CK 3 were unsuccessful despite the fact that CK3 is prominent in the corneal epithelium. This may reflect a problem with the antibody of species difference. It was therefore decided to use a PAN Anti-Cytokeratin Ab which reacted with a wide range of cytokeratin isoforms. Cytokeratin (CK) nos. 3, 5 and 12 are the most abundant ones in the adult cornea and they are expressed uniformly all over the tissue. The PAN Cytokeratin Ab that was used for this study does not stain for CK 12. However, CK 12 forms a heterodimer with CK3 in the cornea and therefore after staining CK3, CK12 is also co-localized. CKs nos 4, 14, 15 and 19 are also present in minor amounts. In light micrographs for cytokeratin it is obvious that the staining is denser at the upper part of the epithelium. It should be taken into consideration that CK 4 is expressed only in the upper corneal epithelial cells from about the third layer upwards. Additionally, CK 19 expression is restricted to the peripheral regions of the corneal epithelium (Kasper *et al* 1988). Therefore, the existence of additional CK isoforms in the upper levels of the corneal epithelium makes CK immunostaining denser along the periphery.

The histological evaluation of LASIK-like injured corneas revealed a rapid epithelial wound healing response and a rather delayed stromal repair. A plug was created at the site of injury and covered the stromal gaps at the incision site. This plug was later confirmed to consist of terminally differentiated epithelial cells indicating a rapid epithelial wound healing response. Although the epithelial plug was created very quickly after injury, epithelial cells carried on migrating towards the stroma even at later stages of the organ culture time span, as the epithelial wound healing response is known to reach completion at approximately 1month after injury.

It appears that the epithelium possibly has an evolutionary mechanism for smoothing the anterior surface of the cornea in cases where it is disrupted by various external factors, such as injury. According to Dawson *et al.* (2005b) mild focal or moderate, diffuse stromal loss can be compensated with hypotropic or hypertropic epithelial cell adjustments. This response takes place only at the basal epithelial cells, but the reason is yet unknown. In the case of the LASIK-like injuries studied in the present work, the epithelium was obviously thicker than normal at the incision site.

Myofibroblast expression was only observed in an area underneath the epithelial plug in LASIK-like injured corneas. Cell density was increasing during the first three weeks after injury, but it seemed to stabilise after this period. These findings confirmed a minor stromal wound healing response that was only observed in an area close to the stromal-epithelial interface. During the 4week organ culture time span there was not any evident stromal wound healing response either in the middle of the flap or at the hinge area. Additionally, histology also confirmed that the incision within the stroma was still intact by the end of the organ culture period. αSMA staining was negative in these areas confirming the absence of any active myofibroblasts. A likely explanation for this could be the absence of certain cytokines that are being released by the epithelium in response to injury and transform quiescent keratocytes into myofibroblasts. The epithelium that lies above the middle of the flap or the hinge is not injured and cytokines that are released by the epithelium at the incision site might not be able physically to reach areas deeper in the stroma towards central flap areas.

In conclusion, this *in vitro* model closely mimics the cellular events observed in previous studies *in vivo.* Within 24hrs after inducing a LASIK-like injury a normal epithelial repair was observed and confirmed. In contrast, impaired stromal wound healing was observed, as myofibroblast expression was only present in the stromal area at the incision site. The myofibroblast phenotype was totally absent in stromal areas towards the middle or the edge of the LASIK-like flap. The histological evaluation of LASIK-like corneas also confirmed that the scar was still intact within the stroma even 4 weeks after injury. These observations are very important in real time LASIK as impaired wound healing makes the flap unstable and prone to decentration or detachment, raising serious concerns regarding the safety and long term stability of LASIK.

4. Association of myofibroblast induction with LASIK-flap adhesion and corneal transparency

4.1 Introduction

Cytokines are known to play a key role in cellular proliferation and differentiation in biological tissues (Wilson *et al.* 2003). On many occasions growth factors are being used for medical purposes in order to heal or improve certain conditions. For example, NGF has been successfully used for the treatment of neurotrophic and autoimmune corneal ulcers (Lambiase *et al.* 2000).

Considering refractive surgery, one of the major drawbacks of LASIK is that the flap is being reported not to heal completely even after several years postoperatively (Ivarsen 2003). ECM proteins such as fibrinogen and tenascin do not seem to appear after LASIK and hence the wound healing process depends only on the epithelial-stromal interaction. The strict localisation of fibrosis marginally at the flap edge, contrary to the minimal fibrosis below the entire flap, suggests that the LASIK interface never heals (Ivarsen 2003). The limited peripheral wound healing response after LASIK is not usually enough to secure the flap and make it resistant to dislocation under mechanical stress (Crawford 2003). Myofibroblast expression was only observed in stromal areas proximal to the epithelial plug (Chapter 3). The fact that there was no myofibroblast phenotype expressed at the bed of the flap leads to the assumption that cytokines that are released from the epithelium do not physically reach areas at the bed of the flap. Therefore, a series of experiments was designed in order to supply the flap with certain cytokines in various dilutions and monitor the wound healing response in culture for up to four weeks.

The effectiveness of the cytokines that were applied to the corneas was assessed at initial stages by judging the mechanical strength and transparency of the samples. Considering the fact that the cornea is the major refractive part of the eye, any biological or mechanical alteration in the tissue will influence optical performance. Maintenance of transparency in any attempt to improve wound healing in LASIK flaps is a very important issue, as the further objective is the maintenance of a normal visual function. In addition, enhancing the wound healing response in LASIK flaps aims to increase the mechanical strength of the corneas and therefore avoid any keratectasia.

Four cytokines were selected and applied at the flap interface (i.e. TNF-α, IL-1α, Fas-ligand and TGF-β_1). It has already been proposed that cultured corneal keratocytes exposed to TNF-α have increased cellular proliferation in the stroma (Mohan *et al.* 2000). Hong *et al.* (2001) suggested that human IL-1α induced apoptosis in human corneal keratocytes. Fas-ligand (Wilson *et al.* 1996) and TGF-β_1 induce apoptosis to corneal keratocytes. However, to date there has not been any experimental evidence to support the amount of these factors required in order for apoptosis to be triggered in keratocytes. A series of various dilutions of these proteins was applied to the tissue to investigate the effect of these cytokines on tissue wound healing, increase in mechanical strength and the maintenance of corneal transparency.

4.2 Experimental design

4.2.1 Organ Culture

Bovine corneas were organ cultured as detailed in section 2.3.1. Three different groups of corneas (n=304) were cultured (Table 4.1). Two hundred and eighty eight (288) were wounded in a LASIK-like fashion using the custom made eye holder (section 2.2.2). Thirty two (32) samples were treated with carrier solution (PBS/BSA or HCl/BSA). Two hundred and fifty six (256) corneas were treated with cytokine solution (i.e. TNF-α, IL-1α, FasL and TGF-β_1/R&D Systems) in various dilutions (i.e. 0.1, 10, 50 and 100ng/ml). The corneas were cultured for 1, 2, 3 and 4 weeks. Four corneas were put in culture for each cytokine dilution for each time point. Sixteen corneas were not wounded and acted as controls (Fig. 4.1). At the end of each culture all samples were fixed in 10% neutral buffered formalin and processed into wax. Control corneas were cut into halves before fixation, whereas LASIK-like corneas were trimmed close to the flap area before fixation.

		No of corneas in culture						
		Control	PBS/BSA	HCl/BSA	TNF-α	IL-1α	Fas-ligand	TGF-β_1
Weeks in culture	1	4	4	4	16	16	16	16
	2	4	4	4	16	16	16	16
	3	4	4	4	16	16	16	16
	4	4	4	4	16	16	16	16
	Total	16	16	16	64	64	64	64

Table 4.1: Number of corneal samples put in culture for each cytokine dilution for each time-point

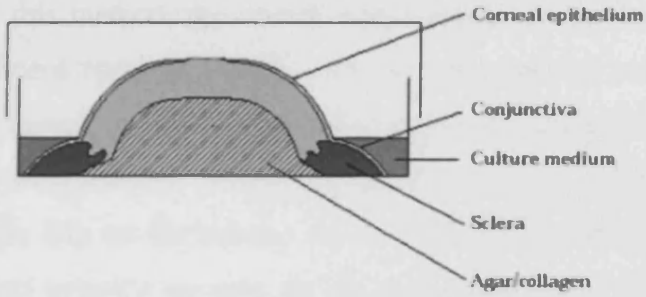

Figure 4.1: The organ culture set up.
(Picture adapted from Foreman *et al.* 1996)

4.2.2 Evaluation of transparency

Organ culture Petri dishes were placed on a grid (Fig. 4.2). Corneal transparency was assessed by three independent observers each time.

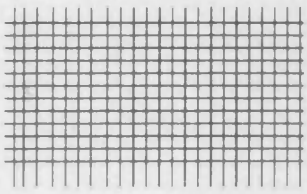

Figure 4.2: Sample of the grids that were used to assess the transparency of control and cytokine treated corneas.

Corneal samples were characterized for their transparency based on a scale of 0 (the control sample that remained clear at all times) to 100% (when the cornea is opaque) (Fig. 4.3).

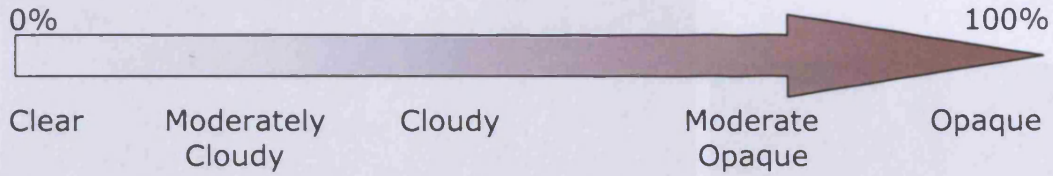

Figure 4.3: Scale for assessing corneal transparency

4.2.3 Assessment of mechanical strength/adhesion of the flap

A Lloyd instruments tensiometer (Lloyd Instruments Ltd, Hampshire, UK) was used in order to assess the extent of adhesion of the flap. The "pull to break" test was performed. In this method, the cornea was clamped on the machine by gluing equal size of cardboard paper in exactly opposite sites and the anterior (middle of flap) and posterior cornea. It was then pulled in opposite vertical directions until the flap was lifted and detached (Fig. 4.4B). The upper arm of the machine was clamped on the middle of the flap on the anterior of the cornea whereas the lower arm was clamped on the exact opposite position on the posterior part of the cornea. This test measured the force that was required to break the flap. The data was recorded using a Nexygen 4.1 software package and it was stored in an MS Windows operated workstation (Fig. 4.4A).

Once a complete set of data was recorded, a non-parametric statistical analysis (i.e. Kruskal-Walis) was performed in SPSS. Three samples were used for each sample dilution at each time-point in order for the statistical analysis to be viable.

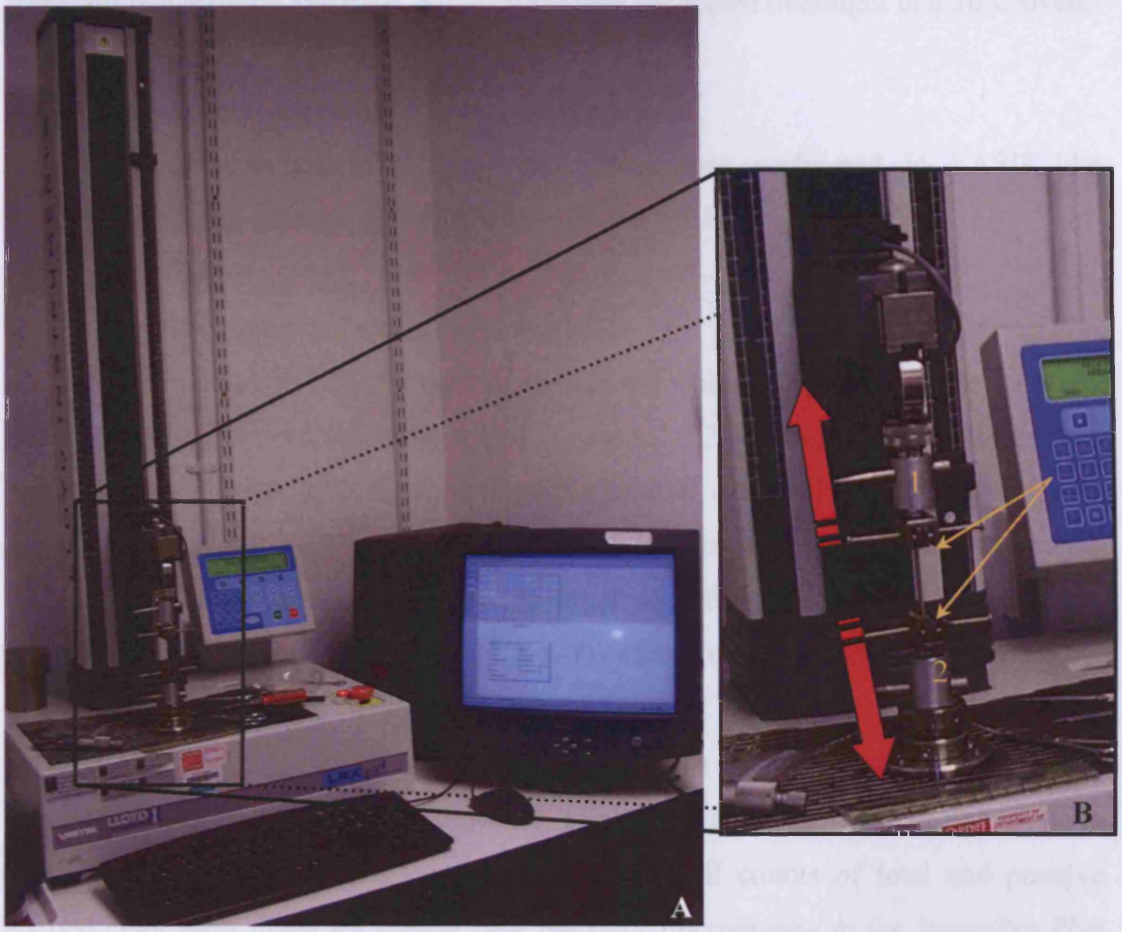

Figure 4.4: Lloyd tensiometer set up (A) Each cornea was clamped on the two metal arms (yellow arrows-upper arm 1, lower arm 2) of the tensiometer and was pulled apart in opposite vertical directions (red arrows) (B).

4.2.4 Wax embedding and tissue sectioning

LASIK-like injured corneas were embedded in paraffin wax perpendicular to the surface of the wax pot. Before processing a thread was placed at the hinged part in the middle of the flap. Tissue blocks were left in 4°C overnight before attempting to cut sections. Each block containing a LASIK-like injured cornea was then clamped on the microtome in such a way that a cross section would be obtained, cutting from the flap hinge towards the flap edge. The wax block was then trimmed until the thread in the middle of the flap was obvious. Finally, a series of 10μm thick corneal cross sections were cut from the middle of the flap. Series of 10μm thick corneal cross sections from central regions of control/uninjured corneas were also obtained. The

sections were floated as described in section 2.3.2.3 and collected using SuperFrost slides for better tissue adhesion. Slides were then incubated overnight in a 56°C oven.

4.2.5 Immunohistochemistry

Immunohistochemistry using anti αSMA was performed in LASIK-like injured and control corneas as described in section 2.3.2.7.

4.2.6 Myofibroblast cell counts and statistics

LASIK-like (n=12) and control (n=12) corneal cross sections were dewaxed and dehydrated as previously described (section 2.3.2.4). Corneal samples that had been in culture for 0, 1, 2, 3, 4 weeks were stained with anti αSMA as previously described (section 2.3.2.7) and counterstained with biz-benzimide to identify nuclei. Slides were then placed on the viewing stage of a fluorescent microscope (Leica, UK). Colour photographs of a stromal area proximal to the epithelial plug and below the incision were taken at 20x magnification using the FW400 (Leica) software package (Fig. 4.2.5.1). Images were captured using a digital camera (Leica), which was attached to the microscope. Blue (i.e. total cells) and green (i.e. αSMA positive cells) composite pictures were saved separately. Cell counts of total and positive stained cells were made by transferring the light micrographs to the ImagePro Plus software package. For each sample, the whole of the picture was selected and cell counts were performed using the software options. For each time-point, three control sections and three LASIK-like injured samples were photographed, in order for the subsequent statistical analysis to be viable.

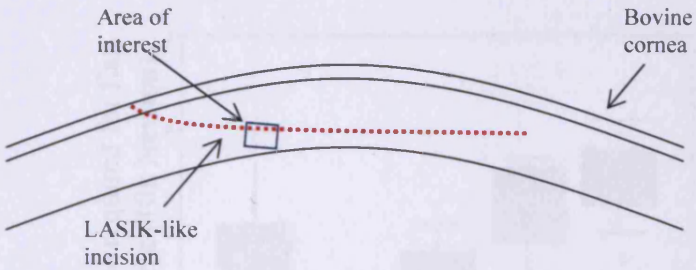

Figure 4.5: Diagram representing a LASIK-like injured cornea indicating the area of interest, in the flap bed, for counting total cells and αSMA positive cells.

The statistical analysis was carried out in SPSS 11. Using the αSMA positive and the total cell numbers, the percentage of αSMA positive cells was calculated. The

data was then checked for normality and Kruskal-Wallis and Mann-Whitney tests were performed in order to check the increase in the percentage of positive αSMA cells during the culture period.

4.3 Results

4.3.1 Evaluation of transparency, corneal mechanical strength/flap adherence and myofibroblast cellular expression and density in response to exogenous factors

4.3.1.1 Control/untreated corneas

At preliminary stages of the experiment, corneas were left in culture over a period of four weeks. The samples were injured in a LASIK-like fashion and left untreated without any cytokine solution. The wound healing response was monitored during this time.

Time in culture (weeks)	Mean force required for flap detachment (Newton)
0 hours	0.04500
1 week	0.03733
2 weeks	0.04433
3 weeks	0.05100
4 weeks	0.05500

Table 4.2: Mean force required to detach control non-cytokine treated corneas over a period of 4 weeks in culture.

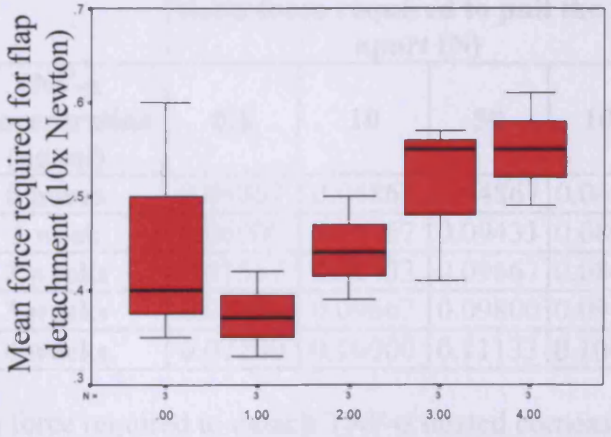

Figure 4.6: Graph showing the flap adherence of non-cytokine treated corneas

The mean force that was required to detach the flap in non-cytokine treated corneas increases gradually over the four week culture time span (Fig. 4.6). However, statistics proved that there are not significant differences in mean force values between 0 and 4 weeks ($p>0.05$). Therefore it can be concluded that flap adherence is still poor 4 weeks after injury, an observation that is in accordance with mid-stromal or LASIK like injuries.

	PBS/ BSA
0 hours	Clear
1 week	Clear
2 weeks	Clear
3 weeks	Clear
4 weeks	Clear

Table 4.3: Visual transparency assessment of control non-cytokine treated corneas over a 4 week period in culture.

LASIK like injured, non-cytokine treated corneas acted as controls when compared to cytokine treated corneas. However, control corneas maintained their transparency at all times during the organ culture period confirming the integrity and reliability of the culture technique.

4.3.1.2 Tumour Necrosis Factor alpha (TNF-α) treated corneas

TNF-α caused an effect on the treated corneas as various concentrations of the cytokine increased adherence and cloudiness to the tissue (Tables 4.4 and 4.5)

	Mean force required to pull the flap apart (N)			
TNF-α Concentration (ng/ml)	**0.1**	**10**	**50**	**100**
0 hours	0.04867	0.04867	0.04867	0.04867
1 week	0.06900	0.08767	0.09433	0.08067
2 weeks	0.07567	0.09433	0.09667	0.08467
3 weeks	0.08367	0.09667	0.09800	0.09467
4 weeks	0.07200	0.10000	0.11133	0.10067

Table 4.4: Mean force required to detach TNF-α treated corneas over a period of 4weeks in culture.

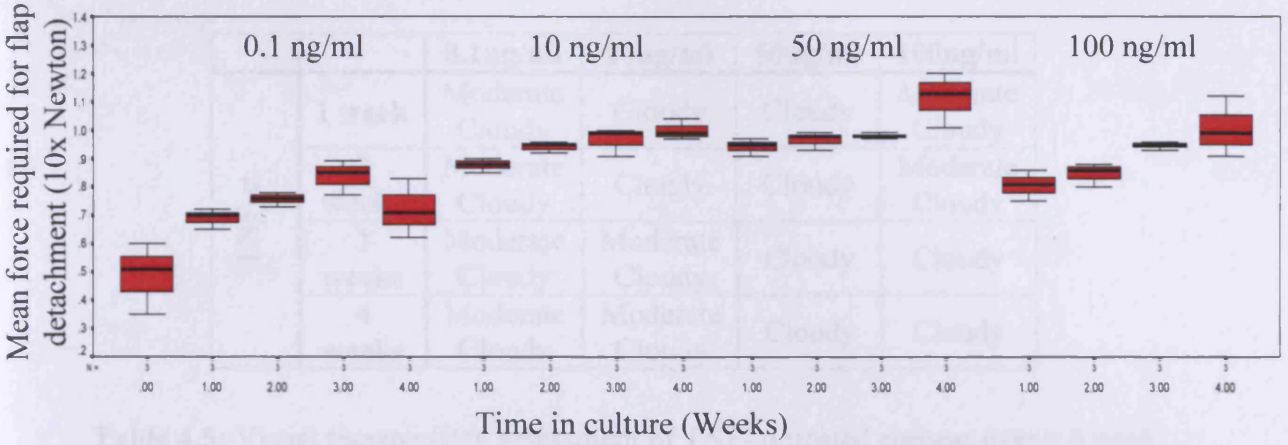

Figure 4.7: Graphs showing the effect of various concentrations of TNF-α on the flap adhesion

The mean force required for flap detachment increased rapidly during the first week in culture and then it kept increasing gradually (Fig. 4.7). The same pattern is observed in all four dilutions with little differences between each one of them. Flap adherence kept increasing with a slower rate (i.e. significant increase every two weeks for most of the samples; $p>0.05$).

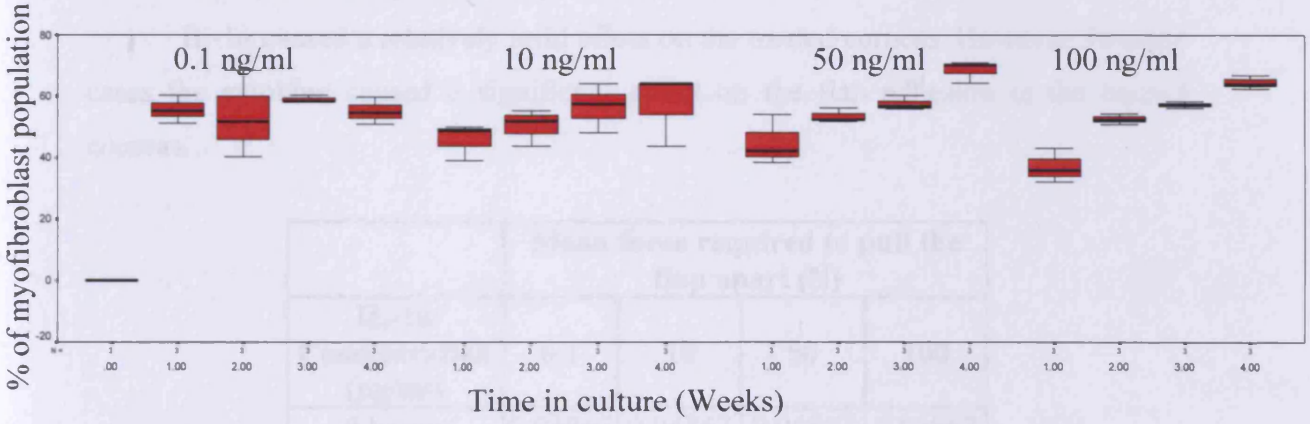

Figure 4.8: Graphs showing the effect of various concentrations of TNF-α on myofibroblast proliferation on the flap bed.

Both 0.1 and 10 ng/ml of TNF-α caused an immediate increase in myofibroblast population on the flap bed, but cell numbers do not increase significantly ($p>0.05$) for the rest of the organ culture time span. However, 50ng/ml and 100ng/ml caused a gradual, significant increase ($p<0.05$) in myofibroblast population (Fig. 4.8).

		0.1ng/ml	10ng/ml	50ng/ml	100ng/ml
TNF-α	1 week	Moderate Cloudy	Cloudy	Cloudy	Moderate Cloudy
	2 weeks	Moderate Cloudy	Cloudy	Cloudy	Moderate Cloudy
	3 weeks	Moderate Cloudy	Moderate Cloudy	Cloudy	Cloudy
	4 weeks	Moderate Cloudy	Moderate Cloudy	Cloudy	Cloudy

Table 4.5: Visual transparency assessment of TNF- α treated corneas over a 4 week period in culture.

Mid range concentrations of TNF-α (i.e. 10ng/ml and 50ng/ml) caused severe cloudiness in the corneas during the early stages of the organ culture (Table 4.5). Lower concentration of the cytokine caused a moderate effect on corneal transparency. However, 100ng/ml triggered a mild effect on the corneas, which became more severe at later stages of the organ culture period.

4.3.1.3 Interleukin 1 alpha (IL-1α) treated corneas

IL-1α caused a relatively mild effect on the treated corneas. However, in some cases the cytokine caused a significant effect on the flap adhesion in the treated corneas.

	Mean force required to pull the flap apart (N)			
IL-1α Concentration (ng/ml)	**0.1**	**10**	**50**	**100**
0 hours	0.04867	0.04867	0.04867	0.04867
1 week	0.06733	0.07333	0.08500	0.08200
2 weeks	0.07200	0.07400	0.09067	0.10100
3 weeks	0.07833	0.08667	0.09200	0.10733
4 weeks	0.08733	0.09033	0.10667	0.10500

Table 4.6: Mean force required to detach IL-1α treated corneas over a period of 4 weeks in culture.

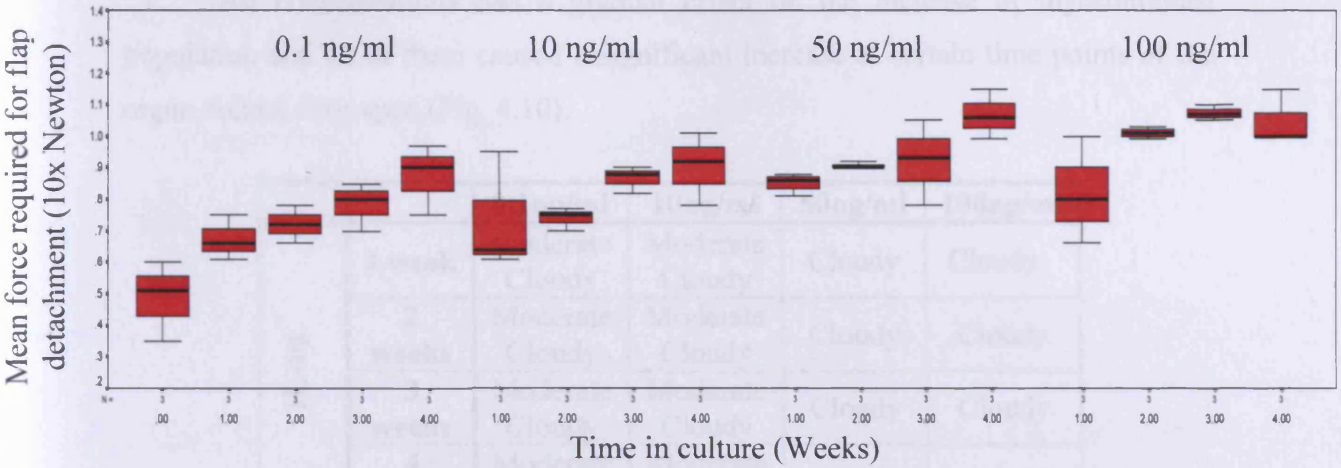

Figure 4.9: Graphs showing the effect of various concentrations of Il-1α on the flap adhesion

In lower IL-1α concentrations (i.e. 0.1 ng/ml and 10 ng/ml), flap detachment was not significantly increased when compared to control during the first week in culture after injury. IL-1α had a relatively mild effect in treated corneas and, for the 0.1ng/ml dilution, there was no significant increase in the mean force required for flap detachment ($p>0.05$). Additionally, at 10ng/ml there was also no significant increase during the first two weeks in culture. However, there is a significant increase in the mean force that was required for flap detachment between the second and the third week after injury. The value of the mean force seems to stabilise after the third week after injury.

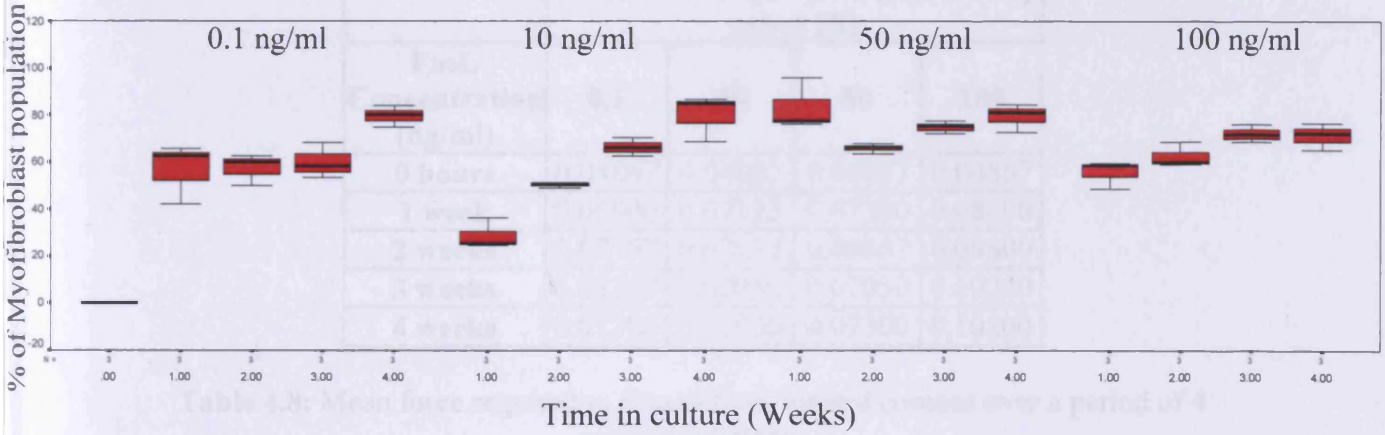

Figure 4.10: Graphs showing the effect of various concentrations of IL-1α on myofibroblast proliferation on the flap bed.

All concentrations had a gradual effect on the increase of myofibroblast population and all of them caused a significant increase at certain time points of the organ culture time span (Fig. 4.10).

		0.1ng/ml	10ng/ml	50ng/ml	100ng/ml
IL-1α	1 week	Moderate Cloudy	Moderate Cloudy	Cloudy	Cloudy
	2 weeks	Moderate Cloudy	Moderate Cloudy	Cloudy	Cloudy
	3 weeks	Moderate Cloudy	Moderate Cloudy	Cloudy	Cloudy
	4 weeks	Moderate Cloudy	Moderate Cloudy	Cloudy	Cloudy

Table 4.7: Visual transparency assessment of IL-1α treated corneas over a 4 week period in culture.

Only high concentrations of IL-1α caused severe opacities in the corneas. Lower concentrations caused a moderate effect on the clarity of the treated corneas (Table 4.7).

4.3.1.4 Fas Ligand (FasL) treated corneas

Fas-ligand had the mildest effect among the four cytokines that were applied to the LASIK like injured corneas.

	Mean force required to pull the flap apart (N)			
FasL Concentration (ng/ml)	**0.1**	**10**	**50**	**100**
0 hours	0.04867	0.04867	0.04867	0.04867
1 week	0.06900	0.07133	0.07300	0.08400
2 weeks	0.07567	0.07133	0.06867	0.09800
3 weeks	0.08367	0.07050	0.07050	0.10200
4 weeks	0.07200	0.07800	0.07300	0.10200

Table 4.8: Mean force required to detach FasL treated corneas over a period of 4 weeks in culture.

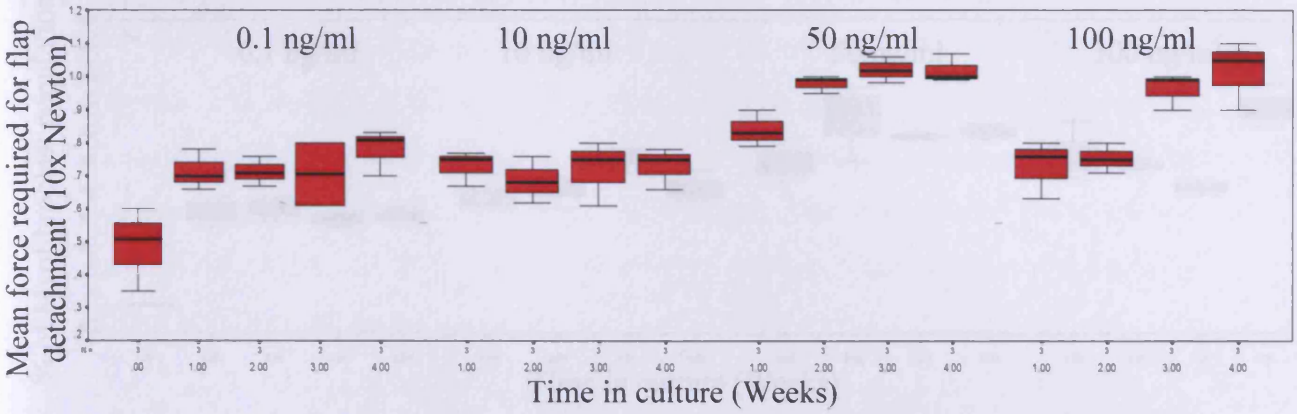

Figure 4.11: Graphs showing the effect of various concentrations of FasL on the flap adhesion

Low concentrations of the cytokine (i.e. 0.1 and 10 ng/ml) caused a significant increase in the mean force that it is required for flap detachment when compared to control untreated samples as shown in the graphs (Fig. 4.11). However, for these concentrations mean force values do not increase significant for the treated samples from 0 to 4 weeks after injury, as p value was too low ($p>0.05$). This a common statistical and in this case it will be considered that low concentrations of FasL do not increase significantly the mean force that it is required for flap detachment and therefore this concentration of the cytokine does not contribute to the improvement of flap adherence in LASIK-like corneal injuries. Higher concentrations of the cytokine, 50ng/ml and 100ng/ml, caused a statistically significant increase in the mean force that it is required for flap detachment during the second and the third week after injury respectively ($p<0.05$, Fig. 4.11). However, it was observed that there was not any further increase in mean force values thereafter. For example, in 50ng/ml samples there is a rapid increase in flap adherence during the first two weeks after injury. It then tends to stabilise towards the end of the organ culture time span (Fig. 4.11). For the 100ng/ml samples flap adherence increases during the first week, tends to stabilise and then it increases again during the third week after injury.

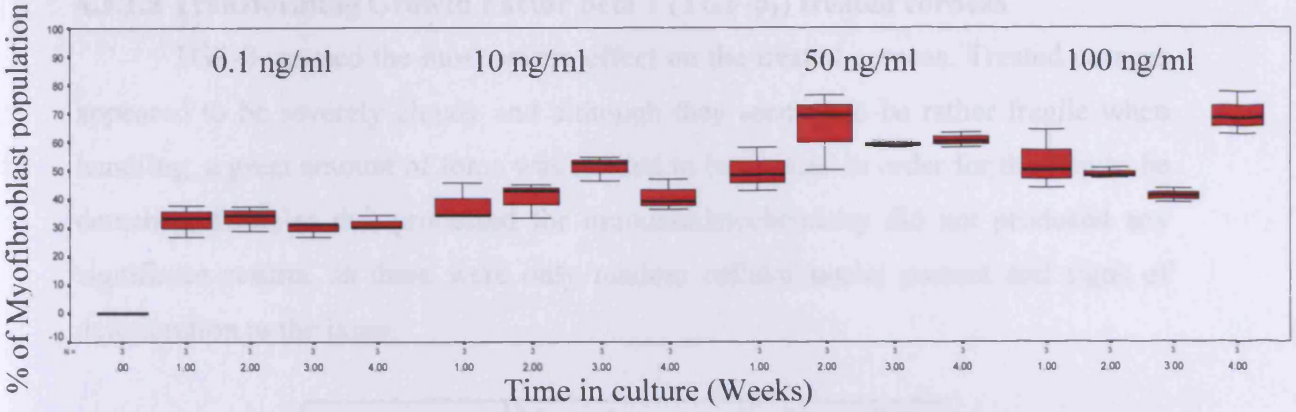

Figure 4.12: Graphs showing the effect of various concentrations of FasL on myofibroblast proliferation on the flap bed.

0.1ng/ml of FasL did not cause any significant increase in myofibroblast population during the four week culture time span ($p>0.05$, Fig. 4.12). 10ng/ml caused a significant increase in myofibroblast cell numbers between the second and the third week after injury ($p<0.05$). 50 and 100 ng/ml samples had a more significant effect in the increase of cell numbers towards early and late stages of the organ culture, respectively ($p<0.05$).

		0.1ng/ml	10ng/ml	50ng/ml	100ng/ml
Fas Ligand	1 week	Moderate Cloudy	Moderate Cloudy	Cloudy	Moderate Cloudy
	2 weeks	Moderate Cloudy	Moderate Cloudy	Cloudy	Moderate Cloudy
	3 weeks	Moderate Cloudy	Moderate Cloudy	Cloudy	Cloudy
	4 weeks	Moderate Cloudy	Moderate Cloudy	Cloudy	Cloudy

Table 4.9: Visual transparency assessment of FasL treated corneas over a 4 week period in culture.

FasL caused moderate opacities when it was applied at low dilutions in injured corneas (Table 4.9). 50ng/ml had the most severe effect in the clarity of the treated corneas, as it caused cloudiness in the corneas during the whole of the organ culture time span. Finally, 100ng/ml had a milder effect than the previous concentration as significant cloudiness was observed in the corneas after the third week in culture.

4.3.1.5 Transforming Growth Factor beta 1 (TGF-β_1) treated corneas

TGF-β_1 caused the most severe effect on the treated corneas. Treated corneas appeared to be severely cloudy and although they seemed to be rather fragile when handling, a great amount of force was needed to be applied in order for the flap to be detached. Samples that processed for immunohistochemistry did not produced any significant results, as there were only random cellular nuclei present and signs of deterioration to the issue.

	Mean force required to pull the flap apart (N)			
TGF-β_1 Concentration (ng/ml)	**0.1**	**10**	**50**	**100**
0 hours	0.04867	0.04867	0.04867	N/A
1 week	0.07100	0.07467	0.13800	N/A
2 weeks	0.06733	0.09000	0.13967	N/A
3 weeks	0.07733	0.12200	N/A	N/A
4 weeks	0.08400	0.13800	N/A	N/A

Table 4.10: Mean force required to detach TGF-β_1 treated corneas over a period of 4 weeks in culture.

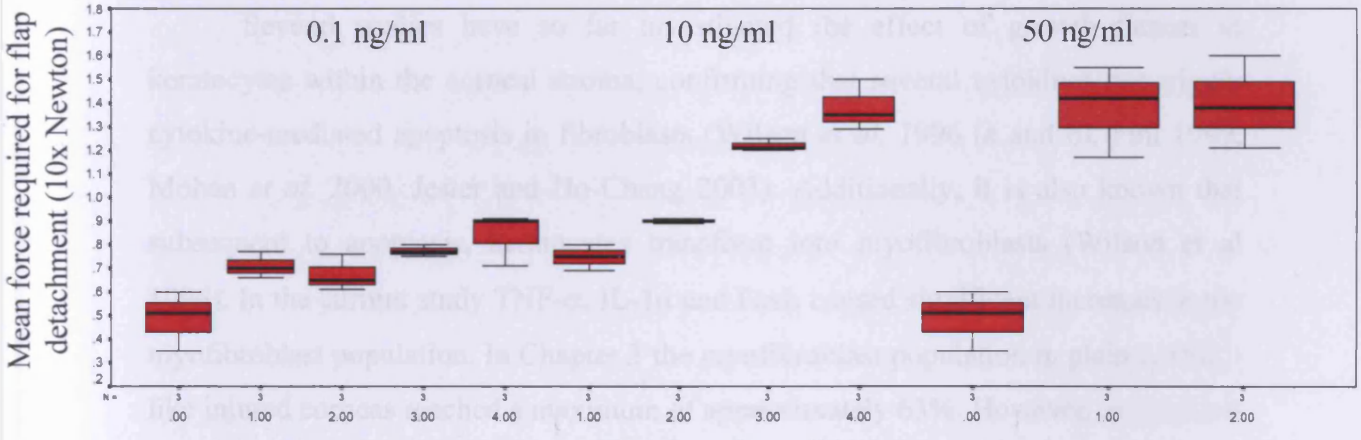

Figure 4.13: Graphs showing the effect of various concentrations of TGF-β_1 on the flap adhesion.

0.1ng/ml and 50ng/ml of the cytokine caused a gradual increase in the flap adherence. The effect of the cytokine was more rapid in the 10ng/ml treated samples as flap adherence kept increasing significantly every single week.

		0.1ng/ml	10ng/ml	50ng/ml	100ng/ml
TGF-β_1	1 week	Moderate Cloudy	Moderate Cloudy	Moderate Opaque	Opaque
	2 weeks	Moderate Cloudy	Moderate Cloudy	Moderate Opaque	Opaque
	3 weeks	Moderate Cloudy	Moderate Opaque	Opaque	Opaque
	4 weeks	Moderate Cloudy	Moderate Opaque	Opaque	Opaque

Table 4.11: Visual transparency assessment of TGF-β_1 treated corneas over a 4 week period in culture.

TGF-1β had the strongest effect on the corneas, as higher concentrations of the cytokine caused severe opacities and signs of deterioration to the tissue.

4.4 Discussion and conclusions

The main aim of this experimental set up was to enhance the appearance of myofibroblats in the stroma of injured corneas. This was achieved by treating injured corneas with growth factors that are known to cause either apoptosis (i.e. TNF-α, IL-1α, FasL) or myofibroblast transformation (TGF-β_1) to quiescent keratocytes in the corneal stroma.

Several studies have so far investigated the effect of growth factors in keratocytes within the corneal stroma, confirming that several cytokines can trigger cytokine-mediated apoptosis in fibroblasts (Wilson *et al.* 1996 (a and b), Fini 1999, Mohan *et al.* 2000, Jester and Ho-Chang 2003). Additionally, it is also known that subsequent to apoptosis, keratocytes transform into myofibroblasts (Wilson et al 1996). In the current study TNF-α, IL-1α and FasL caused significant increases in the myofibroblast population. In Chapter 3 the myofibroblast population in plain LASIK-like injured corneas reached a maximum of approximately 63%. However, in cytokine treated corneas, myofibroblast population clearly became denser and reached up to 80% for some of the dilutions of FasL and IL-1α. TNF-α also caused an increase in myofibroblast cell numbers (max≈70%) but it was not as intense as the effect that IL-1α and FasL had. There is no myofibroblast data for TGF-β_1 as stained samples had signs of deterioration of the tissue. Physically the tissue itself had visual signs of deterioration as it was extremely cloudy and fragile at the periphery. The preparation of the tissue was repeated several times and it always seemed to have the same

appearance. These observations lead to the conclusion that applying TGF-β directly onto the corneal stroma in such concentrations (i.e. 0.1, 10, 50 and 100 ng/ml) can be rather toxic for the tissue itself. The main role of TGF-β_1 is to induce the transformation of keratocytes to myofibroblasts (Wilson *et al.* 1996). Given that the quantity and the concentration of the applied cytokine were high, it triggered a very intense response in cell transformation. This disrupted the balance within the tissue that had fatal effects for the treated corneas.

All four cytokines applied to LASIK-like corneas in the current study increased significantly the flap adherence. However, flap adherence did not increase significantly for non-cytokine treated samples over the 4 week organ culture time span. This confirms that 4 weeks after injury flap recovery is poor and the cornea very unstable. However, previous studies have revealed that LASIK flap adhesion increases significantly 3 months after surgery (Kim *et al.* 2006). All concentrations of TNF-α, IL-1α and TGF-β_1 caused significant increase in flap adherence. FasL had the mildest effect as lower concentrations of the cytokine did not cause any significant increase in flap adherence. However, TGF-β_1 caused the maximum flap adherence among the four cytokines that were used. TGF-β_1 had the most severe effect in the corneas in all the assessments that were made, mainly because this cytokine has an immediate effect in myofibroblast transformation (Carrington *et al.* 2005). In fact, it has already been proposed that dilutions as low as 15 ng/ml of TGF-β_1 are known to cause maximal expression of αSMA in treated keratocytes (Micera *et al.* 2006). Additionally, according to Saika (2004) wound healing problems in the cornea can be treated by manipulating TGF-β signals. The findings of the current study and the suggestions in the literature imply that the application of TGF-β_1 can be ideal for increasing flap adherence and therefore corneal stability in LASIK-like injured corneas. However, a smaller quantity of the cytokine in a lower dilution is clearly required.

Samples that were characterised with the same visual assessment in terms of transparency (i.e. clear, moderately cloudy, etc) seem to have similar values of flap pulling forces as well as myofibroblast increases. This observation implies that there might be a possible correlation between the degree of transparency, hence myofibroblast expression and the extent of flap adherence. Therefore, the application of certain cytokines for the improvement of flap adherence might be useful in further medical practice It is obvious that different, lower dilutions need to be applied in

order to avoid compromising the clarity of the corneas, a vital feature for the function of the tissue. Therefore, it is possible to improve flap adherence using these cytokines, but this is achieved at the expense of corneal clarity. Maintaining corneal transparency is essential for a normal visual function to occur. Therefore, it is important to determine an optimal correlation between cytokine type/dilution and improved flap adherence.

5. Investigation of collagen ultrastructure in normal, LASIK-like and trephine wounded corneas

5.1 Introduction

X-ray diffraction experiments have been widely used to gain important information about the ultrastructure of connective tissue. In the current study synchrotron radiation was used (Daresbury Laboratories, UK- Fig. 5.1) to obtain information about the structure of collagen within the cornea following trephine and LASIK-like wounding and healing in the culture system.

Accelerating an electron beam within a magnetic field to the speed of light produces synchrotron radiation. A series of magnets is used in order to bend the electron beam and accelerate it into a circular shape. As they pass these "bending" magnets, the path of the electrons is deflected and they emit an intense beam of light, known as synchrotron radiation. The beam has the shape of a cone in front of the electron. The spectrum of synchrotron radiation covers the part of the electromagnetic spectrum from infra-red through to gamma-rays (Margaritondo 1988, Meek and Quantock 2001).

Figure 5.1: Aerial photo of the Synchrotron Radiation Source (SRS) in Daresbury, UK (Picture taken from http://es1.ph.man.ac.uk/research/sync/daresburyr.jpg)

Synchrotron radiation is much more intense than common laboratory radiation sources and therefore it enables scientists to run experiments in a relatively short time and hence obtain readings from multiple samples. This is also very important as the tissue is not exposed for a long time and therefore there are minimal degradation effects on the

samples.

For convenience, x-rays are passed through the entire thickness of the cornea, parallel to the optical axis. The x-ray beam has a finite cross-section so x-ray diffraction yields the average values of ultrastructural parameters by averaging the whole depth of the area of the cornea that is examined. By scanning across the tissue, patterns from each position allow spatial variations in these structural parameters to be mapped and to be compared between wounded and unwounded tissues.

5.2 Methods

5.2.1 Sample preparation

Bovine corneas were wounded (either trephined or in a LASIK-like fashion) and organ cultured as previously described (section 2.1). Unwounded clear corneas were also organ cultured and were used as controls. Corneal samples were removed from the organ culture at various time points (i.e. 0, 1, 2, 3 and 4 weeks), wrapped in Clingfilm and immediately frozen in liquid N_2. Samples were then kept at -80°C until they were transferred to Synchrotron Radiation Source (Daresbury, UK); freezing does not affect the structural parameters being measured (Fullwood and Meek 1994). While transferring to the SRS stations samples were kept in an isothermic box containing dry ice and placed in a -80°C freezer upon arrival. The samples were finally thawed before exposed to the x-ray beam.

5.2.2 X-ray diffraction

LASIK-like and trephine wounded and unwounded control corneas were scanned at stations 2.1 and 14.1 in Daresbury SRS (Fig: 5.1). Station 2.1 (small angle), has a long camera and this allows us to measure parameters such as the centre to centre collagen inter fibrillar spacing (IFS) and fibrillar diameter. The set up in station 14.1 (wide angle), is suitable for measuring molecular parameters of collagen such as direction and distribution.

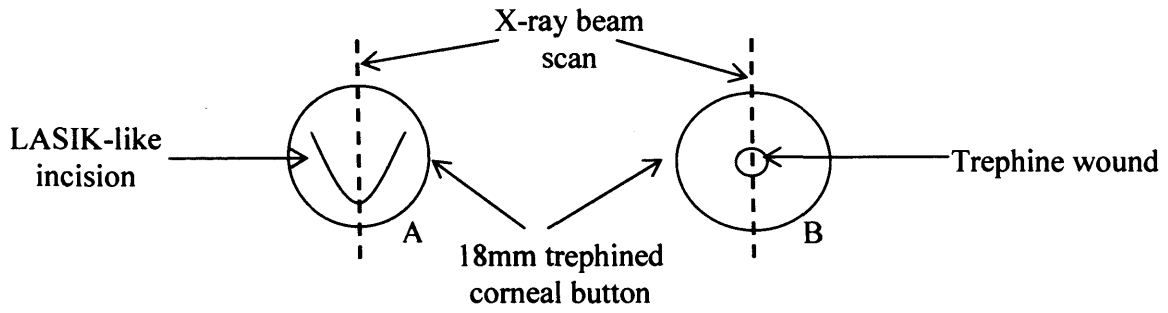

Figure 5.2: 18mm corneal circular area including the LASIK-like incision. For the wide angle x-ray diffraction experiments the whole area was scanned. For small angle experiments a cross section of the cornea (blue dashed line) was scanned (A). 18mm corneal circular area with a 5mm trephine wound in the middle. A cross section of the cornea was scanned (blue, dashed line) in order to observe interfibrillar spacing (IFS) and fibrillar diameter variation outside the wound, whereas the whole corneal button was scanned for wide-angle experiments (B).

During data collection all samples were wrapped in cling film and placed in an airtight Perspex/Mylar chamber in order to prevent dehydration of the tissue. X-rays were passed through the anterior corneal face, parallel to the optical axis, and the small and wide angle diffraction patterns recorded on a detector situated behind the specimen. Before data collection the x-ray beam had to be located. This was achieved by exposing a piece of green x-ray sensitive paper that was mounted on graph paper and placed in the sample holder for 10 sec. A red dot was created by the x-ray beam on the green paper and with the use of the attached graph paper the exact position of the x-ray beam was located.

Small angle x-ray scattering (SAXS) was performed in station 2.1 at the UK Synchrotron Radiation Source (Daresbury laboratories) using an evacuated camera of length 8.25m and a focused monochromatic beam x-ray beam (λ=0.154nm). These series of experiments were performed in order to measure fibrillar diameter and spacing as previously described by Meek and Quantock (2001). The x-ray patterns were recorded at different positions across the cornea as shown in Fig. 5.2. For trephine wounded samples point 0,0 was placed right in the middle of the wound and 9mm scans were performed towards the periphery on either sides. The LASIK-like samples were scanned in a similar

manner, by positioning point 0,0 in the flap incision and extending 11mm towards the nasal and 6mm towards the temporal regions of the corneal button. The size of the beam was 1mm^2, the step size was 1mm and the exposure time was 90sec.

Wide angle x-ray scattering (WAXS) was performed in station 14.1. at the UK Synchrotron Radiation Source (Daresbury laboratories). This method was used to map the collagen distribution and orientation across the cornea as described by Aghamohammadzadeh *et al.* (2004). The whole of the 18mm corneal button was scanned using a 1mm^2 beam, at 1mm steps, with exposure time of 30sec. A lead backstop was positioned between the detector and the sample in order to stop any undeviated rays. The ion chamber was placed in between the incident x-ray beam and the specimen.

5.2.3 Data analysis for SAXS

Data analysis for SAXS experiments was performed using a Unix based graphics program (Fit2D, produced by Dr Hamersley, ESRF, Grenoble, France) and Windows based programs (Statsoft Statistica and Microsoft Excel).

Initially, each data file was normalised against the appropriate ion chamber reading in order to compensate for any beam current decay during data collection. Then, the detector response pattern was removed from each normalised image to obviate systematic error caused by the detector's non-uniform response. An intensity profile of the x-ray pattern was then created by taking a vertical centrally located transect of the pattern. The intensity pattern was then folded in the middle of the pattern, as it is symmetrical, to increase the signal/noise ratio. The scatter intensity (I) was then multiplied by the radial position (R); because only a small sample of the pattern was used, the integrated intensity distribution profile and therefore the use of a linear scan across the x-ray pattern, had to be corrected.

Bragg's law states:

$$n\lambda = 2M\sin\theta$$

where n is the order of diffraction, λ is the wavelength of the radiation, M is the Bragg spacing and 2θ is the scattering angle. The size of the structure that causes the scattering is therefore inversely related to the scattering angle. At this stage of the analysis, the intensity distribution is described as a function of radial distance (R) from the centre of

the pattern in pixels. The first step, therefore, was to calibrate the system and this was done using the 67nm meridional reflection from wet rat-tail tendon. Because the patterns were obtained at very low angles, the small angle approximation could be used, whereby $\sin\theta \approx \tan\theta \approx \theta$. With this approximation, one can obtain the Bragg spacing corresponding to the interfibrillar spacing using:

$$M = 67 \times R_{RTT} / R_c,$$

where R_c is the position of the interfibrillar peak in the corneal x-ray pattern and R_{RTT} is the position of the first order in the meridional pattern from rat tail tendon. Collagen fibrils are thought to be arranged with liquid-like packing, so the Bragg spacing is multiplied by the factor 1.12 to obtain the interfibrillar spacing (Worthington and Inouye 1985, Meek and Quantock 2001).

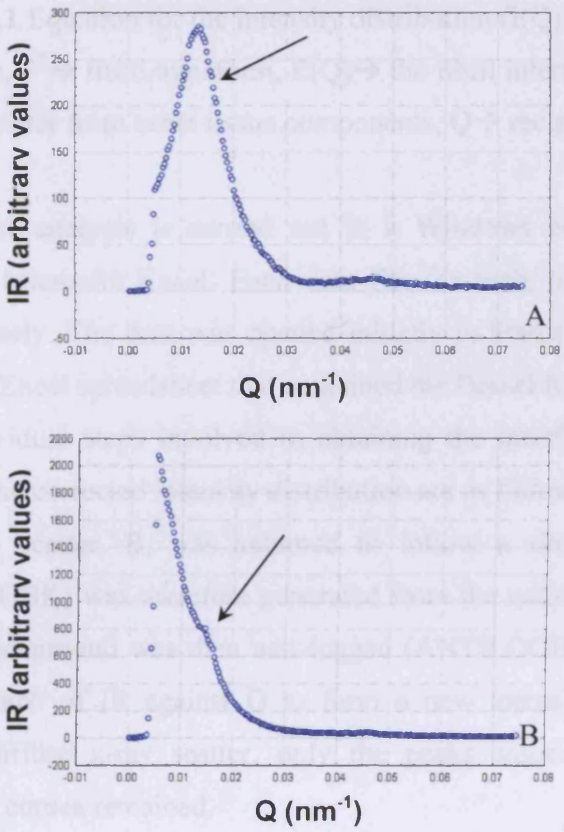

Figure 5.3: A common intensity profile, first order collagen pointed out by arrow (A) and a highly disordered pattern, where first order collagen peak appeared as a small shoulder (arrow in B). Both patterns were taken from a LASIK-like injured bovine cornea.

Figure 5.3 shows intensity profiles from two adjacent areas in a LASIK-like injured cornea; the second graph represents the incision site. X-ray intensity is plotted against the reciprocal space co-ordinate Q (=1/M). The first peak arises from the interference function and the subsidiary peak from the fibril transform (Meek and Quantock 2001). A sharp first peak indicates ordered collagen whereas a diffuse peak or shoulder indicates a more disordered packing. Equation 5.1 is the mathematical basis of Figure 5.3 showing how the observed intensity I(Q), the fibril transform, and the interference function due to the fibril packing E(Q), are related

$$I(Q)=F^2 E(Q)+B$$

Equation 5.1 Equation for the intensity distribution (I(Q)→ integrated intensity distribution, F^2→ fibril transform, E(Q)→ the fibril interference function, B→ background scatter from other tissue components, Q→ reciprocal space coordinate).

At this stage, the analysis is carried out in a Windows environment using StatSoft Statistica 6 and Microsfot Excel. Each data file for each 1mm that was scanned was processed separately. The data was opened initially in Statistica and each Statistica file was linked to an Excel spreadsheet that contained the Bessel function.

The individual steps involved in obtaining the interfibrillar spacings and fibril diameters from the corrected intensity distribution are as follows:

The background scatter, B, was assumed to follow a simple power law. A linear background (LOGBK) was therefore generated from the natural log graph of IR against Q. The linear background was then anti-logged (ANTILOGB) and subtracted from the image profile graph of IR against Q to form a new intensity profile (IR_B). After removing this diffuse x-ray scatter, only the peaks associated with the low angle reflections of the cornea remained.

Collagen fibrils can be considered as non-ending cylindrical structures. Scattering from such cylinders (the fibril transform) takes the mathematical form of a 1st order Bessel function. This has a low broad peak as a subsidiary maximum that appears close to the 3rd order of the collagen meridional reflection. In order to calculate the fibril diameter,

a Bessel function graph was plotted superimposed on the IR_B vs Q graph. The program allowed the height and position of the Bessel peak to be adjusted to achieve the best fit with the IR_B graph. The first maximum in a Bessel function appears at a distance that it is inversely related to collagen fibrillar diameter (d). Considering the fact that the distance of the Bessel peak is inversely proportional to the Braggs spacing (M) in its maximum, there is a simple relationship between M and d and using the following equation (Eq. 5.1) it is possible to calculate the fibril diameter of collagen.

$$d = 2 \times \frac{5.14M}{2\pi}$$

Equation 5.2: Equation for calculating collagen fibrillar diameter (d, fibril diameter; M, Bragg spacing of the subsidiary maximum)

5.2.4 Data analysis for WAXS

Data analysis for WAXS experiments was performed using a Unix based graphics program (Fit2D, produced by Dr Hamersley, ESRF, Grenoble, France) and Windows based programs (Microsoft Excel and Media Cybernetics Optimas 6.5).

In order to correct the beam current decay during data collection an x-ray intensity value was calculated by multiplying the average ion reading from each exposure by the exposure time in sec (i.e. 30sec). This value was then used to normalise the corneal x-ray pattern.

Each of the 200–400 lamellae in the path of the x-ray beam produces an equatorial diffraction pattern (Meek and Quantock 2001). Because lamellae occur at all angles within the plane of the cornea, this pattern appears as a number of concentric circles that span out from the centre of the pattern. The centre of the pattern and the intensity of 120 circles for bovine corneas were determined using Optimas 6.5 in the current study.

In brief, each circular diffraction pattern was divided into 256 equal sectors and the average intensity was calculated for each one of them. Then, the integrated intensity was plotted as a function of radial distance from the centre of the pattern for each sector producing 256 graphs. Background scatter varies with radial distance from the centre of

the pattern and it had to be removed. A power law curve was fitted to either side of the collagen peak on the plot of scattering intensity versus radial distance for each pattern resulting to the subtraction of the fitted curve from the original data and therefore the removal of the background scatter (Daxer and Fratzl 1997).

A single intensity value from each point of the circumference of the collagen reflection was obtained by integrating radially all the 256 normalised plots. The profile of collagen x-ray scatter intensity relative to radial position was then converted to a profile of collagen x-ray scatter to angular position around the x-ray diffraction circular pattern. The profiling started at 3 o'clock position of the circular pattern and carried on in an anticlockwise direction (covering 0-360 degrees). At this stage, the area below the graph line represents the total collagen mass, which consists of both collagen lying in all directions (isotropic collagen) and fibrillar collagen with a preferred orientation (aligned collagen) (Fig. 5.4B). The index of orientation is then the ratio between the scattering of preferentially aligned collagen and the total scattering of collagen.

During the last stage of the analysis polar plots were created in order to have a visual, more comprehensive representation of the actual orientation of collagen, as well as its relative quantity towards a given direction of preferred orientation. The scattering from isotropically orientated collagen was removed leaving just the aligned collagen scatter relative to angular position (Fig. 5.4C). The data for the aligned collagen was then shifted along the x-axis by 90°, as x-rays once they hit the collagen they scatter at right angles to the direction of the fibril axis. A new graph was then created showing the preferentially aligned scatter intensity versus the angle of molecular orientation. This data was also plotted in Microsoft Excel as a propeller-shaped 360° polar plot. A polar plot represents the preferred orientation of collagen towards a given direction in a particular point of the tissue. The maximum dimension of a polar plot is representative of the amount of fibrils in a given direction.

Total scatter from each diffraction pattern was found by integrating the area under the scattering intensity versus rotation angle graph (Figure 5.4B). This was done for the collagen diffraction maxima from each scattering pattern, resulting in a matrix of 32 × 36 intensity values. These data were displayed as a contour plot using Microsoft Excel software. A contour plot displaying total scatter from only the preferentially aligned

collagen was produced in the same way, except that only the preferentially aligned scatter (unshaded region in Fig. 5.4B) was integrated.

5.2.5 Statistical analysis

All statistical analysis was performed using the statistics software package SPSS. Three samples of control and wounded corneas were used for each time-point. Initially all data was tested for its normality and then a one-way ANOVA test was performed between control and wounded corneas for each different scan (points between -9 to 9 for trephined wounded corneas and -6 to 11 for LASIK-like ones). Finally, an independent t-test was used in order to compare overall the data between wounded and control corneas for each time point.

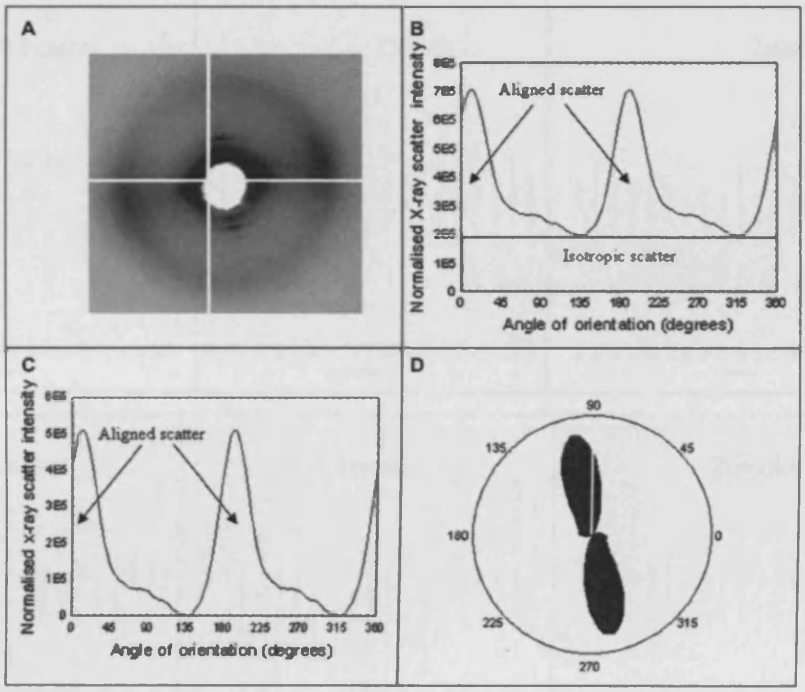

Figure 5.4: Part of the analysis for wide angle x-ray scattering. Initially, an x-ray scattering pattern that was created by passing a beam of X-rays through the cornea parallel to the optical axis (A). Intensity profiles of total and isotropic collagen X-ray scatter (B) and preferentially aligned collagen alone (C) as a function of angular position around the scatter pattern. Example of a polar plot (D). The size of the polar plot and its radial extent in any given direction represents the amount of collagen preferentially orientated in that direction (Picture taken from Hayes *et al.* 2007).

5.2.6 Transmission electron microscopy (TEM)

TEM was used in this project purely to visualise the ultrastructure of the bovine corneal stroma. The procedure was performed as previously described in chapter 2.

5.3 Results

5.3.1 Small angle x-ray scattering (SAXS)

Trephine wounded corneas

Fibrillar diameter and IFS in control corneas

Neither fibrillar diameter nor IFS was affected by the culture system and both these variables remain constant during the organ culture time-span (Fig. 5.5). The IFS increased slightly during the third week in culture.

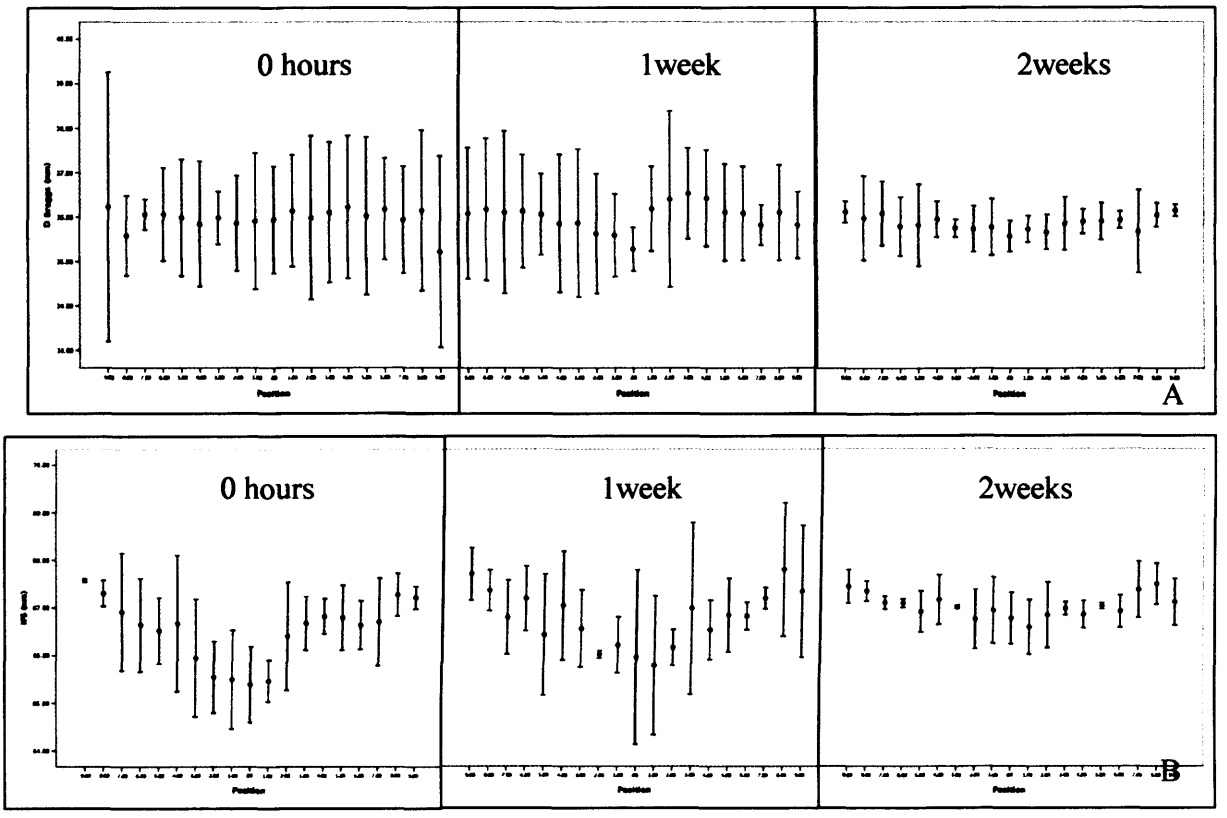

Figure 5.5: Graphs representing Bragg fibril diameter (A) and interfibrillar spacing (B) for control corneas over a time of two weeks in culture- Error bars represent standard error of mean.

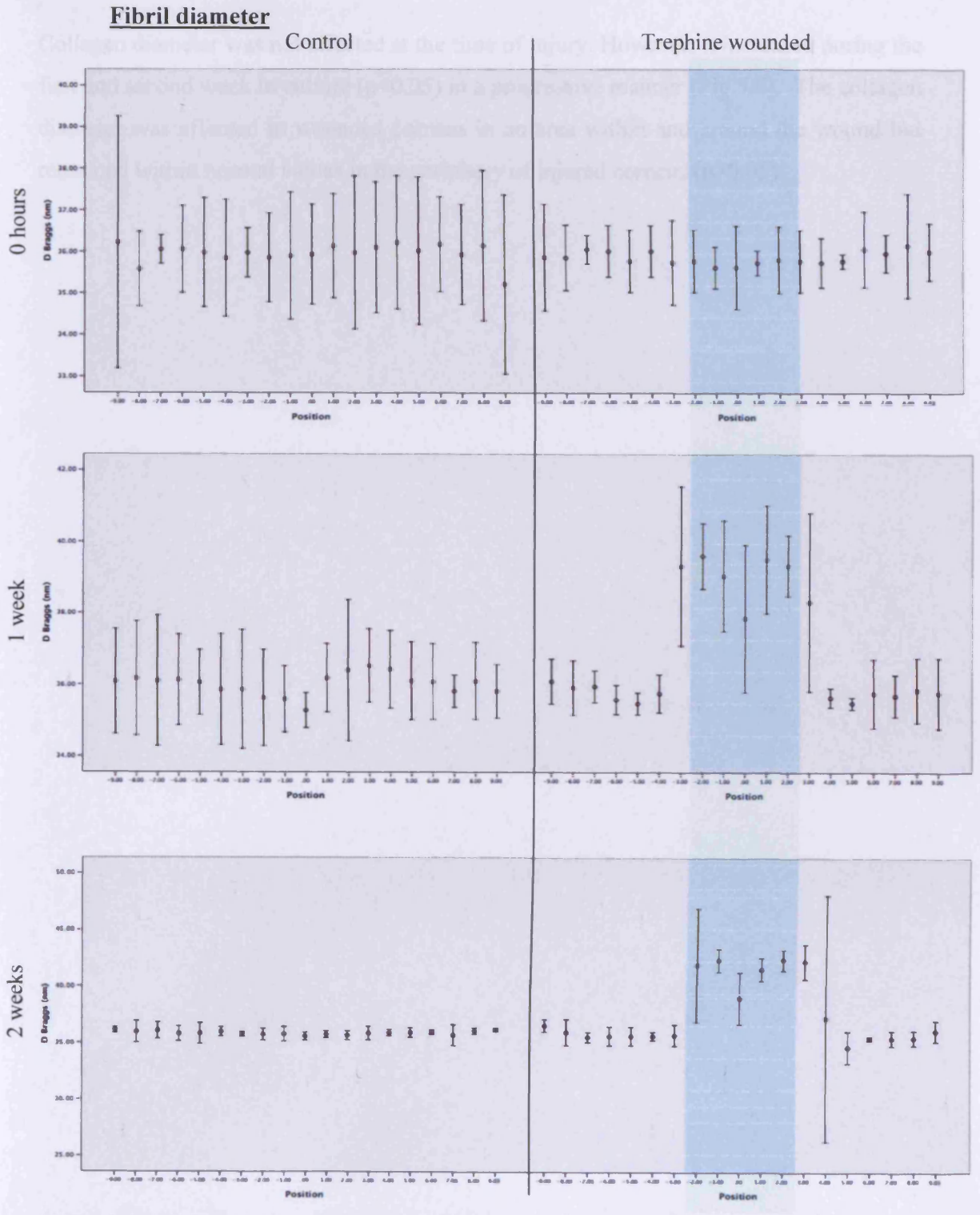

Figure 5.6: Collagen fibril diameter for control and trephine wounded corneas for a two weeks organ culture time span (Pale blue area indicates the position of the wound- Error bars represent standard error of mean)

Collagen diameter was not affected at the time of injury. However, it increased during the first and second week in culture ($p<0.05$) in a progressive manner (Fig.5.6). The collagen diameter was affected in wounded corneas in an area within and around the wound but remained within normal values in the periphery of injured corneas ($p>0.05$).

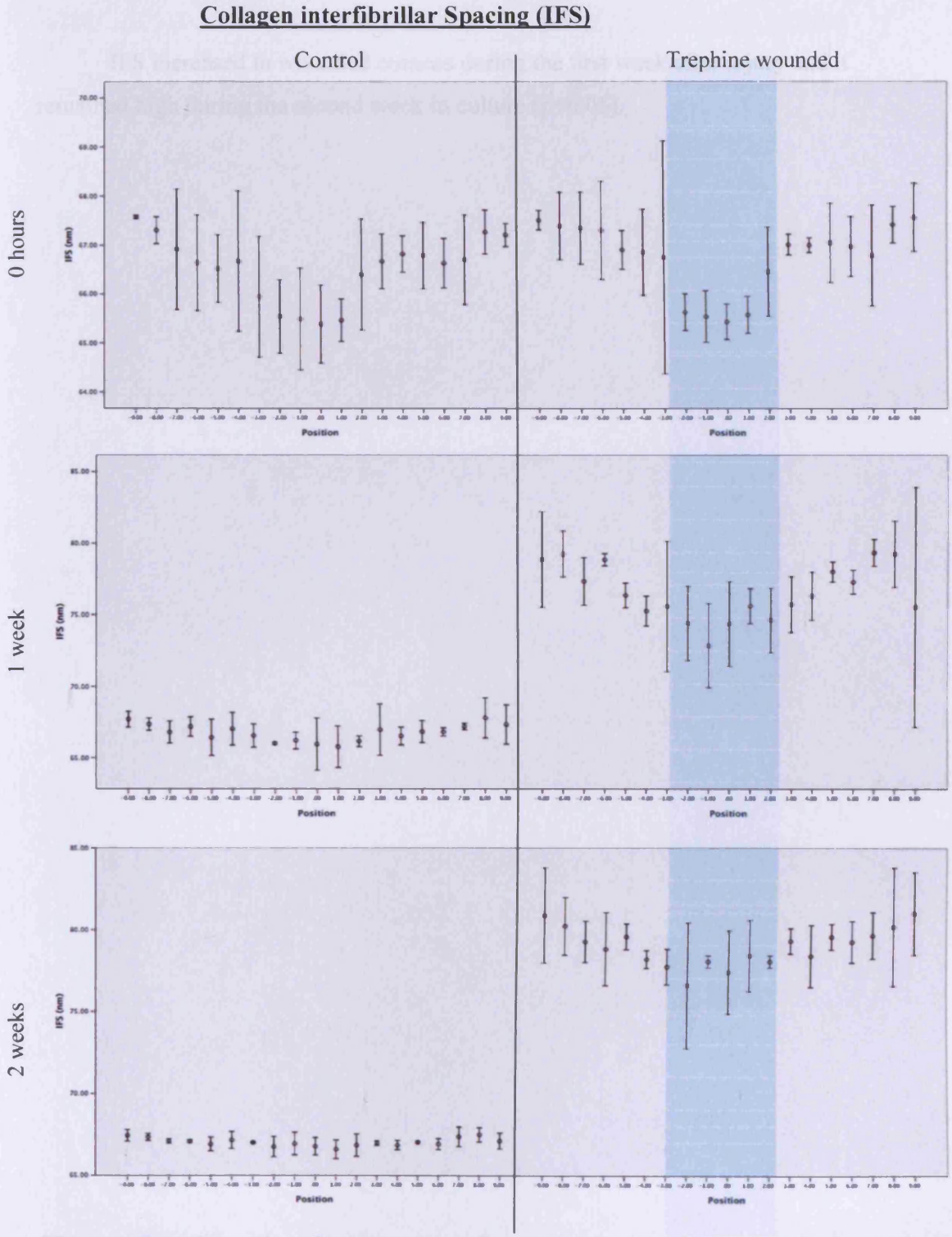

Figure 5.7: Collagen interfibrillar spacing for control and trephine wounded corneas for a two weeks organ culture time span (Pale blue area indicates the position of the wound- Error bars represent standard error of mean)

IFS increased in wounded corneas during the first week after injury and it remained high during the second week in culture ($p<0.05$).

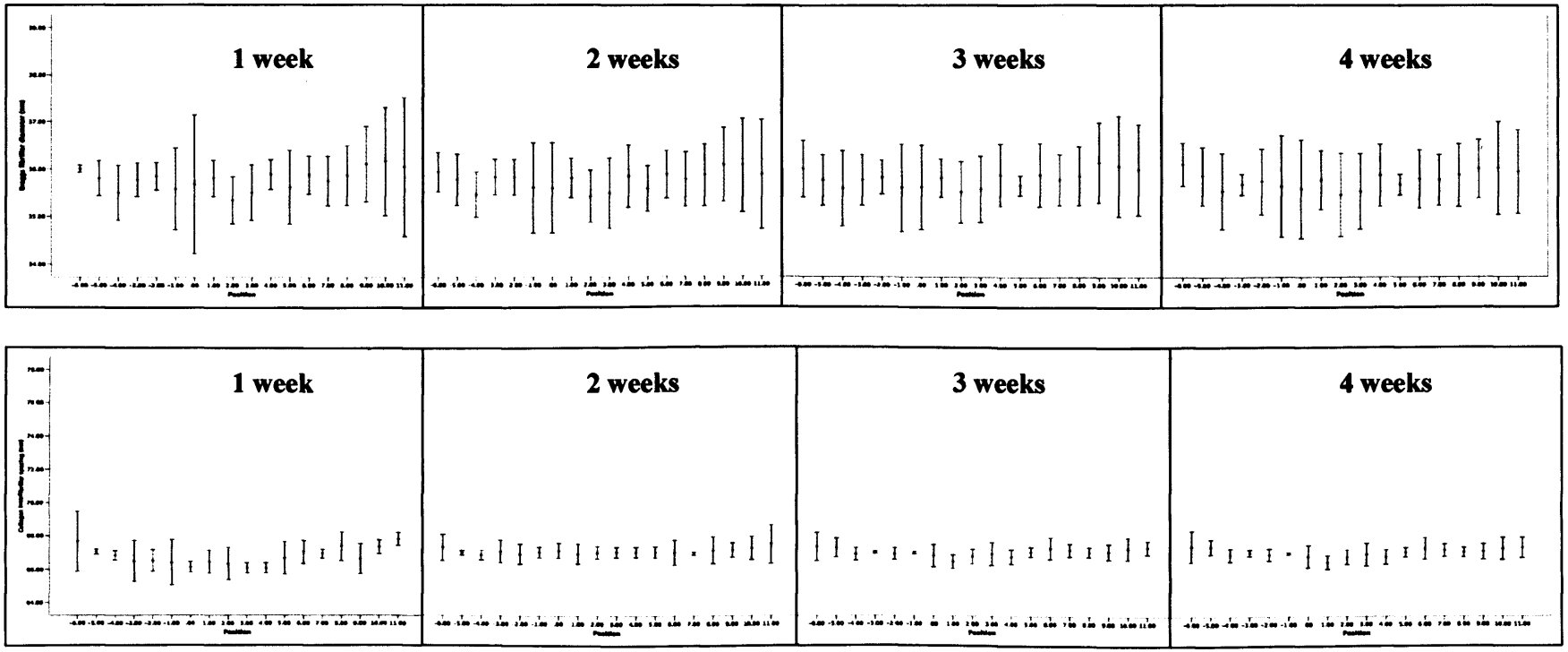

Figure 5.8: Graphs representing fibril diameter and interfibrillar spacing for control corneas over a time of four weeks in culture-Error bars represent standard error of mean.

Neither fibril diameter nor IFS was affected by the culture system and both these variables remained constant during the organ culture time-span (Fig. 5.8).

Fibril diameter

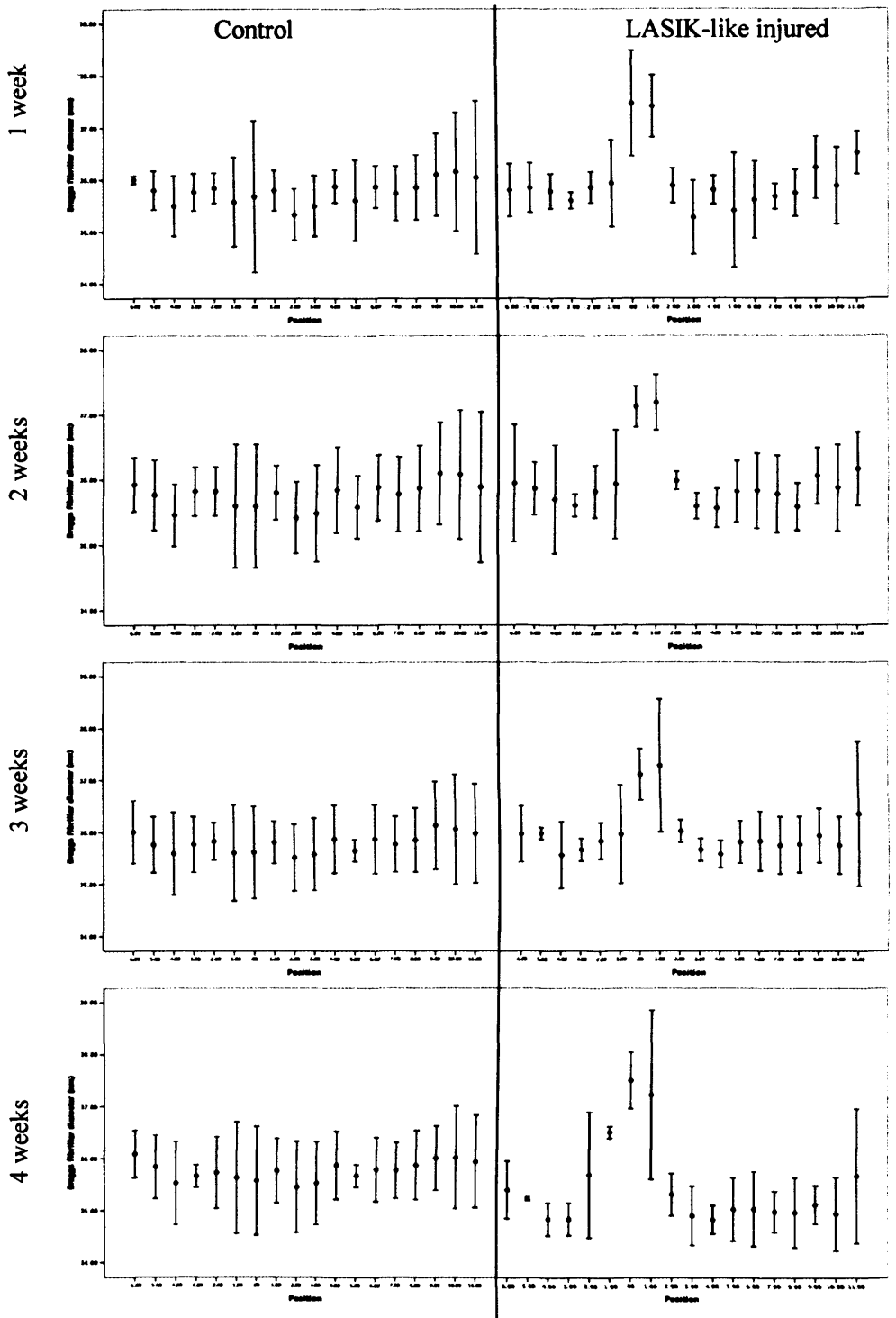

Figure 5.9: Collagen diameter for control and LASIK-like injured corneas for a four weeks organ culture time span (incision site for LASIK-like flap at 0,0- Error bars represent standard error of mean)

Collagen diameter increased after the first week in culture ($p<0.05$) in a progressive manner (Fig.5.9) in an area in and around the incision site only. Collagen diameter remained within normal values in the periphery of injured corneas ($p>0.05$) and mid flap areas.

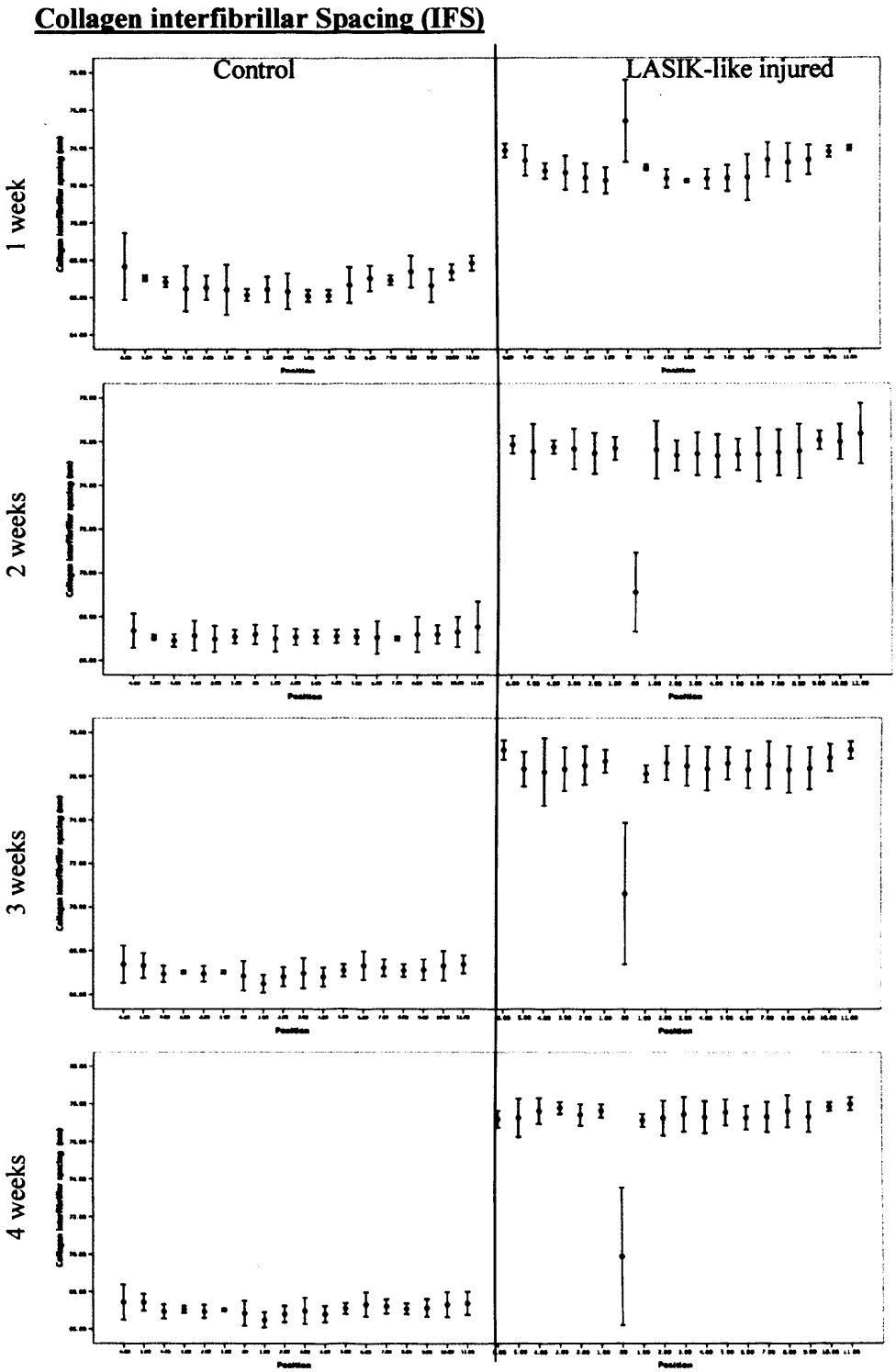

Figure 5.10: Interfibrillar spacing for control and LASIK-like injured corneas for a four weeks organ culture time span (incision site for LASIK-like flap at 0,0- Error bars represent standard error of mean)

Collagen interfibrillar spacing increased in injured corneas during the organ culture time span and provided that this was not the case with the corresponding controls, it can be concluded that corneas swell during the wound healing process. The interfibrillar spacing did not show a consistent change at the incision site, but that was a sign of the high disorder of the tissue in this specific area.

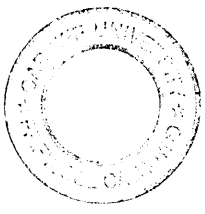

5.3.2 Transmission electron microscopy (TEM)

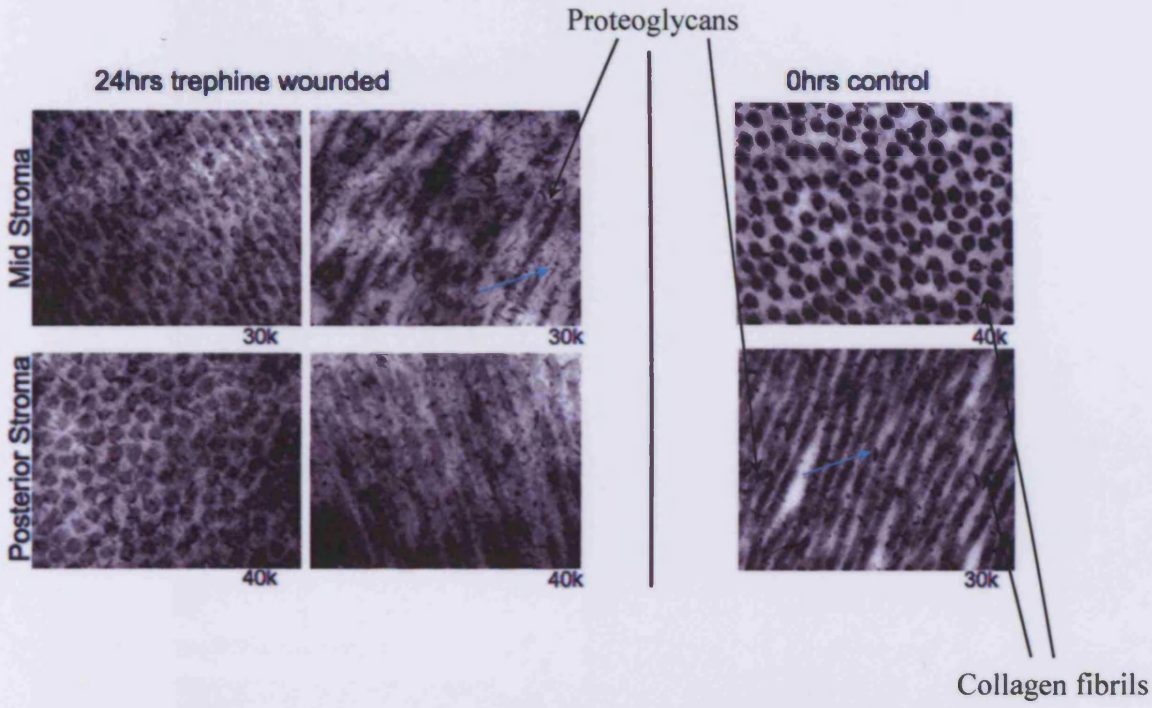

Figure 5.11: Electron micrographs, obtained using the critical electrolyte method, representing area in mid and posterior stroma of trephine wounded corneas within 24hrs of injury (A). Control cornea in a posterior site of the stroma (B). Turquoise arrows point out the difference in size between proteoglycan molecules in injured and uninjured corneas.

Shortly after injury abnormally large proteoglycan molecules appear in an area proximal to the trephine wound. There is an obvious difference in the size of the proteoglycans found in mid stroma of injured corneas and the ones found in control corneas (Fig. 5.11 A and B).

5.3.3 Wide angle X-ray scattering (WAXS)

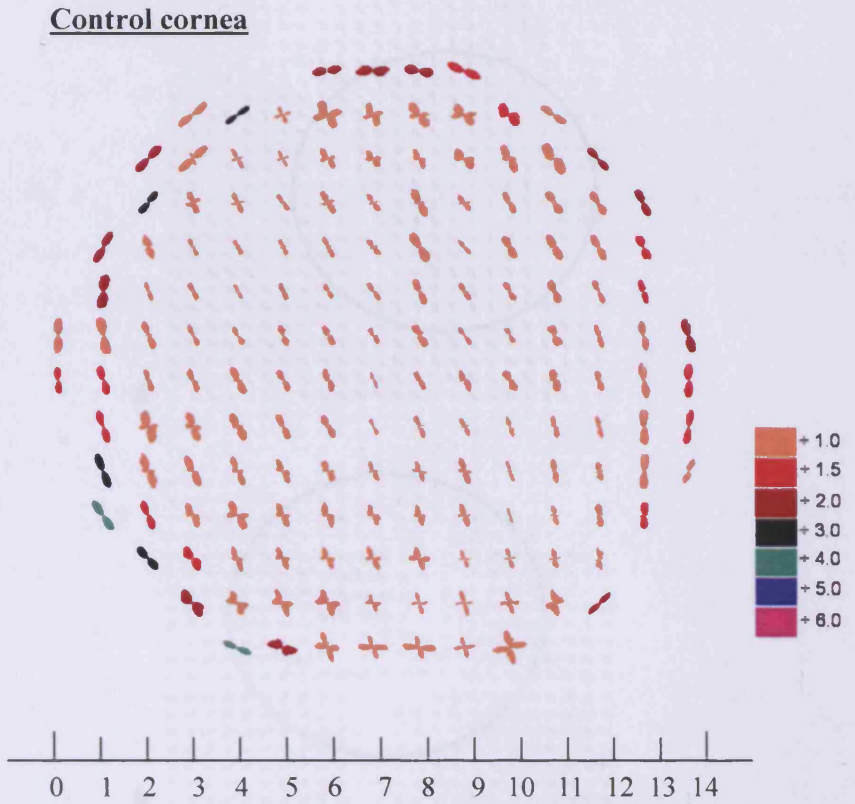

Figure 5.12: Polar plot map showing the preferred orientation of fibrils in a control bovine cornea. Fibrils tend to have a vertical preferred orientation (the map is switched 30 degrees anticlockwise off in vivo orientation). Plots have been scaled down by the factors shown in the colour key and metric scale is in millimeters-Courtesy of Dr S Hayes

Collagen fibrils in bovine corneas tend to have a vertical preferred orientation in a major part of the tissue. However in the periphery of the cornea this pattern obtains a circular orientation.

Trephine wounded corneas

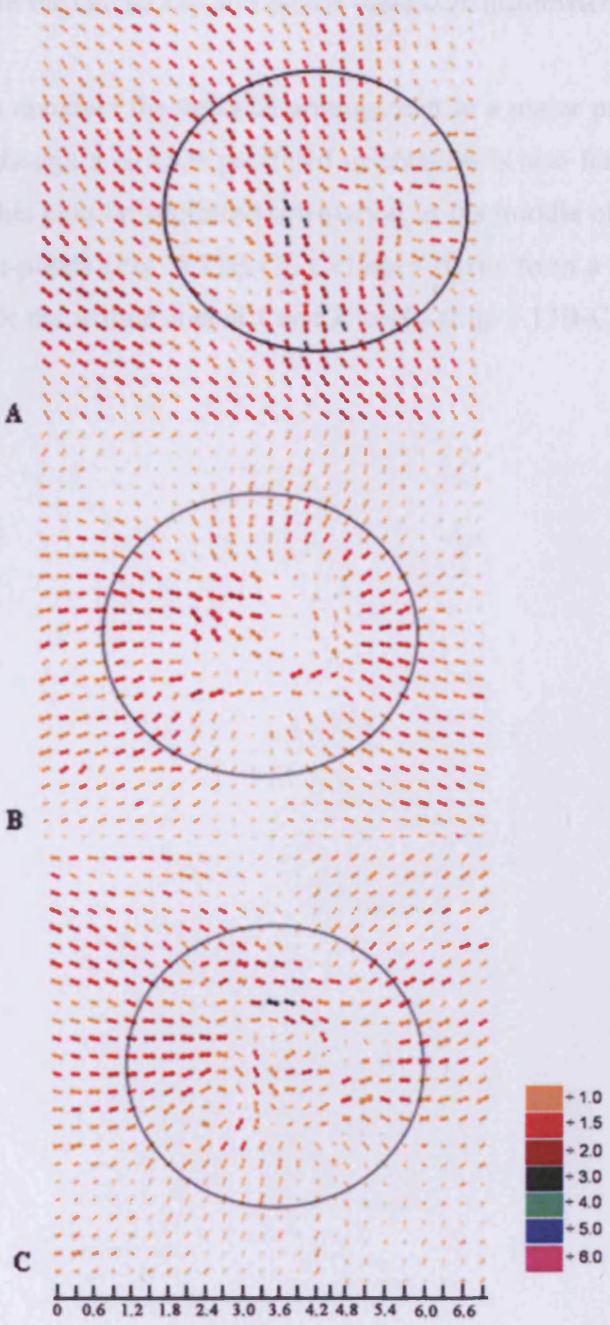

Figure 5.13: Polar plot map showing the preferred orientation of fibrils in a centrally located 6.9×6.9mm area from a trephine wounded cornea over a two week culture time span (A-C). The wound was placed in the middle of the scan and the pictures depict trephine wounded corneas at 0hrs (A), 1 week (B) and 2 weeks (C). Solid circle

represents the size and approximate position of the wound. Plots have been scaled down by the factors shown in the colour key and metric scale is in millimeters.

Fibrils tend to maintain the uniaxial arrangement in a major part of the cornea at 0hrs (Fig. 5.13A), although a circular proffered orientation is also formed in the middle of the wound area. This circular preferred orientation in the middle of the wound is also observed at later time-points (Fig. 5.13B-C). Collagen fibrils form a radial arrangement both outside and inside the wound area at 1 and 2 weeks (Fig. 5.13B-C).

LASIK-like wounded corneas

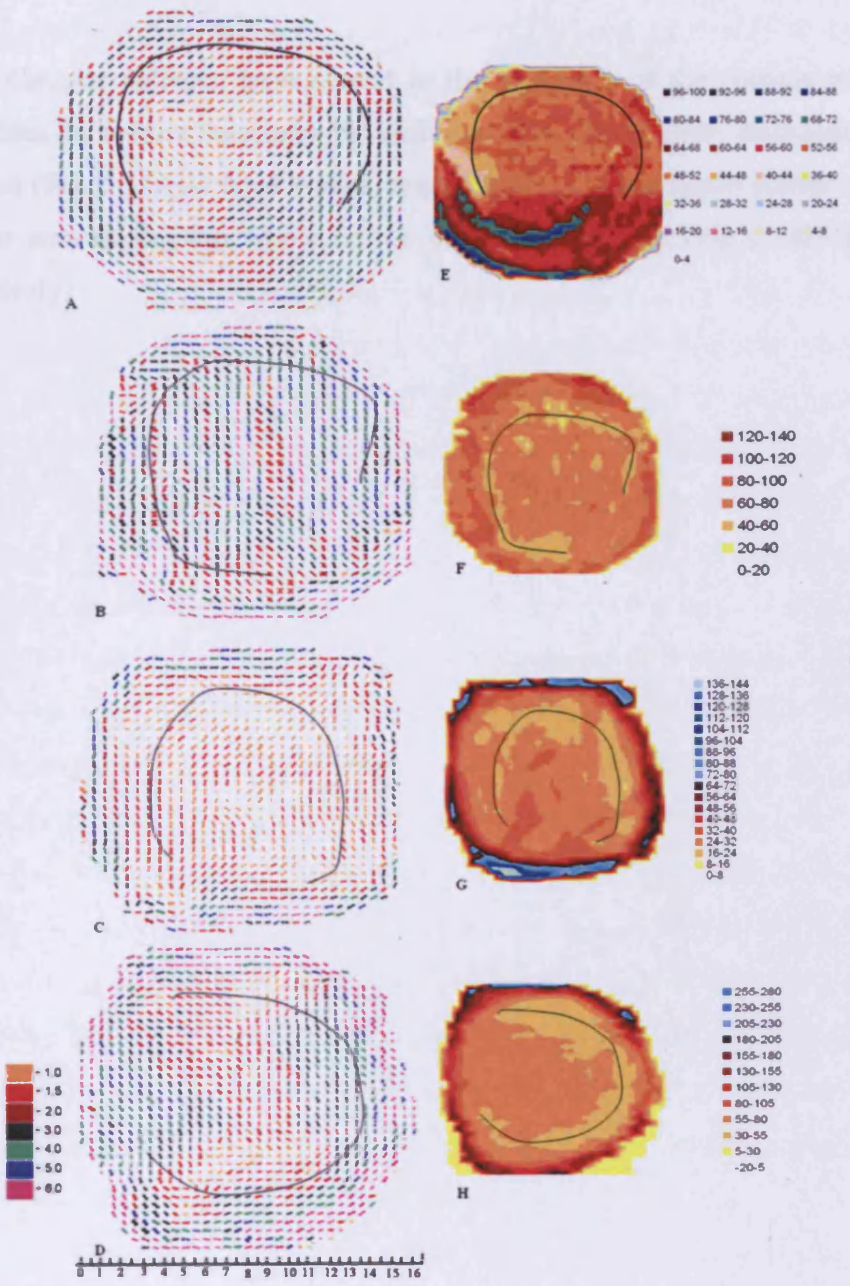

Figure 5.14: Polar plot maps of x-ray scatter (A-D) and contour maps of total collagen (E-H) showing the orientation and distribution, respectively, of fibrillar collagen across LASIK-like injured corneas at 1, 2, 3 and 4 week after injury. The scan covered an area

that included the whole of the flap as well as the hinge. Plots have been scaled down by the factors shown in the colour key and metric scale is in millimeters.

Circular collagen arrangement in the periphery of the corneas was maintained throughout the culture time span, but collagen seemed to be fairly disorganized within the flap area (Fig. 5.14A-D→1-4 weeks, respectively). Total collagen scatter was less in the incision area during the whole of the organ culture time (Fig 5.14E-H→1-4 weeks, respectively)

5.4 Discussion and conclusions

The present study revealed important information about the collagen ultrastructural changes in bovine corneas shortly after injury. Fibril diameter increased during the first week in culture and it kept increasing in a progressive manner for the rest of the organ culture time span showing that a stromal repair process had been in progress. Fibril diameter in trephined corneas increased in an area within the wound but also in an area beyond the wound margin of about 1mm. The interfibrillar spacing increased throughout the whole of the corneal buttons within a week after injury and it kept increasing during the rest of the organ culture time. However, in trephine wounded corneas the interfibrillar spacing was increased compared to the corresponding controls, but the spacing was lower in the middle of the tissue, at the wound area, than the periphery. According to Connon and Meek (2004) the presence of a disorganized fibril arrangement inhibits the normal swelling of the scar tissue, and therefore interfibrillar spacing remained reduced in full-penetrating corneal wounds in rabbits. The extent of swelling in injured corneas was more severe in trephine-wounded samples than in LASIK-like ones. What is more, at the incision site in LASIK-like corneas, the interfibrillar spacing was lower than the rest of the cornea. According to Rawe *et al.* (1994) the gradual reduction in the spread of interfibrillar spacing is possibly related to the progressive decrease in the light scattered from the tissue as the wound heals. McCally *et al.* (2007) suggest that the wound site in fully penetrating wounds in rabbit corneas continues to scatter a significant amount of light even 4.5years after wounding. The unusual pattern that was observed in the IR_B versus Q graph during data analysis in scans from the incision site also indicates a high level of disorder at the incision site, a finding that supports even more the fact that collagen fibrils were highly disordered at the incision site.

Upon injury, for trephined samples, the whole 5mm was excised and the corneas were left to heal in culture. On the contrary, in LASIK-like samples, the corneal stroma was sliced and the flap was repositioned back in place. Therefore, the trephine wounding is a more severe kind of injury that effectively disrupts the whole homeostasis of the tissue, by thinning the cornea and exposing a considerable amount of the stromal surface to the air. Provided that a considerable area of the stroma was exposed without having the

barrier of the epithelium to control water uptake from the environment and also having an immediate and intense wound healing response naturally from the tissue itself in order to recover the piece that was removed, swelling effects are a lot more severe for trephine wounds than other more gentle methods of injury (i.e. LASIK-like ones). Additionally, the appearance of high numbers of larger proteoglycan molecules within the extracellular matrix during the repair process is already reported in the literature (Funderburgh *et al.* 1998), but also large proteoglycan molecules were visually obvious in the present study in electron micrographs taken from the wound bed. The existence of these molecules also contributes to swelling effects during the wound healing process in the cornea.

Polar plot maps revealed a strong tendency of the collagen fibrils in trephine-wounded corneas to form a circular pattern within the wound but, because this happens from the moment of injury, it is considered to be an artefact caused by the need to pull upwards on the trephined button in order to cut it away from the underlying stroma. However, the cornea outside the wound is not affected by artefact, and the arrangement that was observed at later stages of the culture period is a result of the healing process and a response of the tissue upon wounding.

The polar plots from the trephined wounds were noted to become smaller outside the wound area as the wounds healed (Figures 5.13 B and C). This phenomenon is due to swelling that occurred in the tissue during wound healing. The effect was not observed in LASIK-like wounds because the extent of the wound healing, and hence the swelling, was not so pronounced. Figures 5.13 B and C also revealed a radical re-alignment of collagen in trephine wounded samples, with collagen fibrils bending towards the wound area in the middle of the tissue at later stages of the organ culture. It is likely that this specific collagen arrangement is the result of wound contraction that occurs during the wound healing process though it could occur as a natural response of the tissue to reinforce the central area of the cornea that became considerably thinner upon wounding with the trephine. Unlike trephine-wounds, the LASIK-like wounds showed no clear evidence of wound contraction, probably because the stromal wound-healing response is minimal and is restricted to the flap periphery (Perez-Santoja 1998, Ivarsen 2003, Phillipp 2003).

In the LASIK-like injured corneas collagen orientation did not adopt such a critical pattern as it did in the trephine-wounded ones. After injury, the collagen seemed to be highly disorganized and appeared to have a completely different pattern within the flap area compared to the control/uninjured sample. This suggests that the process of creating then repositioning the flap, at least in the bovine cornea, distorts the collagen lamellae. X-ray diffraction provides averaged data throughout the corneal thickness, so we cannot say if the distortion is in the flap, the bed, or both. However, it is likely to be in the flap, as this is the part that was displaced during the induction of the wound.

However, it must be taken into consideration that an *in vitro* system lacks certain factors present in a live organism. Such parameters are the absence of nerve responses and intraocular pressure fluctuations in response to injury that potentially can affect the mechanical properties of the tissue. However, the lack of these parameters has not been an issue in previous *in vitro* corneal wound healing studies (Carrington and Boulton 2005, Carrington *et al.* 2006, Zhao *et al.* 2006) and, in particular, this has not been related to the orientation of collagen.

In conclusion, the extent of the wound healing response in the cornea depends on the type of injury. In the present study, the events of the repair process were more dramatic in trephine-wounded samples than in LASIK-like ones, because the first type of injury is more severe than the latter one. In trephine injured corneas collagen fibrils had a preferred orientation pattern to form a ring within and around the wound area. However, this might be induced upon wounding with the circular 5mm trephine. In LASIK-like ones collagen fibrils tend to form a pattern that follows the incision. This pattern appears at the third week after injury and becomes more apparent at the fourth week. It can also be concluded that the observations and the conclusions drawn in the present study are not artefacts of the *in vitro* system that was used. The ultrastructure of the tissue was clearly not affected in control corneas that remained normal without any swelling effects during the 4week organ culture time-span.

6. Homology-based molecular modelling of the bovine corneal biglycan core protein

6.1 Introduction

Collagen/Proteoglycan interactions within the extracellular matrix (ECM) play a key role in the maintenance and function of connective tissue. ECM consists predominantly of collagen, proteoglycans and other minor proteins (Hockin *et al.* 1998). For instance, corneal transparency is an essential requirement in order for visual function to occur and it is maintained due to the collagen and proteoglycan organisation within the corneal stroma. Collagen spacing is mainly controlled by proteoglycans that establish ionic interactions with the collagen fibrils within the stroma and fill the space between the fibrils. Therefore, the physical and chemical properties of proteoglycans play an important role in establishing and maintaining corneal transparency.

The ground substance of the corneal extracellular matrix is made up of proteoglycans. Proteoglycans are macromolecules composed of a protein core and a carbohydrate glycosaminoglycan (GAG) side chain. GAG's are highly hydrophilic, negatively charged molecules located at specific sites around each collagen fibril (Scott and Haigh 1996, Remington 1998). The core protein of a proteoglycan seems to be the most active part of the molecule, since it interacts with the collagen fibrils and the extracellular matrix at specific sites. According to Cintron *et al.* (1989) the precise arrangement of PGs presumably reflects specific intermolecular interactions with collagens. Therefore, loss of PGs might cause alterations to the collagen organisation and hence to connective tissue stability. According to Cintron *et al.* (1989) the precise arrangement of PGs presumably reflects specific intermolecular interactions with collagens. Therefore, loss of PGs might cause alterations to the collagen organisation and hence to corneal transparency.

The corneal stroma contains two major classes of proteoglycans containing either keratan sulphate side chains or dermatan/chondroitin sulphate side chains (Zieske 2001). Lumican, keratocan and mimecan are the major keratan sulphate PG's, whereas decorin and biglycan are dermatan/chondroitin PGs. Keratan sulphate is the major glycosaminoglycan in healthy corneal stroma, whereas dermatan/chondroitin sulphate molecule levels are lower under normal conditions. However, upon wounding dermatan/chondroitin sulphate content increases during tissue remodelling. Specifically, decorin levels increase by twofold, whereas biglycan increases seven times during the wound healing process (Funderburgh *et al.* 1998).

Dermatan sulphate proteoglycans are small leucine rich proteins (SLRPs) with an "arc" shaped spatial conformation and tend to form dimers. The amino-acid sequence of these proteins is characterised by long arrays of leucine-rich repeat motifs of about 24 amino acids in length (Jolles 1994). A feature that is of great interest about SLRPs is that they contain an amphipathic consensus sequence, with leucine as the predominant hydrophobic residue placed in conserved positions (Hocking *et al.* 1998). This pattern is highly likely to be involved with protein-protein or protein lipid interactions (Krantz *et al.* 1991). With respect to collagen/proteoglycan interactions several theories have been proposed to date, with the majority of them suggesting the idea that interactions with collagen are being established at the inner site of the "horseshoe" shaped molecule (Weber *et al.* 1996, Vesentini *et al.* 2005). Bearing in mind that the concave surface is involved in a high-affinity dimer interaction, this theory is now being debated (Scott *et al.* 2006, Vesentini *et al.* 2006). However, it should be taken into consideration that there might be a dimer-to-monomer transition of proteoglycans in collagen/proteoglycan interactions. For example, dermatan sulphate proteoglycans bind collagen as a dimer, conservation analysis across class I SLRPs revealed a clustering of partially conserved residues on the sugar-free surface of LRRs IV-VI, a region that has been implicated in collagen binding. This theory though has yet to be confirmed by further biochemical studies (Scott *et al.* 2004).

Biglycan is a dermatan sulphate proteoglycan and it receives its name because it is substituted more often with two glycosaminoglycan chains at the N-terminus (Kresse *et al.* 1994, Naito 2005). It is expressed in a variety of epithelial tissues throughout the body, such as the lung, spleen, bone, liver, cartilage, tendon, skin, kidney, heart, sclera and cornea (Wegrowski *et al.* 1995, Hocking *et al.* 1998, Watson and Young 2004). Biglycan interacts with fibrillar collagen and based on immunohistochemical analysis it has been proven that the core protein of the proteoglycan interacts directly with the collagen fibril (Schonherr *et al.* 1995).

In this study the 3D structure of the core protein of biglycan was determined by means of homology based molecular modelling. Descent from a common ancestor, i.e. homology, can be hypothesised when similar properties are detected in biological objects (Grishin 2001). It is also widely accepted that statistically significant homology detected from the sequence alone reflects descent from a common ancestor (Aravid and Koonin 1999). Comparative homology-based modelling is based on the observation

that sequence correlation above a certain proportion implies structural similarity. Thus, a protein of a known structure and sequence can be used as a template for the construction of a 3D model of another protein with a sequence similar to the template (D'Alfonso *et al.* 2001). Additionally, it should be taken into consideration that structure is conserved to a much greater extent than sequence and that there is a limited number of backbone motifs (Chothia 1992, Baxevanis and Ouellette 2001). A relative minimum percentage of homology between two protein sequences that can ensure the construction of a reliable model is ≥40% (MOE 2005). Template and model homology sequences identity that greater than 50% normally have 90% or more of the individual structures within the common cores and an RMSD (root mean square) value smaller than 1Å, ensuring reliability of the proposed model (Chothia and Lesk 1986). The aim of this chapter is to predict the 3-dimensional structure of the core protein of the bovine corneal biglycan molecule.

6.2 Materials and methods

6.2.1 Molecular Modelling

All calculations were performed on a dual Pentium 4 workstation running Linux and using the Molecular Operating Environment (MOE) 2005.03 software package developed by Chemical Computing Group (Montreal, Canada).

6.2.2 Sequence alignment

The amino acid sequence of biglycan was obtained from the protein database from NCBI (http://www.ncbi.nlm.nih.gov/protein) (gi|30315664). The PSI-BLAST algorithm was used to identify homologous structures for biglycan by searching the structural database of protein sequences in the Protein Data Bank (PDB) (Berman HM 2002). The crystal structure of decorin (PDB code 1XKU) (resolution 1.5 Å) was selected as template structures for homology modelling of the biglycan protein. The selection of these structures was based on the highest sequence similarity (56.7% similarity). Sequence alignments were created with ClustalW (Thompson 1994).

6.2.3 Homology modelling

The homology model was constructed using MOE version 2005.03. As indicated above, the homology model of biglycan was based on the crystal structure of

1XKU, which shares 56.7% similarity with the sequence of biglycan. The first requirement in the construction of a biglycan model structure is a multiple sequence alignment against its template. The sequence alignment is based on identifying structurally conserved regions (SCRs) common between the model and the template. An initial 3D structure of biglycan was obtained by transferring the backbone coordinates from the template residues to the corresponding residues of biglycan, except for several variable regions (LOOPs). To construct the structural variable regions, a loop-searching and generating algorithm over the databank of known crystal structures was used from within MOE. Through the procedure mentioned above, an initial 3D model was thus completed. The quality of this model was examined by WHATCHECK and ProCheck. The three-dimensional model was subjected to molecular mechanics energy minimization calculations using the updated MMFF94x and Amber algorithms implemented in MOE. The refinement of the homology model was carried out through energy minimization: 500 iterations of steepest descent (SD) calculation were performed and then the conjugated gradient (CG) calculation was carried out until achieving 0.1 kcal/mol $Å^{-1}$ of convergence on the gradient.

6.2.4 Molecular dynamics (MD) simulations

MD simulations were performed using MOE version 2005.03 and its built-in Molecular Dynamics module using an NVT ensemble. The protein was solvated in a cubic periodic box containing water molecules in order to perform simulations in an aqueous environment. Firstly, the model structure was refined by adding all hydrogen atoms and subsequent energy minimization with the MMFF94x molecular mechanics module of MOE to ensure overall neutrality of the simulated system. The time step was 2 fs and all simulations were conducted at 300 K.

The model was first equilibrated for 100 ps keeping the whole protein fixed to allow the water molecules to relax. A subsequent 100 ps of equilibration with the protein backbone fixed was carried out. After the equilibration phase, we obtained 1 ns MD trajectory for the biglycan model. Additionally, in order to assess the structural stability of the protein, 500 pico-second snapshots of the molecular dynamics simulation trajectory were taken. This revealed 9 conformations that were superimposed together. Each snapshot conformation was coloured with its unique colour.

Finally, a conjugate gradient energy minimization of the full protein was performed until the root mean-square (rms) gradient energy was lower than 0.001 kcal/mol $Å^{-1}$. In this step, the quality of the initial model was improved. After the optimization procedure, the structure was checked again by ProCheck.

6.3 Results

6.3.1 Sequence alignment

The sequence that was modelled into a 3D molecule in this study was the bovine biglycan core protein. A comparison between the sequences of this protein from various mammalian species revealed high homology (Fig. 6.1B).

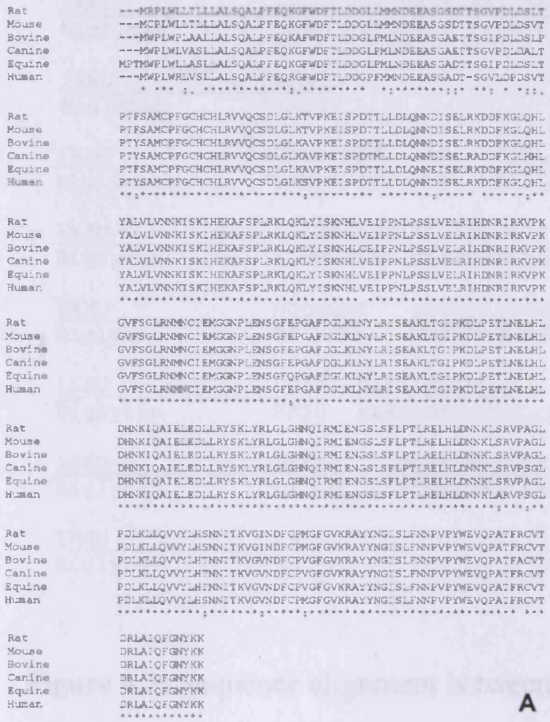

SeqA	Name	Length(aa)	SeqB	Name	Length(aa)	Score
1	Bovine	369	2	Rat	369	95
1	Bovine	369	3	Mouse	369	94
1	Bovine	369	4	Canine	369	96
1	Bovine	369	5	Human	368	94
1	Bovine	369	6	Equine	372	97
2	Rat	369	3	Mouse	369	99
2	Rat	369	4	Canine	369	95
2	Rat	369	5	Human	368	95
2	Rat	369	6	Equine	372	96
3	Mouse	369	4	Canine	369	94
3	Mouse	369	5	Human	368	95
3	Mouse	369	6	Equine	372	96
4	Canine	369	5	Human	368	94
4	Canine	369	6	Equine	372	97
5	Human	368	6	Equine	372	95

B

Figure 6.1: Sequence alignment between biglycan core proteins of different species produced by the ClustalX program (A). Homology scores from sequence alignment between the sequences of biglycan core protein from different mammal species. Alignment scores were between 94-99% suggesting high homology and structural conservation of biglycan core protein throughout mammal species (B).

Additionally, biglycan protein sequence is the same size in many mammal species (Fig. 6.1). Sequence alignment between decorin and biglycan core protein sequences revealed a high homology score (i.e. 56.7%) (Fig. 6.2A).

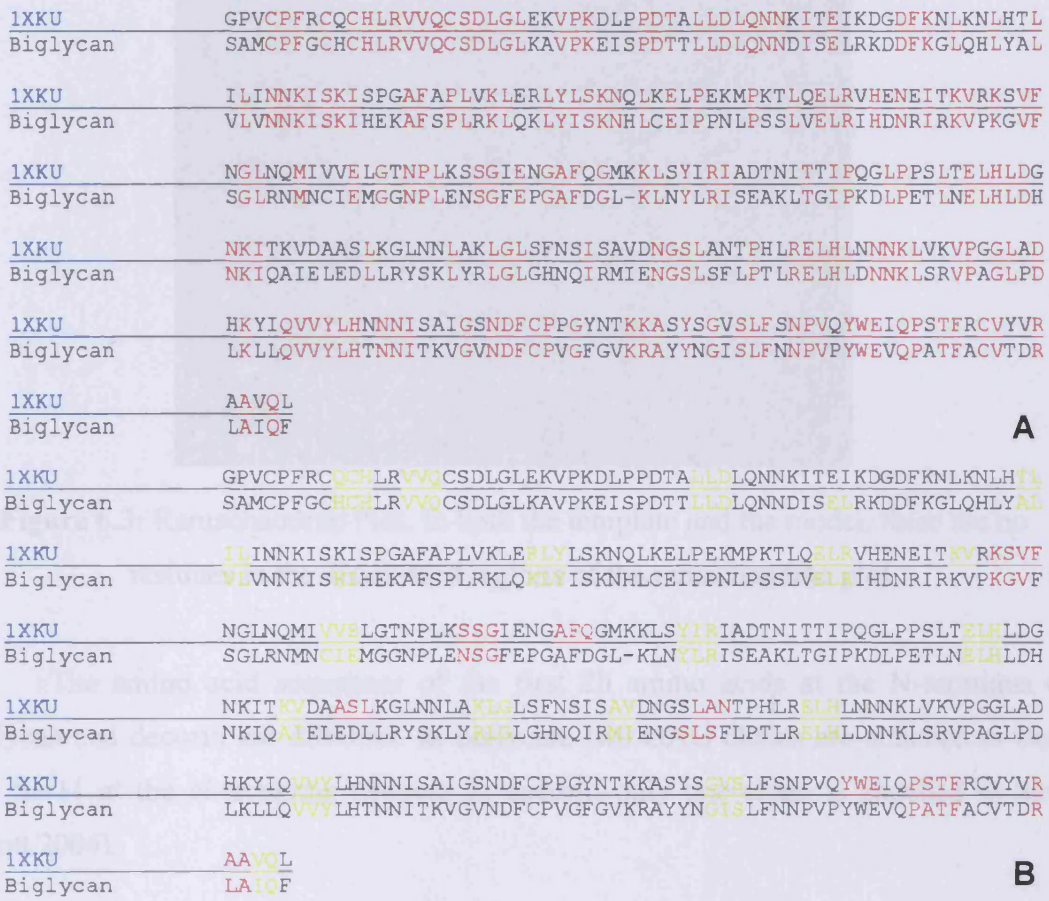

Figure 6.2: Sequence alignment between decorin (1XKU) and biglycan produced by the ClustalX program. Homology score between the two proteins was 56.7%. (A) Secondary structure features prediction. Red: α-helical secondary elements, Black: β-sheet pattern (B).

6.3.2 Secondary features and model evaluation

The β-sheet pattern has been completely conserved between the model and the template. On the other hand the template's α-helix distribution was not exactly assigned to the model. There are 3 α-helical secondary elements missing from the model, when compared to the template (Fig. 6.2B).

The ProCheck/WHATCHECK evaluation of the model revealed that 95% of its residues were found in the core regions and another 5% in the allowed regions of the Ramachandran plot (Fig. 6.3).

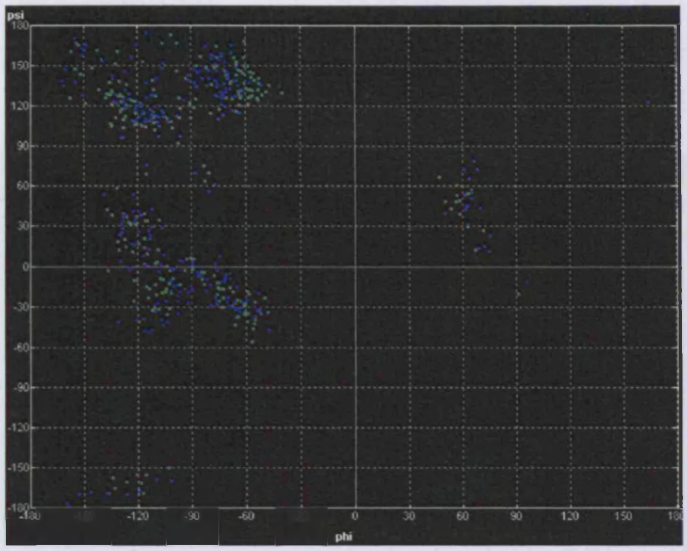

Figure 6.3: Ramachandran Plot. In both the template and the model, there are no residues in the disallowed regions of the ramachandran plot.

The amino acid sequences of the first 20 amino acids at the N-terminus of biglycan and decorin are different. In biglycan, two GAG chains are attached to Ser5 and Ser11 at the N-terminus whereas in decorin only one chain is attached to Ser4 (Scott 2004).

6.3.3 Molecular dynamics

The Molecular Dynamics functions that were used in the present simulations solve the equations of motion for a molecular system and store the resulting trajectory information to a database. These functions depend on the current state of the system, in particular, the force field, the potential setup and the current restraint configuration.

The molecular dynamics simulation serves two purposes in the current study. Firstly after 4 ns the protein is completely relaxed and close to its global energetic minimum (Fig. 6.4, chart 1). Secondly, the extended molecular dynamics simulation does impose a serious structural test to the folding stability of the model. It was proved firstly from the energy graph and secondly from the Hamiltonian graph that the energy of the system was reduced while its structure was conserved during the MD simulation (Fig. 6.4, chart 2). The Hamiltonian is the value of the full (extended system) at time *t*.

In a properly functioning simulation, this quantity is conserved at all times (although fluctuations will be present). Drift in hamiltonian value (*H*) is evidence of too large a time step.

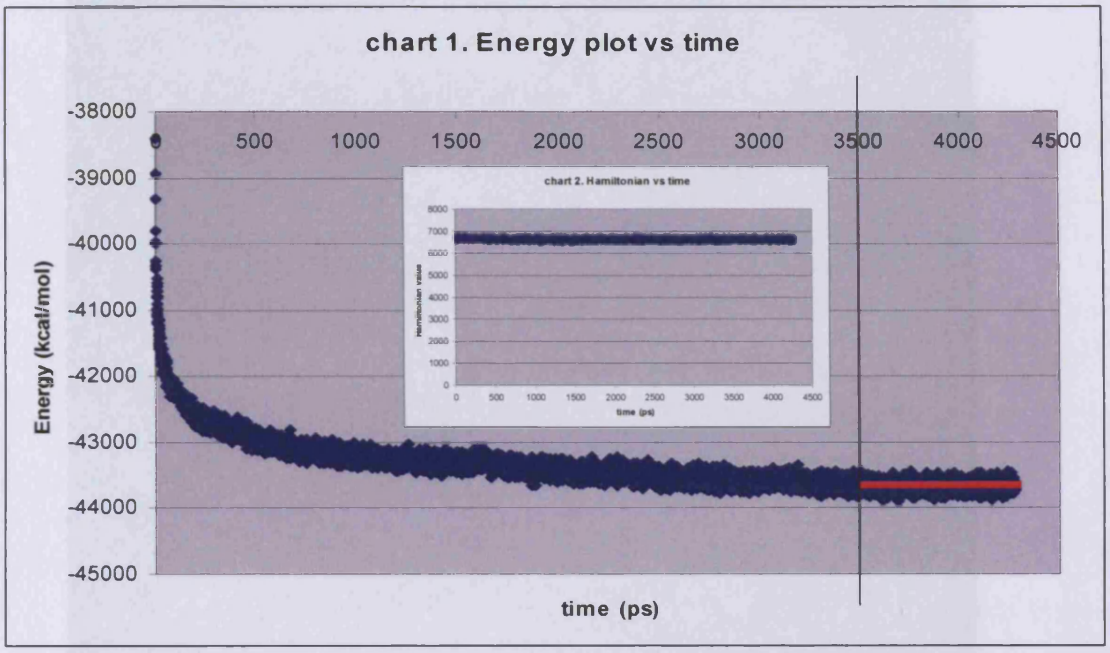

Figure 6.4: The model quickly reached a plateau, which is considered to be its global energy minimum (Chart 1). A constant Hamiltonian value revealed that the molecular system was stable throughout the course of the molecular dynamics simulation (Chart 2).

The evaluation for the structural stability of biglycan model showed that the inner cliff of the protein, where the parallel β-sheet motif is found, is much more stable than the rest of the protein. Visual investigation of the 9 conformations revealed that the inner region of the protein (β-sheet motif) is not as colourful as the rest of the protein (Data not shown). That proves that the β-sheet motif of the biglycan protein is a very stable and conserved motif, whose residues are energetically and conformationally more stable than the rest residues of the protein.

6.3.4 Model evaluation

Superimposition of biglycan proposed model to decorin crystal structure revealed obvious similarity in the spatial arrangement as well as the structural motives of both proteins (Fig. 6.5).

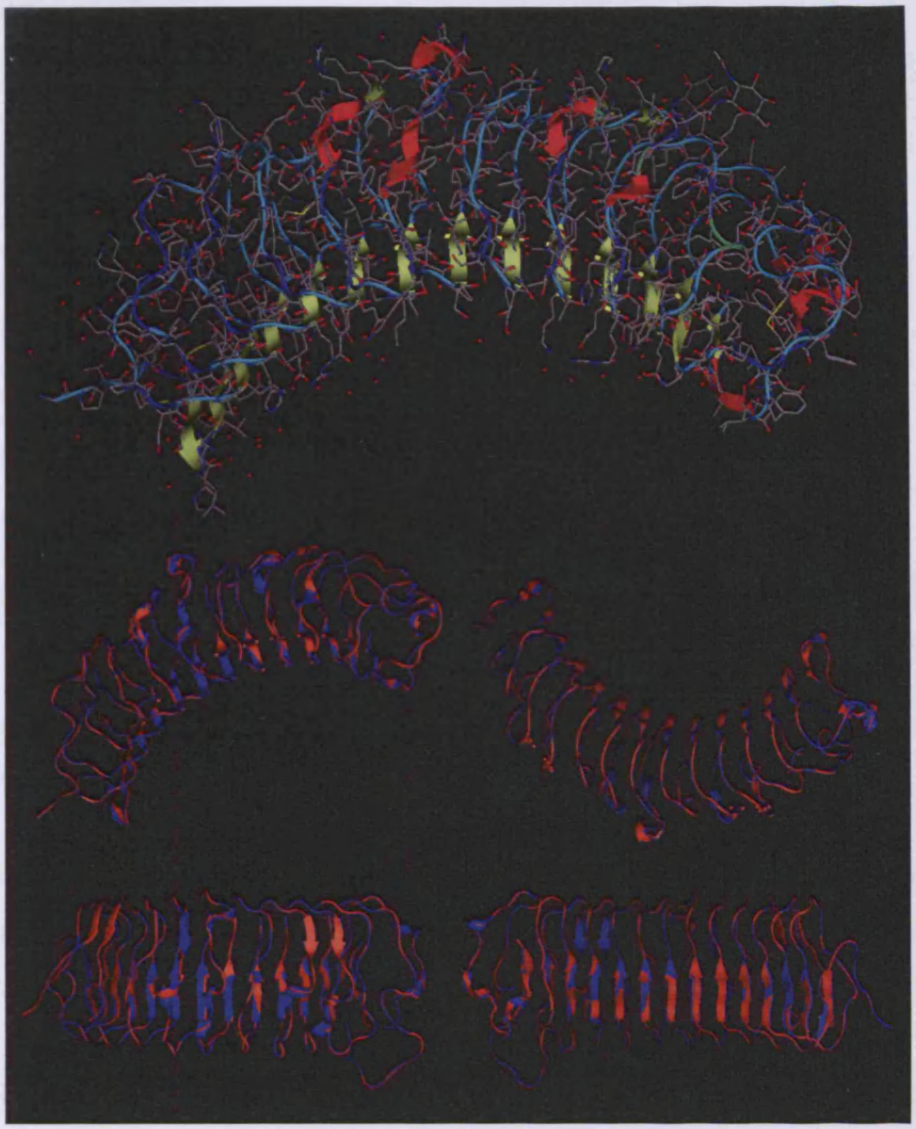

Figure 6.5: The structure of biglycan superimposed with its template. Reasonably high homology identity guaranteed the retention of the major secondary elements and shape. The above structure has been obtained after a 2 nanosecond molecular dynamics simulation.

Also, the proposed model for biglycan appears to obtain an "arc" shape spatial arrangement, which is in consistency with the rest of the RSLPs (Fig. 6.6). The inner cliff of the protein consists of parallel β-sheets made mainly of hydrophobic amino acids.

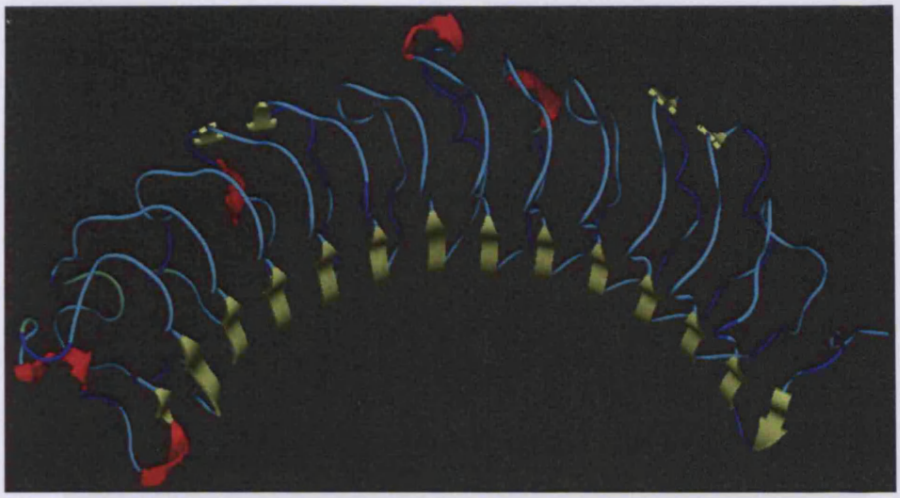

Figure 6.6: Proposed homology model for the structure of the biglycan core protein.

6.3.5 Comparison of theoretical model to its crystal structure

The crystal structure of biglycan has recently been released (Scott 2006) and a comparison of the homology model with the x-ray structure was performed. The secondary elements of the structure (i.e. α-helices and β-sheets) were found to be highly similar. The main differences between the model and the x-ray data lie in two extra α-helical loops the homology model has on its outer surface between residues 206-207 and 248-250, respectively (Fig. 6.7A). The areas of interest, such as the inner cliff of the protein and N- and C- terminal regions were the same between the two molecules. Superimposition of the two models revealed an RMSD of 1.32Å (Figure 6.7B).

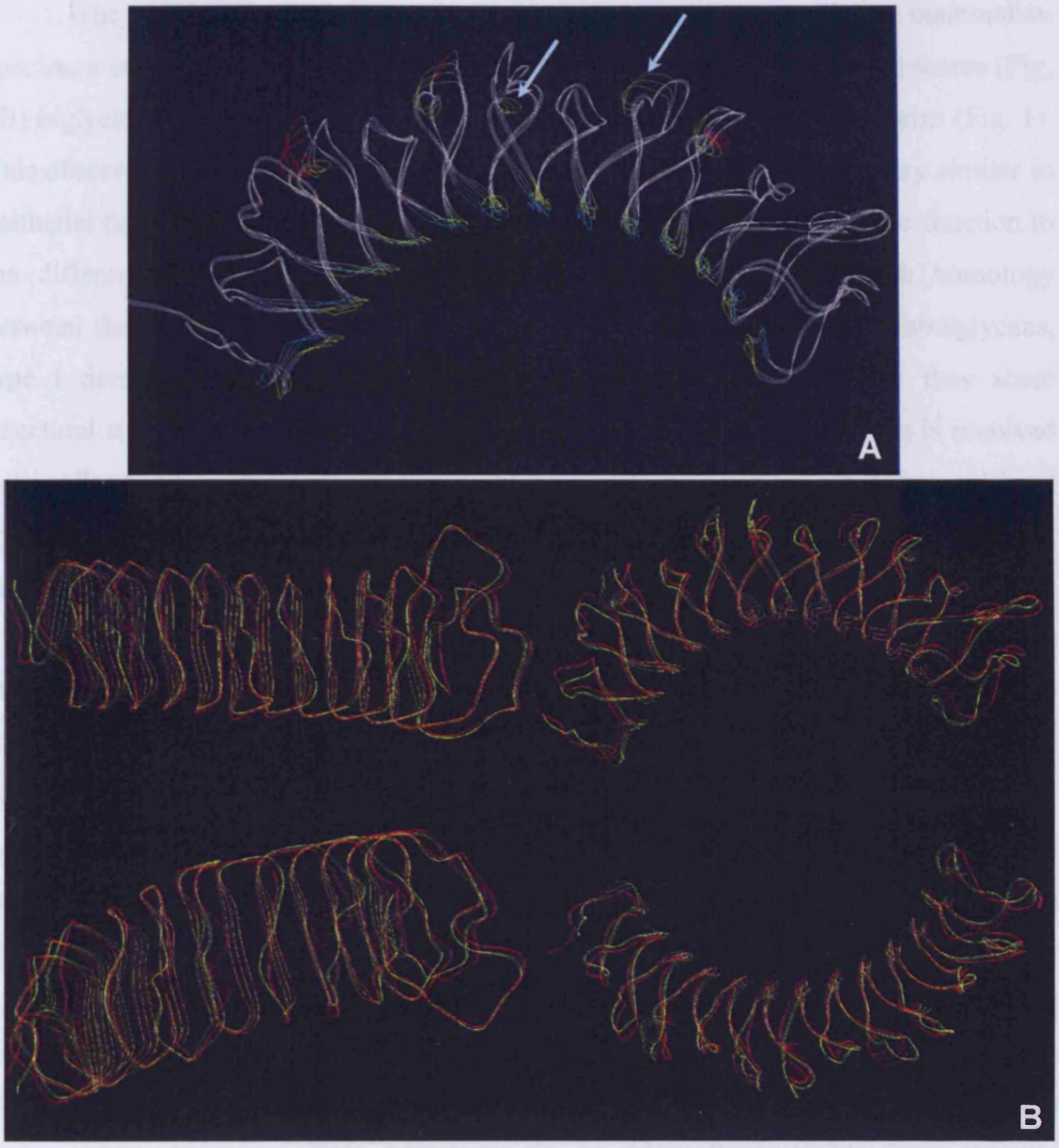

Figure 6.7: The structure of the homology model was very similar to the crystal structure. Superimposition of the two structures revealed the existence of two loops at the surface of the molecule (indicated by turquoise arrows). Key: Green and aqua→ α-helix and β-sheet, respectively, for the homology model; Red and yellow→ α-helix and β-sheet, respectively, for the crystal structure (A). The homology model of biglycan superimposed with the crystal structure of the same protein. Key: Yellow→ X-ray structure, Red→ homology model (B).

6.4 Discussion and conclusions

The sequence of biglycan is highly conserved among higher mammalian species, a common characteristic of SLRPs. In addition to high homology scores (Fig. 1B) biglycan sequences from different mammalian species have the same size (Fig. 1). This observation suggests that biglycan structure and hence function is very similar in epithelial tissues of various mammals. Therefore, biglycan serves the same function to the different species. Additionally, biglycan and decorin share a high homology between their sequences. These proteins belong to the same family of proteoglycans, type I dermatan sulphate. Although their function differs structurally they share structural similarities. In previous studies it has been observed that decorin is involved with collagen fibrilogenesis, whereas biglycan is not. Additionally, decorin is released by keratocytes, whereas biglycan is the result of myofibroblast activity in epithelial tissues (Funderburgh 2001, Funderburgh 2003)

It was also observed that the inner cavity of the "arc" shaped molecule consists mainly of hydrophobic amino acids, whereas the outer surface of the molecule consisted of hydrophilic amino acids. This explains the arc shape of the molecule, as an adaptive response to "hide" these amino acids in aqueous biological environments. Additionally, parallel β-sheets are known to have a tighter spatial arrangement than antiparallel β-sheets (Zubai 1998). This shape obtained for biglycan is consistent with the rest of the known SLRPs.

Findings confirm that a possible interaction site for the collagen fibrils is the inner cavity of the arc-shaped molecule. This is supported by three different arguments. Firstly, by structurally evaluating the model of biglycan, it appears that it has the correct dimensions to accommodate a collagen fibril (Scott 1996). Secondly, the presence of hydrophobic residues implies they must be covered by a second molecule to avoid exposure to the aqueous phase. Thirdly, the inner cavity of the biglycan model is a beta-sheet motif, which is highly conserved among other collagen interacting proteins of the same families. That is shown in the alignment between the template and the model too.

A preliminary data investigation of the relevant literature, combined with the findings of this study, poses important questions such as: how does biglycan interact with collagen fibrils? The proposed patterns of interaction can be investigated in a future protein-protein docking / interaction *in silico* investigation. Biglycan and collagen can be imported to the MOE docking algorithm and after the final interaction

conformations are obtained and the stability and biological viability of the system can be verified by means of Molecular Dynamics. A separate MD simulation will be performed for each viable docking conformation and the various energies will be compared. Finally, a mode of association and interaction will be suggested. However, the means of technology that are currently available are not powerful enough to simulate a whole collagen fibril.

Previous studies suggest a collagen binding domain both in the C- and N-terminal regions of the core protein of decorin (Scott *et al.* 2004, McEwan 2006) . Data suggest a collagen binding site at the N-terminal half of the decorin core protein. The importance of amino acids 125-158 of the mature core protein is further supported by the finding that these amino acids are likely to be on the surface of the molecule according to computer modelling and antibody-binding studies (Scott, 2004).

In conclusion, the comparison between the proposed theoretical model for biglycan and the recently released x-ray structure for the same protein revealed high similarities between the two proteins. The low RMSD value confirms the accuracy of the theoretical model as well as the reliability of the homology methods and algorithms that were used for the current study.

7. General discussion

Wound healing is a complex process that, especially in the ocular surface, demands to be performed in such a way that the clarity of the tissue is not being compromised in the long term. The extent and severity of the wound healing response in the cornea clearly depend on the type of injury. In the present study the repair process in bovine corneas after trephine wounding and LASIK-like incisions was closely investigated. The cellular expression of the tissue during wound healing was investigated by monitoring epithelial cell and myofibroblast expression. However, in normal corneal tissue there are other cell types expressed such as the quiescent keratocytes, limbal stem cells of the epithelium, bone marrow derived cells in the stroma and the endothelial cells. Keratocytes are the main cell type in the stroma. Limbal stem cells are located at the basal layer of the corneal epithelium in the limbus and they differentiate and proliferate in epithelial cells in order to recover the corneal surface upon injury (Wilson 1999). The existence of bone marrow derived keratocytes that give rise to either bone marrow haemopoetic stem cells or major histo-compatibility complex (MHC) class II macrophages has also been confirmed (Sosnova *et al.* 2005). Lastly, the endothelial cells form a layer over the posterior part of the tissue providing regulation of fluid uptake in the cornea.

In vitro models have become increasingly popular in studying the short term effects of corneal wound healing (Richard et al. 1991, May *et al.* 2004, Zhao *et al.* 2006). In the current study, a simple air interface organ culture method was used (Foreman *et al.* 1996) as this culture system achieves excellent re-epithelialisation (Foreman *et al.* 1996, Zhao *et al.* 2006). Additionally, it doesn't appear to induce any swelling effects to the tissue, as corneal thickness remains stable during the maximum term of culture (i.e. 4 weeks) (Carrington, personal communication 2004). In the current study, swelling effects in the cultured corneas were monitored by measuring the interfibrillar spacing of control/uninjured bovine corneas (Chapter 5). During the four weeks in culture interfibrillar spacing increased only slightly indicating that there were no swelling effects induced in the tissue by the culture system. This observation confirmed the reliability of this organ culture method for the *in vitro* study of wound healing in corneal tissue, as it keeps the endothelial barrier intact and fully functional.

The external surface of the human body (i.e. skin, ocular surface) consists of stratified squamus epithelium that protects and provides a physical barrier from the external environment. Part of the immunohistochemical investigation in this study focused in the expression of epithelial cells in the cornea after injury (Chapter 3). In LASIK-like incisions the epithelium reacted rapidly at the incision, forming an epithelial plug that covered stromal gaps in the stroma. At later stages of the organ culture this plug had a tendency to increase in size and also epithelial cells migrated towards inner parts of the stroma. Positive cytokeratin staining confirmed the cell type of these cells as cytokeratins 3, 5 and 12 are known cells markers for corneal epithelial cells (Kasper *et al.* 1988). This is a common observation in LASIK, known as epithelial ingrowth that is often associated with haze and diffuse lamellar keratitis (Vesaluoma *et al.* 2000).

In this study it was observed that stromal wound healing response events were more severe for trephine injured corneas than LASIK-like ones. Cellular expression for myofibroblasts and tissue swelling were more obvious in trephine-wounded corneas than in LASIK-like samples (Chapters 3 and 5). Stromal swelling is a part of the wound healing process and it was estimated by determining the interfibrillar spacing of collagen fibrils. Corneal hydration and therefore swelling is monitored by the epithelium/ endothelium barriers and also the extracellular matrix components of the stroma (i.e. proteoglycans, cells). It was noted to be extensive in trephine wounded corneas within a short period of time after injury. Swelling occurred in LASIK-like corneas as well but it was not so extensive. During wound healing there is a series of events that take place in both the corneal stroma and the epithelium and cause swelling to the tissue as part of a normal repair process. Initially, cytokines released by the epithelium (i.e. IL-1β) cause stromal cell transformation into myofibroblasts and subsequent proliferation (Wilson 2002). Secondly, during the wound healing process elevated numbers of abnormally large proteoglycans appear in the extracellular matrix (Fundeburgh *et al.* 1998). This was also confirmed by transmission electron microscopy (Chapter 5) and the molecular modelling study (Chapter 6).

The three dimensional structure of biglycan was constructed *in silico*. Proteoglycan molecules play a key role in corneal hydration, hence swelling, and their levels are affected in pathologic situations (Funderburgh 1998, Funderburgh 2001). In particular,

biglycan, a dermatan sulphate proteoglycan, levels increase seven fold during the healing process (Funderburgh 1998). The present study revealed that the core protein of biglycan appears to be highly reactive with numerous potential interaction sites throughout the molecule, for the formation of dimers and also with collagen. This, physically increases the water uptake in the cornea and considering the dramatic increase in protein levels during wound healing, as proteoglycans are highly hydrophilic water uptake in the tissue increases also. Biglycan molecules exist in between the collagen fibrils and when they are hyper-hydrated they increase the collagen interfibrillar spacing inducing swelling effects. However, in the current study fibrillar spacing was increased not only at areas proximal to the wound but throughout the whole cornea, implying a disruption of the function of the endothelial barrier. Nevertheless, it needs to be considered that water uptake in the cornea is also increased during the wound healing process, as the energy requirements of the tissue increase.

All the above events take place in the injured cornea regardless of the type of injury. However, it has been reported that the function of the endothelium is compromised after severe injury (Edelhauser 2000). Kim *et al.* (1997) proposed that during ablation it is crucial to leave a residual stromal thickness of 200μm above the corneal endothelium that should not be ablated to protect the corneal endothelial structure and barrier function. According to Edelhauser (2000) LASIK doesn't affect the endothelial architecture as the flap is normally 160μm thick and the flap bed is thicker than 200μm. In the same study laser ablation was also performed in corneas that caused a deeper, more severe type of injury that left less than 200μm of residual stroma above the endothelium. In this case it was observed a loss of the hexagonal morphology in cells and the endothelial barrier function was also compromised. Therefore, in the present study, swelling was not as extensive in LASIK-like incisions, as the function of the endothelium was not seriously affected by the injury. In trephine wounds swelling was extensive, indicating that the severity of the injury had impaired the function of the endothelial barrier.

In scar tissue, fibrils in newly deposited collagen are thicker than normal (Connon 2004) and that is the reason that fibrillar diameters were found to increase in the wound area or the incision site in the injured corneas in the present work. In trephine wounded corneas, fibril diameter was also affected in an area of about 1mm around the wound

(Chapter 5). This could be explained by the results in Chapter 3, where histology revealed that the stromal area under normal epithelium proximal to the trephine wound was also affected by the cut. In addition, cytokines by the injured epithelium affect a stromal area under non-affected epithelium, close to the wounded area. In LASIK-like corneas, fibrillar diameter increased only around and at the incision site, finding that it is consistent with the findings from immunohistochemistry. Additionally, histology/cell counts revealed a decrease in the flap bed in LASIK-like injured corneas, an observation that it is consistent to previous studies (Ivarsen 2004). α-smooth muscle actin was positive in a stromal area close to the incision site only, indicating the existence of active myofibroblasts in this area only. There were no signs of myofibroblast expression anywhere in the flap bed. Therefore, it was concluded that cytokines released by the epithelium play a crucial role in the initiation of the stromal wound healing response. Subsequently, it was assumed that in the case of LASIK-like incisions the cytokines released by the epithelium could only reach a stromal area at the incision site, where the adjacent epithelium was being injured.

In the current study an attempt was made to improve the wound healing response in the cornea (Chapter 4). In the past the effects of UV radiation has been applied to cause collagen cross linking in the corneal stroma and therefore improve the wound healing response (Nagy *et al.* 1997). However, in this project it was already obvious that epithelial cytokines could not physically reach stromal areas further inside the flap. Therefore, a series of different cytokines (i.e. TNF-α, IL-1α, FasL and TGF-β1) were tested in LASIK-like injured corneas and their effect on transparency, myofibroblast proliferation and tissue mechanical strength was monitored for up to four weeks in culture. It was observed that there might be a possible correlation between the extent of transparency, hence myofibroblast expression, and the extent of flap adherence. However, it was obvious that the stronger the effect of the cytokine in flap adherence the more the clarity of the corneas was compromised. This is mainly to the fact that the more severe the wound healing response becomes under the effects of cytokines, the more swelling occurs to the tissue. In addition, myofibroblast cell numbers were also noted to increase in all cytokine treated corneas. Corneal crystallins are expressed in lower levels in myofibroblasts during wound repair, and this is reported to be associated with a loss of

cell transparency (Stramer and Fini 2004, Jester *et al.* 1999). These findings imply that further investigation is needed in order to find an optimum relationship between using the appropriate quantity and type of cytokine to secure the flap, but still maintain the clarity of the cornea.

7.1 Future work

The x-ray diffraction technique in general averages out the parameters it is measuring throughout the depth of the area that it is scanned. Considering that the changes in the interfibrillar spacing were very weak for the LASIK-like corneas it would be worth, in the future, to take slices of injured corneas from certain depths of the tissue and scan them separately. Additionally, it would be very interesting to scan separately the upper flap and the flap bed in order to see in which part fibrillar diameter and interfibrillar spacing changes more severely.

In the current study wide angle x-ray diffraction experiments revealed remarkable collagen orientation patterns in wounded corneas. This is an observation made for the first time and it is important in providing us with information about the structure and the stability of the tissue during wound healing. However, the factors that cause the change in collagen orientation are still unknown. Multi-photon confocal microscopy utilising second harmonic imaging is a new technique that allows individual collagen fibrils or bundles of fibrils to be visualised. It would be useful to use this method to see the direction of fibrils in specific points in the tissue and therefore discover the factors that affect collagen orientation during wound healing.

The series of experiments that tested the effect of various growth factors in the cornea proved that there is a correlation between the type/quantity of growth factors and their influence on the effectiveness of the wound healing response and the maintenance of the transparency of the tissue. So far it was shown that growth factors improve the healing of the tissue, but in all cases the transparency was compromised. Therefore, a series of weaker growth factor solutions should be used in order to see if the clarity of the cornea can be retained.

Corneal transparency is compromised during wound healing. One of the basics of corneal transparency is collagen-proteoglycan interactions. Therefore, in order to gain a

better understanding of corneal wound healing, it is needed to gain a better insight in tissue ultrastructure and specifically collagen-proteoglycan interactions. Theoretical techniques and specifically molecular modelling can be a valuable tool in the prediction of interactions between molecules of the extracellular matrix. However, to date, processing power is insufficient to be able to simulate a whole collagen fibril. In the future, with the development of technology, this might be an achievable task that could save scientists a lot of time and effort in performing long laboratory based experiments.

APPENDICES

Appendix 1 - Nomenclature

Symbol used for abbreviation	Original Term
αSMA	α-Smooth Muscle Actin
Ab	Antibody
ASCRS	American Society of Cataract and Refractive Surgery
ATP	Adenosine Triphosphate
BSA	Bovine Serum Albumin
CK	Cytokeratin
D	Collagen periodicity
DAB	Deaminobenzidine
ddH_2O	Double distilled Water
Dp	Diopter
ECM	Extracellular matrix
EGF	Epidermal Growth Factor
EM	Electron Microscopy
FACIT	Fibril Associated Collagens with Interrupted Triple helices
FasL	Fas Ligandx
d	Collagen fibril diameter
FITC	Fluorescein Isothiocyanate
GAG	Glycosaminoglycan
Gly	Glycine
H&E	Haematoxylin and Eosin
HGF	Hepatocyte Growth Factor
hrs	Hours
I	X-ray scatter intensity
IF	Intermediate Filament
IgA	Immunoglobulin A
IgG	Immunoglobulin
IL	Interleukin
IVCM	*In vitro* Confocal Microscopy
KGF	Keratocyte Growth Factor

kV	Kilovolt
LASEK	Laser Epithelial Keratomileusis
LASIK	Laser *in situ* Keratomileusis
MD	Molecular Dynamics
mg	Milligram
min	Minutes
MM	Molecular Mechanics
MMP	Matrix Metalloproteinase
N	Newton
NBF	Neutral Buffer Formalin
nm	Nanometre
O/N	Overnight
^{o}C	Degrees centigrade
PBS	Phosphate Buffer Saline
PDGF	Platelet-Derived Growth Factor
PFA	Paraformaldehyde
PG	Proteoglycan
PGF	Prostaglandin F
PMN	Polymorphonuclear
PRK	Photorefractive Keratectomy
R	Radial position/distance from the centre of an x-ray scatternpattern
RK	Radial Keratotomy
RMSD	Root Mean Square Deviation
RT	Room Temperature
SAXS	Small Angle X-ray Scattering
SLRP	Small Leucine Rich Proteins
TAC	Transient Amplified Cell
TDC	Terminally Differentiated Cell
TEM	Transmission Electron Microscopy
TGF	Transforming Growth Factor
Ua	Uranil Acetate
WAXS	Wide Angle X-ray Scattering

XRD	X-Ray Diffraction
µl	Microliter
µm	Micrometer

Appendix 2- List of materials

Material	Supplier
0.2 μm filters	Fisher
Acetone	BDH
Alexa Fluor® 488 Goat anti-mouse IgG (H+L) 2° Ab	Molecular Probes
Anti α-smooth muscle actin	Sigma
Anti-Cytokeratin 3	ICN
Anti-PAN Cytokeratin	DAKO
Anti-Vimentin	Sigma
Betadine	AAH
Bovine Serum Albumin	Sigma
Calcium Chloride	BDH
Chloroform	BDH
DAB	Sigma
Disodium Hydrogen Orthophosphate	Gibco
Eagle's Minimal Essential Medium	Gibco
Eosin	BDH
Ethanol	BDH
Forceps	Fisher
Formaldehyde	BDH
Formalin	BDH
Fungizone	Gibco
Goat anti-mouse IgG Biotinylated 2° Ab	DAKO
Goat Serum	Sigma
Haematoxylin	BDH
HCl	Sigma
Human recombinant FasL	R&D Systems
Human recombinant TGF-β1	R&D Systems
Human recombinant IL-1α	R&D Systems
Human recombinant TNF-α	R&D Systems
Hydrogen Peroxide	Sigma
Hydromount	BDH

Methanol	BDH
Microtome Disposable Blade	Lamb
Paraffin Wax	Lamb
Potassium Chloride	BDH
Potassium Orthophosphate	BDH
Proteinase K	Qiagen
Resin Kit	Agar
Scalpel blades	Fisher
Sodium Chloride	BDH
SuperFrost Plus Slides	BDH
Tissue-Tek OCT compound	Agar
Triton X-100	Sigma
Trypsin	Sigma
Xylene	BDH

Appendix 3– Solution preparation

Solutions for the organ culture

Agar/Gelatin

2 g Agar

2 g Gelatin

200 ml ddH_2O

Autoclave

Place agar, gelatine and ddH_2O quantities into a 300ml bottle and autoclave at 120°C for 20mins.

Agar/Gelatin Support

200 ml Agar/Gelatin

20 ml 10xMEM

10 ml 7.4% sodium bicarbonate

2 ml Antibiotics

1 ml Fungazone

Heat agar/gelatin mixture using the microwave in low power. Filter (0.2 μm) the rest of the solutions into the agar gelatin solution and mix.

Trowells T8 Medium

500 ml Trowels T8

5 ml Antibiotics

5 ml Fungizone

Filter (0.2 μm) the antibiotics and the fungizone into the Trowells T8 bottle.

7.4% Sodium Bicarbonate

22.2 g Sodium Bicarbonate

300 ml ddH_2O

Mix until dissolved at RT.

25% (v/v) Betadine Solution

100 ml Betadine

400 ml ddH_2O

Mix and shake well before use.

Buffers and Solutions for Immunohistochemistry

PBS (1X)

40 g NaCl

1 g KCl

5.75 g Na2HPO4

1 g KH2PO4

5 l distilled H_2O

10% NBF

60 ml Na2HPO4

40 ml KH2PO4

900 ml dd H2O

Take 900 ml of the above mixture and add 100 ml formaldehyde.

9 g NaCl

Adjust pH to 6.8

Trypsin Buffer (0.1 mg/ ml)

0.675 g TRIS

80 ml ddH2O

0.1 g $CaCl_2.2H_2O$

Adjust Ph to 7.8 with 1N HCl

Bring up to volume (100ml) with ddH2O

10 mg of Trypsin

0.6% H_2O_2

0.4 ml 30% H_2O_2

19.6 ml Methanol

3% H_2O_2

2 ml 30% H_2O_2

18 ml ddH_2O

Buffers and solutions for cytokine treated corneas

PBS, 0.1% BSA

0.05g BSA

50ml PBS

Mix and filter through a 45μm filter

4mM HCL, 0.1% BSA

0.05g BSA

50ml 4mM HCl

Mix and filter through a 45μm filter

Human recombinant TNF-α

100μg/ml→ 100μg of protein in 1ml PBS, 0.1% BSA stock solution 1

100ng/ml→ 1μl of stock solution 1 in 1ml PBS, 0.1%BSA solution A

50ng/ml→ 500μl solution A in 500μl PBS, 0.1%BSA

10ng/ml→ 10μl solution A in 90μl PBS, 0.1%BSA

0.1ng/ml→ 1μl solution A in 1ml PBS, 0.1%BSA

Human recombinant IL-1α

2μg/ml→ 2μg of protein in 1ml PBS, 0.1% BSA stock solution 2

100ng/ml→ 5μl of stock solution 2 in 95μl PBS, 0.1%BSA solution B

50ng/ml→ 30μl solution B in 30μl PBS, 0.1%BSA

10ng/ml→ 10μl solution B in 90μl PBS, 0.1%BSA

0.1ng/ml→ 1μl solution B in 1ml PBS, 0.1%BSA

Human recombinant FasL

10μg/ml→ 5μg of protein in 500μl PBS, 0.1% BSA stock solution 3

100ng/ml→ 10μl of stock solution 3 in 1ml PBS, 0.1%BSA solution C

50ng/ml→ 100μl solution B in 100μl PBS, 0.1%BSA

10ng/ml→ 10μl solution B in 90μl PBS, 0.1%BSA

0.1ng/ml→ 1μl solution B in 1ml PBS, 0.1%BSA

Human recombinant TGF-β_1

1µg/ml→ 1µg of protein in 1ml HCl, 0.1% BSA stock solution 4

100ng/ml→ 100µl of stock solution 4 in 900µl HCl, 0.1%BSA solution D

50ng/ml→ 100µl solution B in 100µl HCl, 0.1%BSA

10ng/ml→ 10µl solution B in 90µl HCl, 0.1%BSA

0.1ng/ml→ 1µl solution B in 1ml HCl, 0.1%BSA

Buffers and solutions for TEM

4% PFA

8 g PFA

100 ml 1X PBS

Stir and heat for 1 hr

Add NaOH drop wise until the solution becomes clear.

Filter through a 0.5 µm filter.

Adjust pH to 7.4

Freeze aliquots for further use.

Before use, defrost aliquot and dilute it with equal volume of 1X PBS.

Cuprolinic Blue stain

1.05 g $MgCl_2$ in 20 ml ddH_2O

0.1025 g Sodium Acetate in 20 ml ddH_2O

Mix the above solutions

3 ml Glutamine

7 ml ddH_2O

Take 20 ml of the above buffer and add 0.01 g Cuprolinic Blue.

Appendix 4: Raw data and statistics for stromal cells and myofibroblast cell counts

Stromal cells

Cornea Number	Number of keratocytes in control cornea			Cornea Number	Number of keratocytes in control cornea		
0 hrs	Limbus (1)	Equidistant (2)	Mid Cornea (3)	2 weeks	Limbus (1)	Equidistant (2)	Mid Cornea (3)
1	12	21	23	1	13	21	23
2	17	21	18	2	17	21	18
3	16	15	16	3	16	15	16
24 hrs				3 weeks			
1	15	15	19	1	15	15	19
2	24	17	16	2	24	17	16
3	9	12	16	3	9	12	16
72 hrs				4 weeks			
1	22	16	16	1	22	16	16
2	15	15	20	2	15	15	20
3	20	13	17	3	20	13	17
7 days							
1	13	8	11				
2	10	7	8				
3	18	14	11				

Table 1: Raw data for stromal cell counts in control corneas

Cornea	Incision Site (1)		Equidistant (2)		Flap Edge (3)	
0hrs	**Above**	**Below**	**Above**	**Below**	**Above**	**Below**
1	6	22	7	6	8	18
2	13	10	12	11	12	18
3	12	10	17	12	16	13
p value1	0.155		0.827		0.117	
p value2	0.155	0.827	1.117	0.027	0.088	0.374
24hrs	**Above**	**Below**	**Above**	**Below**	**Above**	**Below**
1	34	38	26	20	13	9
2	19	16	22	14	26	26
3	14	14	20	29	21	14
p value1	0.027		0.088		0.374	
p value2	0.442	0.240	0.703	0.198	0.486	0.903
72hrs	**Above**	**Below**	**Above**	**Below**	**Above**	**Below**
1	20	15	14	16	21	21
2	17	11	11	13	16	16
3	6	17	9	14	8	14
p value1	0.5		0.047		0.211	
p value2	0.380	0.162	0.121	0.802	0.539	0.795
1week	**Above**	**Below**	**Above**	**Below**	**Above**	**Below**
1	8	11	8	13	9	10
2	12	14	12	11	17	18
3	16	20	11	11	11	14
p value1	0.442		0.493		0.025	
p value2	0.638	0.725	0.025	0.431	0.421	0.187
2 weeks	**Above**	**Below**	**Above**	**Below**	**Above**	**Below**
1	22	18	11	13	16	13
2	13	17	6	8	11	6
3	12	11	15	12	11	16
p value1	0.45		0.43		0.387	
p value2	1.00	0.927	0.064	0.034	0.076	0.113
3 weeks	**Above**	**Below**	**Above**	**Below**	**Above**	**Below**
1	12	12	10	12	11	10
2	10	8	11	11	8	8
3	13	14	12	11	9	11
p value1	0.371		0.371		0.371	
p value2	0.385	0.377	0.079	0.089	0.05	0.05
4 weeks	**Above**	**Below**	**Above**	**Below**	**Above**	**Below**
1	13	26	8	8	8	8
2	15	22	6	9	7	6

3	11	28	7	8	6	9
p value1	0.026		0.135		0.317	
p value2	0.065	0.081	0.003	0.002	0.001	0.003

Table 2: Raw data and student's t-test results comparing the number of cells at specific sites in the stroma above and below the incision in LASIK-like wounded corneas. p value1→ comparison between cell numbers above and above the incision in the same cornea, p value2→ against controls

Days in culture	Incision site		Corneal periphery control (No of cells /mm^2)
	No of cells above/mm^2	No of cells below/mm^2	
0	500.00	700.00	750.00
1	1100.00	1150.00	800.00
3	700.00	700.00	950.00
7	600.00	750.00	700.00
14	800.00	750.00	750.00
21	600.00	550.00	800.00
28	650.00	1250.00	950.00

Days in culture	Equidistance		Equidistance control (No of cells/mm^2)
	No of cells above/mm^2	No of cells below/mm^2	
0	600.00	500.00	950.00
1	1150.00	1050.00	750.00
3	550.00	700.00	750.00
7	500.00	600.00	500.00
14	550.00	550.00	950.00
21	550.00	550.00	750.00
28	350.00	400.00	750.00

Days in culture	Flap edge		Mid Cornea control (No of cells/mm^2)
	No of cells above/mm^2	No of cells below/mm^2	
0	600.00	800.00	950.00
1	1000.00	800.00	850.00
3	750.00	850.00	900.00
7	600.00	700.00	500.00
14	650.00	600.00	950.00
21	450.00	500.00	850.00
28	350.00	400.00	900.00

Table 3: Total cell counts/mm^2 for stromal cells from different areas along the LASIK-like flap.

Myofibroblasts

Timepoint (weeks)	αSMA positive cells	Total cells	%of positive cells
0	0.00	0.00	0.00
0	0.00	0.00	0.00
0	0.00	0.00	0.00
1	8.00	33.00	24.24
1	10.00	36.00	27.78
1	9.00	38.00	23.68
2	14.00	43.00	32.56
2	15.00	45.00	33.33
2	13.00	42.00	30.95
3	28.00	43.00	65.12
3	27.00	48.00	56.25
3	30.00	45.00	66.67
4	24.00	47.00	51.06
4	34.00	50.00	68.00
4	40.00	58.00	68.97

Table 4: Raw data for myofibroblast cell counts

Test Statistics[a,b]

	PERCENT
Chi-Square	9.462
df	3
Asymp. Sig.	.024

a. Kruskal Wallis Test

b. Grouping Variable: TIMEPOIN

Figure 1: Results for Kruskal Wallis test for myofibroblast cell counts

Test Statistics[b]

	PERCENT
N	12
Median	42.1986
Chi-Square	12.000[a]
df	3
Asymp. Sig.	.007

a. 8 cells (100.0%) have expected frequencies less than 5. The minimum expected cell frequency is 1.5.

b. Grouping Variable: TIMEPOIN

Figure 2: Results for median test for myofibroblast cell counts

Appendix 5: Raw data and statistics for the effect of growth factors in LASIK-like injured corneas

Mechanical strength

Control samples

Time in culture (weeks)	Force (10^{-1}N)
0	0.35
0	0.60
0	0.40
1	0.37
1	0.42
1	0.33
2	0.39
2	0.50
2	0.44
3	0.41
3	0.55
3	0.57
4	0.49
4	0.61
4	0.55

Table 5: Raw data for force required to detach the flap in a control/non cytokine treated LASIK-like corneas.

Test Statistics[a,b]

	LSK
Chi-Square	5.952
df	4
Asymp. Sig.	.203

a. Kruskal Wallis Test

b. Grouping Variable: TIME

Figure 3: Kruskal Wallis statistical test results

Test Statistics[b]

	LSK
N	15
Median	.4400
Chi-Square	6.964[a]
df	4
Asymp. Sig.	.138

a. 10 cells (100.0%) have expected frequencies less than 5. The minimum expected cell frequency is 1.4

b. Grouping Variable: TIME

Figure 4: Median statistical test results

TNF-α treated corneas

Time in Culture weeks	Force (10^{-1}N)			
	0.1ng/ml	10ng/ml	50ng/ml	100ng/ml
0	0.35	0.35	0.35	0.35
0	0.60	0.60	0.60	0.60
0	0.51	0.51	0.51	0.51
1	0.65	0.85	0.91	0.75
1	0.70	0.90	0.95	0.81
1	0.72	0.88	0.97	0.86
2	0.78	0.92	0.98	0.80
2	0.73	0.95	0.93	0.86
2	0.76	0.96	0.99	0.88
3	0.77	0.91	0.97	0.93
3	0.85	0.99	0.98	0.95
3	0.89	1.00	0.99	0.96
4	0.62	0.99	1.01	0.91
4	0.83	0.97	1.13	0.99
4	0.71	1.04	1.20	1.12

Table 6: Raw data for force required to detach the flap in a TNF-α treated LASIK-like corneas.

Test Statistics[a,b]

	C0.1	C10	C50	C100
Chi-Square	10.900	11.930	11.972	12.380
df	4	4	4	4
Asymp. Sig.	.028	.018	.018	.015

a. Kruskal Wallis Test

b. Grouping Variable: TIME

Figure 5: Kruskal Wallis statistical test results

Test Statistics[b]

	C0.1	C10	C50	C100
N	15	15	15	15
Median	.7200	.9200	.9700	.8600
Chi-Square	12.321[a]	9.643[a]	9.643[a]	12.321[a]
df	4	4	4	4
Asymp. Sig.	.015	.047	.047	.015

a. 10 cells (100.0%) have expected frequencies less than 5. The minimum expected cell frequency is 1.4.

b. Grouping Variable: TIME

Figure 6: Kruskal Wallis statistical test results

IL-1α treated corneas

Time in Culture weeks	Force (10^{-1}N)			
	0.1ng/ml	10ng/ml	50ng/ml	100ng/ml
0	0.35	0.35	0.35	0.35
0	0.60	0.60	0.60	0.60
0	0.51	0.51	0.51	0.51
1	0.61	0.61	0.81	0.66
1	0.75	0.95	0.88	1.00
1	0.66	0.64	0.86	0.80
2	0.66	0.75	0.90	1.01
2	0.78	0.70	0.90	0.99
2	0.72	0.77	0.92	1.03
3	0.70	0.82	0.78	1.07
3	0.85	0.90	1.05	1.10
3	0.80	0.88	0.93	1.05
4	0.90	0.78	1.15	1.15
4	0.75	1.01	0.99	1.00
4	0.97	0.92	1.06	1.00

Table 7: Raw data for force required to detach the flap in an IL-1α treated LASIK-like corneas.

Test Statistics[a,b]

	C0.1	C10	C50	C100
Chi-Square	10.429	9.733	11.253	11.012
df	4	4	4	4
Asymp. Sig.	.034	.045	.024	.026

a. Kruskal Wallis Test

b. Grouping Variable: TIME

Figure 3: Kruskal Wallis statistical test results

Test Statistics [c]

	C0.1	C10	C50	C100
N	15	15	15	15
Median	.7200	.7700	.9000	1.0000
Chi-Square	6.964[a]	12.321[a]	9.444[b]	9.444[b]
df	4	4	4	4
Asymp. Sig.	.138	.015	.051	.051

a. 10 cells (100.0%) have expected frequencies less than 5. The minimum expected cell frequency is 1.4.

b. 10 cells (100.0%) have expected frequencies less than 5. The minimum expected cell frequency is 1.2.

Figure 8: Median statistical test results

FasL treated corneas

Time in Culture weeks	Force (10^{-1}N)			
	0.1ng/ml	10ng/ml	50ng/ml	100ng/ml
0	0.35	0.35	0.35	0.35
0	0.60	0.60	0.60	0.60
0	0.51	0.51	0.51	0.51
1	0.66	0.67	0.90	0.63
1	0.78	0.77	0.79	0.76
1	0.70	0.75	0.83	0.80
2	0.67	0.76	0.95	0.80
2	0.76	0.62	0.99	0.71
2	0.71	0.68	1.00	0.75
3	0.80	0.80	0.98	0.90
3	0.61	0.61	1.06	0.99
3	0.61	0.75	1.02	1.00
4	0.70	0.75	1.00	1.05
4	0.81	0.66	0.99	0.90
4	0.83	0.78	1.07	1.10

Table 8: Raw data for force required to detach the flap in a FasL treated LASIK-like corneas.

Test Statistics[a,b]

	C0.1	C10	C50	C100
Chi-Square	8.113	7.084	11.474	12.327
df	4	4	4	4
Asymp. Sig.	.088	.132	.022	.015

a. Kruskal Wallis Test

b. Grouping Variable: TIME

Figure 9: Kruskal Wallis statistical test results

Test Statistics[d]

	C0.1	C10	C50	C100
N	14	15	15	15
Median	.7000	.6800	.9800	.8000
Chi-Square	3.792[a]	4.286[b]	9.643[b]	15.000[c]
df	4	4	4	4
Asymp. Sig.	.435	.369	.047	.005

a. 10 cells (100.0%) have expected frequencies less than 5. The minimum expected cell frequency is .9.

b. 10 cells (100.0%) have expected frequencies less than 5. The minimum expected cell frequency is 1.4.

c. 10 cells (100.0%) have expected frequencies less than 5. The minimum expected cell frequency is 1.2.

d. Grouping Variable: TIME

Figure 10: Median statistical test results

TGF-β_1 treated corneas

Time in Culture weeks	Force (10^{-1}N)			
	0.1ng/ml	10ng/ml	50ng/ml	100ng/ml
0	0.35	0.35	0.35	N/A
0	0.60	0.60	0.60	N/A
0	0.51	0.51	0.51	N/A
1	0.77	0.69	1.42	N/A
1	0.66	0.80	1.17	N/A
1	0.70	0.75	1.55	N/A
2	0.76	0.89	1.38	N/A
2	0.61	0.91	1.21	N/A
2	0.65	0.90	1.60	N/A
3	0.80	1.20	N/A	N/A
3	0.77	1.21	N/A	N/A
3	0.75	1.25	N/A	N/A
4	0.71	1.29	N/A	N/A
4	0.90	1.35	N/A	N/A
4	0.91	1.50	N/A	N/A

Table 9: Raw data for force required to detach the flap in a TGF-β_1 treated LASIK-like corneas.

Test Statistics[a,b]

	C0.1	C10	C50
Chi-Square	10.160	13.500	5.422
df	4	4	2
Asymp. Sig.	.038	.009	.066

a. Kruskal Wallis Test

b. Grouping Variable: TIME

Figure 11: Kruskal Wallis statistical test results

Test Statistics [c]

	C0.1	C10	C50
N	15	15	9
Median	.7100	.9000	1.2100
Chi-Square	6.964[a]	12.321[a]	3.600[b]
df	4	4	2
Asymp. Sig.	.138	.015	.165

a. 10 cells (100.0%) have expected frequencies less than 5. The minimum expected cell frequency is 1.4.

b. 6 cells (.0%) have expected frequencies less than 5. The minimum expected cell frequency is 1.3.

c. Grouping Variable: TIME

Figure 12: Median statistical test results

Cell counts

Control samples

→ Please refer to Appendix 4-Myofibroblast cell counts

TNF-α treated corneas

Time in Culture weeks	Myofibroblast population											
	0.1ng/ml			10ng/ml			50ng/ml			100ng/ml		
	+	T	%	+	T	%	+	T	%	+	T	%
0	0	0	0	0	0	0	0	0	0	0	0	0
0	0	0	0	0	0	0	0	0	0	0	0	0
0	0	0	0	0	0	0	0	0	0	0	0	0
1	28	73	38	30	77	39	41	80	51	25	78	32
1	40	74	54	38	76	50	50	83	60	35	81	43
1	30	71	42	39	80	49	36	65	55	27	75	36
2	45	80	56	42	81	52	43	83	52	43	82	52
2	40	77	52	46	83	55	29	72	40	49	90	54
2	43	82	52	36	82	44	50	73	68	49	96	51
3	50	88	57	38	79	48	53	91	58	56	98	57
3	56	93	60	55	86	64	56	93	60	58	99	59
3	53	95	56	42	73	58	52	89	58	53	94	56
4	60	93	65	45	70	64	60	110	55	75	120	63
4	66	93	71	39	89	44	54	106	51	79	118	67
4	69	98	70	48	75	64	59	99	60	77	120	64

Table 10: Raw data for changes in myofibroblast population in TNF-α treated LASIK-like corneas (+→ positivevely stained cells for αSMA, T→total cell counts, % → % of myofibroblasts put of total cell population).

Test Statistics[a,b]

	C0.1	C10	C50	C100
Chi-Square	12.791	8.494	7.621	13.597
df	4	4	4	4
Asymp. Sig.	.012	.075	.106	.009

a. Kruskal Wallis Test

b. Grouping Variable: TIMEPOIN

Figure 13: Kruskal Wallis statistical test results

Test Statistics[b]

	C0.1	C10	C50	C100
N	15	15	15	15
Median	54.0541	48.7500	54.5455	52.4390
Chi-Square	12.321[a]	4.286[a]	6.964[a]	12.321[a]
df	4	4	4	4
Asymp. Sig.	.015	.369	.138	.015

a. 10 cells (100.0%) have expected frequencies less than 5. The minimum expected cell frequency is 1.4.

b. Grouping Variable: TIMEPOIN

Figure 14: Median statistical test results

IL-1α treated corneas

	Myofibroblast population											
Time in Culture weeks	**0.1ng/ml**			**10ng/ml**			**50ng/ml**			**100ng/ml**		
	+	**T**	**%**	**+**	**T**	**%**	**+**	**T**	**%**	**+**	**T**	**%**
0	0	0	0	0	0	0	0	0	0	0	0	0
0	0	0	0	0	0	0	0	0	0	0	0	0
0	0	0	0	0	0	0	0	0	0	0	0	0
1	21	50	42	21	82	26	42	55	76	54	92	59
1	15	24	63	25	69	36	35	45	78	61	102	60
1	25	38	66	11	45	24	48	50	96	42	86	49
2	29	58	50	32	65	49	50	75	67	66	110	60
2	35	56	63	36	70	51	51	80	64	68	115	59
2	36	60	60	35	69	51	59	87	68	75	109	69
3	40	75	53	50	80	63	65	90	72	80	116	69
3	45	77	58	55	83	66	70	93	75	76	106	72
3	52	76	68	57	81	70	69	89	78	90	118	76
4	60	80	75	78	90	87	80	110	73	89	123	72
4	63	75	84	66	96	69	92	109	84	96	125	77
4	72	90	80	85	100	85	78	96	81	85	130	65

Table 11: Raw data for changes in myofibroblast population in TNF-α treated LASIK-like corneas (+→ positivevely stained cells for αSMA, T→total cell counts, % → % of myofibroblasts put of total cell population).

Test Statistics[a,b]

	C0.1	C10	C50	C100
Chi-Square	10.956	13.329	11.818	12.187
df	4	4	4	4
Asymp. Sig.	.027	.010	.019	.016

a. Kruskal Wallis Test

b. Grouping Variable: TIMEPOIN

Figure 15: Kruskal Wallis statistical test results

Test Statistics[b]

	C0.1	C10	C50	C100
N	15	15	15	15
Median	60.0000	50.7246	72.7273	60.0000
Chi-Square	6.964[a]	12.321[a]	9.643[a]	12.321[a]
df	4	4	4	4
Asymp. Sig.	.138	.015	.047	.015

a. 10 cells (100.0%) have expected frequencies less than 5. The minimum expected cell frequency is 1.4.

b. Grouping Variable: TIMEPOIN

Figure 16: Median statistical test results

FasL treated corneas

Time in Culture weeks	Myofibroblast population											
	0.1ng/ml			10ng/ml			50ng/ml			100ng/ml		
	+	T	%	+	T	%	+	T	%	+	T	%
0	0	0	0	0	0	0	0	0	0	0	0	0
0	0	0	0	0	0	0	0	0	0	0	0	0
0	0	0	0	0	0	0	0	0	0	0	0	0
1	9	27	33	11	32	34	15	35	43	20	40	50
1	8	30	27	13	38	34	16	33	48	18	41	44
1	11	29	38	16	35	46	18	31	58	27	42	64
2	12	35	34	15	35	43	21	42	50	25	52	48
2	15	40	38	13	39	33	29	38	76	27	53	51
2	11	38	29	18	40	45	25	36	69	28	59	47
3	14	45	31	20	38	53	30	50	60	29	75	39
3	15	48	31	23	42	55	32	55	58	26	63	41
3	12	45	27	19	41	46	34	58	59	30	69	43
4	16	53	30	18	46	39	39	65	60	50	80	63
4	18	60	30	20	55	36	40	69	58	55	81	68
4	20	58	34	25	53	47	45	71	63	61	79	77

Table 12: Raw data for changes in myofibroblast population in TNF-α treated LASIK-like corneas (+→ positivevely stained cells for αSMA, T→total cell counts, % → % of myofibroblasts put of total cell population).

Test Statistics[a,b]

	C0.1	C10	C50	C100
Chi-Square	7.509	10.643	9.964	12.523
df	4	4	4	4
Asymp. Sig.	.111	.031	.041	.014

a. Kruskal Wallis Test

b. Grouping Variable: TIMEPOIN

Figure 17: Kruskal Wallis statistical test results

Test Statistics[b]

	C0.1	C10	C50	C100
N	15	15	15	15
Median	30.1887	39.1304	58.0645	47.4576
Chi-Square	4.286[a]	6.964[a]	9.643[a]	9.643[a]
df	4	4	4	4
Asymp. Sig.	.369	.138	.047	.047

a. 10 cells (100.0%) have expected frequencies less than 5. The minimum expected cell frequency is 1.4.

b. Grouping Variable: TIMEPOIN

Figure 18: Median statistical test results

Appendix 6: Raw data and statistics for x-ray diffraction experiments

Trephine wounded corneas

Controls

Independent Samples Test

		Levene's Test for Equality of Variances		t-test for Equality of Means						
									95% Confidence Interval of the Difference	
		F	Sig.	t	df	Sig. (2-tailed)	Mean Difference	Std. Error Difference	Lower	Upper
C2WKSIFS	Equal variances assumed	16.000	.016	-1.000	4	.374	-.3333	.33333	-1.25882	.59215
	Equal variances not assumed			-1.000	2.000	.423	-.3333	.33333	-1.76755	1.10088

A

Independent Samples Test

		Levene's Test for Equality of Variances		t-test for Equality of Means						
									95% Confidence Interval of the Difference	
		F	Sig.	t	df	Sig. (2-tailed)	Mean Difference	Std. Error Difference	Lower	Upper
C1WKIFS	Equal variances assumed	16.000	.016	1.000	4	.374	.0600	.06000	-.10659	.22659
	Equal variances not assumed			1.000	2.000	.423	.0600	.06000	-.19816	.31816

B

Figure 19: Independent sample t-test comparing IFS in control corneas. 0hrs and 1weeks (A) and 0hrs and 2weeks (B)

0hrs

Position of scan	Control Fd	Trephine wounded Fd	Control IFS	Trephine wounded Fd
-9.00	36.98	36.22	67.58	67.59
-9.00	34.82	36.10	67.59	67.43
-9.00	36.88	35.27	67.56	67.52
-8.00	35.50	36.10	67.42	67.10
-8.00	35.27	35.98	67.20	67.65
-8.00	35.98	35.50	67.30	67.42
-7.00	35.98	36.22	67.43	67.01
-7.00	35.98	35.98	66.87	67.56
-7.00	36.22	35.98	66.44	67.47
-6.00	36.10	36.22	66.22	67.00
-6.00	35.62	35.74	66.70	67.76
-6.00	36.46	36.10	67.00	67.15
-5.00	35.74	35.74	66.75	67.00
-5.00	35.62	35.50	66.60	66.99
-5.00	36.59	36.10	66.21	66.72
-4.00	35.74	36.10	66.97	66.74
-4.00	35.34	35.74	67.04	67.25
-4.00	36.46	36.22	66.01	66.57
-3.00	35.98	35.98	65.67	67.24
-3.00	35.74	35.27	66.52	67.36
-3.00	36.22	35.98	65.65	65.65
-2.00	35.74	35.74	65.82	65.51
-2.00	35.50	35.50	65.59	65.59
-2.00	36.34	36.10	65.22	65.80
-1.00	35.39	35.74	65.65	65.31
-1.00	35.74	35.39	65.81	65.72
-1.00	36.59	35.74	65.02	65.60
0.00	35.86	35.86	65.61	65.30
0.00	35.50	35.16	65.53	65.42

0.00	36.46	35.86	65.02	65.59
1.00	35.98	35.74	65.66	65.72
1.00	35.74	35.86	65.32	65.59
1.00	36.71	35.62	65.42	65.42
2.00	35.62	38.18	65.89	66.76
2.00	35.50	35.62	66.76	66.05
2.00	36.84	35.62	66.56	66.56
3.00	35.74	35.74	66.55	67.00
3.00	35.74	36.10	66.53	67.10
3.00	36.84	35.50	66.93	66.93
4.00	35.98	35.50	66.88	67.01
4.00	35.74	35.98	66.65	67.05
4.00	36.96	35.74	66.93	66.93
5.00	35.74	35.74	67.10	67.20
5.00	35.50	35.74	66.59	67.26
5.00	36.84	35.86	66.67	66.67
6.00	35.98	35.74	66.78	66.98
6.00	35.86	36.46	66.40	67.21
6.00	36.71	35.98	66.72	66.72
7.00	35.86	35.87	67.10	67.20
7.00	35.50	35.86	66.64	66.78
7.00	36.46	38.18	66.37	66.37
8.00	36.22	35.62	67.10	67.25
8.00	35.39	36.22	67.25	67.54
8.00	36.84	36.62	67.46	67.46
9.00	34.74	35.74	67.15	67.50
9.00	34.70	35.98	67.16	67.87
9.00	36.22	38.20	67.32	67.32

Table 13: Raw data for fibril diameter (Fd) and interfibrillar spacing (IFS) for trephine wounded corneas and their corresponding controls at 0hrs.

ANOVA

		Sum of Squares	df	Mean Square	F	Sig.
CONTROL	Between Groups	3.070	18	.171	.454	.963
	Within Groups	14.281	38	.376		
	Total	17.351	56			
TWOHRS	Between Groups	5.293	18	.294	.752	.738
	Within Groups	14.867	38	.391		
	Total	20.160	56			

Figure 20: One-way ANOVA statistical test results comparing fibril diameter according to the position of scan

ANOVA

		Sum of Squares	df	Mean Square	F	Sig.
CONTROLI	Between Groups	23.822	18	1.323	12.302	.000
	Within Groups	4.088	38	.108		
	Total	27.909	56			
TREPHINE	Between Groups	26.839	18	1.491	13.568	.000
	Within Groups	4.176	38	.110		
	Total	31.015	56			

Figure 21: One-way ANOVA statistical test results comparing interfibrillar spacing according to the position of scan

Independent Samples Test

		Levene's Test for Equality of Variances		t-test for Equality of Means						
									95% Confidence Interval of the Difference	
		F	Sig.	t	df	Sig. (2-tailed)	Mean Difference	Std. Error Difference	Lower	Upper
DBRAGGS	Equal variances assumed	1.329	.252	.024	112	.981	.0026	.10840	-.21216	.21742
	Equal variances not assumed			.024	111.375	.981	.0026	.10840	-.21217	.21743

Figure 22: Independent sample T-test comparing fibril diameter according to type (i.e. wounded/unwounded)

Independent Samples Test

		Levene's Test for Equality of Variances		t-test for Equality of Means						
									95% Confidence Interval of the Difference	
		F	Sig.	t	df	Sig. (2-tailed)	Mean Difference	Std. Error Difference	Lower	Upper
IFS	Equal variances assumed	.175	.676	-1.754	112	.082	-.2382	.13587	-.50745	.03096
	Equal variances not assumed			-1.754	111.690	.082	-.2382	.13587	-.50746	.03097

Figure 23: Independent sample T-test comparing interfibrillar spacing according to type (i.e. wounded/unwounded)

1week

Position of scan	Control Fd	Trephine wounded Fd	Control IFS	Trephine wounded Fd
-9.00	36.65	36.16	67.96	80.00
-9.00	35.47	36.68	67.59	77.38
-9.00	36.14	36.22	67.56	79.23
-8.00	35.98	35.78	67.55	80.00
-8.00	36.89	36.22	67.22	78.83
-8.00	35.65	36.46	67.30	78.94
-7.00	36.90	36.38	66.93	78.00
-7.00	35.45	36.22	67.02	76.66
-7.00	35.98	35.98	66.44	77.38
-6.00	36.64	35.74	67.50	79.00
-6.00	35.62	35.98	67.06	78.92
-6.00	36.14	35.62	67.00	78.67
-5.00	36.46	35.74	67.01	76.76
-5.00	35.98	35.50	66.06	76.10
-5.00	35.74	35.74	66.21	76.24
-4.00	36.22	35.74	66.58	75.75
-4.00	36.22	35.97	67.04	75.05
-4.00	35.14	36.22	67.50	75.00
-3.00	36.59	40.86	66.23	76.67
-3.00	35.74	40.22	66.56	76.65
-3.00	35.27	38.88	66.88	73.49
-2.00	36.22	40.34	65.98	74.24
-2.00	35.50	40.71	66.04	75.54
-2.00	35.16	39.88	66.02	73.49
-1.00	35.50	40.00	65.98	72.19
-1.00	36.00	40.16	66.21	74.23
-1.00	35.27	38.87	66.45	72.19
0.00	35.22	39.00	66.00	74.42
0.00	35.12	37.27	66.67	75.54

0.00	35.50	38.74	65.20	73.17
1.00	36.39	40.86	66.45	76.01
1.00	35.74	40.22	65.55	75.77
1.00	36.42	39.49	65.35	75.06
2.00	37.00	39.71	65.99	74.22
2.00	35.50	40.44	66.28	74.02
2.00	36.71	39.87	66.21	75.67
3.00	36.14	38.82	67.68	76.56
3.00	36.48	37.74	66.23	75.02
3.00	36.96	40.00	67.03	75.62
4.00	36.46	35.98	66.68	76.77
4.00	35.97	35.74	66.67	75.54
4.00	36.84	35.84	66.24	76.63
5.00	35.98	35.74	66.48	77.75
5.00	35.74	35.68	67.05	78.31
5.00	36.59	35.59	66.98	77.96
6.00	36.16	35.62	66.95	77.00
6.00	35.62	36.46	66.78	77.22
6.00	36.46	35.85	66.73	77.66
7.00	35.85	35.62	67.10	79.00
7.00	35.62	35.97	67.28	79.29
7.00	35.98	36.14	67.20	79.75
8.00	36.46	35.62	68.45	79.34
8.00	35.62	36.22	67.42	80.14
8.00	36.22	36.40	67.53	78.28
9.00	35.85	35.50	66.82	79.36
9.00	35.50	36.10	67.27	72.98
9.00	36.10	36.37	67.93	74.26

Table 14: Raw data for fibril diameter (Fd) and interfibrillar spacing (IFS) for trephine wounded corneas and their corresponding controls at 1week.

ANOVA

		Sum of Squares	df	Mean Square	F	Sig.
CONTROL	Between Groups	5.035	18	.280	1.101	.388
	Within Groups	9.656	38	.254		
	Total	14.692	56			
TREPHINE	Between Groups	188.741	18	10.486	36.567	.000
	Within Groups	10.897	38	.287		
	Total	199.637	56			

Figure 24: One-way ANOVA statistical test results comparing fibril diameter according to the position of scan

ANOVA

		Sum of Squares	df	Mean Square	F	Sig.
CONTROLI	Between Groups	18.567	18	1.031	6.254	.000
	Within Groups	6.267	38	.165		
	Total	24.834	56			
TREPHI_A	Between Groups	204.434	18	11.357	8.656	.000
	Within Groups	49.861	38	1.312		
	Total	254.295	56			

Figure 25: One-way ANOVA statistical test results comparing interfibrillar spacing according to the position of scan

Independent Samples Test

		Levene's Test for Equality of Variances		t-test for Equality of Means						
									95% Confidence Interval of the Difference	
		F	Sig.	t	df	Sig. (2-tailed)	Mean Difference	Std. Error Difference	Lower	Upper
DBRAGGS	Equal variances assumed	134.747	.000	-5.020	112	.000	-1.3009	.25912	-1.81430	-.78746
	Equal variances not assumed			-5.020	64.198	.000	-1.3009	.25912	-1.81851	-.78325

Figure 26: Independent sample T-test comparing fibril diameter according to type (i.e. wounded/unwounded)

Independent Samples Test

		Levene's Test for Equality of Variances		t-test for Equality of Means						
									95% Confidence Interval of the Difference	
		F	Sig.	t	df	Sig. (2-tailed)	Mean Difference	Std. Error Difference	Lower	Upper
IFS	Equal variances assumed	55.764	.000	-33.155	112	.000	-9.8043	.29571	-10.39023	-9.21840
	Equal variances not assumed			-33.155	66.834	.000	-9.8043	.29571	-10.39459	-9.21404

Figure 27: Independent sample T-test comparing interfibrillar spacing according to type (i.e. wounded/unwounded)

2weeks

Position of scan	Control Fd	Trephine wounded Fd	Control IFS	Trephine wounded Fd
-9.00	36.22	36.34	67.46	82.00
-9.00	36.10	36.77	67.29	80.95
-9.00	36.03	36.48	67.57	79.67
-8.00	35.55	35.50	67.26	81.02
-8.00	36.10	36.42	67.33	80.00
-8.00	36.28	35.98	67.43	79.66
-7.00	36.28	35.74	67.15	78.96
-7.00	35.75	35.50	67.10	79.00
-7.00	36.22	35.39	67.04	79.86
-6.00	35.66	35.39	67.05	78.28
-6.00	35.62	35.49	67.12	78.34
-6.00	36.10	36.01	67.09	79.86
-5.00	35.75	35.50	67.01	79.24
-5.00	35.49	35.39	67.01	79.66
-5.00	36.22	36.01	66.71	79.86
-4.00	36.10	35.62	67.05	78.26
-4.00	35.78	35.49	67.40	78.39
-4.00	35.98	35.79	67.03	77.96
-3.00	35.84	35.39	67.00	77.24
-3.00	35.68	35.68	67.02	78.03
-3.00	35.74	36.14	67.00	77.96
-2.00	35.86	39.84	66.50	78.29
-2.00	35.50	42.00	66.74	76.25
-2.00	35.86	43.88	67.00	75.27
-1.00	35.49	42.24	66.94	78.24
-1.00	35.86	42.79	67.21	78.00
-1.00	35.98	41.98	66.65	77.96
0.00	35.74	38.29	66.73	78.06
0.00	35.49	38.64	66.57	76.24

0.00	35.50	40.02	67.00	77.96
1.00	35.74	41.24	66.45	77.96
1.00	35.62	41.35	66.45	77.88
1.00	35.86	42.00	66.85	79.43
2.00	35.49	42.00	67.07	77.96
2.00	35.74	42.42	66.53	78.00
2.00	35.78	42.74	66.91	78.24
3.00	35.86	42.42	66.91	79.42
3.00	35.62	42.71	67.00	78.98
3.00	36.10	41.52	67.01	79.58
4.00	35.98	42.28	66.98	79.27
4.00	35.78	35.04	66.78	77.86
4.00	35.96	34.37	66.78	78.07
5.00	35.86	34.15	67.00	79.86
5.00	35.78	34.59	67.05	79.64
5.00	36.10	35.27	67.03	79.24
6.00	36.00	35.50	66.98	79.00
6.00	35.98	35.38	66.76	78.95
6.00	35.86	35.50	67.01	79.86
7.00	35.78	35.39	67.10	79.96
7.00	35.27	35.27	67.46	79.00
7.00	36.00	35.78	67.55	80.01
8.00	36.01	35.27	67.68	81.86
8.00	35.98	35.42	67.34	79.35
8.00	36.18	35.78	67.45	79.35
9.00	36.20	35.74	67.34	82.00
9.00	36.18	36.14	67.00	79.98
9.00	36.10	36.48	67.00	81.03

Table 15: Raw data for fibril diameter (Fd) and interfibrillar spacing (IFS) for trephine wounded corneas and their corresponding controls at 2weeks.

ANOVA

		Sum of Squares	df	Mean Square	F	Sig.
CONTROL	Between Groups	1.435	18	.080	1.675	.089
	Within Groups	1.808	38	.048		
	Total	3.243	56			
TREPHINE	Between Groups	450.410	18	25.023	18.075	.000
	Within Groups	52.606	38	1.384		
	Total	503.016	56			

Figure 28: One-way ANOVA statistical test results comparing fibril diameter according to the position of scan

ANOVA

		Sum of Squares	df	Mean Square	F	Sig.
CONTROLI	Between Groups	3.249	18	.181	5.870	.000
	Within Groups	1.169	38	.031		
	Total	4.418	56			
TREPHI_A	Between Groups	74.152	18	4.120	6.538	.000
	Within Groups	23.943	38	.630		
	Total	98.094	56			

Figure 29: One-way ANOVA statistical test results comparing interfibrillar spacing according to the position of scan

Independent Samples Test

		Levene's Test for Equality of Variances		t-test for Equality of Means						
									95% Confidence Interval of the Difference	
		F	Sig.	t	df	Sig. (2-tailed)	Mean Difference	Std. Error Difference	Lower	Upper
DBRAGGS	Equal variances assumed	189.240	.000	-4.342	112	.000	-1.7277	.39787	-2.51605	-.93939
	Equal variances not assumed			-4.342	56.940	.000	-1.7277	.39787	-2.52446	-.93098

Figure 30: Independent sample T-test comparing interfibrillar spacing according to type (i.e. wounded/unwounded)

Independent Samples Test

		Levene's Test for Equality of Variances		t-test for Equality of Means						
									95% Confidence Interval of the Difference	
		F	Sig.	t	df	Sig. (2-tailed)	Mean Difference	Std. Error Difference	Lower	Upper
IFS	Equal variances assumed	51.842	.000	-66.695	112	.000	-11.9523	.17921	-12.30736	-11.59720
	Equal variances not assumed			-66.695	61.034	.000	-11.9523	.17921	-12.31062	-11.59394

Figure 31: Independent sample T-test comparing interfibrillar spacing according to type (i.e. wounded/unwounded)

LASIK-like injured corneas

Controls

Independent Samples Test

		Levene's Test for Equality of Variances		t-test for Equality of Means						
									95% Confidence Interval of the Difference	
		F	Sig.	t	df	Sig. (2-tailed)	Mean Difference	Std. Error Difference	Lower	Upper
C1WKIFS	Equal variances assumed	4.119	.112	.391	4	.716	.1667	.42592	-1.01589	1.34922
	Equal variances not assumed			.391	2.196	.730	.1667	.42592	-1.51803	1.85136
C2WKSIFS	Equal variances assumed	.244	.648	.513	4	.635	.1667	.32462	-.73462	1.06795
	Equal variances not assumed			.513	3.513	.638	.1667	.32462	-.78607	1.11940

A

Independent Samples Test

		Levene's Test for Equality of Variances		t-test for Equality of Means						
									95% Confidence Interval of the Difference	
		F	Sig.	t	df	Sig. (2-tailed)	Mean Difference	Std. Error Difference	Lower	Upper
C1WKIFS	Equal variances assumed	4.119	.112	.391	4	.716	.1667	.42592	-1.01589	1.34922
	Equal variances not assumed			.391	2.196	.730	.1667	.42592	-1.51803	1.85136
C3WKSIFS	Equal variances assumed	3.479	.136	-.030	4	.977	-.0067	.22010	-.61776	.60443
	Equal variances not assumed			-.030	2.878	.978	-.0067	.22010	-.72420	.71087

B

Independent Samples Test

		Levene's Test for Equality of Variances		t-test for Equality of Means						
									95% Confidence Interval of the Difference	
		F	Sig.	t	df	Sig. (2-tailed)	Mean Difference	Std. Error Difference	Lower	Upper
C1WKIFS	Equal variances assumed	4.119	.112	.391	4	.716	.1667	.42592	-1.01589	1.34922
	Equal variances not assumed			.391	2.196	.730	.1667	.42592	-1.51803	1.85136
C4WKSIFS	Equal variances assumed	1.247	.327	-.242	4	.821	-.0633	.26202	-.79082	.66416
	Equal variances not assumed			-.242	3.447	.823	-.0633	.26202	-.83925	.71258

C

Figure 32: Independent sample t-test comparing IFS in control corneas. 1weeks and 2weeks (A), 1week and 2weeks (B), 1week and 3weeks (C)

1week

Position of scan	Control Fd	Trephine wounded Fd	Control IFS	Trephine wounded Fd
11.00	36.66	36.66	67.97	74.00
11.00	35.48	36.34	67.88	73.89
11.00	36.00	36.57	67.66	73.96
10.00	36.29	35.92	67.55	73.75
10.00	36.54	35.57	67.22	73.89
10.00	35.65	36.16	67.32	73.65
9.00	36.24	36.48	66.93	73.05
9.00	36.33	36.23	66.75	73.25
9.00	35.74	36.00	66.24	73.68
8.00	36.00	35.74	67.50	73.00
8.00	35.57	35.93	67.66	72.92
8.00	36.01	35.57	67.00	73.67
7.00	35.69	35.74	67.01	73.74
7.00	35.98	35.57	66.96	73.01
7.00	35.57	35.74	66.81	73.24
6.00	35.93	35.57	66.75	72.95
6.00	36.00	35.93	67.04	72.24
6.00	35.69	35.34	67.30	72.00
5.00	35.88	35.36	66.23	72.15
5.00	35.69	35.00	66.96	72.24
5.00	35.27	35.88	66.81	72.67
4.00	35.98	35.74	66.00	72.24
4.00	35.93	35.93	66.04	72.55
4.00	35.74	35.74	66.23	72.15
3.00	35.50	35.57	66.00	72.19
3.00	35.74	35.26	66.04	72.24
3.00	35.27	35.00	66.23	72.19
2.00	35.22	35.74	66.00	72.55
2.00	35.23	35.93	66.75	72.24

2.00	35.57	36.00	66.23	72.19
1.00	35.69	37.69	66.23	72.95
1.00	35.74	37.27	66.75	73.00
1.00	35.98	37.28	66.35	72.88
.00	36.34	37.69	66.00	76.35
.00	35.50	37.72	66.23	75.25
.00	35.21	37.00	66.21	74.61
-1.00	35.24	35.57	66.00	72.15
-1.00	35.57	36.00	66.23	72.02
-1.00	35.93	36.23	67.03	72.55
-2.00	35.74	35.98	66.68	72.19
-2.00	35.97	35.74	66.67	72.24
-2.00	35.83	35.86	66.23	72.74
-3.00	35.93	35.57	66.48	72.74
-3.00	35.74	35.68	66.00	72.24
-3.00	35.65	35.57	66.98	72.95
-4.00	35.24	35.67	66.95	72.68
-4.00	35.57	35.74	66.78	72.94
-4.00	35.69	35.93	66.75	72.64
-5.00	35.85	35.64	67.10	73.00
-5.00	35.64	35.93	67.03	73.65
-5.00	35.93	36.00	66.98	73.25
-6.00	36.00	35.64	68.45	73.68
-6.00	35.98	36.03	67.03	73.89
-6.00	36.04	35.74	67.53	73.96
2.00	35.23	35.93	66.75	72.24
2.00	35.57	36.00	66.23	72.19
1.00	35.69	37.69	66.23	72.95

Table 16: Raw data for fibril diameter (Fd) and interfibrillar spacing (IFS) for LASIK-like injured corneas and their corresponding controls at 1week.

ANOVA

		Sum of Squares	df	Mean Square	F	Sig.
CONTROL	Between Groups	2.488	17	.146	1.643	.103
	Within Groups	3.206	36	.089		
	Total	5.694	53			
LSK	Between Groups	18.054	17	1.062	18.030	.000
	Within Groups	2.121	36	.059		
	Total	20.175	53			

Figure 33: One-way ANOVA statistical test results comparing fibril diameter according to the position of scan

ANOVA

		Sum of Squares	df	Mean Square	F	Sig.
CONTROLI	Between Groups	14.258	17	.839	7.795	.000
	Within Groups	3.873	36	.108		
	Total	18.131	53			
LSKIFS	Between Groups	35.319	17	2.078	18.090	.000
	Within Groups	4.135	36	.115		
	Total	39.454	53			

Figure 34: One-way ANOVA statistical test results comparing interfibrillar spacing according to the position of scan

Independent Samples Test

		Levene's Test for Equality of Variances		t-test for Equality of Means						
									95% Confidence Interval of the Difference	
		F	Sig.	t	df	Sig. (2-tailed)	Mean Difference	Std. Error Difference	Lower	Upper
DBRAGGS	Equal variances assumed	6.779	.011	-2.141	106	.035	-.2035	.09507	-.39201	-.01503
	Equal variances not assumed			-2.141	80.709	.035	-.2035	.09507	-.39269	-.01435

Figure 35: Independent sample T-test comparing fibril diameter according to type (i.e. wounded/unwounded)

Independent Samples Test

		Levene's Test for Equality of Variances		t-test for Equality of Means						
									95% Confidence Interval of the Difference	
		F	Sig.	t	df	Sig. (2-tailed)	Mean Difference	Std. Error Difference	Lower	Upper
IFS	Equal variances assumed	4.457	.037	-44.166	106	.000	-6.2649	.14185	-6.54610	-5.98365
	Equal variances not assumed			-44.166	93.218	.000	-6.2649	.14185	-6.54654	-5.98320

Figure 36: Independent sample T-test comparing interfibrillar spacing according to type (i.e. wounded/unwounded)

2weeks

Position of scan	Control Fd	Trephine wounded Fd	Control IFS	Trephine wounded Fd
11.00	36.26	36.36	67.98	76.23
11.00	35.37	36.24	67.56	75.89
11.00	36.05	35.92	67.05	76.98
10.00	36.18	36.00	67.35	75.74
10.00	36.43	35.57	67.55	75.89
10.00	35.65	36.06	67.00	76.36
9.00	36.23	35.93	67.23	76.05
9.00	36.33	36.26	67.33	76.23
9.00	35.74	36.00	67.00	75.89
8.00	36.00	35.57	67.00	75.00
8.00	35.57	35.74	67.56	75.95
8.00	36.05	35.45	67.00	75.74
7.00	35.65	36.04	67.00	75.74
7.00	36.05	35.74	66.96	75.01
7.00	35.65	35.57	67.03	75.74
6.00	36.00	35.57	66.75	75.95
6.00	36.00	36.00	67.04	75.24
6.00	35.65	35.93	67.35	75.00
5.00	35.74	35.69	67.23	75.24
5.00	35.65	36.04	67.00	75.24
5.00	35.37	35.74	67.01	75.74
4.00	36.00	35.57	67.00	75.24
4.00	36.00	35.69	67.04	75.78
4.00	35.54	35.45	67.23	75.01
3.00	35.57	35.69	67.00	75.24
3.00	35.74	35.54	67.04	75.89
3.00	35.16	35.57	67.23	75.18
2.00	35.24	35.93	67.00	75.68
2.00	35.37	36.00	66.96	75.24

2.00	35.67	36.04	67.23	75.18
1.00	35.69	37.00	67.23	75.95
1.00	35.74	37.33	66.75	75.00
1.00	36.00	37.25	67.00	75.89
.00	36.00	37.15	67.00	68.40
.00	35.57	37.25	67.23	69.85
.00	35.24	37.00	67.35	69.12
-1.00	35.24	35.57	67.00	75.47
-1.00	35.57	36.01	67.23	75.68
-1.00	36.00	36.23	67.03	75.89
-2.00	35.74	36.00	66.96	75.24
-2.00	36.00	35.69	66.75	75.89
-2.00	35.74	35.77	67.23	75.24
-3.00	36.00	35.57	67.45	75.78
-3.00	35.74	35.69	67.00	75.24
-3.00	35.74	35.57	66.96	75.95
-4.00	35.24	35.34	66.95	75.68
-4.00	35.57	35.77	66.78	75.89
-4.00	35.57	36.00	67.00	75.68
-5.00	35.74	35.69	67.10	75.00
-5.00	35.57	35.93	67.03	75.64
-5.00	36.00	36.00	67.00	76.00
-6.00	36.00	36.29	67.56	75.68
-6.00	36.05	36.00	67.00	75.89
-6.00	35.74	35.57	67.53	76.00
2.00	36.26	36.36	67.98	76.23
2.00	35.37	36.24	67.56	75.89
1.00	36.05	35.92	67.05	76.98

Table 17: Raw data for fibril diameter (Fd) and interfibrillar spacing (IFS) for LASIK-like injured corneas and their corresponding controls at 2weeks.

ANOVA

		Sum of Squares	df	Mean Square	F	Sig.
CONTROL	Between Groups	2.007	17	.118	1.565	.127
	Within Groups	2.716	36	.075		
	Total	4.723	53			
LSK	Between Groups	10.985	17	.646	14.482	.000
	Within Groups	1.606	36	.045		
	Total	12.591	53			

Figure 37: One-way ANOVA statistical test results comparing fibril diameter according to the position of scan

ANOVA

		Sum of Squares	df	Mean Square	F	Sig.
CONTROLI	Between Groups	1.162	17	.068	1.310	.241
	Within Groups	1.878	36	.052		
	Total	3.041	53			
LSKIFS	Between Groups	124.496	17	7.323	43.704	.000
	Within Groups	6.032	36	.168		
	Total	130.528	53			

Figure 38: One-way ANOVA statistical test results comparing interfibrillar spacing according to the position of scan

Independent Samples Test

		Levene's Test for Equality of Variances		t-test for Equality of Means						
									95% Confidence Interval of the Difference	
		F	Sig.	t	df	Sig. (2-tailed)	Mean Difference	Std. Error Difference	Lower	Upper
DBRAGGS	Equal variances assumed	3.502	.064	-2.659	106	.009	-.2069	.07778	-.36106	-.05265
	Equal variances not assumed			-2.659	87.855	.009	-.2069	.07778	-.36143	-.05228

Figure 39: Independent sample T-test comparing fibril diameter according to type (i.e. wounded/unwounded)

Independent Samples Test

		Levene's Test for Equality of Variances		t-test for Equality of Means						
									95% Confidence Interval of the Difference	
		F	Sig.	t	df	Sig. (2-tailed)	Mean Difference	Std. Error Difference	Lower	Upper
IFS	Equal variances assumed	9.669	.002	-37.760	106	.000	-8.1574	.21603	-8.58574	-7.72913
	Equal variances not assumed			-37.760	55.468	.000	-8.1574	.21603	-8.59029	-7.72458

Figure 40: Independent sample T-test comparing interfibrillar spacing according to type (i.e. wounded/unwounded)

3weeks

Position of scan	Control Fd	Trephine wounded Fd	Control IFS	Trephine wounded Fd
11.00	36.33	36.23	67.56	77.22
11.00	35.57	36.98	67.29	77.02
11.00	36.05	35.88	67.26	77.33
10.00	36.28	35.57	67.57	77.00
10.00	36.33	35.69	67.03	76.98
10.00	35.57	36.00	67.33	76.56
9.00	36.33	36.16	67.05	76.05
9.00	36.33	35.93	67.35	76.23
9.00	35.74	35.74	67.00	76.79
8.00	36.00	36.00	67.05	76.17
8.00	35.57	35.57	67.22	75.95
8.00	36.00	35.74	67.00	76.78
7.00	35.57	36.00	67.05	76.77
7.00	36.00	35.57	67.25	76.00
7.00	35.75	35.69	67.35	76.74
6.00	36.00	35.57	67.05	76.68
6.00	36.06	36.00	67.35	76.24
6.00	35.57	35.93	67.57	76.00
5.00	35.74	35.69	67.00	76.24
5.00	35.65	36.00	67.05	76.74
5.00	35.57	35.75	67.22	76.77
4.00	36.00	35.57	66.74	76.24
4.00	36.05	35.69	66.67	76.78
4.00	35.57	35.48	67.00	76.00
3.00	35.75	35.74	67.00	76.24
3.00	35.74	35.57	67.22	76.89
3.00	35.26	35.69	66.67	76.28
2.00	35.24	35.93	66.73	76.78
2.00	35.57	36.05	66.67	76.24

2.00	35.75	36.10	67.00	76.78
1.00	35.75	36.98	66.35	76.00
1.00	35.69	37.00	66.45	76.05
1.00	36.00	37.88	66.67	76.29
.00	36.00	37.00	67.00	71.36
.00	35.57	37.35	66.53	69.11
.00	35.29	37.01	67.00	71.37
-1.00	35.26	36.00	67.00	76.47
-1.00	35.57	35.57	67.05	76.69
-1.00	36.00	36.33	67.01	76.89
-2.00	35.75	35.78	67.00	76.89
-2.00	36.00	36.00	67.05	76.24
-2.00	35.75	35.74	66.78	76.33
-3.00	36.00	35.69	67.00	76.24
-3.00	35.75	35.57	67.05	76.74
-3.00	35.57	35.74	67.03	75.95
-4.00	35.29	35.27	66.98	75.68
-4.00	35.57	35.74	66.76	76.89
-4.00	35.93	35.69	67.05	76.00
-5.00	35.74	36.01	67.15	76.30
-5.00	35.57	35.93	67.58	76.64
-5.00	36.00	36.01	67.23	76.00
-6.00	36.05	36.17	67.58	77.00
-6.00	36.23	35.74	66.98	77.24
-6.00	35.75	36.00	67.57	77.35
2.00	36.33	36.23	67.56	77.22
2.00	35.57	36.98	67.29	77.02
1.00	36.05	35.88	67.26	77.33

Table 17: Raw data for fibril diameter (Fd) and interfibrillar spacing (IFS) for LASIK-like injured corneas and their corresponding controls at 3weeks.

ANOVA

		Sum of Squares	df	Mean Square	F	Sig.
CONTROL	Between Groups	1.593	17	.094	1.192	.319
	Within Groups	2.831	36	.079		
	Total	4.424	53			
LSK	Between Groups	11.690	17	.688	10.281	.000
	Within Groups	2.408	36	.067		
	Total	14.099	53			

Figure 41: One-way ANOVA statistical test results comparing fibril diameter according to the position of scan

ANOVA

		Sum of Squares	df	Mean Square	F	Sig.
CONTROLI	Between Groups	2.926	17	.172	4.377	.000
	Within Groups	1.416	36	.039		
	Total	4.342	53			
LSKIFS	Between Groups	103.458	17	6.086	28.963	.000
	Within Groups	7.564	36	.210		
	Total	111.022	53			

Figure 42: One-way ANOVA statistical test results comparing interfibrillar spacing according to the position of scan

Independent Samples Test

		Levene's Test for Equality of Variances		t-test for Equality of Means						
									95% Confidence Interval of the Difference	
		F	Sig.	t	df	Sig. (2-tailed)	Mean Difference	Std. Error Difference	Lower	Upper
DBRAGGS	Equal variances assumed	3.803	.054	-2.461	106	.015	-.1980	.08045	-.35746	-.03847
	Equal variances not assumed			-2.461	83.280	.016	-.1980	.08045	-.35796	-.03796

Figure 43: Independent sample T-test comparing fibril diameter according to type (i.e. wounded/unwounded)

Independent Samples Test

		Levene's Test for Equality of Variances		t-test for Equality of Means						
									95% Confidence Interval of the Difference	
		F	Sig.	t	df	Sig. (2-tailed)	Mean Difference	Std. Error Difference	Lower	Upper
IFS	Equal variances assumed	8.388	.005	-45.478	106	.000	-9.1307	.20077	-9.52879	-8.73269
	Equal variances not assumed			-45.478	57.139	.000	-9.1307	.20077	-9.53276	-8.72873

Figure 44: Independent sample T-test comparing fibril interfibrillar spacing to type (i.e. wounded/unwounded)

4weeks

Position of scan	Control Fd	Trephine wounded Fd	Control IFS	Trephine wounded Fd
11.00	36.28	36.33	67.66	78.17
11.00	36.00	36.76	67.24	77.89
11.00	35.57	35.93	67.22	78.00
10.00	36.28	35.69	67.57	77.94
10.00	36.23	35.57	67.03	77.89
10.00	35.57	36.01	67.34	77.76
9.00	35.74	35.93	67.05	77.05
9.00	36.23	36.00	67.35	77.24
9.00	36.06	35.77	67.00	77.68
8.00	35.57	35.77	67.05	77.24
8.00	36.00	36.00	67.22	77.89
8.00	36.06	35.57	67.00	77.76
7.00	35.75	35.69	67.05	77.05
7.00	35.57	35.74	67.25	77.24
7.00	36.00	35.93	67.35	77.68
6.00	35.57	35.57	67.05	77.24
6.00	36.06	36.00	67.35	77.55
6.00	35.75	35.93	67.57	77.05
5.00	35.69	35.69	67.00	77.24
5.00	35.57	36.05	67.05	77.76
5.00	35.74	35.74	67.22	77.68
4.00	36.05	35.57	66.74	77.24
4.00	35.57	35.69	66.67	77.00
4.00	36.00	35.74	67.00	77.68
3.00	35.74	35.57	67.00	77.25
3.00	35.69	35.93	67.22	77.89
3.00	35.16	35.69	66.67	77.24
2.00	35.06	35.93	66.73	77.00
2.00	35.74	36.04	66.67	77.68

2.00	35.57	36.19	67.00	77.07
1.00	35.69	37.00	66.35	77.00
1.00	35.57	37.76	66.45	77.15
1.00	36.05	38.00	66.67	77.28
.00	35.57	37.66	67.00	68.40
.00	36.00	37.76	66.53	71.36
.00	35.16	38.00	67.00	69.85
-1.00	35.16	37.00	67.00	77.48
-1.00	36.00	37.05	67.05	77.68
-1.00	35.75	36.98	67.01	77.76
-2.00	35.57	36.77	67.00	77.68
-2.00	36.05	36.00	67.05	77.34
-2.00	35.57	36.30	66.78	77.24
-3.00	35.69	35.69	67.01	77.74
-3.00	35.74	35.77	67.15	77.69
-3.00	35.57	35.57	67.03	77.93
-4.00	35.16	35.77	67.00	77.89
-4.00	35.69	35.69	66.76	77.68
-4.00	35.74	35.57	67.05	77.34
-5.00	35.57	36.00	67.49	77.00
-5.00	36.04	35.98	67.58	77.74
-5.00	35.93	36.00	67.23	77.05
-6.00	36.05	36.33	67.69	77.00
-6.00	36.29	36.00	67.00	77.24
-6.00	35.93	36.05	67.62	77.35
2.00	36.28	36.33	67.66	78.17
2.00	36.00	36.76	67.24	77.89
1.00	35.57	35.93	67.22	78.00

Table 18: Raw data for fibril diameter (Fd) and interfibrillar spacing (IFS) for LASIK-like injured corneas and their corresponding controls at 4weeks.

ANOVA

		Sum of Squares	df	Mean Square	F	Sig.
CONTROL	Between Groups	1.734	17	.102	1.193	.318
	Within Groups	3.078	36	.085		
	Total	4.812	53			
LSK	Between Groups	21.624	17	1.272	23.929	.000
	Within Groups	1.914	36	.053		
	Total	23.538	53			

Figure 45: One-way ANOVA statistical test results comparing fibril diameter according to the position of scan

ANOVA

		Sum of Squares	df	Mean Square	F	Sig.
CONTROLI	Between Groups	3.263	17	.192	4.572	.000
	Within Groups	1.511	36	.042		
	Total	4.774	53			
LSKIFS	Between Groups	167.076	17	9.828	50.817	.000
	Within Groups	6.962	36	.193		
	Total	174.039	53			

Figure 46: One-way ANOVA statistical test results comparing interfibrillar spacing according to the position of scan

Independent Samples Test

		Levene's Test for Equality of Variances		t-test for Equality of Means						
									95% Confidence Interval of the Difference	
		F	Sig.	t	df	Sig. (2-tailed)	Mean Difference	Std. Error Difference	Lower	Upper
DBRAGGS	Equal variances assumed	16.220	.000	-3.965	106	.000	-.3946	.09953	-.59195	-.19731
	Equal variances not assumed			-3.965	73.800	.000	-.3946	.09953	-.59295	-.19631

Figure 47: Independent sample T-test comparing fibril diameter according to type (i.e. wounded/unwounded)

Independent Samples Test

		Levene's Test for Equality of Variances		t-test for Equality of Means						
									95% Confidence Interval of the Difference	
		F	Sig.	t	df	Sig. (2-tailed)	Mean Difference	Std. Error Difference	Lower	Upper
IFS	Equal variances assumed	7.017	.009	-39.940	106	.000	-9.9832	.24996	-10.47877	-9.48764
	Equal variances not assumed			-39.940	55.906	.000	-9.9832	.24996	-10.48395	-9.48246

Figure 48: Independent sample T-test comparing interfibrillar spacing according to type (i.e. wounded/unwounded)

Differential Regulation of Key Stages in Early Corneal Wound Healing by TGF-β Isoforms and Their Inhibitors

Louise M. Carrington,[1,2] *Julie Albon,*[1,2] *Ian Anderson,*[3] *Christina Kamma,*[1,2] *and Mike Boulton*[1,2]

Purpose. Inhibition of TGF-β reduces myofibroblast differentiation and fibrosis in the cornea. Determining the actions of distinct TGF-β isoforms and their inhibitors during early corneal wound healing is an essential step in guiding therapeutic intervention.

Methods. Bovine serum-free corneal cell and wounded organ cultures were challenged with a range of concentrations of TGF-β_1, -β_2, and -β_3; IL-10; and neutralizing human monoclonal antibodies (mAbs) against TGF-β_1 (CAT-192) or -β_2, (CAT-152). Cultures were assessed for re-epithelialization, proliferation (cell counts and cresyl violet assay), morphology (histologic examination), repopulation of the area under the wound, and myofibroblast transformation (α-smooth muscle actin) between 0 and 5 days.

Results. TGF-β_1 delayed re-epithelialization, increased repopulation of the stroma, increased keratocyte proliferation and was the only isoform to promote myofibroblast differentiation. The anti-TGF-β_1 mAb, CAT-192 promoted re-epithelialization and reduced repopulation of the stroma. Exogenous TGF-β_3 had little effect on re-epithelialization but reduced repopulation of the stroma. IL-10 promoted corneal re-epithelialization at low doses but inhibited this response at high doses. Stromal repopulation was prevented by all doses of IL-10. TGF-β_2 or the anti-TGF-β_2 mAb, CAT-152 had little effect on any repair parameter.

Conclusions. The results confirm TGF-β_1 as the principal isoform in corneal wound healing and suggest that inhibition of the action of TGF-β_1 can promote corneal wound healing. Treatment with the anti-TGF-β_1 mAb CAT-192 accelerates corneal re-epithelialization but reduces cell repopulation of the stroma. The cytokines TGF-β_3 and IL-10 have opposing actions to that of TGF-β_1. (*Invest Ophthalmol Vis Sci.* 2006;47: 1886-1894) DOI:10.1167/iovs.05-0635

From the [1]Cell and Molecular Unit, School of Optometry and Vision Sciences, Cardiff University, Cardiff, United Kingdom; the [2]Cardiff Institute of Tissue Engineering and Repair, Cardiff University, Cardiff, United Kingdom; and [3]Cambridge Antibody Technology, Cambridge, United Kingdom.

Presented in part at the annual meeting of the Association for Research in Vision and Ophthalmology, Fort Lauderdale, Florida, May 2001.

Supported by the Wellcome Trust, BBSRC, the Guide Dogs for the Blind Association, and Cambridge Antibody Technology.

Submitted for publication May 22, 2005; revised November 12, 2005, and January 4, 2006; accepted March 17, 2006.

Disclosure: **L.M. Carrington**, Cambridge Antibody Technology (F); **J. Albon**, None; **I. Anderson**, Cambridge Antibody Technology (E); **C. Kamma**, None; **M. Boulton**, Cambridge Antibody Technology (F)

The publication costs of this article were defrayed in part by page charge payment. This article must therefore be marked "*advertisement*" in accordance with 18 U.S.C. §1734 solely to indicate this fact.

Corresponding author: Mike Boulton, School of Optometry and Vision Sciences, Cardiff University, Redwood Building, King Edward VII Avenue, Cardiff CF103NB, UK; boultonm@cf.ac.uk.

TGF-β has been established as a major regulator of wound healing in most species and tissues, including the cornea.[1-3] To date, TGF-β_1 and -β_2 have been localized to both the corneal epithelium and stroma, and both are constituents of the tear fluid (Vesaluoma M, et al. *IOVS* 1996;37:ARVO Abstract 3912).[4-9] Although mRNA of the β_3 isoform has been isolated from whole rat corneas at very low levels, its tissue location is unclear, and the protein has yet to be detected in the nonpathologic cornea.[6,10]

The TGFβ receptors RI and RII are located in epithelial, stromal, and endothelial layers of the cornea.[11-13] RI and RII are present predominantly in the basal layer of corneal epithelial cells, with receptor density increasing proximal to the limbus in many species, including humans. The nonsignaling TGFβ-RIII (β-glycan receptor) has been located on both the epithelium and endothelium in vivo, but appears to be absent in keratocytes in vivo.[11]

As with many other growth factor signaling systems the levels and spatial location of each component in the TGF-β system alters dramatically after a corneal wound. All three isoforms are present in the corneal epithelium,[4,14-16] and corneal epithelial cells in culture release TGF-β_1 and -β_2.[17,18] TGF-β_2 is reported to be more strongly expressed than the other two isoforms[4] and throughout wound healing after PRK and TGF-β_1, -β_2, and -β_3 are present in the corneal epithelium.[19] In stromal cells TGF-β is upregulated,[15] but isoforms cannot be detected immunohistochemically until 2 days after PRK, when rounded cells in the ablated area express all three isoforms. TGF-β_1, -β_2, and -β_3 expression is delayed in spindle shaped fibroblasts until 10 days after PRK. Expression of all three isoforms returns to normal after 30 days. In addition, levels of TGF-β_1 in the tear film increase dramatically (Vesaluoma M, et al. *IOVS* 1996;37:ARVO Abstract 3912). Of particular interest is the finding that topical administration of 1D11, a TGF-β_1-, -β_2-, and -β_3-neutralizing antibody, to rabbit corneas after PRK and lamellar keratectomy wounds, results in a reduction in the appearance of myofibroblasts, and substantially decreases the incidence of haze in rabbits.[2,3] Taken together, this indicates a pivotal role for the TGF-β system in corneal maintenance and wound repair.

The TGF-β superfamily is a structurally related group of bioactive ubiquitous proteins with diverse and pleiotropic activities. TGF-β1 and -β2 share 80% sequence homology but can have opposite actions on biological processes such as proliferation, migration, and differentiation.[1] The role of the various isoforms of TGF-β in corneal wound healing is not fully understood, and therefore optimal treatment may rely on selective inhibition of one or more TGF-β isoforms. To manipulate the cytokine environment of the healing cornea after either trauma or elective surgery, it is necessary to understand the actions of each TGF-β isoform. It appears increasingly likely that the events occurring within the earliest stages of corneal wound healing alter prognosis.[2,3] Herein, we describe the very different actions of the three TGF-β isoforms in early corneal wound-healing events and their inhibition by human isoform-specific neutralizing antibodies. The action of the cytokine IL-10, a potential antagonist of TGF-β, was also evaluated. The results

of the study have been reported in part in abstract form (Carrington LM, et al. *IOVS* 2001;42:ARVO Abstract 5018).

Methods

Cell Culture

Nonactivated bovine keratocytes were cultured based on established methods.[3,20] In brief, the epithelial and endothelial layers were scraped from the stroma which was incubated in 2 mg/mL collagenase (wt/vol RPMI at 37°C; Invitrogen-Gibco, Paisley, Scotland, UK) overnight at 37°C. Isolated cells were plated at 1×10^4 cells/well (24-well plate) in 1 mL of serum-free RPMI containing nonessential amino acids (Invitrogen-Gibco), glutamine, antibiotics, amphotericin B. Cultures were maintained in medium at 37°C in a standard 5% CO_2-95% air atmosphere for 48 hours, to allow attachment. Medium was replaced with fresh medium containing 0.1, 1, or 10ng/mL TGFβ_1, -β_2, or -β_3 or IL-10 (R&D, Abingdon, UK). Diluents were used as the control: 10 μL of phosphate buffered saline (PBS) containing 0.1% BSA and 0.01 M HCl (TGF-β isoform diluent) or 10 μL of PBS containing 0.1% BSA (IL-10 diluent). All treatments were applied in triplicate for up to 5 days in culture, and experiments were performed at least three times.

Organ Culture

Bovine corneas were centrally wounded with a 5-mm trephine, as previously described,[21] and the disc of epithelial-stromal tissue within the wound was excised. Sterile, serum-free DMEM containing 1% agar and 1% gelatin (BDH, Poole, UK) was used as a support, and serum-free Trowell's T8 medium (Invitrogen-Gibco) containing antibiotics, amphotericin B, and glutamine was added to the dish to a level just below the limbal region. Twice daily, 100 μL of fresh serum-free T8 medium was pipetted onto the surface of the cornea containing 1, 10, or 100 ng/mL TGFβ_1, -β_2, or -β_3 or IL-10 (R&D Systems); or neutralizing mAb against either active hTGFβ_1 (CAT-192; 0.1 nM–10 μM human IgG4; Cambridge Antibody Technology, Cambridge, UK); or hTGFβ_2 (CAT-152; 10 μM human IgG4; Cambridge Antibody Technology); or 10 μL of PBS containing 0.1% BSA (IL-10 and neutralizing antibody diluent) or 10 μL of PBS containing 0.1% BSA, and 0.01 M HCl (TGF-β isoform diluent). Cultures were maintained in serum-free T8 medium for up to 5 days (n = 6, per time, per treatment).

Re-epithelialization

Re-epithelialization was assessed as previously described,[20,21] by using captured macroimages of the wound area, where both the original wound cut and the leading edge of the epithelium could be seen. Re-epithelialization was expressed as the percentage of the original wound area that was re-covered.

Morphologic Assessment of Epithelium

Wounded and unwounded corneas were fixed overnight in 10% neutral buffered formalin (NBF), processed into wax. Seven-micrometer sections were stained with Harris hematoxylin and eosin.

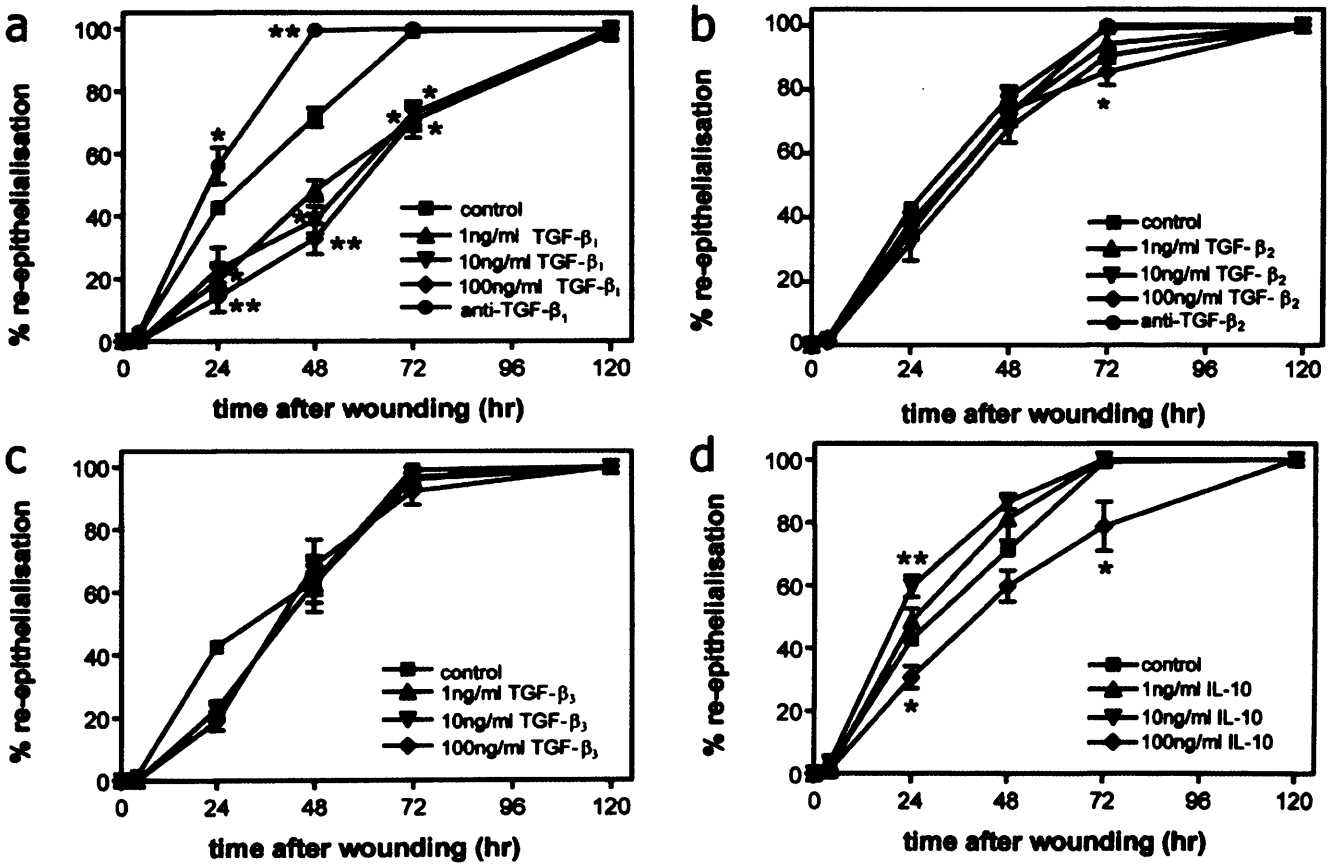

FIGURE 1. Percentage re-epithelialization of bovine corneal trephine wounds treated with 100 μL of serum-free medium twice daily, containing 1% growth factor diluent (PBS+0.1% BSA+HCL) or 1, 10, or 100 ng/mL (a) TGF-β_1 and 10 μM neutralizing mAb against hTGF-β_1, (b) TGF-β_2 and 10 μM neutralizing mAb against hTGF-β_2, (c) TGF-β_3, or (d) IL-10. Each point represents the average of at least six corneas ± SEM. Significant differences were determined by Student's t-test $^*P < 0.05$, $^{**}P < 0.01$.

Assessment of Proliferation in Cell Culture Using the Cresyl Violet Assay

Briefly, cells were fixed in 70% ethanol for 10 minutes at room temperature and incubated with a 0.5% solution of cresyl violet (BDH) for 1 minute at room temperature. After washing with PBS, acetic acid (33%, vol/vol ddH_2O) was added to the wells to elute the dye. The absorbance of the wells was read at 540 nm, with an ELISA reader, and wells containing 33% acetic acid were used as a blank.

Stromal Cell Density beneath the Wound

Corneas were fixed in 10% NBF overnight and processed into wax. Seven-micrometer sections were floated and incubated in 1 μg/mL bisbenzimide solution (Sigma-Aldrich, Poole, UK) for 10 minutes. Images of stained sections were captured, and the number of nuclei in the area 100 μm below the wound surface was analyzed (ImagePro Plus software; Media Cybernetics, Silver Spring, MD).

Identification of Myofibroblasts

Cultured cells were fixed at 0, 1, 2, 3, 4, and 5 days after treatment in 1% paraformaldehyde for 5 minutes. Corneal organ cultures were snap frozen in liquid nitrogen at 0, 1, 2, 3, and 5 days after treatment; embedded in optimal cutting temperature compound (OCT); and sectioned at 5-μm intervals. Cultures and sections were pretreated with 0.1% Triton-X-100 for 20 minutes, incubated with a monoclonal anti-α smooth muscle actin antibody (Sigma-Aldrich) for 2 hours followed by an Alexafluor 488-conjugated goat anti-mouse IgG (Invitrogen, Eugene, OR) for 1 hour. Counterstaining of nuclei was obtained using bisbenzimide solution incubation for 10 minutes. Cell cultures were also costained with TRITC-conjugated phalloidin (5 μg/mL in PBS; Sigma-Aldrich) for 2 hours, to identify F-actin.

Statistical Analysis

Cell counts beneath the wound were compared by using the nonparametric Mann-Whitney test. Proliferation was compared with unpaired, two-way *t*-tests (Prism 3.0; GraphPad Software, San Diego, CA) Corneal re-epithelialization was compared at each time point using either the Kruskal-Wallis test (nonparametric ANOVA) with Dunn's post test or Mann-Whitney test, as appropriate. The rate of re-epithelialization was assessed with a least-squares regression function of data between 24 and 48 hours and was expressed as the percentage of the wound area re-epithelialized in 1 hour. The calculated EC_{50} for CAT-192 in the re-epithelialization assay is indicated as the geometric mean with associated 95% confidence limits.

Results

Epithelial Wound Healing

Re-epithelialization followed a pattern similar to that previously described for this organ culture model.[20,21] Epithelial migration commenced within 12 hours after wounding, and, by 72-hours, wounds had completely re-epithelialized for corneas treated with medium alone or medium containing diluent (Fig. 1). The rate of re-epithelialization was calculated to be 1.56% ± 0.07% h^{-1}.

Corneal re-epithelialization was differentially sensitive to the three TGF-β isoforms tested. TGF-β_1 was the most potent inhibitor of re-epithelialization, inhibition was greatest at 100 ng/mL and halved the rate of re-epithelialization compared with the control (0.71% ± 0.3% h^{-1}; $P < 0.05$). The rate of re-epithelialization for corneas treated with TGF-β_2 or -β_3 was similar to that for the control ($P > 0.05$), except that TGF-β_2 at 100 ng/mL caused a small delay in re-epithelialization at 72 hours (Figs. 1b, 1c).

Administration of CAT-192 (100 μg/mL) resulted in an accelerated rate of regrowth of the corneal epithelium such that complete cover was established at 48 hours, corresponding to a re-epithelialization rate of 2.11% ± 0.1% h^{-1} ($P < 0.05$ compared with the rate observed in vehicle-treated controls, 1.56% ± 0.07% h^{-1}, Fig. 1b). In a separate experiment the concentration-response for CAT-192 was evaluated at a single time point. CAT-192 (10 ng/mL–100 μg/mL) applied to wounded corneas resulted in a concentration-related enhancement of corneal re-epithelialization measured at 40 hours, with a calculated EC_{50} of 0.51 μg/mL (0.23–1.10, 95% confidence limits; $n = 12$, Fig. 2). Neither CAT-152 or a null control IgG4 had a significant effect on the rate of re-epithelialization (Figs. 1b, 2)

IL-10 exhibited a pleiotropic effect on re-epithelialization (Fig. 1d): 1 ng/mL had no effect, 10 ng/mL increased re-epithelialization, and 100 ng/mL decreased re-epithelialization (without apparent cytotoxicity using the trypan blue assay, data not shown).

Epithelial Morphology

Epithelial morphology during re-epithelialization in control corneas and those receiving diluent was similar to that previously described for this model[20,21] and as depicted in Figure 3. Initial rounding off and retraction of the epithelium from the wound site at 4 hours was followed by migration onto the denuded stroma at 12 hours with the leading edge of the epithelium one cell deep, with no obvious stratification. Migration continued across the wound, with the leading edge of epithelium increased to 3 to 4 cells and slight hypercellularity at the original wound edge evident. By 72 hours, wound closure had occurred with the epithelium at the closure site thinner and less differentiated than the distal epithelium. After 5 days in culture the entire epithelium within the wound site

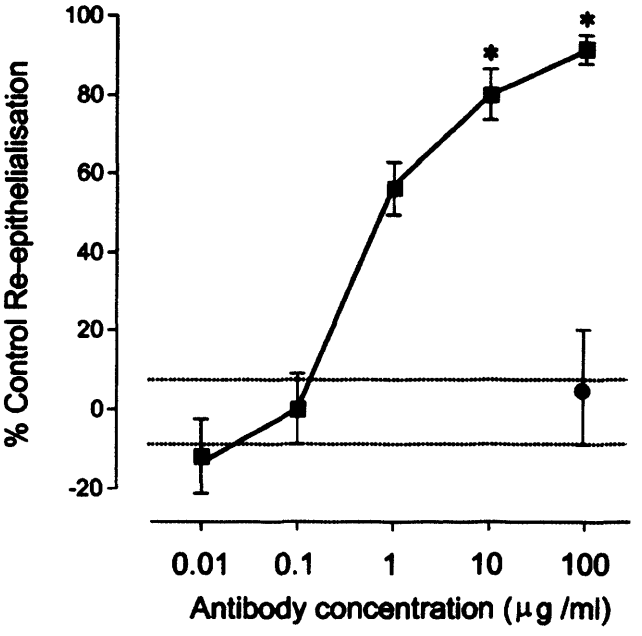

FIGURE 2. Dose response to CAT-192 during corneal re-epithelialization after an excisional trephine wound. The EC_{50} for CAT192 was 0.51 mg/mL (95% CI, 0.23–1.10; $n = 12$). Data are expressed as the percentage change in re-epithelialization of the vehicle-treated control group. *Dotted lines*: SEM of the vehicle control group data. A null IgG4 antibody control group (CAT-001, $n = 6$) was included. Each point represents the mean; vertical bars, SEM. The effect of the different doses of CAT-192 was compared with control treatment using the Kruskal-Wallis and Dunn tests. *$P < 0.01$.

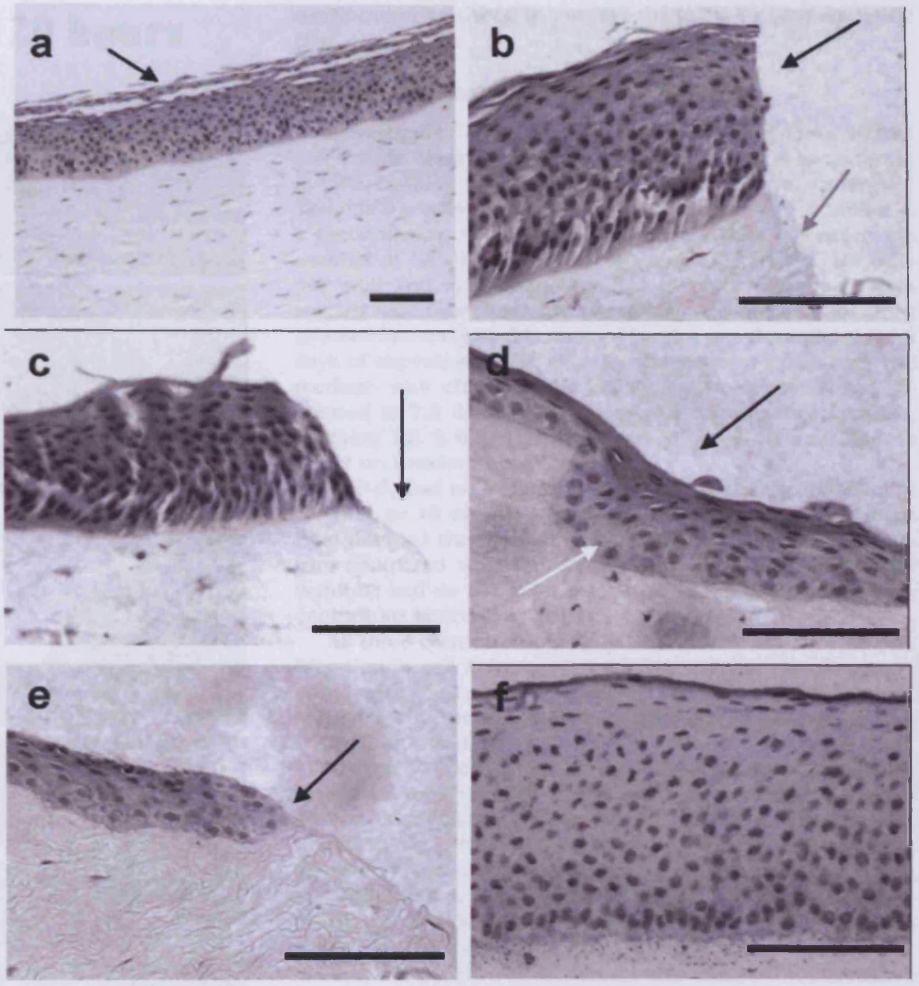

FIGURE 3. Epithelial morphology of wounded corneas at various stages of re-epithelialization. Unwounded bovine corneas (**a**) contained 8 to 10 layers of cells within the epithelium and 1 to 2 layers of desquamating, flattened superficial epithelial cells (*black arrow*). Corneas that had undergone wounding with a trephine, showed clean, sharply cut edges (**b**) through the epithelium immediately after wounding (*black arrow*), stromal cutting was less defined (*grey arrow*). Four hours after wounding (**c**), the epithelium had retracted from the cut edge of the stroma (*black arrow*). As the epithelium migrated across the denuded stroma (**d**), the epithelium over the corner of the original cut (*black arrow*) had thinned to one to three layers deep, whereas hypercellularity was often observed within the wound's edge (*white arrow*). (**e**) The leading edge of the epithelium had lost stratification and become one to two cells deep (*black arrow*). By 120 hours (**f**), stratification of the healed epithelium was evident with a slight thickening compared with unwounded corneas. Scale bar, 100 μm.

exhibited good stratification, although slight thickening of the epithelium within the wound area was common.

Morphologic differences were observed in corneas treated with TGF-β_1 (Fig. 4). This included considerable thinning of the epithelium in the wound site at all time points and was more pronounced in the corneas receiving 100 ng/mL TGF-β_1 (Fig. 4b). Stratification of the epithelium migrating into the wound was always evident, although the layers were thinner than those in control corneas. By 120 hours, re-epithelialization was complete, confirming the results of macroscopic image analysis. Corneas treated with the anti-TGF-β_1 antibody CAT-192 were similar to the control, although the epithelium appeared slightly thinner (Figs. 4c, 4d).

Corneas receiving 1 ng/mL TGF-β_2 showed a retraction of the wound edge that was not observed at higher concentrations (Fig. 4e). Thinning of the epithelium was particularly obvious at 100 ng/mL, especially at the interface between wounded and unwounded stroma. By 48 hours in culture, hypercellularity was evident at all TGF-β_2 concentrations, with sparse populations of cell nuclei in the superficial layers and loss of stratification correlated with increasing doses of TGF-β_2, and at 100 ng/mL no obvious basal cells or superficial epithelium were observed. Patches of acellularity were observed within the epithelium (Fig. 4f). By 120 hours in culture all wounds had closed, stratification of the epithelium was poor in corneas treated with higher doses of TGF-β_2. Corneas receiving a neutralizing antibody against TGF-β_2, CAT-152, showed morphologic features similar to those observed in the control corneas (Fig. 4g, 4h).

TGF-β_3, at all doses, showed considerable epithelial retraction from the wound edge at 4 hours and some cellular debris (Fig. 4i). Morphology of the epithelium was reasonably normal with some thinning toward the epithelial edge in corneas treated with higher doses. By 24 hours, migration into the wound had begun but was less advanced than in the control. Hypercellularity and extreme thinning of the epithelium was evident at the wound edge and stratification, as indicated by lack of columnar cells in Fig 4j, became less evident with increasing TGF-β_3 concentrations. By 120 hours in culture, the epithelium had an increased thickness throughout the wound, compared with the control (Fig. 4j).

IL-10 produced contrasting results, depending on dose. At 4 hours after wounding 1 ng/mL IL-10 showed neither retraction nor migration, but the epithelium was thinned to three to four cell layers, 10 ng/mL resulted in extreme thinning of the leading edge of the epithelium and some retraction, whereas 100 ng/mL prompted migration of a very thin leading edge into the wound area (Fig. 4k). At 24 and 48 hours, apart from degree of migration, epithelial morphology was similar for all three doses of IL-10. Stratification was not evident at the leading edge and hypercellularity was evident at the original wound margin. By 72 hours, differentiation of cells was evident but not confined to obvious layers, and basal cells were difficult to distinguish; 1-ng/mL-treated corneas demonstrated an

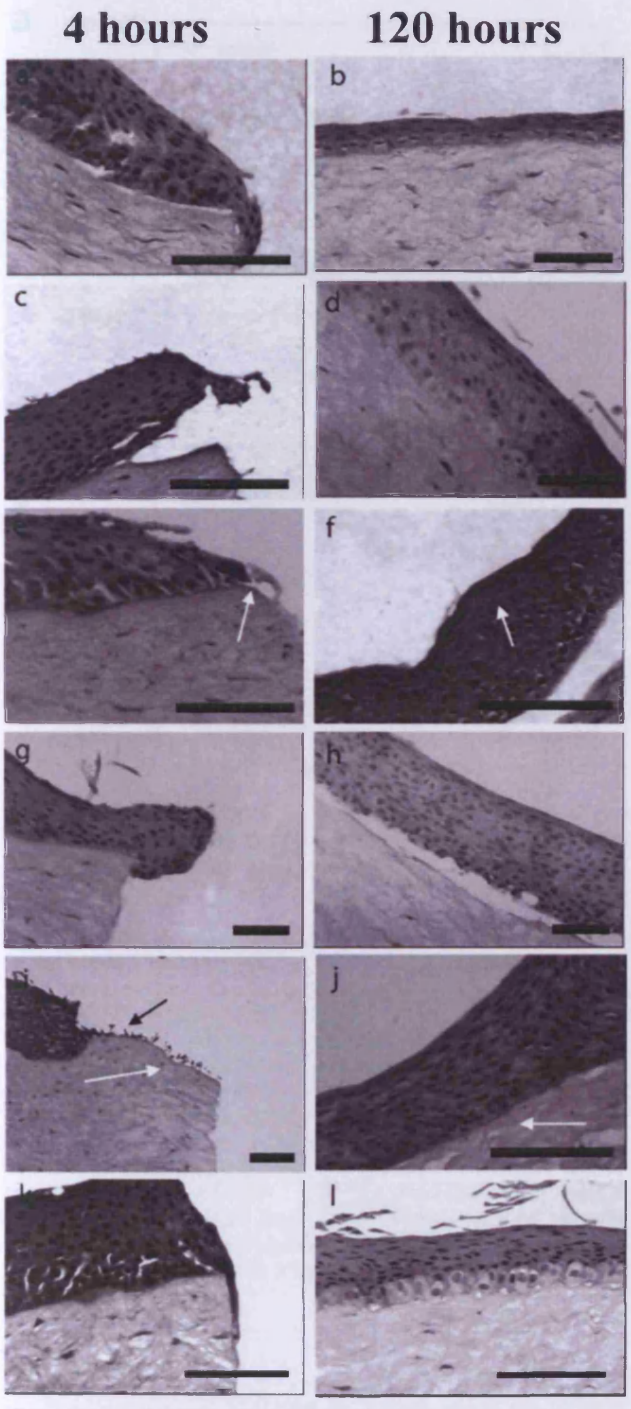

FIGURE 4. Epithelial morphology after trephine wounding 4 (**a**, **c**, **e**, **g**, **i**, **k**) and 120 (**b**, **d**, **f**, **h**, **j**, **l**) hours after treatment with 100 ng/mL TGF-β_1 (**a**, **b**) or anti-TGF-β_1 (**c**, **d**); TGF-β_2 (**e**, 10 ng/mL; **f**, 1 ng/mL; *white arrow*, an area apparently devoid of nuclei) or anti-TGF-β_2 (**g**, **h**); 100 ng/mL TGF-β_3 (**i**, **j**; *black arrow*: cellular debris and retraction of epithelium from the wound edge, *white arrow*); or IL-10 (**k**, 100 ng/mL; **l**, 10 ng/mL). Scale bar, 100 μM.

even epithelium within the wound area with some disruption of the layering, whereas both 10 and 100 ng/mL produced hypercellularity at the wound edges and a thinning of the epithelium at the site of wound closure. At 120 hours, good stratification was seen in corneas treated with all three doses (Fig. 4l).

Keratocyte Proliferation

Keratocyte Cell Culture. Bovine keratocytes in serum-free cell culture retained a stellate morphology similar to that seen in vivo, forming a monolayer with interconnecting processes. The initial seeding density of 1×10^4 cells per well, resulted in a preconfluent culture; however, after 2 days in culture the number of cells had increased to approximately 4×10^4 cells per well and the keratocytes had extended long processes toward each other, forming a network. The culture conditions allowed low-level proliferation of keratocytes throughout the 5 days of experimentation (Fig. 5). Twenty-four hours after the medium was changed, the number of keratocytes had increased to $7.3 \pm 0.1 \times 10^4$ cells and continued to increase, reaching $1.8 \pm 0.2 \times 10^5$ cells at 120 hours. Diluents had no effect on keratocyte proliferation.

TGF-β_1 had no significant effect on keratocyte numbers at either 1 or 10 ng/mL. However, at 0.1 ng/mL, TGF-β_1 more than doubled the number of keratocytes at 120 hours of culture compared with the control ($P < 0.001$; Fig. 5a). Other isoforms had no effect on keratocyte proliferation at the concentrations tested (Fig. 5b, 5c).

All three concentrations of IL-10 stimulated keratocyte proliferation in cell culture, with the cell number doubling compared with the control ($P < 0.011$; Fig. 5d). The proliferative response appeared to be initiated earlier in cultures treated with 10 ng/mL IL-10.

Trephine-Wounded Corneas. The number of keratocytes decreased to 56% ± 2% compared with unwounded control corneas immediately after wounding, and a maximum reduction to 33% ± 1.5% was measured 4 hours after wounding. Thereafter, the number of keratocytes gradually increased in the wound area, and, by 120 hours, the number of cells beneath the wound had increased to 60% ± 7.5% of that in unwounded corneas (Fig. 6).

The TGF-β isoforms prompted very different repopulation behavior. In agreement with the results from keratocyte cell culture, the increase in cells under the wound was evident only in corneas treated with the lowest concentration of TGF-β_1 (1 ng/mL), where, by 4 and 120 hours, the repopulation of cells under the wound had increased from 33% ± 1.5% to 83% ± 4.0%, respectively, of the unwounded control (Fig. 6a). In contrast, the TGF-β_1 neutralizing mAb CAT-192 dramatically decreased keratocyte numbers at all time points, compared with the control (Fig. 6a). TGF-β3 significantly decreased the cell density under the wound at all concentrations tested (Fig. 6c). Similarly, addition of IL-10 decreased the number of cells beneath the wound (Fig. 6d). Neither TGF-β_2 nor CAT-152 had a significant effect on this response (Fig. 6b).

Myofibroblast Differentiation

Keratocytes cultures maintained in medium alone or plus diluent retained a stellate morphology and were α-smooth muscle actin negative. β-Actin was located perinuclearly and throughout the cytoplasm with no obvious stress fiber bundles (Fig. 7a). Of all the factors tested in cell culture, only high-dose TGF-β_1 prompted the differentiation of keratocytes into myofibroblasts. Prominent stress fibers were obvious when cells were stained with phalloidin, the cells lost their stellate shape and elongated into spindles (Fig. 7b). More than half of the cells staining positive for α smooth muscle actin which appeared to be organized in bundles similar to the β-actin filaments.

Only very occasional cells, if any, were α-smooth muscle actin positive in control cornea organ cultures (Figs. 7e) with

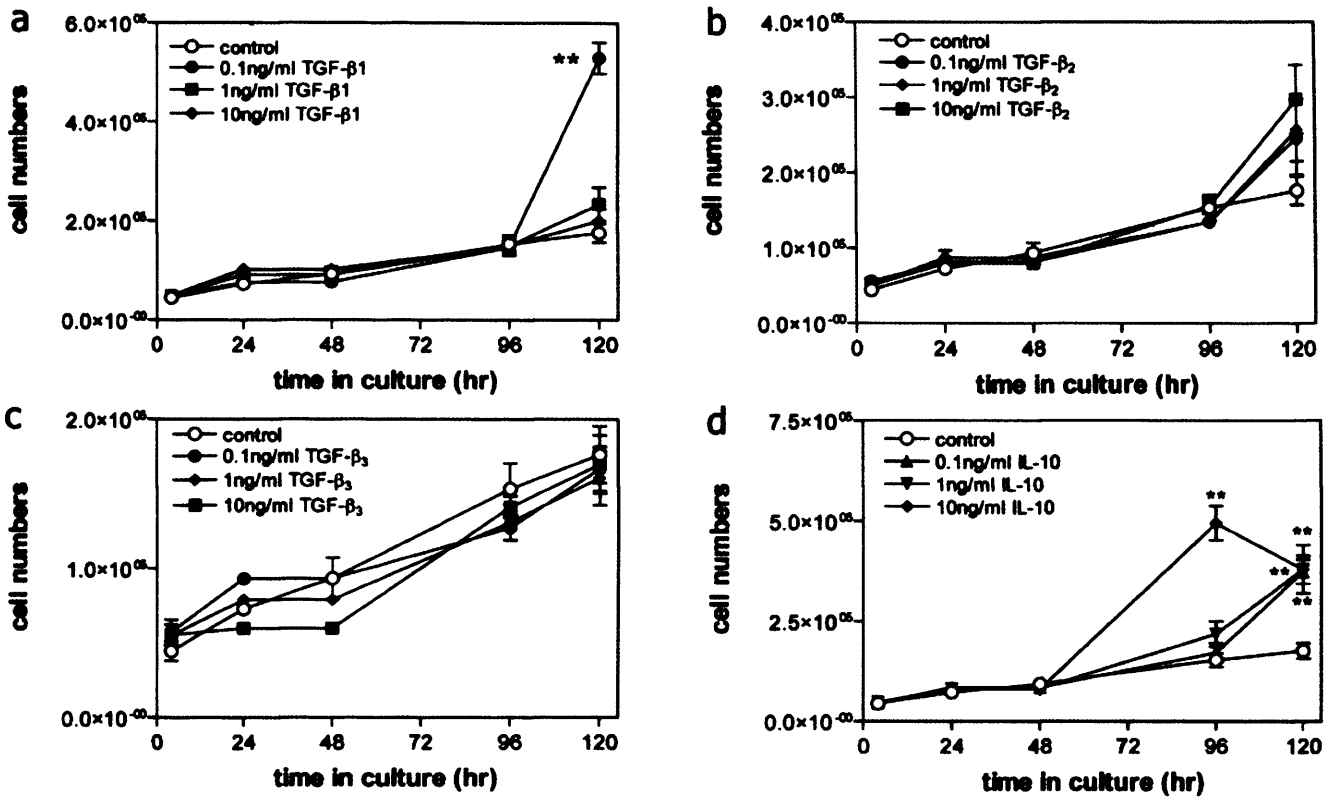

FIGURE 5. The effect of (a) TGF-β_1, (b) TGF-β_2, (c) TGF-β_3, and (d) IL-10 on the number of keratocytes in serum-free cell culture assessed using the cresyl violet assay. Each point is the average of three experiments of triplicate wells. Error bars, SEM. Data were analyzed using the Students *t*-test. $^*P < 0.05$; $^{**}P < 0.01$.

the exception of cells surrounding the lumen of blood vessels in the corneal limbus (Figs. 7c, 7d). Very occasionally, isolated cells were evident in the area under the wound after re-epithelialization had occurred. Myofibroblasts became evident in the stroma of corneas treated with 100 ng/mL of TGF-β_1 (Figs. 7f). These were located in the area directly under the wound, within the upper 150 μm of the stroma at the edge of the wound face, with isolated cells (<1% of stromal cells) appearing at 72 hours after wounding. At 120 hours, the number of α-smooth muscle actin-positive cells had significantly increased to 65.97% ± 13.57%, compared with control corneas at the same time point ($P < 0.001$). The stromal cells of corneas treated with CAT-192 (anti-TGF-β_1), TGF-β_3 or IL-10 had no obvious α-smooth muscle actin positive cells at any time point.

Discussion

We present evidence that TGF-β isoforms differentially regulate several key events in early corneal wound healing. TGF-β_1 appeared to be the most active corneal isoform and was able to delay re-epithelialization, increase proliferation of keratocytes, enhance repopulation of the periwound area, and promote myofibroblast transformation. Moreover, neutralization of endogenously produced TGF-β_1 after treatment with the anti-TGF-β_1 mAb, CAT-192, mediated an effect opposite the response to exogenously added TGF-β_1. In contrast to the TGF-β_1 isoform, TGF-β_3 reduced the keratocyte repopulation of the periwound area. TGF-β_2 or neutralization of TGF-β_2 with the selective antibody CAT-152 had little effect on corneal wound healing.

The effects of TGF-β_1 reported in this study concur with the findings of other investigators in various species. First, TGF-β_1 was the only factor capable of inducing α-smooth muscle actin expression in stromal cells in cell and organ culture, a well-documented phenomenon.[3,22] Second, TGF-β_1 increased the number of cells under the wound in wounded, organ-cultured corneas, a finding in common with reports in the literature involving rabbits.[3] Third, a neutralizing antibody against the active form of TGF-β_1, inhibits the slow repopulation of stromal cells under the wound as previously shown after laser keratectomy.[23] Although not examined in this study, it is likely that these events are, at least in part, mediated via connective tissue growth factor.[24]

TGF-β_3 inhibited not only the repopulation of the stroma observed in the control but also decreased the number of cells below that seen at any time point in untreated corneas. Of note, neutralizing TGF-β_3 had no effect, either on the number of cells beneath the wound or the expression of laminin and fibronectin in the cornea,[23] and thus may act by inhibiting the action of endogenous TGF-β_1 as occurs during wound healing in the skin.[25] TGF-β_3 knockout mice demonstrate scarring in the fetal stage that does not occur after wounding in the wild-type equivalent,[26] and it appears that the ratio of TGF-β_1 to -β_3 is critical in determining the extent of fibrosis. Thus, TGF-β_3 may be a candidate for therapeutic interventions, especially because it had no detrimental effect on corneal re-epithelialization in this study.

Møller-Pedersen et al. [2] have reported that a pan neutralizing antibody (1D11) able to block all isoforms of TGFβ reduced keratocyte activation and transformation and inhibited stromal fibrosis in a rabbit model of PRK. However, in this rabbit

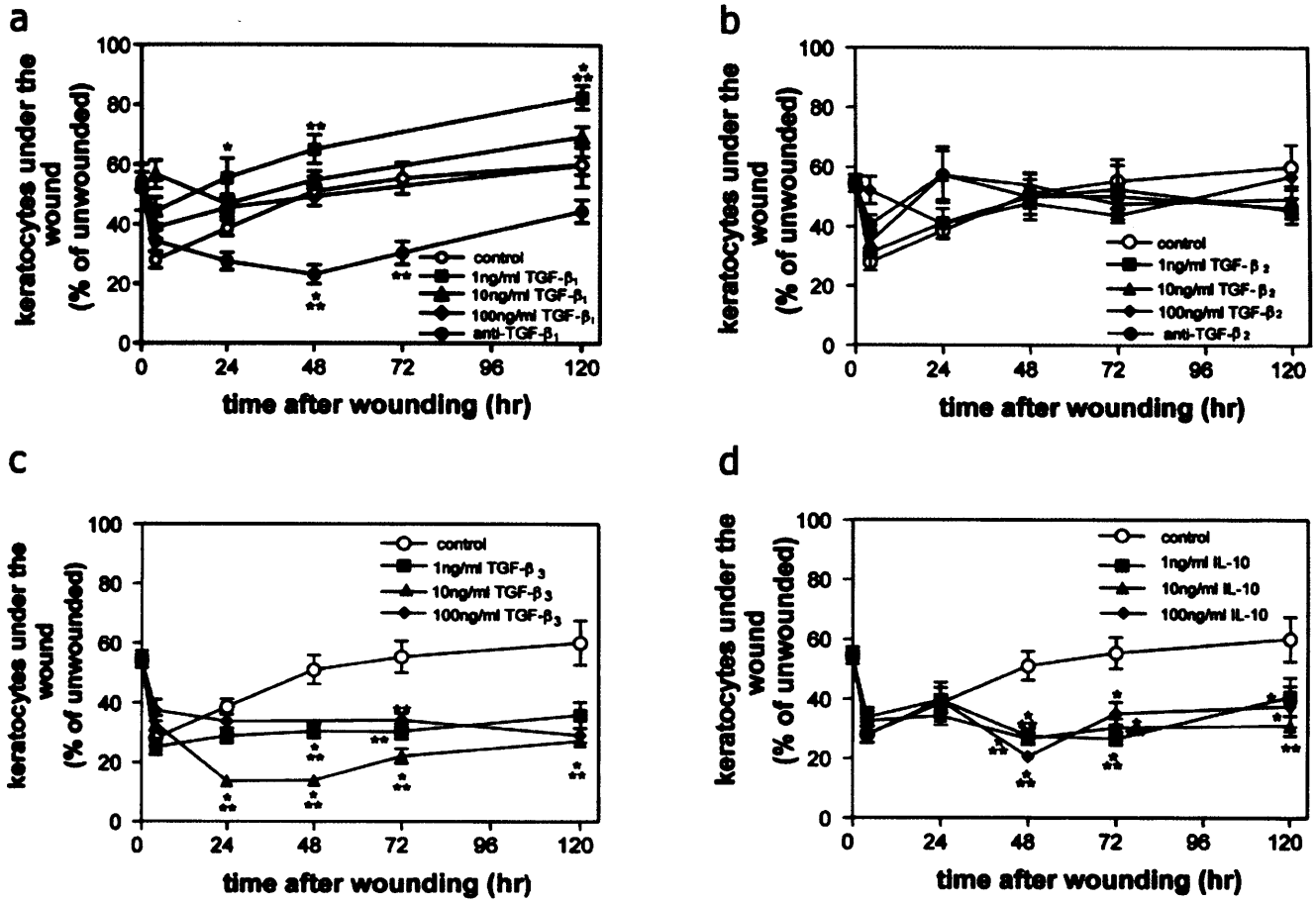

FIGURE 6. The effect of (a) TGF-β_1 and anti-TGF-β_1, (b) TGF-β_2 and anti-TGF-β_2, (c) TGF-β_3, and (d) IL-10 on the number of keratocytes beneath a trephine wound in organ-cultured corneas between 0 and 120 hours after wounding. Points represent the average number of cells under the wound as a percentage of the number at a comparable depth in that unwounded control. Each point is the average of six corneas per treatment and error bars, SEM. Data were analyzed using the Kruskal-Wallis test (*$P < 0.05$; **$P < 0.01$). Significance symbols for 4-hour time points are not shown due to lack of space.

model, the regrowth of the stroma was unaffected by pan isoform neutralization with 1D11. Our results suggest that while neutralizing TGF-β_1 may be important in preventing fibrosis, the neutralization of TGF-β_3 may well be agonistic to TGF-β_1 action. One may postulate that the best outcome (of a single agent) would be selective neutralization of TGF-β_1, and this could be achieved with the human monoclonal antibody CAT-192. This approach may reduce fibrosis, keratocyte transformation (and hence light-reflective keratocytes), as well as repopulation of the stroma. Rapid re-epithelialization would also limit additional stromal trauma. This approach would be worthy of study in a model system such as experimental PRK.

IL-10 is classically regarded as a potent anti-inflammatory cytokine and most studies into its function and effect have centered on this premise. This study is the first to report the effect of IL-10 on corneal wound healing. IL-10 was seen to have a pleiotropic effect on the epithelium, increasing re-epithelialization at 10 ng/mL, but suppressing wound coverage at 100 ng/mL.

Sources for IL-10 include TH_2 cells[27] and monocytes,[28] both of which should have no access to the cornea in nonpathologic situations. IL-10 mRNA has been isolated from the corneas of mice both before and after alkali burns[29] and in humans during corneal transplant surgery.[30] Corneal epithelial cells are a likely candidate, as the epithelia of other organs including skin produce IL-10.[31–33] Previous studies have shown that IL-10 treatment can reduce the migration of T-cells and neutrophils into HSV-1-infected mouse corneas,[34] reduce HLA-DR expression on corneal cells and infiltrating leukocytes of human herpetic stromal keratitis specimens,[35] and decrease corneal opacification in HSV-1-infected BALB/c mice.[34,36] All of these in vivo experiments were performed in the presence of a functioning immune system and were characterized by immune cell infiltration of the cornea, which could have mediated the effects of IL-10 on the corneal cells. The current study is therefore the first to show that corneal cells, in the absence of lymphocytes, can respond to IL-10 treatment and as such provides compelling evidence that the cornea contains the IL-10 receptor. Indeed, the upregulation of IL-10 Rc mRNA expression has been identified in corneas after excimer laser injury.[37]

Little is known about the mechanism by which IL-10 regulates epithelial cells and fibroblasts. IL-10 has been shown to have antagonistic effects to the actions of TGF-β,[38] although how this is achieved is unclear. IL-10 has been shown to modulate extracellular matrix components by downregulating type I collagen expression and upregulating collagenase and stomelysin mRNA in human skin fibroblasts[39]; reducing constitutive and transforming growth factor-β-stimulated, type I collagen mRNA expression in human lung fibroblast cells[40]; and downregulating the biosynthesis of fibrinogen in smooth muscle cells,[41] all of which may contribute to modulation of fibrosis.

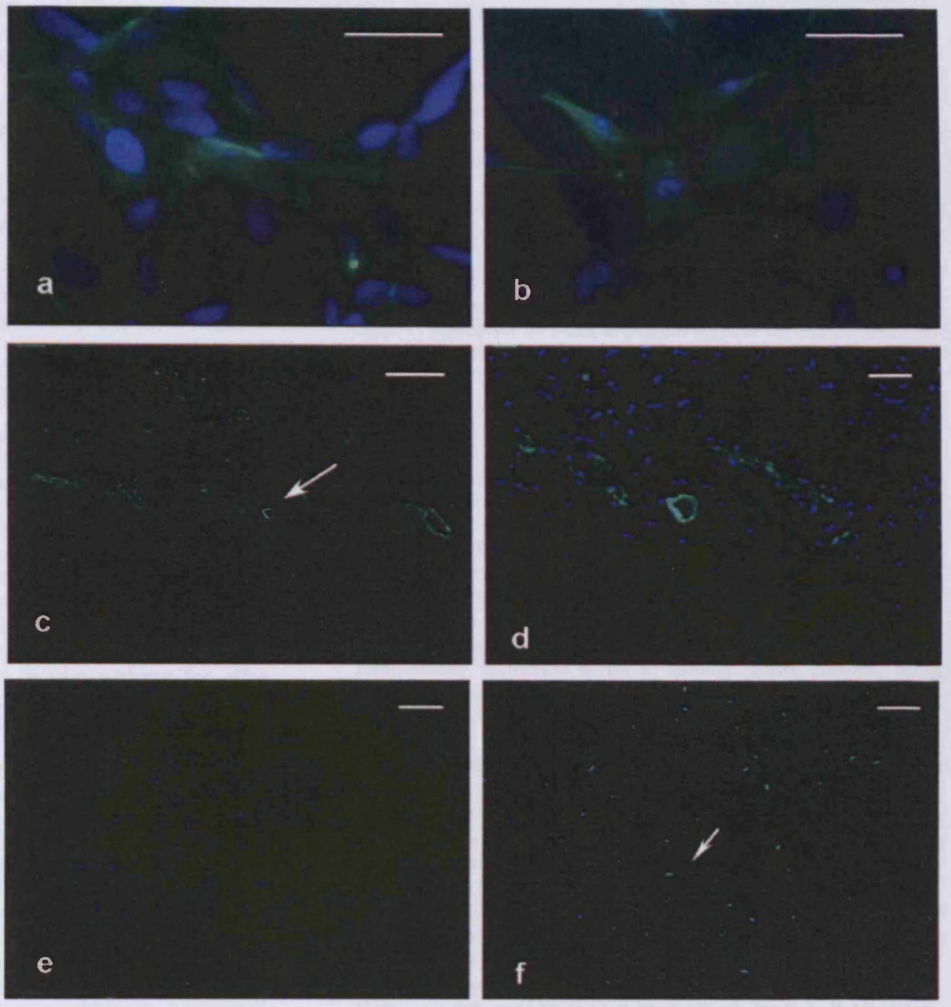

FIGURE 7. α-Smooth muscle actin staining in myofibroblasts. In serum-free cell culture, untreated keratocytes did not express α-smooth muscle actin (not shown); however, serum-treated cultures (**a**) developed α-smooth actin expression apparently within stress fibers in groups of cells after 5 days, commonly these cells were overlying the initial monolayer. In cultures treated with 10 ng/mL TGF-β_1, ~50% of cells expressed α-smooth muscle actin after 5 days (**b**). Untreated wounded bovine corneas, except for the limbal vasculature (*arrow* denotes blood vessel), which acted as an internal positive control (**c**), shown at higher magnification in (**d**), were negative for α-smooth muscle actin (**e**). Corneas treated with 100 ng/mL TGF-β_1 for 5 days contained cells within the stroma, immediately beneath the wound site, that expressed α-smooth muscle actin (**f**), indicating the presence of myofibroblasts (*arrow*). Scale bar: (**a**, **b**) 50 μm; (**c**) 100 μm; (**d**) 20 μm; (**e**) 40 μm.

Our study confirms the primary role of the β_1 isoform of TGF during corneal wound healing. Furthermore, it identifies IL-10 and TGF-β_3 as potential therapeutic regulators of corneal repair and the prevention of fibrosis. It is also likely that early application of treatment will be essential to minimize adverse healing and optimize repair. A postoperative indication such as corneal refractive surgery could be benefited by this type of biological therapy.

References

1. O'Kane S, Ferguson M. Transforming growth factor betas and wound healing. *Int J Biochem Cell Biol*. 1997;29:63–78.
2. Møller-Pedersen T, Cavanagh H, Petroll W, Jester J. Neutralising antibody to TGF-beta modulates stromal fibrosis but not regression of photoablative effect following PRK. *Curr Eye Res*. 1998;17:736–747.
3. Jester JV, BarryLane PA, Petroll WM, Olsen DR, Cavanagh HD. Inhibition of corneal fibrosis by topical application of blocking antibodies to TGF(beta) in the rabbit. *Cornea*. 1997;16:177–187.
4. Nishida K, Kinoshita S, Yokoi N, et al. Immunohistochemical localization of transforming growth factor-beta-1, factor-beta-2, and factor-beta-3 latency-associated peptide in human cornea. *Invest Ophthalmol Vis Sci*. 1994;35:3289–3294.
5. Nishida K, Sotozono C, Adachi W, Yamamoto S, Yokoi N, Kinoshita S. Transforming growth factor β1, -β2 and -β3 mRNA expression in human cornea. *Curr Eye Res*. 1995;14:235–241.
6. Pasquale LR, Dorman-Pease ME, Lutty GA, et al. Immunolocalization of Tgf-beta-1, Tgf-beta-2, and Tgf-beta-3 in the anterior segment of the human eye. *Invest Ophthalmol Vis Sci*. 1993;34:23–30.
7. Abrahamian A, Xi MS, Donnelly JJ, Rockey JH. Effect of interferon-gamma on the expression of transforming growth-factor-beta by human corneal fibroblasts: role in corneal immunoseclusion *J Interferon Cytokine Res*. 1995;15:323–330.
8. Chen KH, Harris DL, Joyce NC. TGF-beta 2 in aqueous humor suppresses S-phase entry in cultured corneal endothelial cells. *Invest Ophthalmol Vis Sci*. 1999;40:2513–2519.
9. Gupta A, Monroy D, Ji Z, Yoshino K, Huang A, Pflugfelder S. Transforming growth factor beta-1 and beta-2 in human tear fluid. *Curr Eye Res*. 1996;15:605–614.
10. Chen C, Michelini-Norris B, Stevens S, et al. Measurement of mRNAs for TGF beta and extracellular matrix proteins in corneas of rats after PRK. *Invest Ophthalmol Vis Sci*. 2000;41:4108–4116.
11. Joyce N, Zieske J. Transforming growth factor beta-receptor expression in the human cornea. *Invest Ophthalmol Vis Sci*. 1997;38:1922–1928.
12. Obata H, Kaburaki T, Kato M, Yamashita H. Expression of TGF-beta type I and type II receptors in rat eyes. *Curr Eye Res*. 1996;15:335–340.
13. Obata H, Kaji Y, Yamada H, Kato M, Tsuru T, Yamashita H. Expression of transforming growth factor-beta superfamily receptors in rat eyes. *Acta Ophthalmol Scand*. 1999;77:151–156.
14. Wilson S, He Y, Lloyd S. EGF, EGF receptor, basic FGF, TGF beta-1, and IL-1 alpha mRNA in human corneal epithelial cells and stromal fibroblasts. *Invest Ophthalmol Vis Sci*. 1992;33:1756–1765.
15. Hayashi GF, Wolf G, Kenyon K. Expression of transforming growth factor-beta in wound healing of vitamin A-deficient rat corneas. *Invest Ophthalmol Vis Sci*. 1989;30:239–247.

16. Mita T, Yamashita H, Kaji Y, et al. Effects of transforming growth factor beta on corneal epithelial and stromal function in a rat wound healing model. *Graefes Arch Clin Exp Ophthalmol* 1998 236:834-843.
17. Strissell K, Rinehart W, Fini M. A corneal epithelial inhibitor of stromal cell collagenase synthesis identified as TGFβ2. *Invest Ophthalmol Vis Sci.* 1995;36:151-162.
18. Pancholi S, Tullo A, Khaliq A, Foreman D, Boulton M. The effects of growth factors and conditioned media on the proliferation of human corneal epithelial cells and keratocytes. *Graefes Arch Clin Exp Ophthalmol.* 1998;235:1-8.
19. Kaji Y, Mita T, Obata H, et al. Expression of transforming growth factor beta superfamily and their receptors in the corneal stromal wound healing process after excimer laser keratectomy. *Br J Ophthalmol.* 1998;82:462-463.
20. Carrington L, Boulton M. HGF and KGF regulate both epithelial and stromal corneal wound healing. *J Cataract Refract Surg.* 2005;31:412-423.
21. Foreman D, Pancholi D, Jarvis-Evans J, McLeod D, Boulton M. A simple organ culture model for assessing the effects of growth factors on corneal reepithelialisation. *Exp Eye Res.* 1996;62:555-564.
22. Jester J, Barry P, Cavanagh M, Petroll W. Induction of alpha smooth muscle actin expression and myofibroblast transformation in cultured corneal keratocytes. *Cornea.* 1996;115:505-516.
23. Mita T, Yamashita H, Kaji Y, et al. Functional difference of TGF-beta isoforms regulating corneal wound healing after excimer laser keratectomy. *Exp Eye Res.* 1999;68:513-519.
24. Blom IE, van Dijk AJ, Wieten L, et al. In vitro evidence for differential involvement of CTGF, TGF beta, and PDGF-BB in mesangial response to injury. *Nephrol Dialysis Transplant.* 2001;16:1139-1148.
25. Shah M, Foreman D, Ferguson M. Neutralisation of TGF-beta 1 and TGF-beta 2 or exogenous addition of TGF-beta 3 to cutaneous rat wounds reduces scarring. *J Cell Sci.* 1995;108:985-1002.
26. Cowin AJ, Holmes TM, Brosnan P, Ferguson MW. Expression of TGF-beta and its receptors in murine fetal and adult dermal wounds. *Eur J Dermatol.* 2001;11:424-431.
27. Fiorentino DF, Bond MW, Mosmann TR. Two types of mouse T helper cell IV Th2 clones secrete a factor that inhibits cytokine production by Th1 clones. *J Exp Med.* 1989;170:2081-2095.
28. Serot JM, Bene MC, Foliguet B, Faure GC. Monocyte-derived IL-10-secreting dendritic cells in choroid plexus epithelium. *J Neuroimmunol.* 2000;105:115-119.
29. Sotozono C, He JC, Matsumoto Y, Kita M, Imanishi J, Kinoshita S. Cytokine expression in the alkali-burned cornea. *Curr Eye Res.* 1997;16:670-676.
30. King WJ, Comer RM, Hudde T, Larkin DF, George AJ. Cytokine and chemokine expression kinetics after corneal transplantation. *Transplantation.* 2000;70:1225-1233.
31. Enk AH, Katz SI. Identification and induction of keratinocyte-derived Il-10. *J Immunol.* 1992;149:92-95.
32. Dosanjh A, Morris RE, Wan B. Bronchial epithelial cell-derived cytokine IL-10 and lung fibroblast proliferation. *Transplant Proc.* 2001;33:352-354.
33. Yoshida M, Takeuchi M, Streilein JW, et al. Participation of pigment epithelium of iris and ciliary body in ocular immune privilege. 1. Inhibition of T-cell activation in vitro by direct cell-to-cell contact. *Invest Ophthalmol Vis Sci.* 2000;41:811-821.
34. Tumpey TM, Cheng H, Yan XT, Oakes JE, Lausch RN. Chemokine synthesis in the HSV-1-infected cornea and its suppression by interleukin-10. *J Leukocyte Biol.* 1998;63:486-492.
35. Boorstein SM, Elner SG, Meyer RF, et al. Interleukin-10 Inhibition of HLA-DR expression in human herpes stromal keratitis. *Ophthalmology.* 1994;101:1529-1535.
36. Minagawa H, Sakai Y, Li Y, Ishibashi T, Inomata H, Mori R. Suppression of infectious virus spread and corneal opacification by the combined use of recombinant interferon beta and interleukin-10 following corneal infection with herpes simplex virus-1 in mice. *Antiviral Res.* 1997;36:99-105.
37. Cao Z, Wu HK, Bruce A, Wollenberg K, Panjwani N. Detection of differentially expressed genes in healing mouse corneas, using cDNA microarrays. *Invest Ophthalmol Vis Sci.* 2002;43:2897-2904.
38. Carrington L, McLeod D, Boulton M. IL-10 and antibodies to TGF-beta(2) and PDGF inhibit RPE-mediated retinal contraction. *Invest Ophthalmol Vis Sci.* 2000;41:1210-1216.
39. Reitamo S, Remitz A, Tamai K, Uitto J. Interleukin-10 modulates type I collagen and matrix metalloproteinase gene expression in cultured human skin fibroblasts. *J Clin Invest.* 1994;94:2489-2492.
40. Arai T, Abe K, Matsuoka H, et al. Introduction of the interleukin-10 gene into mice inhibited bleomycin-induced lung injury in vivo. *Am J Physiol Lung Cell Mol Physiol.* 2000;278:L914-L922.
41. Vasse M, Paysant I, Soria J, Mirshahi SS, Vannier JP, Soria C. Down-regulation of fibrinogen biosynthesis by IL-4, IL-10 and IL-13. *Br J Haematol.* 1996;93:955-961.

Bibliography

Aghamohammadzadeh H, Newton RH and Meek KM (2004) X-Ray Scattering Used to Map the Preferred Collagen Orientation in the Human Cornea and Limbus. *Structure* 12: 249–256.

Alberts B, Bray D, Lewis J, Raff M, Roberts K and Watson JP (1994) *Molecular Biology of the Cell.* 3 ed. New York: Garland Publishing.

Ang RT, Dartt DA and Tsubota K (2001) Dry eye after refractive surgery. *Current Opinion in Opthalmology* 12: 318-322.

Aravind L, and Koonin EV (1999) Gleaning non-trivial structural, functional and evolutionary information about proteins by iterative database searches *J Mol Biol.* 287: 1023.

Arnold A, Bordoli L, Kopp J and Schwede G (2006) The SWISS-MODEL workspace: a web-based for protein structure homology modelling. *Bioinformatics* 22: 195-201.

Azar DT (1997) *Refractive Surgery.* Stamford: Appleton and Lange.

Azar DT, and Farah SG (1998a) LASIK vs PRK: An Update on Indications and Safety. *Opthalmology* 105: 1357-1358.

Azar DT, Pluznik D, Jain S and Khoury JM (1998b) Gelatinase B and A expression after laser in situ keratomileusis and photorefractive keratectomy. *Arch Ophthalmol* 116: 1206-1208.

Baldwin HC, and Marshall J (2002) Growth factors in corneal wound healing following refractive surgery: A review. *Acta Ophthalmologica Scandinavica* 80: 238-248.

Bansal AK, and Veenashree MP (2001) Laser Refractive Surgery: Technological Advance and Tissue Responce. *Bioscience Reports* 21: 491-512.

Baxevanis AD, and Ouellette F (2001) Predictive methods using protein sequences. In: 2 [ed.] *Bioinformatics: A Practical Guide to the Analysis of Genes and Proteins,*. John Wiley & Sons, Inc.

Baxevanis AD, Bryant SH and Landsman D (1995) Homology model building of the HMG-1 box structural domain. *Nucleic Acids Research* 23: 1019.

Beecher N, Chakravarti S, Joyce S, Meek KM and Quantock AJ (2006) Neonatal development of the corneal stroma in wild-type and lumican-null mice. *Invest Ophthalmol Vis Sci.* 47: 146-155.

Berman HM, Battistuz T, Bhat TN, Bluhm WF, Bourne PE, Burkhardt K, Feng Z, Gilliland GL, Iype L, Jain S, Fagan P, Marvin J, Padilla D, Ravichandran V, Schneider B, Thanki N, Weissig H, Westbrook JD, Zardecki C (2002) The Protein Data Bank. *Acta Crystallogr D Biol Crystallogr.* 58: 899.

Berthiaume F, Moghe PV, Toner M and Yarmush ML (1996) Effect of extracellular matrix topology on cell structure, function, and physiological responsiveness: hepatocytes cultured in a sandwich configuration. *FASEB J.* 10: 1471-1484.

Boote C, Dennis S, Huang Y, Quantock AJ and Meek KM (2005) Lamellar orientation in human cornea in relation to mechanical properties. *J Struct Biol.* 149: 1.

Boote C, Hayes S, Abahussin M and Meek KM. (2006) Mapping collagen organization in the human cornea: left and right eyes are structurally distinct. *Invest Ophthalmol Vis Sci.* 47: 901-908.

Cameron GJ, Alberts IL, Laing JH and Wess TJ (2002) Structure of type I and type III heterotypic collagen fibrils: an X-ray diffraction study. *J Struct Biol* 137: 15-22.

Carlson EC, Wang IJ, Liu CY, Brannan P, Kao CW and Kao WW (2003) Altered KSPG expression by keratocytes following corneal injury. *Mol Vis.* 21: 615-623.

Carrington LM, Albon J, Anderson I, Kamma C and Boulton M (2006) Differential regulation of key stages in early corneal wound healing by TGF-beta isoforms and their inhibitors. *Invest Ophthalmol Vis Sci* 47: 1886-1894.

Carrington LM, and Boulton M (2005) Hepatocyte growth factor and keratinocyte growth factor regulation of epithelial and stromal corneal wound healing. *J Cataract Refract Surg.* 31: 412-423.

Chang S W, Benson A, and Azar D T (1998) Corneal light scattering with stromal reformation after laser in situ keratomileusis and photorefractive keratectomy. *J Cataract Refract Surg* 24: 1064-1069.

Chaudhry MI, Conti ER and Steinert RF. (1999) Advances in refractive surgery: new options expand the scope of corrective procedures. *Postgrad Med* 106: 129-137.

Chawla JS (2003) Complications of LASIK: Part 1-Epithelial Defects. *OT* 13: 26-27.

Chothia C (1992) One thousand families for the molecular biologists. *Nature* 357: 543-544.

Chothia C, and Lesk AM (1986) The relation between the divergence of sequence and structure in proteins. *The EMBO Journal* 5: 823.

Cintron C (1989) The Function of Proteoglycans in Normal Healing Cornea. In: Beuerman RW, C C, Kaufman HE [ed.] *Healing Processes in the Cornea.* Vol. 1. Texas: The Portfolio Publishing Company.

Connon CJ, and Meek KM (2003) Organization of corneal collagen fibrils during the healing of trephined wounds in rabbits. *Wound Repair Regen.* 11: 71-78.

Connon CJ, and Meek KM (2004) The structure and swelling of corneal scar tissue in penetrating full-thickness wounds *Cornea.* 23: 165-171.

Corbett MC, and Marshall J (1996) Corneal Haze after PRK. *Lasers and Light* 7: 173-196.

Crawford JB, Aldave AJ, McLeod S, Howes E and Schwartz D (2003) Histopathological analysis of the cornea after laser in situ keratomileusis. *Arch Ophthalmol.* 121: 896-898.

Cunha BA (2000) Antibiotic selection for diabetic foot infections: a review. *J Foot Ankle Surg.* 39: 253-257.

D'Alfonso G, Tramontano A and Lahm A (2001) Structural conservation in single-domain proteins: implications for homology modeling. *J Struct Biol.* 134: 246.

Daniels JT, and Khaw PT (2000) Temporal stimulation of corneal fibroblast wound healing activity by differentiating epithelium in vitro. *Invest Ophthalmol Vis Sci.* 41: 3754-3762.

Dawson DG, Holley GP, Geroski DH, Waring GO, Grossniklaus HE and Edelhauser HF (2005a) Ex vivo confocal microscopy of human LASIK corneas with histologic and ultrastructural correlation. *Ophthalmology.* 112: 634-644.

Dawson DG, Kramer TR, Grossniklaus HE, Waring GO and Edelhauser HF (2005b) Histologic, ultrastructural, and immunofluorescent evaluation of human laser-assisted in situ keratomileusis corneal wounds. *Arch Ophthalmol.* 123: 741-756.

Derwin KA, Soslowsky LJ, Kimura JH and Plaas AH (2001) Proteoglycans and glycosaminoglycan fine structure in the mouse tail tendon fascicle. *J Orthop Res.* 19: 269-277.

Dilly PN (1994) Structure and function of the tear film. *Adv. Exp. Med. Biol.* 350: 239-247.

Donzis PB, and Mondino BJ (1987) Management of noninfectious corneal ulcers. *Surv Ophthalmol* 32: 94-110.

Edelhauser H (2000) The Resiliency of the Corneal Endothelium to Refractive and Intraocular Surgery. *Cornea* May 19: 263-273.

Esquenazi S, He J, Bazan NG and Bazan HE (2005) Comparison of corneal wound-healing response in photorefractive keratectomy and laser-assisted subepithelial keratectomy. *J Cataract Refract Surgery* 31: 1632-1639.

Fagerholm P (2000) Wound Healing after PRK. *J Cataract Refract Surgery* 26: 432-447.

Fatima A, Vemuganti GK, Iftekhar G, Rao GN and Sangwan VS (2007) In vivo survival and stratification of cultured limbal epithelium. *Clin Experiment Ophthalmol* 35: 96-98.

Fini ME (1999) Keratocyte and fibroblast phenotypes in the repairing cornea. *Prog Retin Eye Res.* 18: 529-551.

Fitton JH, Ziegelaar BW, Hicks CR, Clayton AB, Crawford GJ,Constable IJ and Chirila TV. (1998) Assessment of anticollagenase treatments after insertion of a keratoprosthetic material in the rabbit cornea. *Cornea* 17: 108-114.

Foreman DM, Pancholi S, Jarvis-Evans J, McLeod D and Boulton ME (1996) A Simple Organ Culture Model for Assesing the Effects of Growth Factors on Corneal Re-epithelization. *Exp Eye Res* 62: 555-564.

Freegard TJ (1997) The physical basis of transparency of the normal cornea. *Eye* 11: 465-471.

Fuchsluger T, Tuerkeli E, Westekemper H, Esser J, Steuhl K P, and Meller D (2007) Rate of epithelialisation and re-operations in corneal ulcers treated with amniotic membrane transplantation combined with botulinum toxin-induced ptosis. *Graefes Arch Clin Exp Ophthalmol.*

Funderburgh JL, Funderburgh ML, Mann MM, Corpuz L and Roth MR (2001) Proteoglycan expression during transforming growth factor beta -induced keratocyte-myofibroblast transdifferentiation. *J Biol Chem.* 276: 44173.

Funderburgh JL, Hevelone ND, Roth MR, Funderburgh ML, Rodrigues MR, Nirankari VS and Conrad GW (1998) Decorin and biglycan of normal and pathologic human corneas. *Invest Ophthalmol Vis Sci* 39: 1957-1964.

Funderburgh JL, Mann MM and Funderburgh ML (2003) Keratocyte phenotype mediates proteoglycan structure: a role for fibroblasts in corneal fibrosis. *J Biol Chem.* 278: 45629.

Gao XF, Huang XR and Sun CC (2006) Role of each residue in catalysis in the active site of pyrimidine nucleoside phosphorylase from Bacillus subtilis: A hybrid QM/MM study. *Journal of Structural Biology* 154: 20-26.

Gellert A, Salanki K, Naray-Szabo K and Balazs E (2006) Homology modelling and protein structure based functional analysis of five cucumovirus coat proteins. *Journal of Molecular Graphics and Modelling* 24: 319-327.

Gough J, and Chothia C (2004) The Linked Conservation of Structure and Function in a Family of High Diversity: The Monomeric Cupredoxins. *Structure* 12: 917-925.

Green C (2003) Keratocytes: more than a framework for the window. *Clin Exp Opth* 31: 91-92.

Greenhalgh DG (2003) Wound healing and diabetes mellitus. *Clin Plast Surg.* 30: 37-45.

Grimmett MR, and Holland EJ (1996) Complications of Small-Clear zone after PRK. *Opthalmology* 103: 1348-1356.

Grishin NV (2001) Fold Change in Evolution of Protein Structures. *Journal of Structural Biology* 134: 167.

Hart RW, and Farrell RA (1969) Light scattering in the cornea. *J Opt Soc Am* 59: 766-774.

Hedbys BO, and Dohlman CH (1963) A new method for the determination of the swelling pressure of the corneal stroma in vitro. *Exp Eye Res.* 2.

Heickell AG, Vesaluoma MH, Tervo TM, Vannas A and Krootila K (2004) Late traumatic dislocation of laser in situ keratomileusis flaps. *J Cataract Refract Surg.* 30: 253-256.

Helena MC, Baerveldt F, Kim WJ and Wilson SE (1998) Keratocyte Apoptosis after Corneal Surgery. *Invest Opthalmol Vis Sci* 39: 276-283.

Helena M C, Baerveldt F, Kim W J, and Wilson S E (1998) Keratocyte apoptosis after corneal surgery. *Invest Ophthalmol Vis Sci* 39: 276-283.

Hendrickson RC (1986) Space charge drift from a +/- 400-kV direct current transmission line. *Bioelectromagnetics.* 7: 369-379.

Hocking AM , Shinomura T and McQuillan DJ (1998) Leucine-Rich Repeat Glycoproteins of the Extracllular Matrix. *Matrix Biology* 17: 1-19.

Hocking AM S R, Ramamurthy P and McQuillan DJ (1996) Eukaryotic Expression of Recombinant Biglycan. *The Journal of Biological Chemistry* 271: 19571-19577.

Hodson S, Guggenheim J, Kaila D and Wigham C (1991) Anion pumps in ocular tissues. *Biochem Soc Trans.* 19: 849-852.

Hogan MJ, Alvarado JA and Weddell JE (1971) The cornea.*Histology of the human eye*. Philaderphia: WB Saunders.

Huang AJ, Li DQ, Li CH, Shang TY and Hernandez E (2005) Modulation of corneal vascularization. *Ocul Surf* 3: S190-193.

Iocono JA *e a* (1998) The biology of healing. In: KG, L D a H [ed.] *Wounds: biology and management*. Oxford: Oxford Medical Publications.

Ishizaki M, Wakamatsu K, Matsunami T, Yamanaka N, Saiga T,Shimizu Y, Zhu G and Kao WW (1994) Dynamics of the expression of cytoskeleton components and adherens molecules by fibroblastic cells in alkali-burned and lacerated corneas. *Exp Eye Res.* 59: 537-549.

Iskander NG, Peters NT, Anderson Penno E and Gimbel HV (2001) Late traumatic flap dislocation after laser in situ keratomileusis. *J Cataract Refract Surg.* 27: 1111-1114.

Ivarsen A, and Moller-Pedersen T (2005) LASIK induces minimal regrowth and no haze development in rabbit corneas. *Curr Eye Res* 30: 363-373.

Ivarsen A, Laurberg T and Moller-Pedersen T (2003) Characterisation of corneal fibrotic wound repair at the LASIK flap margin. *Br J Ophthalmol.* 87: 1272-1278.

Ivarsen A, Laurberg T and Moller-Pedersen T (2004) Role of keratocyte loss on corneal wound repair after LASIK. *Invest Ophthalmol Vis Sci* 45: 3499-3506.

Jeffcoate WJ, and Harding KG (2003) Diabetic foot ulcers. *The Lancet* 361: 1545-1551.

Jester JV, and Ho-Chang J (2003) Modulation of cultured corneal keratocyte phenotype by growth factors/cytokines control in vitro contractility and extracellular matrix contraction. *Exp Eye Res.* 77: 581-592.

Jester JV, Moller-Pedersen T, Huang J, Sax CM, Kays WT, Cavangh HD, Petroll WM and Piatigorsky J (1999) The cellular basis of corneal transparency: evidence for "corneal crystallins". *J Cell Sci.* 112:613-622.

Johnson ME, and Murphy PJ (2004) Changes in the tear film and ocular surface from dry eye syndrome. *Prog Retin Eye Res.* 23: 449-474.

Kasper M, Moll R, Stosiek P and Karsten U (1988) Patterns of cytokeratin and vimentin expression in the human eye. *Histochemistry.* 89: 369-377.

Kim JY, Kim MJ, Kim TI, hoi HJ, Pak JH and Tchah H (2006) A femtosecond laser creates a stronger flap than a mechanical microkeratome. *Invest Ophthalmol Vis Sci.* 47:599-604.

Kim KS, Jean SJ and Edelhauser HF (1997) Corneal endothelial morphology and barrier function following excimer laser photorefractive keratectomy. In: Lass J, e a [ed.] *Advances in corneal research.* New York: Plenum Press, pp. 329–342.

Kitzmann AS, Bourne WM and Patel SV (2007) Confocal microscopy of a femtosecond laser LASIK flap before separation. *Am J Ophthalmol* 143: 691-693.

Knudson CV, and Knudson W (2001) Cartilage proteoglycans. *seminars in CELL & DEVELOPMENTAL BIOLOGY* 12.

Kopp J, and Schwede T (2006) The SWISS-MODEL Repository: new features and functionalities. *Nucleic Acids Research.* 34: 315-318.

Kramer RZ B J, Mayville P, Brodsky B and Berman HM (1999) Sequence dependent conformational variations of collagen triple-helical structure. *Nature Structural Biology* 6: 454-457.

Krantz DD, Zidovetzki R, Kagan BL and Zipursky SL (1991a) Amphipathic beta structure of a leucine-rich repeat peptide. *J Biol Chem.* 266: 16801.

Krantz DD Z R, Kaganll BL and Zipursky SL (1991b) Amphipathic b Structure of a Leucine-rich Repeat Peptide. *The Journal of Biological Chemistry* 266: 16801-16807.

Kresse H, Liszio C, Schonherr E and Fisher LW (1997) Critical Role of Glutamate in a Central Leucine-rich Repeat of Decorin for Interaction with Type I Collagen. *The Journal of Biological Chemistry* 272: 18404.

Kymionis GD, Tsiklis NS, Pallikaris AI, Kounis G, Diakonis VF, Astyrakakis N and Siganos CS (2006) Long-term follow-up of Intacs for post-LASIK corneal ectasia. *Ophthalmology.* 113.

Lambiase A, Manni L, Bonini S, Rama P, Micera A and Aloe L (2000) Nerve growth factor promotes corneal healing: structural, biochemical, and molecular analyses of rat and human corneas. *Invest Ophthalmol Vis Sci* 41: 1063-1069.

Landau D, Levy J, Solomon A, Lifshitz T, Orucov F, Strassman E and Frucht-Pery J (2006) Traumatic corneal flap dislocation one to six years after LASIK in nine eyes with a favorable outcome. *J Refract Surg* 22: 884-889.

Laube T, Wissing S, Theiss C, Brockmann C, Steuhl K P, and Meller D (2004) Decreased keratocyte death after laser-assisted subepithelial keratectomy and photorefractive keratectomy in rabbits. *J Cataract Refract Surg* 30: 1998-2004.

Levy Y, Zadok D and Barenboim E (2003) Laser in situ keratomileusis in a combat jet aircraft pilot. *J Cataract Refract Surg.* 29: 1239-1241.

Li DQ, and Pflugfelder SC (2005) Matrix metalloproteinases in corneal inflammation. *Ocul Surf* 3: S198-202.

Lim M, Goldstein MH, Tuli S and Schultz GS (2003) Growth Factor, Cytokine and Protease Interactions During Corneal Wound Healing. *Ocul Surf.* 1: 53-65.

Litwak S, Zadok D, Garcia-de Quevedo V, Robledo N and Chayet AS (2002) LASEK vs PRK for the correction of myopia. *J Cataract Refract Surgery* 28: 1330-1333.

Lu L (2001) Corneal Epithelial Wound Healing. *Exp Biol Med* 226: 653-664.

MacDougall IJA, Lewis PJ and Griffith R (2005) Homology modelling of RNA polymerase and associated transcription factors from Bacillus subtilis. *Journal of Molecular Graphics and Modelling* 23: 297-303.

Maguen E, Zorapapel NC, Zieske JD, Ninomiya Y, Sado Y, Kenney MC and Ljubimov AV (2002) Extracellular Matrix and Matrix Metalloproteinase Changes in Human Corneas After Complicated Laser-Assisted In Situ Keratomileusis (LASIK). *Cornea* 21: 95-100.

Malik NS, Moss SJ, Ahmed N, Furth AJ, Wall RS and Meek KM (1992) Ageing of the human corneal stroma: structural and biochemical changes. *Biochim Biophys Acta.* 1138: 222-228.

Margaritondo G (1988) *Introduction to Synchrotron Radiation.* Oxford: Oxford University Press.

Marshall GE, Konstas AG and Lee WR. (1991) Immunogold fine structural localization of ECM components in aged human cornea: II. Collagen types V and VI. *Graefe's Arch Clin Exp Opthalmol* 229: 164-171.

Marshall J, Trokel SL, Rothery S and Krueger RR (1988) Long-term healing of the central cornea after photorefractive keratectomy using an excimer laser. *Ophthalmology.* 95: 1411-1421.

Masket S, and Belani S (2007) Proper wound construction to prevent short-term ocular hypotony after clear corneal incision cataract surgery. *J Cataract Refract Surg* 33: 383-386.

Maurice DM (1957) The structure and transparency of the cornea. *J Physiol.* 136: 263-286.

May CA, Priglinger SG, Neubauer AS, Alge CS, Ludwig K, Kampik A, Welge-Lu U □ (2004) Laser in situ keratomileusis in human corneas: New organ culture model *J Cataract Refract Surg.* 30.

McCally RL, Freund DE, Zorn A, Bonney-Ray J, Grebe R, de la Cruz Z and Green WR (2007) Light-scattering and ultrastructure of healed penetrating corneal wounds. *Invest Ophthalmol Vis Sci.* 48: 157-165.

McNeil R (2003) Refractive Surgery update: Safer surgery and better vision. *OT* 13: 21.

Meek KM (1981) The use of glutaraldehyde and tannic acid to preserve reconstituted collagen for electron microscopy. *Histochemistry.* 73: 115-120.

Meek KM (2002) The Corneà. In: D, R [ed.] *Signals and Perception: The Fundamentals of Human Sensation.* New York: Palgrave McMillan.

Meek KM, and Boote C (2004) The organization of collagen in the corneal stroma. *Exp Eye Res.* 78: 503-512.

Meek KM, and Fullwood NJ (2001a) Corneal and scleral collagens--a microscopist's perspective. *Micron* 32: 261-272.

Meek KM, and Quantock AJ (2001b) The use of X-ray scattering techniques to determine corneal ultrastructure. *Prog Retin Eye Res.* 20: 95-137.

Meek KM, Leonard DW, Connon CJ, Dennis S and Khan S (2003) Transparency, swelling and scarring in the corneal stroma. *Eye* 17: 1-10.

Melki SA, Talamo JH, Demetriades AM, Jabbur NS, Essepian JP, O'Brien TP and Azar DT (2000) Late traumatic dislocation of laser in situ keratomileusis corneal flaps. *Ophthalmology.* 107: 2136-2139.

Meltendorf C, Burbach G J, Buhren J, Bug R, Ohrloff C and Deller T (2007) Corneal femtosecond laser keratotomy results in isolated stromal injury and favorable wound-healing response. *Invest Ophthalmol Vis Sci* 48: 2068-2075.

Micera A, Lambiase A, Puxeddu I, Aloe L, Stampachiacchiere B, Levi-Schaffer F, Bonini S and Bonini S (2006) Nerve growth factor effect on human primary fibroblastic-keratocytes: possible mechanism during corneal healing. *Exp Eye Res.* 83: 747-757.

Mohan RR, Hutcheon AE, Choi R, Hong J, Lee J, Mohan RR, Ambrosio R Jr, Zieske JD and Wilson SE (2003) Apoptosis, necrosis, proliferation, and myofibroblast generation in the stroma following LASIK and PRK. *Exp Eye Res.* 76: 71-87.

Mohan RR, Mohan RR, Kim WJ, Stark GR and Wilson SE (2000) Defective keratocyte apoptosis in response to epithelial injury in stat 1 null mice. *Exp Eye Res* 70: 485-491.

Mondino BJ (1988) Inflammatory diseases of the peripheral cornea. *Opthalmology* 95: 463-472.

Nagy ZZ, Hiscott P, Seitz B, Shlotzer-Schrehardt U, Simon M Jr, Suveges I and Naumann GO (1997) Ultraviolet-B enhances corneal stromal response to 193-nm excimer laser treatment. *Ophthalmology* 104: 375-380.

Naito Z (2005) Role of the small leucine-rich proteoglycan (SLRP) family in pathological lesions and cancer cell growth. *J Nippon Med Sch.* 72: 137-145.

Pallikaris IG, Kymionis GD and Astyrakakis NI (2001) Corneal Ectasia induced by LASIK. *J Cataract Refract Surgery* 27: 1796-1802.

Patel S, McLaren J, Hodge D and Bourne W (2001) Normal human keratocyte density and corneal thickness measurement by using confocal microscopy in vivo. *Invest Ophthalmol Vis Sci.* 42: 333-339.

Perrella G, Brusini P, Spelat R ,Hossain P ,Hopkinson A and Dua H S (2007) Expression of haematopoietic stem cell markers, CD133 and CD34 on human corneal keratocytes. *Br J Ophthalmol*: 94–99.

Philipp WE, Speicher L and Gottinger W (2003) Histological and Immunohistochemical findings after LASIK in human corneas. *J Cataract Refract Surgery* 29: 808-820.

Poole AC, Brookes NH and Clover GM. (2003) Confocal imaging of the human keratocyte network using the vital dye 5-chloromethylfluorescein diacetate. *Clin Exp Opth* 31: 147-154.

POrez-Santoja JJ L T, Tervo KM, Sakla HF, Alio y Sanz JL and Tervo TM (1998) Corneal Wound Healing after LASIK in Rabbits. *J Refract Surgery* 1998: 602-609.

Priglinger SG, May CA, Alge CS, Wolf A, Neubauer AS, Haritoglou C, Kampik A andWelge-Lussen U (2006) Immunohistochemical findings after LASIK confirm in vitro LASIK model. *Cornea* 25: 331-335.

Pullar CE, Zhao M, Song B, Pu J, Reid B, Ghoghawala S, McCaig C and Isseroff RR (2007) Beta-adrenergic receptor agonists delay while antagonists accelerate epithelial wound healing: evidence of an endogenous adrenergic network within the corneal epithelium. *J Cell Physiol* 211: 261-272.

Qiu P, Kurpakus-Wheater M and Sosne G (2007) Matrix metalloproteinase activity is necessary for thymosin beta 4 promotion of epithelial cell migration. *J Cell Physiol* 212: 165-173.

Quantock AJ, Fullwood NJ, Thonar EJ, Waltman SR, Capel MS, Ito M, Verity SM and Schanzlin DJ (1997) Macular corneal dystrophy type II: Multipe studies on a cornea with low levels of sulphated keratan sulphate. *Eye* 11.

Quantock AJ, Padroni S, Connon CJ, Milne G and Schanzlin DJ (2003) Proteoglycan alterations in the rabbit corneal stroma after a lamellar incision. *J Cataract Refract Surg.* 29: 821-824.

Rabinowitz YS (2006) Ectasia after laser in situ keratomileusis. *Curr Opin Ophthalmol* 17: 421-426.

Rainey JK, and Goh MC (2002) A statistically derived parameterization for the collagen triple-helix. *Protein Sci* 11: 2748-2754.

Rajan MS, Watters W, Patmore A and Marshall J (2005) In vitro human corneal model to investigate stromal epithelial interactions following refractive surgery. *J Cataract Refract Surg.* 31: 1789-1800.

Ranucci CS, Kumar A, Batra SP and Moghe PV (2000) Control of hepatocyte function on collagen foams: sizing matrix pores toward selective induction of 2-D and 3-D cellular morphogenesis. *Biomaterials.* 21: 783-793.

Rawe IM, Meek KM, Leonard DW, Takahashi T and Cintron C (1994) Structure of corneal scar tissue: an X-ray diffraction study. *Biophys J.* 67: 1743-1748.

Reed R H D, Weyers J and Jones A (1998) *Practical Skills in Biomolecular Science*. London: Longman.

Remington LA (1998) *Clinical Anatomy of the Visual System*. Butterworth-Heinemann.

Robert L *et al.* (2000) Corneal Collagens. *Pathol Biol (Paris)* 49: 353-363.

Roughley PZ, Rodriguez E and Lee ER (1995) The interactions of 'non-aggregating' proteoglycans. *Osteoarthritis and Cartilage* 3: 239-248.

Saika S (1998) Alterations in ECM in Experimental Alkali burn of the Cornea. In *Santen International Symposium: Corneal Healing Responces to Injuries and Refractive Surgeries*. The Hague: Kugler Publications.

Saude T (1993) *Occular Anatomy and Physiology*. Oxford: Blackwell Scientific Publications.

Schonherr E, Hausser H, Beavan L and Kresse H (1995) Decorin-type I collagen interaction. Presence of separate core protein-binding domains. *J Biol Chem.* 270: 8877.

Schönherr E W-P P, Harrach B, Robenek H, Rauterberg J and Kresse H (1995) Interaction of Biglycan with type I collagen. *The Journal of Biological Chemistry* 270 2776-2783.

Scott JE (1988a) Proteoglycan-fibrillar collagen interactions. *Biochem. J.* 252.

Scott JE (1996) Proteodermatan and Proteokeratan Sulfate (Decorin, Lumican/Fibromodulin) Proteins Are Horseshoe Shaped. Implications for Their Interactions with Collagen. *Biochemistry* 35: 8795-8799.

Scott JE, and Haigh M (1988b) Identification of specific binding sites for keratan sulphate proteoglycans and chondroitin-dermatan sulphate proteoglycans on collagen fibrils in cornea by the use of cupromeronic blue in 'critical-electrolyte-concentration' techniques. *Biochem J.* 253: 607-610.

Scott JE, and Stockwell RA (1967) On the use and abuse of the critical electrolyte concentration approach to the localization of tissue polyanions. *J Histochem Cytochem.* 15: 111-113.

Scott PG, Bishop PN and Bella J (2006a) On the calculation of the binding force between decorin and collagen. *Journal of Biomechanics* 39: 1159-1160.

Scott PG, Dodd CM, Bergmann EM, Sheehan JK and Bishop PN (2006b) Crystal structure of the biglycan dimer and evidence that dimerisation is essential for folding and stability of class I small leucine rich repeat proteoglycans *J Biol Chem.* 281: 13324.

Scott PG, McEwan PA, Dodd CM, Bergmann EM, Bishop PN and Bella J. (2004) Crystal structure of the dimeric protein core of decorin, the archetypal small leucine-rich repeat proteoglycan. *Proc Natl Acad Sci U S A* 101: 15633.

Scott PJ, McEwan PG, Dodd CM, Bergmann EM, Bishop PN, and Bella J (2004) Crystal structure of the dimeric protein core of decorin, the archetypal small leucine-rich repeat proteoglycan. *PNAS* 101: 15633-15638.

Shah S, and Kumar V (2003) Has LASEK superseded LASIK? *OT* 13: 22-25.

Shah S, Sebai Sarhan AR, Doyle SJ, Pillai CT and Dua HS (2001) The epithelial flap for PRK. *Br J Opthalmol* 85: 393-396.

Shortt AJ, Bunce C and Allan BD (2006) Evidence for superior efficacy and safety of LASIK over photorefractive keratectomy for correction of myopia. *Ophthalmology.* 113: 1897-1908.

Singerman LJ, and Coscas G (1992) *Current Techniques in Opthalmic Laser Surgery.* 3rd ed. USA: BH.

Solomon R, Donnenfeld ED and Perry HD (2004) The effects of LASIK on the ocular surface. *Ocul Surf* 2: 34-44.

Sosnová M, Bradl M and Forrestera JV (2005) CD34+ Corneal Stromal Cells Are Bone Marrow–Derived and Express
Hemopoietic Stem Cell Markers. *Stem Cells* 23: 507–515.

Southard-Smith EM C J, Ellison JS, Smith KJ, Baxevanis AD, Touchman JW, Green ED, Dunham I and Pavan WJ (1999) Comparative analyses of the Dominant megacolon-SOX10 genomic interval in mouse and human. *Mammalian Genome* 10: 744-749.

Stramer BM, and Fini ME. (2004) Uncoupling keratocyte loss of corneal crystallin from markers of fibrotic repair. *Invest Ophthalmol Vis Sci.* 45(11):4010-5.

Steele C (1999) Corneal Wound Healing: a review. *Optometry Today* 24: 28-34.

Sundarraj N F D, Belak R, Sundarraj S, Rada J, Okamoto S and Hassell L J (1998) Proteoglycan Distribution During Healing of Corneal Stromal Wounds in Chick. *Exp. Eye Res.* 67: 433-442.

Terry T (2002) *Lecture Notes: Amino Acids and Proteins.* wwwfac.mcdaniel.edu/.../CH3321JPGs/ Proteins/Collagen.jpg Accessed: 2003

Thompson JD, Higgins DG and Gibson TJ (1994) CLUSTAL W: improving the sensitivity of progressive multiple sequence alignment through sequence weighting, position-specific gap penalties and weight matrix choice. *Nucleic Acids Res* 22: 4673.

Tufvesson E, and Westergren-Thorsson G (2002) Tumour necrosis factor-K interacts with biglycan and decorin. *FEBS Letters* 530: 124-128.

Vesaluoma MH, Petroll WM, Perez-Santonja JJ, Valle TU, Alio JL and Tervo TM (2000) Laser in situ keratomileusis flap margin: wound healing and complications imaged by in vivo confocal microscopy. *Am J Ophthalmol.* 130: 564-573.

Vesentini S, Montevecchi FM, and Redaelli A (2006) Response to letter to the editor: On the calculation of the binding force between decorin and collagen. *Journal of Biomechanics* 39: 1160.

Vesentini S, Redaelli A and Montevecchi FM (2005) Estimation of the binding force of the collagen molecule-decorin core protein complex in collagen fibril. *J Biomech.* 38: 433.

Vigneault F, Zaniolo K, Gaudreault M, Gingras ME and Guerin SL (2007) Control of integrin genes expression in the eye. *Prog Retin Eye Res* 26: 99-161.

Waddington RJ, and Langley MS (1998) Structural Analysis of Proteogtycans Synthesized By Mineralizing Bone Cells In Vitro in the Presence of Fluoride. *Matrix Biology* 17: 255-268.

Waggett AD R J, KwanA, Woodnutt D and Benjamin M (1997) Characterization of Collagens and Proteoglycans at the Insertion of the Human Achilles Tendon. *Matrix Biology* 16: 457-470.

Wakuta M, Morishige N, Chikama T, Seki K, Nagano T and Nishida T (2007) Delayed wound closure and phenotypic changes in corneal epithelium of the spontaneously diabetic Goto-Kakizaki rat. *Invest Ophthalmol Vis Sci* 48: 590-596.

Watson PG, and Young RD (2004) Scleral structure, organisation and disease. A review. *Experimental Eye Research* 78: 609-623.

Weber IT, Harrison RW and Iozzo RV. (1996a) Model structure of decorin and implications for collagen fibrillogenesis. *J Biol Chem.* 271: 31767.

Weber IT H R a I R (1996b) Model Structure of Decorin and Implications for Collagen Fibrillogenesis. *The Journal of Biological Chemistry* 271: 31767-31770.

Wegrowski Y, Paltot V, Gillery P, Kalis B, Randoux A and Maquart FX. (1995) Stimulation of sulphated glycosaminoglycan and decorin production in adult dermal fibroblasts by recombinant human interleukin-4. *Biochem J.* 307.

Weisa SM Z S, Shaha M, Covella JM, Omensa JH, Ross J Jr, Daltonb N, Jonesa Y, Reedd CC, Iozzod RV and McCullocha AD (2005) A role for decorin in the remodeling of myocardial infarction. *Matrix Biology* 24: 313 - 324.

Wilson K, and Walker J (1997) *Principles and Techniques of Practical Biochemistry*. 4 ed. Cambridge: Cambridge University Press.

Wilson SE (1998a) LASIK: Management of Common Complications. *Cornea* 17: 459-467.

Wilson SE (1999a) Stimulus-specific and cell type-specific cascades: emerging principles relating to control of apoptosis in the eye. *Exp Eye Res.* 69: 255-266.

Wilson SE (2002) Analysis of the keratocyte apoptosis, keratocyte proliferation, and myofibroblast transformation responses after photorefractive keratectomy and laser in situ keratomileusis. *Trans Am Ophthalmol Soc* 100: 411-433.

Wilson SE, and Kim WJ (1998b) Keratocyte Apoptosis: Implications on Corneal Wound Healing, Tissue Organisation and Disease. *IOVS* 39: 220-226.

Wilson SE, He YG, Weng J, Li Q, McDowall AW, Vital M and Chwang EL (1996a) Epithelial injury induces keratocyte apoptosis: hypothesized role for the interleukin-1 system in the modulation of corneal tissue organization and wound healing. *Exp Eye Res.* 62: 325-327.

Wilson SE, Li Q, Weng J, Barry-Lane PA, Jester JV, Liang Q and Wordinger RJ (1996b) The Fas-Fas ligand system and other modulators of apoptosis in the cornea. *Invest Ophthalmol Vis Sci* 37: 1582-1592.

Wilson SE, Liu JJ and Mohan RR (1999b) Stromal-epithelial interactions in the cornea. *Prog Retin Eye Res.* 18: 293-300.

Wilson SE, Mohan RR, Hong JW, Lee JS, Choi R and Mohan RR (2001) The wound healing response after laser in situ keratomileusis and photorefractive keratectomy: elusive control of biological variability and effect on custom laser vision correction. *Arch Ophthàlmol* 119: 889-896.

Wilson SE, Mohan RR, Hutcheon AE, Mohan RR, Ambrosio R, Zieske JD, Hong J and Lee J (2003) Effect of ectopic epithelial tissue within the stroma on keratocyte apoptosis, mitosis and myfibroblast transformation. *Exp Eye Res* 76: 193-201.

Windshugel B, Jyrkkarinne J, Vanamo J, Poso A, Honkakoski P and Sippl W (2006) Comparison of homology models and X-ray structures of the nuclear receptor CAR: Assessing the structural basis of constitutive activity. *Journal of Molecular Graphics and Modelling*

Wolff E (1946) Mucocutenous junction of lid margin and distribution of tear fluid. *Trans. Opthal. Soc.* 66: 291-308.

Woodhead-Galloway J (1980) *Collagen: the Anatomy of a Protein.* London: Edward Arnold Ltd

Worthington CR and Inouye H (1985) X-ray diffraction study of the cornea. *Int. J. Biol. Macromol.* **7**: 2–8

Wu J, Rajwa B, Filmer DL, Hoffmann CM, Yuan B, Chiang CS, Sturgis J and Robinson JP (2003) Analysis of orientations of collagen fibers by novel fiber-tracking software. *Microsc Microanal.* 9: 574-580.

Yamagami S, Ebihara N, Usui T, Yokoo S and Amano S (2006) Bone Marrow–Derived Cells in Normal Human Corneal Stroma. *Arch Ophthalmol* 124: 62-69.

Young RD, Tudor D, Hayes AJ, Kerr B, Hayashida Y, Nishida K, Meek KM, Caterson B and Quantock AJ (2005) Atypical composition and ultrastructure of proteoglycans in the mouse corneal stroma. *Invest Ophthalmol Vis Sci* 46: 1973-1978.

Zhao B, Cooper LJ, Brahma A, MacNeil S, Rimmer S and Fullwood NJ (2006) Development of a three-dimensional organ culture model for corneal wound healing and corneal transplantation. *Invest Ophthalmol Vis Sci.* 47: 2840-2846.

Zieske JD (2001) ECM and wound healing. *Current Opinion in Opthalmology* 12: 237-241.

Zubai GL (1998) *Biochemistry*. 4 ed. Boston: McGraw Hill.